SYNTHESIS, CHARACTERIZATION, AND THERMOPHYSICAL PROPERTIES OF MAGHEMITE (γ-Fe_2O_3) NANOFLUIDS WITH AND WITHOUT MAGNETIC FIELDS EFFECT

IRWAN NURDIN

FACULTY OF ENGINEERING
UNIVERSITY OF MALAYA
KUALA LUMPUR

2016

SYNTHESIS, CHARACTERIZATION, AND THERMOPHYSICAL PROPERTIES OF MAGHEMITE (γ-Fe_2O_3) NANOFLUIDS WITH AND WITHOUT MAGNETIC FIELDS EFFECT

IRWAN NURDIN

THESIS SUBMITTED IN FULFILMENT OF THE REQUIREMENTS FOR THE DEGREE OF DOCTOR OF PHILOSOPHY

FACULTY OF ENGINEERING
UNIVERSITY OF MALAYA
KUALA LUMPUR

2016

UNIVERSITY OF MALAYA

ORIGINAL LITERARY WORK DECLARATION

Name of Candidate: Irwan Nurdin

Registration/Matric No: KHA 090058

Name of Degree: Doctor of Philosophy

Title of Project Paper/Research Report/Dissertation/Thesis ("this Work"):

Synthesis, Characterization, And Thermophysical Properties of Maghemite (γ-Fe_2O_3) Nanofluids With And Without Magnetic Fields Effect

Field of Study: Nanomaterials

I do solemnly and sincerely declare that:

(1) I am the sole author/writer of this Work;
(2) This Work is original;
(3) Any use of any work in which copyright exists was done by way of fair dealing and for permitted purposes and any excerpt or extract from, or reference to or reproduction of any copyright work has been disclosed expressly and sufficiently and the title of the Work and its authorship have been acknowledged in this Work;
(4) I do not have any actual knowledge nor do I ought reasonably to know that the making of this work constitutes an infringement of any copyright work;
(5) I hereby assign all and every rights in the copyright to this Work to the University of Malaya ("UM"), who henceforth shall be owner of the copyright in this Work and that any reproduction or use in any form or by any means whatsoever is prohibited without the written consent of UM having been first had and obtained;
(6) I am fully aware that if in the course of making this Work I have infringed any copyright whether intentionally or otherwise, I may be subject to legal action or any other action as may be determined by UM.

Candidate's Signature Date:

Subscribed and solemnly declared before,

Witness's Signature Date:

Name:

Designation:

ABSTRACT

Synthesis, characterization, and thermophysical properties of maghemite nanofluids have been studied with and without magnetic fields effect. The objectives of study are to synthesize maghemite nanoparticles and their characterization using various methods, to prepare stable maghemite nanofluids, and measurement of thermophysical properties of maghemite nanofluids with and without external magnetic fields effect. Maghemite nanoparticles were synthesized by chemical co-precipitation method with different concentrations of nitric acid. Maghemite nanofluids were then prepared and the stability of the nanofluids were characterized by zeta potential and dynamic light scattering at different pH and time of storage. Lastly, measurements of thermal conductivity, viscosity, and electrical conductivity of maghemite nanofluids were taken at various particle volume fraction, temperatures, with and without strengths of magnetic fields. Results show that spherical shape of superparamagnetic maghemite nanoparticles with good thermal and suspensions stability was successfully synthesized within the size range of 9.3 to 14.7 nm. The stability of maghemite nanofluids show that the suspensions remain stable at acidic condition with zeta potential value of 44.6 mV at pH 3.6 and at basic condition with zeta potential -46.2 mV at pH 10.5. The isoelectric point of the maghemite nanoparticles suspensions is obtained at pH 6.7. The maghemite nanofluids remains stable after eight months of storage. The thermal conductivity of maghemite nanofluids linearly increases with increasing of particle volume fraction, temperature, and magnetic fields strengths. The kinematic viscosity of maghemite nanofluids increases with increasing of particle volume fraction and magnetic fields and decrease with increasing of temperature. Electrical conductivity of maghemite nanofluids increases with increasing of particle volume fraction and temperature and no effect with magnetic fields.

ABSTRAK

Sintesis, pencirian, dan sifat termofizikal bendalir maghemite nano telah dikaji dengan dan tanpa kesan medan magnet. Objektif kajian ini adalah untuk mensintesis zarah maghemite nano dan menjalankan pencirian dengan menggunakan pelbagai kaedah, menyediakan bendalir maghemite nano yang stabil, dan pengukuran ciri-ciri termofizikal bendalir maghemite nano dengan dan tanpa pengaruh medan magnetik luaran. Sintesis zarah maghemite nano dengan menggunakan kaedah co-pemendakan kimia. Kepekatan asid nitrik yang berbeza digunakan sebagai pembolehubah, kemudian penyediaan bendalir maghemite nano yang stabil yang dicirikan dengan mengukur keupayaan zeta dan "dynamic light scattering" pada pH dan masa simpanan yang berbeza. Akhirnya, pengukuran kekonduksian terma, kelikatan, dan kekonduksian elektrik bendalir maghemite nano pada pelbagai suhu, kepekatan zarah maghemite nano, dengan dan tanpa kekuatan medan magnetik luar. Hasil uji kaji menunjukkan superparamagnetik zarah maghemite dengan bentuk sfera dan kestabilan haba dan suspensi yang baik dan saiz dalam julat 9.3 – 14.7 nm telah berjaya dihasilkan. Bendalir maghemite nano yang stabil menunjukkan ia berada di keadaan asid dengan nilai keupayaan zeta 44.6 mV pada pH 3.6 dan pada keadaan bes dengan nilai keupayaan zeta -46.2 mV pada pH 10.5. Takat isoletrik pula di perolehi pada pH 6.7. Bendalir maghemite nano masih berada dalam keadaan stabil selepas lapan bulan. Kekonduksian terma bendalir maghemite nano adalah linear meningkat dengan peningkatan kepekatan zarah, suhu dan medan magnet. Kelikatan kinematik bendalir maghemite nano adalah meningkat dengan peningkatan kepekatan jumlah zarah dan medan magnet dan menurun dengan peningkatan suhu. Manakala, kekonduksian elektrik adalah meningkat dengan peningkatan kepekatan zarah, dan suhu dan tidak berkesan dengan medan magnet.

ACKNOWLEDGEMENTS

With deep regards and profound respect, I would like to express my sincere thanks and gratitude toward Prof. Dr. Mohd Rafie Johan and Prof. Dr. Iskandar Idris Yaacob for introducing the present research topic and for their inspiring guidance, constructive criticism, and valuable suggestion throughout this research work. It would have not been possible for me to bring out this thesis without their help and constant encouragement.

Special thanks to my colleague, Ms. Yusrini Marita, Mrs. Ang Bee Chin, Ms. Siti Hajar, Mrs. Fatihah, Mr. Shahadan Mohd Suan, Mrs. Aliya, Mrs. Yusliza, Ms. Syima Razali, Mrs. Asmalina, Mrs. Mariah and Ms. Nadia in sharing their knowledge and ideas with me. Besides that, sincerest appreciation goes to Faculty of Engineering, University of Malaya for providing all the facilities in the Mechanical Department and laboratories. Not forgetting also, the dedicated laboratory assistant Mr. Mohd Said Sakat, Mr. K. Kandasamy and Mr. Suhaimi, Mrs. Norzirah, and Ms. Aida Nur Izzaty for giving their full co-operation while using the equipments.

Last but not least, awards of thanks to my father Nurdin Abidin (alm), my mother, Nuriah Husin and lovely family members and my wife Mrs Nurliza Idris and my children Thariq Irza and Tsaqif Aufa Irza who give me full support in making this research work a success. Thanks for sharing my hard time.

Appreciate the efforts and contributions shared by individuals whose names are not mentioned above.

Thank you so much.

TABLE OF CONTENTS

LIST OF FIGURES

LIST OF TABLES

LIST OF SYMBOLS AND ABBREVIATIONS

Symbol or Abbreviations	Meaning	Unit (SI)
H	Magnetic fields strength	Tesla (T)
B	Magnetic induction	A/m
μ_o	Permeability of free space	4π x 10^{-7}
μ	Permeability of materials	-
μ_r	Relative permeability	-
M	Magnetization	Weber (Wb)
M_s	Saturation magnetization	emu/g
k_{nf}	Thermal conductivity of nanofluids	W/mK
k_{bf}	Thermal conductivity of base fluids	W/mK
k_p	Thermal conductivity of particle	W/mK
ϕ	Particle volume fraction	%
ψ	Particle sphericity	-
μ	Viscosity of suspensions	cst
μ_{bf}	Viscosity of base fluids	cst
μ_{nf}	Viscosity of nanofluids	cst
EDL	Electrical double layer	-
σ_m	Electrical conductivity	S/m
σ_o	Electrical conductivity of base fluids	S/m
α	Electrical conductivity ratio	-
XRD	X-Ray diffraction	-
TEM	Transmission electron spectroscopy	-
AGM	Alternating gradient magnetometer	-
TGA	Thermogravimetry analysis	-

DLS	Dynamic light scattering	-
m_p	Mass of particle	g
m_f	Mass of fluids	g
ρ_l	Density of fluids	g/mL
ρ_p	Density of particle	g/mL
T	Temperature	K
ξ	Zeta potential	mV
d	Diameter of particle	cm
D	Translational diffusion coefficient	

LIST OF APPENDICES

CHAPTER 1: INTRODUCTION

This chapter describes the background, objectives, scope and limitation and the significant research of study on synthesis, characterization, and thermophysical properties of maghemite nanofluids with and without magnetic field effects.

1.1 Background

Understanding and control of the synthesis and properties of engineered materials at scales similar to those of atoms and molecules is of utmost importance as this field of nanotechnology makes its progress in today's science. The uniqueness of the materials created by this technology arises from tailoring their structures at the atomic level, where chemical and physical properties differ from those observed in bulk materials. This visionary discipline is relevant across areas from textiles to medicine, energy, environmental, electronics, and catalytic applications. Most of the materials created within this field consist of small clusters of atoms or molecules. It called by nanoparticles which have the size in range of 1 to 100 nm.

Successful application of this technology not only depends on the special properties exhibited at this scale such as an enhanced electronic, mechanical, physical and chemical response but also on their manipulation to achieve specific objectives. In this sense, magnetic nanoparticles offer a range of opportunities as their response can be tailored by choosing from a variety of magnetic materials with different magnetic properties. They can be manipulated by the use of external magnetic fields and by modification of their surfaces with molecules specific for intended applications. They have received much attention recently because of their unique characteristics. Iron oxide nanoparticles mainly magnetite and maghemite are promising magnetic materials that are intensively explored due to their magnetic properties.

They are used in a wide sort of applications including electronic packaging, mechanical engineering, aerospace, and bioengineering (Abareshi et al., 2010). Suspension of magnetic nanoparticles in aqueous medium creates a new class of liquid called "magnetic fluid." With using external magnetic fields, the flow and energy transport processes of magnetic fluids can be controlled. Hence, the magnetic fluids can be used effectively in thermal engineering applications (Li & Xuan, 2009).

Most of these applications require the magnetic nanoparticles to be uniform in size, shape, and well dispersed in a solvent (Oh & Park, 2011). The stability of the suspension is the most important parameter in the application of magnetic nanoparticles suspensions.

Challenges arise each day as these nanoparticles find their way to emerging technologies. Understanding of their chemical stability, dispersion in different media, particle-particle interactions, surface chemistry and magnetic response are fundamentally for successful implementation. Thus, the need for synthesis techniques that produce magnetic nanoparticles with a controlled size and size distribution and methods of surface modification that can be used to gain insight into the fundamental aspects that govern the exciting properties exhibited by these particles and that make them attractive for a wide range of applications.

Various methods have been reported on the synthesis of magnetic nanoparticles. They included chemical co-precipitation (Bee et al., 1995; Casula et al., 2011; Schwegmann et al., 2010), sol-gel synthesis (Hsieh et al., 2009; Xu et al., 2007), microemulsion (Chin & Yaacob, 2007; Maleki et al., 2012; Vidal-Vidal et al., 2006), thermal decomposition (Asuha et al., 2011Peng et al., 2006), and hydrothermal (Caparrós et al., 2012; Hui Zhang & Zhu, 2012). The simplest and common technique is co-precipitation (Behdadfar et al., 2012; Odenbach, 2004). Most researchers have reported synthesis of magnetite nanoparticles rather than maghemite nanoparticles.

The significant feature of magnetic fluids is their superparamagnetic properties. Meanwhile, the significance of superparamagnetism is that the magnetic flux can be enhanced due to rotation of single domain magnetic particle in the magnetic fields rapidly. When the external magnetic field is removed, there is no net magnetism. Hence, the interaction of magnetic fluids with external magnetic fields leads to various interesting phenomena. The flow and behavior of magnetic fluids can be controlled by external magnetic field for particular applications (Odenbach, 2003).

Particularly, a possibility to induce and control the heat transfer process and fluid flow by means of an external magnetic field opened a window to a spectrum of promising applications. It included magnetically controlled thermosyphon for technological purposes, enhancement of heat transfer for cooling of high-power electric transformers, and magnetically controlled heat transfer in energy conversion systems (Blums, 2002). Other applications like magnetic resonance imaging media, and adsorbent environmental use. Recent investigations have shown that the presence of the nanoparticles in thermosyphons and heat pipes cause a significant enhancement of their thermal characteristics (Goshayeshi et al.; Huminic et al., 2011; Yarahmadi et al., 2015; Župan & Renjo, 2015).

Thus, in such applications, the properties of these magnetic fluids and the effect of external magnetic fields are important issues. These applications require thermophysical properties data such as thermal conductivity and viscosity for increasing the efficiency of cooling and reduce pumping power in the system (Alsaady et al., 2015).

1.2 Problem Statement

Magnetic nanoparticles have been attracted many investigators in recent years due to their unique characteristics. Iron oxide nanoparticles particularly magnetite (Fe_3O_4) and maghemite (γ-Fe_2O_3) are promising magnetic materials that are intensively explored due to their unique magnetic properties. Suspended magnetic nanoparticles in solvent creates

new class of liquids called “magnetic fluids”. These smart materials are unique because of their superparamagnetic property. The movement and energy transport of magnetic fluids can be controlled using external magnetic fields. Hence, the magnetic fluids can be used effectively in thermal engineering applications.

Although many investigations of magnetic nanofluids have been done, there are only focused on magnetite nanoparticles, lacks of data regarding maghemite nanoparticles and their thermophysical measurements in the literatures (Abbas et al., 2015; Ali et al., 2015; Ramimoghadam et al., 2015; Yamaguchi et al., 2010).

1.3 Research Objectives

The main objective of this study is to synthesize maghemite nanoparticles using a chemical co-precipitation method and preparation of maghemite nanofluids and measurement of their thermophysical properties. The specific objectives are:

1. To synthesize maghemite nanoparticles using chemical co-precipitation method and characterize the physical, structural, thermal stability and magnetic properties of the maghemite nanoparticles.
2. To study the effect of pH and time on the stability of the maghemite nanofluids.
3. To determine the effect of particle volume fraction on thermal conductivity, kinematic viscosity, and electrical conductivity of maghemite nanofluids.
4. To determine the effect of temperature on thermal conductivity, kinematic viscosity, and electrical conductivity of maghemite nanofluids.
5. To determine the effect of parallel and perpendicular arrangement of magnetic fields on thermal conductivity, kinematic viscosity, and electrical conductivity of maghemite nanofluids.

1.4 Research Scope and Limitation

Synthesis and stability of maghemite nanofluids play a significant role in utilization of these smart materials. Several characterization methods were performed for maghemite

nanoparticles and their suspensions to analyze the properties of samples. Thermophysical data were measured with and without the effect of magnetic fields.

This investigation was conducted on synthesize, characterize and measure thermophysical properties of maghemite nanofluids with and without the effect of magnetic fields. The synthesis of maghemite nanoparticles has been conducted by co-precipitation methods at different nitric acid concentrations. The stability of maghemite nanofluids is studied at different pHs and time of storage. While thermophysical properties were conducted at different particle volume fraction, temperature, and magnetic fields strength.

1.5 Significance of Research

Maghemite nanofluids have been using in various applications including electronic, mechanical engineering, aerospace, environmental, and bioengineering due to their unique characteristics. By applying external magnetic fields, the flow of maghemite nanofluids and energy transport processes can be controlled. Therefore, maghemite nanofluids can be utilized effectively in thermal engineering applications. The stability of maghemite nanofluids and their thermophysical properties play important role in the applications of this nanofluids. Hence, the results of this study will contribute to the available data of the applications of maghemite nanofluids.

1.6 Thesis Organization

This thesis consists of five chapters. Chapter 1 is an introduction consist of research background, objectives, and the limitations of the conducted studies. Chapter 2 is literature review containing previous works done by other investigators and the relevant literature supporting the present research. The methodology of research includes the methods and procedures for preparation and characterization of maghemite nanofluids

discussed in chapter 3. Results and discussion presented in Chapter 4, conclusions, and recommendations in Chapter 5.

CHAPTER 2: LITERATURE REVIEW

This chapter describes the relevant details in synthesis, characterization, and thermophysical properties of maghemite nanofluids with and without the effect of magnetic fields.

2.1 Nanofluids

Nanofluids is a new class of engineering material consisting of solid nanoparticles with sizes smaller than 100 nm suspended in a base fluid. It provides useful applications in industrial fluids system, including as heat transfer fluids, magnetic fluids, and lubricant fluids (Hwang et al., 2008).

2.1.1 Fundamental of Nanofluids

The concept of nanofluids was first coined by Choi (1995) at Argonne National Laboratory. It interested many investigators due to a dramatic enhancement of heat transfer (Masuda et al., 1993), and mass transfer (Krishnamurthy et al., 2006). Metals in solid form have orders-of-magnitude higher thermal conductivities than those of fluids at room temperature (Kováčik et al., 2015; Ramirez-Rico et al., 2016; Touloukian et al., 1970). For instance, the thermal conductivity of copper is around seven hundred times larger than that of water and about three thousand times bigger than that of engine oil at room temperature, as shown in Table 2.1. The thermal conductivity of metallic liquids is substantially greater than that of nonmetallic liquids. Therefore, the thermal conductivities of metallic fluids could be estimated to be significantly larger than those of conventional heat transfer fluids.

Since then, nanofluids has attracted attention as a new generation of heat transfer fluids with a superior enhancement of heat transfer performance. These fluids obtained by a stable colloidal suspension of a low volume fraction of ultrafine solid particles in nano metric dimension. It dispersed in conventional heat transfer fluid such as water, ethylene

glycol, or propylene glycol to enhance or improve its rheological, mechanical, optical, and thermal properties.

Several researchers found that the thermal conductivity of these fluids significantly increased when compared to the same fluids without nanoparticles. Since the thermal conductivity of solids ordered of magnitude greater than that of liquids, dispersion of solid particles in liquids is assured to increase its thermal conductivity.

Fluids are essential for heat transfer in many engineering types of equipment. Conventional heat transfers fluids, such as, water, oil and ethylene glycol mixture have a significant limitation in improving the performance and compactness of this manufacturing equipment due to the low thermal conductivity. Dispersion of a small volume (<1%) fraction of solid nanoparticles in conventional base fluid drastically increases the thermal conductivity than that of base fluid (Azmi et al., 2016; Chopkar et al., 2006; Chopkar et al., 2007; İlhan et al., 2016).

Table 2.1: Thermal conductivity of various materials at 300 K (Das et al., 2008)

	Materials	Thermal Conductivity (W/mK)
Metallic Solids	Silver	429
	Copper	401
	Aluminum	237
Nonmetallic Solids	Diamonds	3300
	Carbon Nanotube	3000
	Silicon	148
	Alumina	40
Metallic Liquids	Sodium at 644 K	72.3
Non Metallic Liquids	Water	0.613
	Engine Oil	0.145
	Ethylene Glycol	0.253

2.1.2 Impact and Potential Benefit of Nanofluids

The technology of nanofluids is expected to be unlimited potential considering that heat transfer performance of heat exchangers or cooling devices is vital in numerous industries by increasing thermal transport of coolants and lubricants. Hence, it can reduce the dimension and load of thermal management systems vehicle in the transportation industry. Nanofluids offer anomalously great thermal conductivity and numerous benefit (Choi, 1998; Choi et al., 2004; Eggers & Kabelac, 2016; Nitsas & Koronaki, 2016; Zussman, 1997). These advantages include:

2.1.2.1 Improved heat transfers and stability

Heat transfer occasionally takes place at the surface of the particles; it is desirable to use larger surface area particles. The relatively bigger surface areas of nanoparticles compared to microparticles provide significantly improved heat transfer capabilities. Besides, particles finer than 20 nm carry 20% of their atoms on their surface, making them directly available for thermal interaction (Choi et al., 2004). With such ultra-fine particles, nanofluids can flow smoothly in the tiniest of channels such as mini- or micro-channels. It is because the nanoparticles are small, gravity becomes less necessary, and thus chances of sedimentation are less, making nanofluids more stable (Babita et al., 2016; Raja et al., 2016).

2.1.2.2 Microchannel cooling without clogging

Since the high heat loads encountered in the recent application, the utilization of nanofluids become necessary. The nanofluids will be a superior medium for heat transfer in general especially ideal for microchannel applications (Vafaei & Wen, 2014; G. Zhao et al., 2016). The arrangement of microchannels and nanofluids will provide both highly conducting fluids and a large heat transfer area. This condition cannot be attained with macro- or micro-particles because they clog microchannels.

2.1.2.3 Miniaturized systems

Nanofluids technology will support the modern industrial trend toward miniaturing component and system. It will also reduce the design of smaller and lighter heat exchanger systems. Miniaturized systems will decrease the inventory of heat transfer fluid and will result in cost savings.

2.1.2.4 Reduction in pumping power

Improving conventional fluids heat transfer by a factor of two, the pumping power of fluids usually must be increased by a factor of 10. The heat transfer was doubled when the thermal conductivity increased by a factor of three in the same apparatus (Choi, 1995). The improving of the pumping power will be very moderate unless there is a sharp increase in fluid viscosity.

2.1.2.5 Cost and energy savings

The utilization of nanofluids as heat transfer fluids, heat exchanger system can be made smaller and lighter. Hence, it will result in significant energy and cost savings. Stable nanofluids will avoid rapid sedimentation and diminish clogging in the tube walls of heat transfer devices. The greater thermal conductivity of nanofluids translates into higher energy efficiency, better performance and lower operating costs. They can reduce energy consumption by pumping heat transfer fluids. Less inventories of fluids are consumed in miniaturized systems where nanofluids is used. Thermal systems can be smaller and lighter. Smaller components result in improve gasoline mileage, fuel savings, lower emissions, and a cleaner environment in vehicles (Choi et al., 2002).

2.1.3 Potential Applications of Nanofluids

The transport of heat in the nanofluids is a significant parameter in nanotechnology applications (Kim et al., 2001). It is important to learn and control the heat transport at nanoscale dimensions, which without a doubt will open ways to improve new applications. With those mentioned above highly desired thermal properties and potential

benefits, nanofluids can be seen to have a broad sort range of industrial and medical applications.

2.1.3.1 Engineering applications

Nanofluids can be used to improve thermal management systems in many engineering applications including:

(a) **Nanofluids in transportation**

The transportation industry has a high demand to improve the performance of vehicle heat transfer fluids and enhancement in cooling technologies is desired. Because engine coolants, engine oils, automatic transmission fluids, and other synthetic high-temperature fluids possess inherently inadequate heat transfer capabilities, they could profit from the high thermal conductivity offered by nanofluids. The utilization of nanofluids makes the engines, pumps, radiators, and other components will be lighter and smaller.

Lighter vehicles could travel further with the same amount of fuel i.e. more mileage per liter. More energy-efficient vehicles would save money. Moreover, burning less fuel would result in lower emissions and thus reduce environment pollution. Therefore, in transportation systems, nanofluids can contribute substantially. An ethylene glycol and water mixture usually used for the automotive coolant has relatively low heat transfer fluid and engine oils perform even worse as a heat transfer medium.

The addition of nanoparticles to the standard engine coolant influence the automotive and heavy-duty machine cooling rates. The utilization of nanofluids as a heat transfer media reduce the size of the cooling system. It makes cooling system smaller and lighter. Smaller cooling systems lead to smaller and lighter radiators, which improve car and truck performance and lead to saving fuel economy.

Alternatively, more heat from higher horsepower engines with the same size of the coolant system can be removed by improving the cooling rate. The nanofluids also have a high boiling point, which is desirable for maintaining single-phase coolant flow.

Besides, a normal coolant operating temperature can be enhanced by a higher boiling point of nanofluids and can be used to reject more heat through the existing coolant system. More heat rejection allows a variety of design enhancements, including engines with higher horsepower.

(b) **Micromechanics and instrumentation**

Since 1960s, miniaturization has been a major trend in science and technology. Microelectromechanical systems (MEMS) generate a lot of heat during operation. Conventional coolants do not work well with high power MEMS because they do not have enough cooling capability. Moreover, even if large-sized solid particles were added to conventional coolants to enhance their thermal conductivity, they still could not be applied in practical cooling systems. This because the particles would be too big to flow smoothly in the extremely narrow cooling channels required by MEMS. Nanofluids would be suitable for coolants because they can flow in microchannels without clogging. They could enhance cooling of MEMS under extreme heat flux conditions.

(c) **Heating, ventilating and air-conditioning (HVAC) systems**

The application of nanofluids would save energy in heating, ventilating, and air conditioning system. Moreover, it also increases energy efficiency which gives potential utilization in building without increased pumping power. Nanofluids could improve heat transfer capabilities of current industrial HVAC and refrigeration systems. Many innovative concepts are being considered; one involves pumping of coolant from one location where the refrigeration unit is housed in another area. The nanofluid technology could make the process more energy efficient and profitable.

(d) **Electronics Cooling**

The energy density of integrated circuits and microprocessors has increased dramatically in recent years. Future high-performance computers and server's processors

have been projected to dissipate higher power, in the number of one hundred to three hundred W/cm^2. Whether these values become the truth is not as significant as the projection that the general trend in higher energy density of electronics processors will continue. Existing air-cooling procedures for removing this heat are approaching their limits, and liquid cooling technologies are increasingly being and have already been, developed for replacing them. Single-phase fluids, two-phase fluids, and nanofluids are candidate replacements for air. They have increased heat transfer capabilities of air systems, and all are being investigated.

(e) **Space and Defense**

Some military devices and systems involve high-heat-flux refrigerating to the level of tens of MW/m^2. Cooling with conventional fluids is challenging at this level. Cooling of power electronics and directed-energy weapons is one of an example of military application. Providing suitable cooling and the associated power electronic is a critical need. Nanofluids have the potential to provide the required cooling in such applications including in other military systems. Reducing transformer size and weight is important to the Navy as well as the power generation industry. The substitution of conventional transformer oil with nanofluids is a potential alternative in many cases. Such replacement represents considerable cost savings. The using nanoparticle additives in transformer oils, the heat transfer of transformer oils can significantly improve. Recent experiments showed some promising nanofluids with surprising properties. Such as fluids with advanced heat transfer, drag reduction, binders for sand consolidation, gels, products for wettability alteration, and anticorrosive coatings (Chaudhury, 2003; Wasan & Nikolov, 2003).

Nanofluids coolants also have potential application in major process industries, such as materials, chemical, food and drink, oil and gas, paper and printing, and textiles.

2.1.3.2 Medical applications

Nanofluids and nanoparticles have many utilizations in the biomedical industry. For example, iron-based nanoparticles could be used as a delivery agent for drugs or radiation without damaging nearby healthy tissue to avoid some side effects of conventional cancer treatment methods. Such particles could be directed in the bloodstream to a tumor using external magnetic fields to the body. Nanofluids could also be utilized for safer surgery by producing efficient cooling around the surgical region and thereby improving the patient's chance of survival and generating the risk of organ destruction. In an opposing application to cooling, nanofluids could produce a higher temperature around tumors to kill cancerous cells without affecting nearby healthy cells. Magnetic nanoparticles in body fluids (biofluids) can be used as delivery vehicles for drugs or radiation, providing new cancer treatment techniques. Due to their surface properties, nanoparticles are more adhesive to tumor cells than normal cells. Thus, magnetic nanoparticles excited by an AC magnetic field are promising for cancer therapy. The combined effect of radiation and hyperthermia is due to the heat-induced malfunction of the repair process right after radiation-induced DNA damage. Therefore, in future nanofluids can be used as advanced drug delivery fluids. Nanofluids could be used to cool the brain, so it requires less oxygen and thereby improve the patient's chance of survival and decrease the risk of brain destruction during a critical surgery.

2.2 Synthesis of Magnetic Nanoparticles

Numerous methods are known for synthesis of magnetic nanoparticles including physical and chemical methods. Several methods have been employed for synthesis of magnetic nanoparticles, such as chemical co-precipitation (Bee et al., 1995), microemulsion (Chin & Yaacob, 2007; Vidal-Vidal et al., 2006); sol-gel method (Xu et al., 2007), chemical vapor deposition, thermal decomposition (Asuha et al., 2011).

The most convenient way to synthesize iron oxides (either Fe_3O_4 or γ-Fe_2O_3) from aqueous Fe^{2+}/Fe^{3+} salt solutions is a chemical co-precipitation method (Charles, 2002). The size, shape, and composition of the magnetic nanoparticles depend on the type of salts used (e.g. chlorides, sulfates, nitrates). It also depends on the ratio of Fe^{2+}/Fe^{3+}, the reaction temperature, the pH value, and ionic strength of the media. This method has been used extensively to produce magnetic nanoparticles of controlled sizes and magnetic properties in recent years. Several processes have been developed to accomplish this goal. In general, these techniques start with a mixture of $FeCl_2$ and $FeCl_3$ and water. Co-precipitation arises with the addition of ammonium hydroxide and then the system is exposed to dissimilar procedures to peptization, magnetic separation, filtration, and dilution (Cabuil et al., 1993; Massart, 1981).

The procedure involves reactions in aqueous or non-aqueous solutions containing soluble or suspended salts. The precipitate is formed when the solution becomes supersaturated with the product. The formation of nuclei after formation usually proceeds by diffusion. In any case, concentration gradients and reaction temperatures are very crucial parameters in determining the growth rate of the particles, e.g. to form monodispersed particles. All the nuclei should be formed at nearly the same time to prepare un-agglomerated particles with a very narrow size distribution. Moreover, subsequent growth must occur without further nucleation or agglomeration of the particles.

Particle size and particle size distribution, physical properties such as crystallinity and crystal structure, and degree of dispersion can be affected by reaction kinetics (Nalwa, 2001). Moreover, the concentration of reactants, reaction temperature, pH and the order of addition of reactants to the solution are very crucial aspects. Even though a multi-element material is often prepared by co-precipitation of batched ions, it is not always easy to co-precipitate all the desired ions simultaneously as different species may only

precipitate at different pHs. Hence, control of chemical homogeneity and the stoichiometry requires a very precise control of reaction conditions (Nalwa, 2001).

The major advantage of chemical synthesis is its versatility in designing and synthesizing new materials that can be refined into the final product. The principal merit that chemical processes offer over physical methods, as chemical synthesis offers to mix at the molecular level is excellent chemical homogeneity. Understanding how matter is gathered on an atomic and molecular level and the consequent effect on the desired material macroscopic properties can be designed by molecular chemistry. An essential understanding of the principles of crystal chemistry, thermodynamics, phase equilibrium, and reaction kinetics becomes necessary to take advantage of the many benefits that chemical processing has to offer. However, there are certain hurdles in chemical processing. In some synthesis, the chemistry is very hazardous and complex. Contamination may also result from by-products being generated or side reactions in the chemical process. It ought to be minimized to obtain preferred properties in the final product. Agglomeration can also be a major drawback in any phase of the synthetic process, and it can terribly alter the properties of the materials

An interesting feature of co-precipitation method is that the product will contain some amount of associated water even after heating in an alkaline solution for an extended period. The rate of mixing of reagents plays a vital role in the size of the resultant particles. Co-precipitation comprises two processes: nucleation i.e. formation of centers of crystallization followed by growth of particles. Relative rates of these two processes decide the size and polydispersity of precipitated particles. Polydispersed colloids are obtained because of a simultaneous formation of new nuclei and growth of the earlier formed particles. A less dispersed in size colloid is made when the rate of nucleation is high, and the rate of particles growth is weak. This situation relates to a rapid addition and a vigorous mixing of reagents in the reaction.

Slow addition of reagents in the co-precipitation reaction leads to the formation of bigger nuclei than rapid addition. Also, in the case of slow addition of base to a solution of metal salts a separate precipitation takes place due to different pH of precipitation for various metals. Mixed precipitation may increase chemical inhomogeneity in the particles. The mixing of reagents must be accomplished as rapid as possible to obtain smaller size ferrite particles and more chemically homogeneous.

Preparation of magnetic nanoparticle solutions requires the magnetic nanoparticle synthesis and then the formation of a stable colloidal solution. Magnetic nanoparticles must be chemically stable in the liquid carrier and have a convenient size to deliver colloidally stable magnetic fluid.

2.3 Application of Maghemite Nanoparticles

Iron oxide nanoparticles offer broad applications in chemical and biological fields, engineering, and environment applications due to their nanometer size and superparamagnetic property. They are used in comprehensive application especially in magnetic resonance imaging, magnetic separation, nanocatalysis, thermal, and environment applications.

2.3.1 Magnetic Resonance Imaging

Magnetic resonance imaging has become a respected non-invasive diagnostic technique to visualize the structure and function of the body, especially for soft tissues (e.g., brain, liver) since the 1980's (Song et al., 2015) . The image created by MRI usually based on the intrinsic contrast provided by the proton density and spin relaxation that vary throughout the sample. However, MRI suffers from the relative low sensitivity that limits its utility when relying solely upon these inherent contrast mechanisms (Cuny et al., 2015). Exogenous MRI contrast agents have been developed to improve the image resolution and precision in the past twenty years.

Superparamagnetic iron oxide nanoparticles play an important role as MRI contrast agents, to better differentiate healthy and pathological tissues. Recent developments in MR imaging have enabled in vivo imaging at near microscopic resolution (Huang et al., 2010; Blasiak et al., 2013; Johnson et al., 1993; Thomas et al., 2013). It is necessary to tag cells magnetically to visualize and track stem and progenitor cells by MR imaging.

2.3.2 Magnetic Separation

Magnetically susceptible material can be extracted from a mixture by using magnetic separation method. This separation procedure can be useful in mining iron as it is attracted to a magnet.

Magnetic separation is a straightforward application of magnetic nanoparticles. This simple technique, however, has several attractive features in comparison with traditional separation procedures. The whole separation and purification process can be done in one test tube without filtrations or more expensive liquid chromatography systems. In biomedical research and diagnosis, disengagement and accumulation of specific biological entities of interest (e.g., cells, proteins) from biological fluids is often required because of their low concentration and the complexity of sample fluids (Shao et al., 2012). Magnetic nanoparticles offer a unique platform to enrich the target analytes onto the surfaces by the nonspecific adsorption or specific interaction between substrates and ligands on the particle surfaces. Applying an external magnetic field will allow facile separation of target analytes from the solution.

Superconducting magnetic separation is also used in wastewater treatment particularly for chemical oxygen demand (COD) removal (Hao Zhang et al., 2011) and removal phosphate from wastewater (Y. Zhao et al., 2012).

Magnetic separation performed in many fields and industries. The primary usage is to separate magnetic materials from nonmagnetic materials or materials with high magnetic fields from materials with low magnetic fields. This method is suitable for separating

crushed ore at numerous stages of the mining, production of iron, mineral processing, and metallurgy industries. It also used to remove materials with magnetic properties in the processing of food.

Magnetic separation is also used in microbiology where new techniques are being developed on a regular basis. Several applications include diagnostic microbiology, isolating rare cells, studying nano cells in biological processes.

Several researchers have conducted study in this fields (Herrmann et al., 2015; Kim et al., 2011; Kläser et al., 2015; Magnet et al., 2015; Yavuz et al., 2009).

2.3.3 Nanocatalysis

Magnetic nanoparticles have the potential use as a catalyst or catalyst support (Galindo et al., 2012). In chemistry, a catalyst support is a material with a high surface area, to which a catalyst affixed. Efforts have been made to maximize the surface area of a catalyst by distributing it over the support in which the reactivity of heterogeneous catalysts occurs. The support may be inert or contribute to the catalytic reactions. Typical supports include several kinds of carbon, alumina, and silica.

Homogeneous catalysts have found numerous applications in both laboratory research and industrial production. However, there is not a simple solution so far to the recycling of homogeneous catalysts. The attachment of homogenous catalysts onto iron oxide nanoparticles is becoming a promising strategy to bridge the gap between homogeneous and heterogeneous catalyses. The magnetic nanoparticle-catalyst systems could possess the advantages of both homogeneous and heterogeneous catalyses. (Rossi et al., 2013; Shin et al., 2009; Varma, 2014)

2.3.4 Thermal Engineering

Numerous applications have been developed since magnetic fluids (ferrofluids) have first been produced in the early 60s. Since then fundamental research involves the study

of its physical properties, such as supermagnetism, magnetic dipolar interaction, and single electron transfer. Magnetic control of a fluid enables the design of applications in numerous fields of technology and thousands of patents for ferrofluid applications have been approved. The most common commercial use of ferrofluids is the cooling of loudspeakers (Odenbach & Thurm, 2002).

Ferrofluid is filled into the gap of the permanent magnet of the loudspeaker. It is placed around the voice coil, which increases the thermal conductivity of this region. It is known that well-designed ferrofluids are five times more thermally conductive than air. The ohmic heat produced in the voice coil can be transferred to the outer structure by the fluid and enhances the cooling process. This result in an increase in the cooling heat transfer process and improves the system efficiency.

Ferrofluids also are used to obtain mechanical resistance, which prevents damping problems. Other applications are possible in sealing technology by bringing a drop of ferrofluid into the gap between a magnet and a high permeable rotating shaft. In the small gap, a strong magnetic field will fix the ferrofluid, and pressure differences of about 1 bar can be sealed without serious difficulties (Schinteie et al., 2013; Sekine et al., 2003).

Thermomagnetic convection cooling is one of the thermal applications of magnetic nanofluids. The application of external magnetic field on magnetic fluids with varying susceptibilities give a non-uniform magnetic body force which leads to the thermomagnetic behavior. Recent development of thermomagnetic cooling devices is mainly motivated by their great potential application for small scale cooling devices such as in miniature micro-scale electronic devices (Li et al., 2008; Xuan & Lian, 2011; Zablotsky et al., 2009).

A recent study regarding the thermal engineering applications of magnetic nanoparticles have been conducted (Carp et al., 2011; Dibaji et al., 2013; Nikitin et al., 2007).

2.3.5 Environmental

Among the many applications of nanotechnology that have environmental effects, remediation of polluted groundwater with zero-valent iron nanoparticles is one of the most prominent cases (Gonçalves, 2016; Tsakiroglou et al., 2016). However, the applications for optimal performance or to assess the risk to human or ecological health still challenging due to many uncertainties concerning the essential features of this technology. This important aspect of nanoparticles needs extensive considerations as well.

Magnetic nanoparticles have an enormous surface area and can be separated by applying a magnetic field. Because of the vast surface to volume ratio, magnetic nanoparticles have a real potential for treatment of contaminated water. In this technique, attachment of EDTA-like chelators to carbon-coated metal nanomagnets effect in a magnetic reagent for the fast removal of heavy metals from solutions or contaminated water. It can be eliminated by three orders of magnitude at concentrations as low as micrograms per litre.

Air pollution is another potential area where nanotechnology has great promise. Filtration techniques similar to the water purification methods described above could be used in buildings to purify indoor air volumes. Nanofilters could be applied to automobile tailpipes and factory smokestacks to separate out contaminants and prevent them from entering the atmosphere.

Environmental remediation includes the degradation, sequestration, or other related approaches that result in reduced risks to human and environmental receptors posed by chemical and radiological contaminants. The benefits, which arise from the application of nanomaterials for remediation, would be more rapid or cost-effective cleanup of wastes.

Nanoparticles could provide very high flexibility for both in situ and ex situ remediations. For example, nanoparticles are easily deployed in ex situ slurry reactors for the treatment of contaminated soils, sediments, and solid wastes. Alternatively, they can be anchored onto a solid matrix such as carbon, zeolite, or membrane for enhanced treatment of water, wastewater, or gaseous process streams. Direct subsurface injection of nanoscale iron particles, whether under gravity-feed or pressurized conditions, has already been shown to effectively degrade chlorinated organics such as trichloroethylene, to environmentally benign compounds.

2.4 Magnetism and Magnetic Properties of Nanoparticles

An understanding of fundamentals of magnetism is required to study the magnetic behavior of materials. It is known that certain materials attract or repel each other depending on their relative orientation. In fact, all materials display some magnetic response to magnets; however, in many cases, the forces involved are exceptionally small.

It is known that there is a connection between magnetic forces and electric currents. Magnetism originates from the movement of electronic charges. Those charges behave as pairs of equal magnitude and opposite sign. A couple of these charges is referred as a dipole. The magnetic force is related from one charge to another through a magnetic field. In a bar magnet, the magnetic force lines flow around the dipole from north to south as shown in Fig. 2.1.

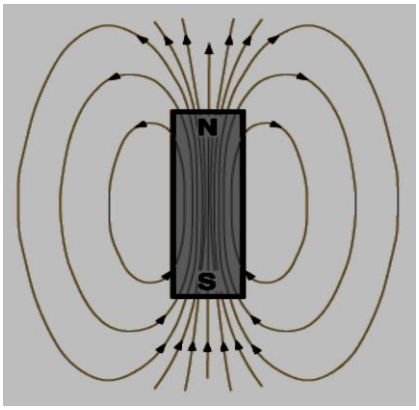

Figure 2.1: Magnetic field lines in a magnet bar (http://hyperphysics.phy-astr.gsu.edu/hbase/magnetic/elemag.html).

There are several relevant parameters related to magnetic materials. The magnetic field strength (H) is a vector that measures the force acting on a unit pole. Magnetic flux density and magnetic induction (B) is the net magnetic response of the material to an applied field (H). It is measured in Tesla (T) in SI units and Gauss (G) in cgs units. If μ_o is defined as the permeability of free space, then the relation of induction and magnetic field strength can be related in vacuum and presented by the equation 2.1 (White, 2012).

$$B = \mu_o H \tag{2.1}$$

If a material is placed in the magnetic field than the relation is similar to,

$$B = \mu \times H \tag{2.2}$$

where: μ is the permeability of that material. Therefore, if a material whose magnetization is M is placed in the magnetic field, the relationship can be defined as:

$$B = \mu \times H = \mu_o (H + M) \tag{2.3}$$

The unit of M is same as magnetic field strength, Am^{-1}. In the Equation (2.3), the term μ_o M represents the additional magnetic induction field associated with the material. The relative permeability, μr of a material is defined as:

$$\mu_r = \mu/\mu_o \tag{2.4}$$

An electromagnet is a type of magnet in which the magnet field is produced by the flow of electric current. When the electric current is off, the magnetic fields disappear. They are commonly used as modules of electrical devices, such as motors, generators, relays, loudspeakers, hard disks, MRI machines, scientific instruments, and magnetic separation equipment. It also being employed as industrial lifting electromagnets for picking up and moving heavy iron objects like scrap iron.

A magnetic field nearby the wire is created by electric current. The wire is wounded by a coil with many turns to focus the magnetic fields in an electromagnet. The magnetic field of wire passes through the center of the coil, making a strong magnetic field. A shape of a straight tube coil (a helix) is called a selenoid. Stronger magnetic fields can be created

if the wire is wounded on a ferromagnetic material, such as soft iron, due to the high magnetic permeability μ of the ferromagnetic material. This assembly is called a ferromagnetic core or iron core electromagnet.

The path of the magnetic field through a coil of wire can be found from a form of the right-hand rule. If the fingers of the right hand are curled around the coil in the direction of current flow (conventional current, flow of positive charge) through the windings, the thumb points in the direction of the field inside the coil. The side of the magnet that the field lines emerge from is defined to be the North Pole (https://www.boundless.com/physics/textbooks/boundless-physics-textbook/magnetism-21/magnets-156/ferromagnets-and-electromagnets-551-6041/).

The great benefit of an electromagnet over a permanent magnet is that the magnetic field can be promptly manipulated over a wide range by controlling the amount of electric current. However, a continuous supply of electrical energy is required to maintain the field.

Many researchers are a focus on nanoparticles and one-dimensional nanostructures in recent years because these materials exhibit unique properties, which cannot be achieved by their bulk counterparts. Magnetic nanoparticles are an important class of functional nanomaterials, which possess unique magnetic properties.

Some basic material properties change significantly, as overall size decreases from bulk to nanosize. Magnetism is one such property. Typically, macroscopic magnetic materials are separated into domains or sections where magnetic spins are cooperatively oriented in the same direction. In the existence of an external magnetic field, these domain spins will tend to align with that field producing an overall magnetic moment.

When single domain particles are subjected to an external magnetic field, the magnetic particle moments align with the field. If there is complete randomization of the

orientations of the particle's magnetic moments when the applied magnetic field is removed, the material is considered superparamagnetic as shown in Fig. 2.2.

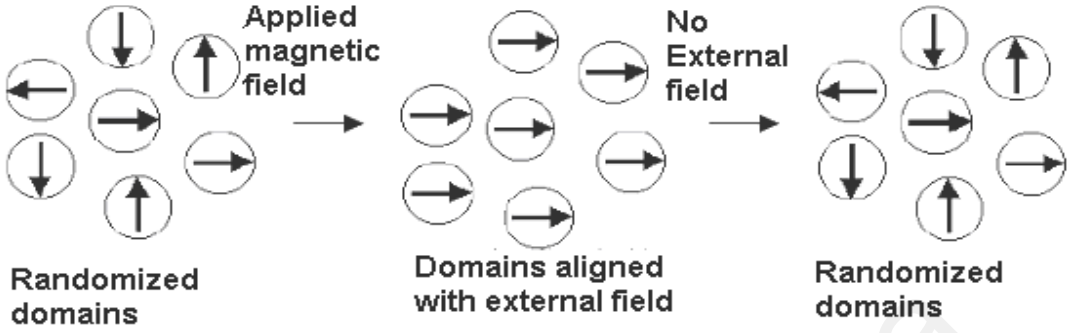

Figure 2.2: Behavior of superparamagnetic particles with and without the presence of an applied external magnetic field.

The magnetic properties of maghemite nanoparticles are studied using hysteresis loops. The magnetic moment, saturation magnetization, coercivity, and initial permeability are important parameters to consider in the investigation.

The magnetic properties of materials can be learned by studying its hysteresis loop. A hysteresis loop shows the relationship between the changes of magnetic moment (M) over the strength of an applied magnetic field (H). It is often stated to as the B-H loop or M-H loop. An example hysteresis loop is shown in Fig. 2.3.

The loop is produced by measuring the magnetic flux of a ferromagnetic material while the magnetizing force is applied. A ferromagnetic material that has never been previously magnetized or has been thoroughly demagnetized will follow the dashed line as H is increased. As the line demonstrates, the greater the amount of current applied (H+), the stronger the magnetic field in the component (M+). At point "a" almost entirely of the magnetic domains are aligned. An additional increase in the magnetizing force will produce a very little increase in magnetic flux and the material has reached the point of magnetic saturation (Ms). When H reduced to zero, the curve will move from point "a" to point "b" where some magnetic flux remains in the material even though the magnetizing force is zero. This point is referred to as the point of retentivity on the graph

and indicates the remanent or level of residual magnetism in the material (remanent magnetic moment, Mr). Some of the magnetic domains remain aligned while some have lost their alignment. As the magnetizing force reversed, the curve moves to point "c", where the flux has been reduced to zero. This point is called the point of coercivity on the curve. The reversed magnetizing force has flipped enough of the domains so that the remaining flux within the material is zero. The force required to eliminate the residual magnetism from the material is called the coercive force or coercivity of the material.

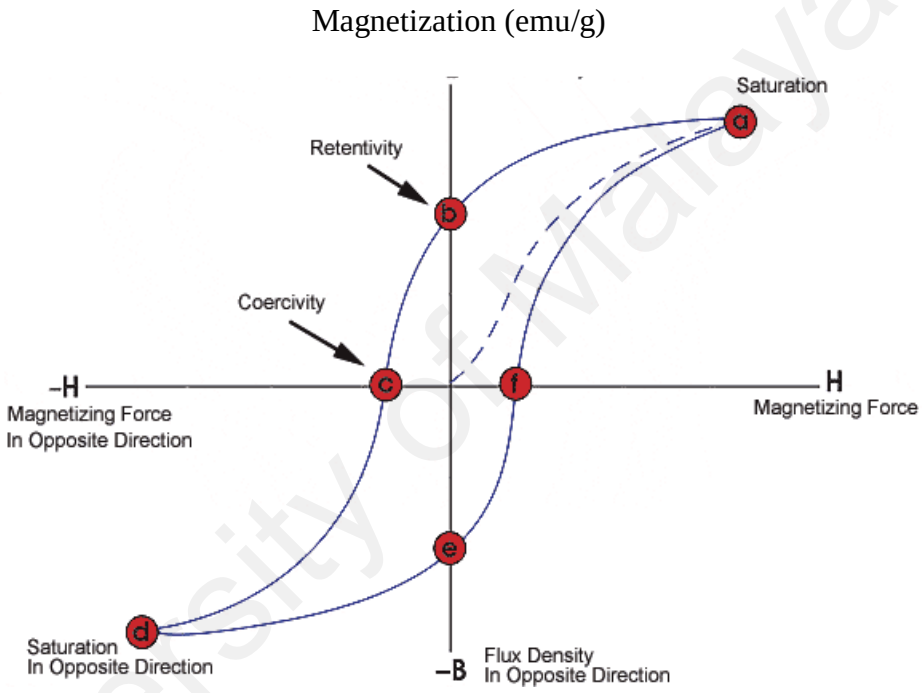

Figure 2.3: Magnetization Curve

As the magnetizing force is enhanced in the negative direction, the material will become magnetically saturated again but in the opposite direction (point "d"). Plummeting H to zero conveys the curve to point "e" which have a level of residual magnetism equal to that reached in other direction. Increasing H back in the positive direction will return M to zero. It shall be noted that the curve did not return to the origin of the graph, as some force is required to remove the residual magnetism. The curve will take a different path from point "f" back to the saturation point where it will complete.

From the hysteresis loop, some primary magnetic properties of a material can be determined.

1. Retentivity (remanent magnetic moment) - A measure of the residual flux density equivalent to the saturation induction of a magnetic material. In other words, it is a material's capability to retain a certain quantity of residual magnetic field if the magnetizing force is removed after reaching.
2. Coercivity - The quantity of reverse magnetic field that must be applied to a magnetic material to make the magnetic flux yield to zero.
3. Permeability, μ - A property of a material that describes the ease with which a magnetic flux is established in the component.

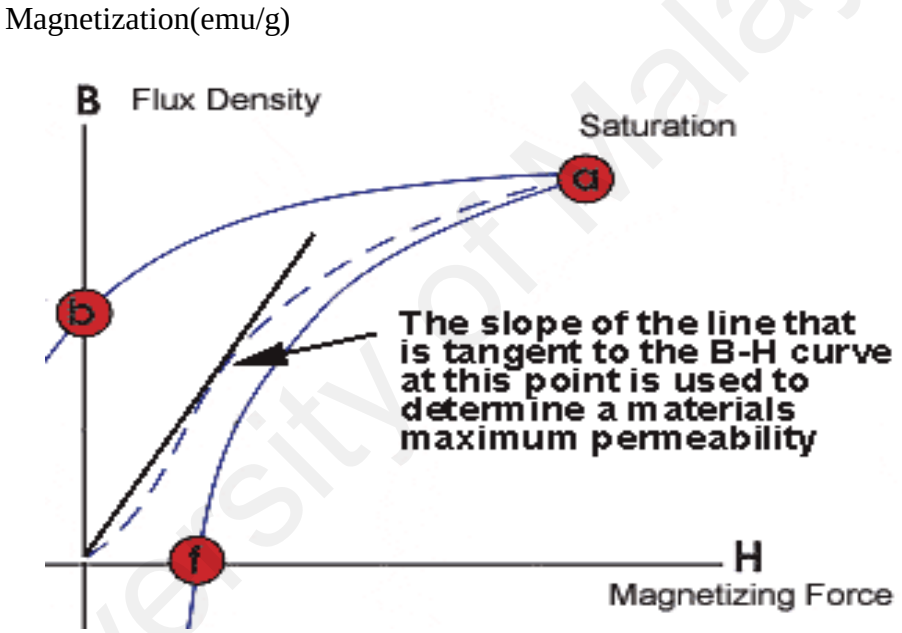

Figure 2.4: Initial Permeability of Magnetization Curve

The beginning of magnetism lies in the orbital and spin motions of electrons and how the electrons interact with one another. The best method to introduce the different types of magnetism is to describe the manner by which materials respond to magnetic fields. Some materials are much more magnetic compared to others. The primary difference is that there is no collective interaction of atomic magnetic moments in some materials, whereas there is a very strong interaction between the atomic moments in other materials.

Most materials display little magnetism and even then only in the presence of an applied field. These are classified as either paramagnetic or diamagnetic. However, some

materials exhibit ordered magnetic states and are magnetic even without a field applied. These materials are classified as ferromagnetic, ferrimagnetic, and antiferromagnetic – prefix denotes to the nature of the coupling interaction between the electrons within the material (Jakubovics & Jakubovics, 1994).

The susceptibility in ordered materials depends not only on temperature but also on H. This phenomenon gives rise to the specific sigmoidal shape of the M-H curve. With M approaching a saturation value at large values of H. Moreover, in ferromagnetic and ferrimagnetic materials hysteresis is commonly observed. This feature is the irreversibility of the magnetization process that is related to the spinning of magnetic domain walls at impurities or grain boundaries within the material as well as intrinsic effects such as the magnetic anisotropy of the crystalline lattice (Pankhurst et al., 2003).

The shapes of these loops determined in part by particle size. In large particles micron or more, there is a multi-domain ground state that leads to a narrow hysteresis loop. It takes little field energy to make the domain walls move. While, for smaller particles, there is a single domain ground state that leads to a broad hysteresis loop. For nanometer-sized particles, superparamagnetism can be observed. The magnetic moment of the particle as a whole is free to change in response to thermal energy while individual atomic moments keep their ordered state about each other.

Magnetic nanoparticles develop a single magnetic domain and keep one large magnetic moment at small sizes. However, thermal energy is sufficient to make a free spin of the particle causing a loss of net magnetization without an external field at sufficiently high temperatures (i.e., blocking temperature).

The superparamagnetic behavior, marked by the absence of remnant magnetization when removal of external fields, allows the particles to retain their colloidal stability and prevent aggregation. This characteristic makes particles feasible for their use in biomedical applications. The coupling interactions within these single magnetic domains

result in much higher magnetic susceptibilities than paramagnetic materials. Although superparamagnetism is a favorable property of small particles, the reduction of particle size is not without some consequences. As particle sizes decrease, surface-to-volume ratios increase resulting in pronounced surface effects, such as noncollinear spins, spin canting, and spin-glass-like behavior, which can significantly influence the magnetic properties of the material. Typically, the saturation magnetization (Ms) values of nanoparticles, corresponding to the complete alignment of all individual moments in a sample, are smaller than their corresponding bulk phases due to disordered crystal structure resulting from high surface curvature, which increases with particle size reduction. Furthermore, significant differences in magnetic properties are observed with magnetic nanoparticles obtained.

2.5 Stability of Maghemite Nanofluids

The stability of dispersion is an important issue in any industry in which settling of particles can result in poor performance. Uniform dispersion and stable suspension of nanoparticles in liquids is the key to most application of nanofluids. Nanofluids are not a simple mixture of liquid and solid particles. Therefore, technique for good dispersion of nanoparticles in liquids or directly producing stable nanofluids are crucial.

Nanoparticles tend to aggregate with time elapsed for its high surface activity. The agglomeration of nanoparticles results in not only the settlement and clogging of microchannel but also decreasing of thermal conductivity.

The dispersion of nanoparticles depends on many factors, including the solvent must wet the particles, the particles must become separated from one another and mixed with the solvent system and they must remain and not reagglomerate. The contact area between particles and the dispersing medium in a colloidal system is very large, as a result, interparticle forces strongly influence suspension behavior (Singh et al., 2004).

There are the number of interparticle forces that play a significant role in dispersing particle suspension. Among those, the dominating force is the van der Waals force which is attractive in nature between like particle and exhibit power moderate distance dependence (Singh et al., 2002). This attractive force has to be minimized to achieve the desired degree of suspension stability; one approach is to generate the charge of sufficient magnitude on the surface of suspended particles. This cause strong electrostatic repulsion between the suspended particles.

Proper dispersion of the colloidal system in aqueous/nonaqueous media is often achieved through control of the charge/zeta potential on the particle. The most significant properties in determining the nature of suspension are including the charge density of the suspended particles and the ionic strength of the medium. The relative magnitude of these two parameters determines the nature of particle interaction in the suspension. When the magnitude of surface charge density relative to ionic strength is high, the particle interaction is repulsive and a low viscosity stable suspension is achieved. In contrast, an agglomerated suspension is achieved when the magnitude of surface charge density relative to ionic strength is small (Singh et al., 2002).

In the maghemite nanofluids, the surface charge and the distribution of maghemite nanoparticles play a significant role in colloidal stability. It can be qualitatively described as the nature and behavior of the surface groups in solution at a definite pH in the presence of an electrolyte. Quantitatively, it can be measured as an electrical potential in the interfacial double layer on the surface of maghemite nanoparticles in suspension.

Zeta potential is an important parameter that is corresponding to nanoparticle stability or aggregation in a dispersion and have significant implications on product performance. A high zeta potential (+ or −) value is an indication of the dispersion stability of maghemite nanoparticles due to the electrostatic interaction.

The pH control is an important parameter for determines the iso electric point (IEP) of suspension to avoid coagulation and instability. A repulsion force between suspended particles is caused by zeta potential that increases with the increase of surface charge of the particles suspended in the solution (Hwang et al., 2007).

The isoelectric point (IEP) is the concentration of potential controlling ions at which the zeta potential is zero (Ghadimi et al., 2011). Zeta potential is an indicator of dispersion stability. The zeta potential of any dispersion is influenced by the surface chemistry. The surface chemistry can be changed by different methods such as the variation of pH value. At the isoelectric point, the repulsive forces among metal oxides are zero and nanoparticles close together at this pH value. Pursuant to the Derjaguin–Landau–Verwey–Overbeek theory (Wamkam et al., 2011), when the pH is equal to or close to the IEP, nanoparticles tend to be unstable, form clusters, and precipitate. Comprehension of pH effects may enable discovery of fundamental nature of nanofluids. Also at the IEP, the surface charge density equals the charge density, which is the start point of the diffuse layer (Ghadimi et al., 2011). As the pH of a solution departs from the IEP of particles, the colloidal particles get more stable and ultimately modify the thermal conductivity of the fluid. It is well noted that, the surface charge is a basic feature which is mainly responsible for increasing thermal conductivity of the nanofluids (Huang et al., 2009).

Sun studied the effect of excess surface concentration of Fe^{2+} or Fe^{3+} ions on the zeta potential of magnetite nanoparticles. According to their results, the zeta potential of magnetite had positive and negative values in the absence of multivalent cations in acidic and basic solutions, respectively. Furthermore, in the presence of excess iron cations, specific adsorption took place at the surface of magnetite, considerably affecting its zeta potential (Sun et al., 1998).

The composition and structure of nanoparticles are very important in their interactions with biological fluids. Magnetite is reported to be an inverse spinel structure with oxygen

forming a face-centred cubic (FCC) closely packed arrangement and Fe cations occupying the interstitial tetrahedral and octahedral sites (Fleet, 1986). The structure of maghemite is similar to that of magnetite except that all Fe ions are in a trivalent state (Fe^{3+}).

Most applications require a stable suspension of magnetic nanoparticles in a liquid carrier. Some applications require this stability to be disrupted either by the application of an external magnetic field or by changes in the environment such as temperature or ionic strength.

2.6 Thermophysical Properties

2.6.1 Thermal Conductivity

Thermal conductivity is the property of a material that indicates its ability to conduct heat. Thermal conductivity, symbolized by "k, expresses the heat flux that will flow through the material if a particular temperature gradient exists over the material. Thermal conductivity is an important property of conduction and convective heat transfer since it explains how heat is transported into and throughout the material.

The important parameter that highly affect the thermal conductivity of nanofluid is the concentration of nanoparticles inside the base fluid. In different reports, concentration has been stated in both types including volume as well as weight percentage.

Reported results of the thermal conductivity of nanofluids as a function of nanoparticle volume fraction from various research groups shown that even for the same nanofluids, different groups reported different enhancements. It is clear that nanofluids exhibit much higher thermal conductivities than their base fluids even when the volume fractions of suspended nanoparticles are very low and they increase significantly with nanoparticle volume fraction.

The particle size is also important because shrinking it down to nanoscale not only increases the surface area relative to volume but also generates some nanoscale

mechanisms in the suspensions (Eastman et al., 2004; Keblinski et al., 2002; Yu & Choi, 2003).

Fluid temperature may play a significant role in enhancing the effective thermal conductivity of nanofluids. Despite the fact that nanofluids may be used under various temperatures, very few studies were performed to investigate the temperature effect on the effective thermal conductivity of nanofluids.

The role of motion as a mechanism for enhanced thermal transport in nanofluids was discussed and raised topics firstly discussed by Wang (Wang et al., 1999). There are three types of motion have been vastly discussed in literature namely:

1. Thermophoretic motion (Motion caused by temperature gradient)
2. Brownian motion (force)
3. Osmophoretic motion (Motion in concentration gradient)

When Das et al. (2003) discovered the fact that nanofluids have temperature-dependent thermal conductivity, and posed motion of particles as an important reason for that. Afterward the motion of particles caused by the temperature gradient, which is called thermophoretic motion, has been investigated more by (Koo & Kleinstreuer, 2004).

However, Brownian motion as the most useful type of movement, which has been investigated by different researchers and has stated as a very effective reason for increasing thermal conductivity of nanofluids.

Keblinski et al. (2002) declared four possible microscopic mechanisms for the rise in the thermal conductivity of nanofluids, and these mechanisms are the Brownian motion of the nanoparticles, liquid layering at the liquid/particle interface, nature of the heat transport in the nanoparticles, and the effect of nanoparticle clustering. They explored particle-particle collision as the effect of Brownian motion which causes heat transfer increment eventually motion was the reason for increasing.

Brownian motion is caused by the random bombardment of liquid molecules. Particles randomly move through the liquid due to the Brownian motion, thereby enabling stronger transport of heat, which can increase the effective thermal conductivity. The more efficient mechanism would have if the Brownian motion to be a significant contributor to the thermal conductivity than thermal diffusion in the fluid. However, by a simple analysis, they showed that the thermal diffusion is much faster than Brownian diffusion, even within the limits of extremely small particles (Keblinski et al., 2002).

When the size of the nanoparticles in a nanofluid becomes less than the phonon mean-free path, phonons no longer diffuse across the nanoparticle but move ballistically without any scattering. However, it is difficult to envision how ballistic phonon transport could be more effective than a very-fast diffusion phonon transport, particularly to the extent of explaining anomalously high thermal conductivity of nanofluids. No further work or analysis has been reported on the ballistic heat transport nature of nanoparticles. Instead, the continuum approach was adopted in all reported works (Murshed et al., 2006, 2008; Wang et al., 2003; Yu & Choi, 2003).

Another responsible mechanism for higher thermal properties of nanofluids was liquid layering around the particle (i.e. nanolayer). The basic idea is that liquid molecules can form a layer around the solid particles and thereby enhance the local ordering of the atomic structure at the interface region. Hence, the atomic structure of such liquid layer is significantly more ordered than that of the bulk liquid. Given that solids, which have much ordered atomic structure, exhibit much higher thermal conductivity than liquids, the liquid layer at the interface would reasonably have a higher thermal conductivity than the bulk liquid. Thus the nanolayer is considered as an important factor enhancing the thermal conductivity of nanofluids.

The effective volume of a cluster is considered much larger than the volume of the particles due to the lower packing fraction (ratio of the volume of the solid particles in

the cluster to the total volume of the cluster) of the cluster. Since heat can be transferred rapidly within such clusters, the volume fraction of the highly conductive phase (cluster) is larger than the volume of solid, thus increasing its thermal conductivity (Hong et al., 2005; Keblinski et al., 2002).

2.6.1.1 Theoretical Formula

The physical mechanism accounting for the thermal conductivity enhancement of nanofluids is not well understood. Maxwell (Maxwell, 1954) was one of the first to analytically investigate conduction through suspended particles. Maxwell formula shows that the effective thermal conductivity of nanofluids relies on the thermal conductivity of spherical particle, the base fluid and the volume fraction of the solid particles. The Maxwell formula considered a very dilute suspension of spherical particles by ignoring the interactions among the particles. The Maxwell equation can be obtained by solving the Laplace equation for the temperature field outside the particles and resulting as follows:

$$k_r = \frac{k_{nf}}{k_{bf}} = \left[\frac{k_p + 2\,k_{bf} + 2\,(k_p - k_{bf})\phi}{k_p + 2\,k_{bf} - 2\,(k_p - k_{bf})\phi}\right] \tag{2.5}$$

where k_p represents the thermal conductivity of solid particles added, k_{bf} is the thermal conductivity of base fluids, and ϕ is particle volume fraction.

The limitation on the particle volume concentration proposed by Maxwell has been improved by Bruggeman (Bruggeman, 1935). The interactions among the randomly distributed particles are considered in the development of an equation in an implicit form and given as

$$k_{nf} = \frac{1}{4}\left[(3\phi - 1)k_p + (2 - 3\phi)k_{bf}\right] + \frac{k_{nf}}{4}\sqrt{\Delta} \tag{2.6}$$

Where $$\Delta = \left[(3\phi - 1)^2(\frac{k_p}{k_{bf}})^2 + (2 - 3\phi)^2 2(2 + 9\phi - 9\phi^2(\frac{k_p}{k_{bf}}\right]$$

The Bruggeman model is valid for spherical particles and considered interaction between particles.

Hamilton and Crosser (Hamilton & Crosser, 1962) developed a modified Maxwell's theory for two-component systems containing different particle shapes and particle sizes ranging between millimeters and micrometers. According to H–C model, k/kf is given by

$$\frac{k_{nf}}{k_{bf}} = \left[\frac{k_p+(n-1)k_{bf}-(n-1)\phi(k_{bf}-k_p}{k_p+(n-1)k_{bf}+\phi(k_{bf}-k_{p)}}\right] \quad (2.7)$$

This model is valid for both spherical and cylindrical particles and n = 3/ψ, where ψ is the particle sphericity.

The Wasp model (Xuan & Li, 2000) was developed for predicting the effective thermal conductivity of a continuum medium with well dispersed solid particles. The Wasp model is the same as the Maxwell model although it is not specified for any particular shape of particles. The Wasp model can be expressed as

$$\frac{k_{nf}}{k_{bf}} = \left[\frac{k_p+2\,k_{bf}-2\phi(k_{bf}-k_p)}{k_p+2\,k_{bf}+2\phi\,(k_{bf}-k_p)}\right] \quad (2.8)$$

The classical models originated from continuum formulations, which typically involve only the particle size/shape and volume fraction and assume diffusive heat transfer in both fluid and solid phases. Although they can give good predictions for micrometer or larger-size multiphase systems, the classical models usually underestimate the enhancement of thermal conductivity increase of nanofluids as a function of volume fraction. Nevertheless, stressing that nanoparticle aggregation is the major cause of thermal conductivity enhancement.

The classical models also were found to be unable to predict the anomalously high thermal conductivity of nanofluids. This is because these models do not include the effects of particle size, interfacial layer at the particle/liquid interface, and Brownian motion of particles, which are considered as important factors for enhancing thermal conductivity of nanofluids (Keblinski et al., 2002; Wang et al., 1999; Yu & Choi, 2003, 2004).

Recently, many theoretical studies have been carried out to predict the anomalously increased thermal conductivity of nanofluids. A detailed summary of recently developed models for the prediction of the effective thermal conductivity of nanofluids is provided in Table 2.2.

Table 2.2: Summary of models developed for thermal conductivity of nanofluids

Researchers	Models/equations	Remarks
(Wang et al., 2003)	$\frac{k_f}{k_{bf}} = \frac{(1-\phi)+3\phi\int_0^\infty \frac{k_{cl}(r)n(r)}{k_{cl}(r)+2k_{bf}}dr}{(1-\phi)+3\phi\int_0^\infty \frac{k_{bf}n(r)}{k_{cl}(r)+2k_{bf}}dr}$	Based on effective medium approximation and fractal theory
(Xuan et al., 2003)	$\frac{k_f}{k_{bf}} = \frac{k_p+2k_{bf}-2\phi(k_{bf}-k_p)}{k_p+2k_{bf}+\phi(k_{bf}-k_p)} + \frac{\phi\rho_p c_p}{2k_{bf}}\sqrt{\frac{K_B T}{3\pi r_c \eta}}$	The first term is the Maxwel models
(Yu & Choi, 2003)	$\frac{k_f}{k_{bf}} = \frac{k_{pc}+2k_{bf}-2\phi(k_{pc}-k_{bf})(1+\beta)^3}{k_{pc}+2k_{bf}-\phi(k_p-k_{bf})(1+\beta)^3}$	Considered interfacial layer when modified Maxwell model
(Yu & Choi, 2004)	$\frac{k_f}{k_{bf}} = 1+\frac{n\phi_f A}{1-\phi_f A^2}$ where $A = \frac{1}{3}\sum_{j=a,b,c}\frac{k_{pj}-k_{bf}}{k_{pj}+(n-1)k_{bf}}$	Considered interfacial layer when modified Hamilton and Crosser model
(Kumar et al., 2004)	$\frac{k_f}{k_{bf}} = 1 + c\frac{2K_B T}{\pi\eta d_p^2}\frac{\phi r_{bf}}{k_{bf}(1-\phi)r_p}$	Based on kinetic theory and Fourier's law
(Leong et al., 2006)	$k_f = \frac{(k_p-k_{bf})\phi_p k_{lr}[2\gamma_l^3-\gamma^3+1]+(k_p+k_{lr})\gamma_l^3[\phi_p\gamma^3(k_{lr}-k_{bf})+k_{bf}]}{\gamma_l^3(k_p+2k_{lr})-(k_p-k_{lr})\phi_p[\gamma_l^3+\gamma^3-1]}$	Considered interfacial layer as separate component and for spherical shape particle
(Jang & Choi, 2004)	$\frac{k_f}{k_{bf}} = 1 + c\frac{d_f}{d_p}k_{bf}\phi R_e^2 d_p P_r$	Based on convection and conduction heat transport
(Xie et al., 2005)	$\frac{k_f}{k_{bf}} = 1+3\Theta\phi+\frac{2\Theta^2\phi^2}{1-\Theta\phi}$	Considered the presence of a nanolayer
(Murshed et al., 2008)	$k_f = \frac{(k_p-k_{lr})\phi_p k_{lr}[\gamma_l^2-\gamma^2+1]+(k_p+k_{lr})\gamma_l^2[\phi_p\gamma^2(k_{lr}-k_{bf})+k_{bf}]}{\gamma_l^2(k_p+k_{lr})-(k_p-k_{lr})\phi_p[\gamma_l^2+\gamma^2-1]}$	For cylindrically shaped particles in base fluid
(Koo & Kleinstreuer, 2004)	$\frac{k_f}{k_{bf}} = \frac{k_{MG}}{k_{bf}} + \frac{1}{k_{bf}}5\ x\ 10^4\beta\phi\rho_p c_p\sqrt{\frac{K_B T}{\rho_p D}}f(T,\phi)$	Assumed randomly moving nanoparticles with surrounding liquid motion having unknown parameters of β and f
(Jang & Choi, 2004)	$\frac{k_f}{k_{bf}} = k_{bf}+(1-\phi)+k_p\phi+\phi h\delta_T$	Considered the thickness liquid layer and Brownian motion of dispersed particles.
(Pak & Cho, 1998)	$\frac{k_f}{k_{bf}} = 1+7.47\phi$	Assumed that k enhancement is due to the suspended particle

(Gupte et al., 1995)	$k_f = k_{bf}(0.0556\,P_e + 0.1649\,P_e^2 - 0.0391\,P_e^3 + 0.0034\,P_e^4)$	Considered the effect of translational motion of nanoparticle
(Evans et al., 2008)	$\frac{k_f}{k_{bf}} = 1 + \phi_p \frac{k_p}{3k_1}$	Considered aggregation and interfacial layer of the particle thermal conductivity
(Timofeeva et al., 2007)	$\frac{k_f}{k_{bf}} = 1 + 3\phi$	Considered the agglomeration of the nanoparticle

2.6.1.2 Experimental Investigation

Most of the investigation of nanoparticles as heat transfer application is the property of thermal conductivity. Due to their higher thermal conductivity of particles compared to base fluids, it is believed that suspended nanoparticle in fluids will enhance thermal conductivity of fluids. For magnetic fluids, investigation of thermal conductivity conducted in the absence and presence of magnetic fields effect.

Experimental investigations on the thermal conductivity of magnetic nanofluids in the absence of magnetic fields show that the increase of thermal conductivity is mainly affected by several parameters. These parameters are volume fraction of magnetic nanoparticles, particle size/particle size distribution, the chemical composition of magnetic nanoparticles, temperature, particle coating layer.

Many investigators show that the thermal conductivity of magnetic fluids increase with the increasing of particles fraction and temperature. Abareshi measured the thermal conductivity of a water based magnetite nanofluids as a function of the particle volume fraction at different temperatures. The thermal conductivity enhanced with the increase of the particle volume fraction and temperature. The largest thermal conductivity ratio observed was 11.5% at a particle volume fraction of 3% at 40 °C (Abareshi et al., 2010).

Li et al. (2005) investigated the effects of particle volume fraction, surfactants and the magnetic field on the transport properties of water based Fe magnetic nanofluids. They observed a thermal conductivity enhancement of magnetic nanofluids with the increase

of particle volume fraction with and without applied magnetic fields. Their results also revealed that the viscosity of magnetic nanofluids increased with the increase of particle volume fraction and the surfactant.

Yu et al. (2010) investigated the effects of the particle volume fraction on the thermal conductivity of a kerosene-based magnetite nanofluid prepared via a phase-transfer method. The results describe that the thermal conductivity ratios increased linearly with the increase of volume fraction and temperature, and the value was up to 34.0 % at 1 vol %. The measurement was conducted in the different temperature range from 10 to 60 ^{o}C in order to investigate the effect of temperature on thermal conductivity. The results revealed that the absolute thermal conductivity improved with increasing temperature. While the thermal conductivity ratio was nearly constant, and the thermal conductivities of the magnetic nanofluids tracked those of the carrier fluid.

Philip et al. (2007) conducted a work on thermal conductivity of magnetic nanofluids prepared via the dispersion of magnetite nanoparticles in water, ethylene glycol, and kerosene as carrier fluids, respectively. Their results revealed that the thermal conductivity ratio increased with the increase of particle volume fraction. (Philip et al., 2007) (Philip et al., 2007) (Philip et al., 2007) (Philip et al., 2007) (Philip et al., 2007) (Philip et al., 2007) (Philip et al., 2007) (Philip et al., 2007) (Philip et al., 2007)

The thermal conductivity enhancement of Fe_3O_4/water nanofluids depends on the particle volume concentration and temperature. Thermal conductivities are higher at higher volume concentrations (Sundar et al., 2013).

Recent work on the control of the thermal conductivity of magnetic nanofluids has received particular interest because the "anomalous" thermal conductivity observed under the influence of an external magnetic field. The thermal conductivity of magnetic nanofluids can be affected by the orientation, and the intensity of the presence of the applied magnetic field. The same techniques as those used in without magnetic fields are

conducted to measure thermal conductivity in the presence of magnetic field and usually performed at room temperature. The magnetic field is created by either electromagnets or permanent magnets.

Krichler & Odenbach (2013) investigated the influence of magnetically driven structure formation on heat flux in magnetic nanofluids. They conducted the measurements of thermal conductivity in the different of external magnetic field. They developed an improved measuring device based on the plane heat source instead of the standard hot wire method was used to enable both parallel and perpendicular orientations of a magnetic field and heat flux. Thermal conductivity measurements were conducted on the variation of strength and direction of an external magnetic field about heat flux. It was concluded that the results showed qualitative consistency with theoretical predictions for both orientations.

Li et al. (2005) also reported on the influence of magnetic field strength and direction on the transport properties of magnetite nanofluids. Their results show that an external magnetic field had outstanding effects on the both thermal conductivity and viscosity of the magnetite nanofluids. Little change in the thermal conductivity of the magnetite nanofluids was found in the magnetic field perpendicular to the temperature gradient, irrespective of the applied magnetic field strength and the volume fraction of particles. The thermal conductivity of the magnetite nanofluids increased with the increase of strength of magnetic field in which parallel to the temperature gradient. The reason for this enhancement was the change of microstructures induced by the external magnetic field in the magnetite nanofluids. They further clarified that when the magnetic field was parallel to the temperature gradient, the formed particle chains give more bridges for energy transport inside the magnetite nanofluids. This phenomenon occurred along the direction of temperature gradient and enhanced the thermal process in the magnetite nanofluids. It was revealed that the viscosity firstly increased with the magnetic field and

finally approached a constant as the magnetization of the magnetic fluid achieved a saturation state. This behavior was also explained by the presence of chain-like structures in magnetic nanofluids with respect to the influence of magnetic fields.

Philip et al. (2007;2008) reported a remarkable enhancement of the thermal conductivity of magnetite-based nanofluids under the effect of magnetic fields along the direction of heat flow. The enhancement of thermal conductivity was within the predicted value for parallel mode conduction. The decrease in thermal conductivity observed after the critical value of the magnetic field was explained by the "zippering" of chains. They claimed that the cluster morphology and distribution of both could have impacts on thermal conductivity enhancement. These behaviors support the transfer of heat through the particles. A magnetically polarizable nanofluid (magnetic nanofluid) could be used as a reversible switchable thermal fluid, such as insulation to high thermal conducting fluid and vice versa, by changing the magnetic fields.

Wensel et al. (2008) investigated the thermal conductivity of nanofluids with metal oxides nanoparticles (Fe_3O_4 and MgO) and carbon nanotubes in the presence of magnetic field. They observed that thermal conductivity increased by up to 10% at a low particle weight fraction of 0.02 wt%. This phenomenon is because of the aggregation of metal oxide on the surface of the nanotube by electrostatic attraction and the formation of chain structure along the nanotube. It was proposed that the investigated nanofluids could be used for coolant applications since their viscosity was similar to that of water.

Nkurikiyimfura et al. (2011) investigated the effects of particle size and particle volume fraction on the thermal conductivity enhancement of an engine oil based magnetite nanofluids in a magnetic field. The results revealed that the thermal conductivity increased with the increase of particle volume fraction for smaller magnetite particles. Besides, the thermal conductivity enhancement corresponding to a magnetic field parallel to temperature gradient. They analyzed that the increase of thermal

conductivity ratio was due to the chain-like structures formed in magnetic nanofluids under the effect of magnetic field. The increased thermal conductivity observed for the smaller particles was justified by the superparamagnetic behavior of the less particulate matter and their influence on the aggregates formation. The magnetic field parallel to temperature gradient exhibited a positive effect on the thermal conductivity of the magnetic nanofluids. However, a high magnetic field set back thermophysical properties such as rheological and thermal conductivity itself (Nkurikiyimfura et al., 2011; Philip et al., 2007). Because of the undesirable clumping and zippering of chains under the effect of high magnetic fields. This restriction calls for the simultaneous treatment of thermal conductivity enhancement with other transport properties, especially, the viscosity (η). Once the thermal conductivity and magnetoviscous effects were taken into account, the improvement could be considered by a ratio of the thermal conductivity to the viscosity (Nkurikiyimfura et al., 2011).

Gavili et al. (2012) conducted an experimental investigation on the thermal conductivity of water-based magnetite nanofluids under the magnetic field using the Helmholtz coils. The magnetic field strength was controlled by an electric current. The saturation time and the reversibility of thermal conductivity were also observed after the magnetic field was turned off. The results revealed that the thermal conductivity increased more than 200% for magnetite nanofluids with 5.0% volume fraction with an average diameter of 10 nm. Furthermore, the variation of thermal conductivity with temperature was also shown.

2.6.2 Viscosity

Viscosity is the friction between neighboring particles in a fluid that are moving at different velocities. When the fluid is forced through a tube, the fluid moves faster near the axis and very slowly near the walls. Therefore, some stress (such as a pressure difference between the two ends of the tube) is required to overcome the friction between

layers and keep the fluid moving. For the same velocity pattern, the stress required is proportional to the fluid's viscosity. A liquid's viscosity depends on the size and shape of its particles and the attractions between the particles.

Viscosity describes the internal resistance of a fluid to flow, and it is an important property for all thermal applications involving fluids (Nguyen et al., 2007b). The pumping power is related to the viscosity of a liquid. In laminar flow, the pressure drop is directly proportional to the viscosity. Furthermore, convective heat transfer coefficient is influenced by viscosity. Hence, viscosity is as important as thermal conductivity in engineering systems involving fluid flow (Kole & Dey, 2010).

Measurement of viscosity is conducted by various types of viscometer and rheometers. A rheometer is used for those liquids that cannot be defined by a single value of viscosity and, therefore, need more parameters to be set and measured than is the case for a viscometer. Temperature control of the liquid is an essential parameter to obtain precise measurements, particularly in materials like lubricants. One of the most common apparatus for measuring kinematic viscosity is the glass capillary viscometer.

2.6.2.1 Theoretical Formula

There are some existing theoretical formulas to estimate the particle suspension viscosities depending on the size and concentration of the solid particles. Some models exist that describe the relative viscosity as a function of volume fraction ϕ of solid particles. Among them, equation suggested by Einstein could be labeled the pioneer one, and most of other derivations have been established from this relation (Einstein, 1906). The assumptions are based on the linear viscous fluid containing dilute, suspended, spherical particles and low particle volume fractions ($\phi < 0.02$). The suggested formula is represented by equation 2.9 as follows:

$$\mu = \mu_{bf}(1 + 2.5\,\phi) \tag{2.9}$$

where μ is the viscosity of suspension; μ_{bf} is the viscosity of the base fluid, and ϕ is the volume fraction of a particle in a base fluid. This equation is a linear increase of the suspension viscosity with increasing solid volume concentration. The Einstein model for nanofluids is according to the assumption of a Newtonian fluid containing suspensions of spherical nanoparticles. It does not take into account temperature dependence and, in general, the viscosity of liquids is strongly dependent on the temperature. Einstein considered non-interacting suspensions. Some factors have been identified as the limitations of this formula as the particle concentrations may not be so small. The structure and the interaction of the particles within the continuous phase may also affect the viscosity of the mixture.

Brinkman extended Einstein's formula to be used with moderate particle concentrations, taking into account the effect of the addition of one solute-molecule to an existing solution, which is considered as a continuous medium. And this correlation has more acceptances among the researchers (Brinkman, 1952). For particle concentrations less than 4%, the expression is represented by equation 2.10.

$$\mu = \mu_{nf}\,(1-\phi)^{2.5} \tag{2.10}$$

Lundgren (Lundgren, 1972) proposed the following equation under the form of a Taylor series in ϕ. The equation is represented by equation 2.11.

$$\mu = \mu_{bf}(1 + 2.5\,\phi + \tfrac{25}{4}\,\phi^2 + f(\phi^3) \tag{2.11}$$

Considering the effect due to the Brownian motion of particles on the bulk stress of an approximately isotropic suspension of rigid and spherical particles; (Batchelor, 1977) proposed the equation as expressed by equation 2.12.

$$\mu = \mu_{bf}(1 + 2.5\,\phi + 6.5\,\phi^2) \tag{2.12}$$

From the above two relations, if a second or higher order of ϕ are ignored, then these formulas will be the same as Einstein's formula. Eq. (2.12) has been validated for a

particle volume fraction up to $\phi \leq 0.1$ where the motion of the single particle and pair-particle interactions is dominant. Batchelor considered the interaction of pair-particles.

There are many of other theoretical formulas developed by researchers for higher particle volume concentration which have not describe here.

2.6.2.2 Experimental Investigation

Due to their unique properties, magnetic nanoparticles have been attracted many researchers to investigate these smart materials. Most of the investigations available in the literature on the viscosity of nanofluids, regarding the effect of volume fraction agree upon the fact that the viscosity of nanofluids increases with increasing the particle volume fractions. This phenomenon also occurs in magnetic nanofluids.

Several authors reported that in the absence of a magnetic field, the viscosity of a fluid with dispersing magnetic nanoparticles is similar to other types of nanofluids. The viscosity increases proportionally with the volume fraction (Mahbubul et al., 2012; Sundar et al., 2013).

The influence of volume fraction and temperature on viscosity of Fe_3O_4-water nanofluids have been investigated by (Sundar et al., 2013). The results show that Fe_3O_4-water magnetic nanofluid exhibited Newtonian behavior. The viscosity of nanofluids increases with an increase in particle volume concentration and decreases with a rise in temperature.

In a strong magnetic field, the magnetic fluids form chains directed to magnetic fields that are zippered and clumped together. It will block the motion of the particle and significantly reduce the flow ability of the fluid, hence increase the viscosity of a condensed magnetic fluids (Genc & Derin, 2014). Many works supported by many workers that the viscosity of magnetic fluids would increase under the existence of a magnetic field (Nowak et al., 2014; Patel et al., 2003). Patel also used a horizontal viscometer to study the effective viscosity as a function of external magnetic field,

parallel, perpendicular, and in other angular directions to the flow. The results also showed that the orientation of the magnetic field played affects greatly the viscosity of magnetic fluids. The viscosity was magnified up to 200% when the magnetic field was shifted from perpendicular to parallel to the flow direction. They also investigated the dependence of viscosity of magnetic fluids on the intensity of the magnetic field and the volume fraction of a particle in the experiment. They found that introducing either a strong field or decrease the volume fraction resulted in the increase of viscosity.

Moeen investigated the rheological properties of magnetic fluids by using a standard rotating rheometer with a variable magnetic field. The results suggested the presence of a remarkable magneto-viscous effect at a low shear rate. The increase in viscosity is due to the magnetic torques spreading though the suspensions which tries to align the particles magnetic moments with the magnetic field direction (Moeen et al., 2012).

Li et al. (2005) study the effect of magnetic particle and surfactant concentrations and magnetic strength on the viscosity of Fe_3O_4-water magnetic fluids using capillary tube viscometer. The results show that the viscosity of magnetic fluids increases with the magnetic particle and surfactant concentrations. The magnetic field strength plays significant roles in affecting the viscosity of magnetic fluids. The viscosity increases with the strength of magnetic field.

2.6.3 Electrical Conductivity

Electrical conductivity of a nanofluid is related to the ability of charged particles (ions) in the suspension to carry the charges (electrons) towards respective electrodes when an electric potential is applied. In nanofluids, the nanoparticles dispersed in a base fluid get charged due to the formation of electrical double layer around the particle surface. These nanoparticles along with the EDL move towards oppositely charged electrode when a potential is applied. This EDL formation depends on the surface charge, size, and volume

fraction of the particles and ionic concentration in the base fluid. Thus, the electrophoretic mobility of charged particles determines the electrical conductivity of a nanofluid.

The electrical conductivity of a suspension depends on the background electrolyte and particle size, charge, and volume fraction (Posner, 2009). When nanoparticles dispersed in fluid, these particles gain surface charge due to the protonation or deprotonation of a surface group such as a hydroxyl ligand (-OH) (Lee et al., 2006). This surface charge, which can be adjusted in electrolyte solutions by altering the pH of the suspension (Li et al., 2008; Lee, 2007) or chemically treating the particle surface (Lee, 2007), causes an electrical double layer EDL of counter-ions to form near the particle surface. For bulk suspensions that are salt-free, the only ions present are those from the charging process of the particles, which are counter-ions formed at the fluid-particle interface. For salt-free suspensions, the effective electrical conductivity is typically increased upon the suspension of particles since the ionic conductivity in the EDL is generally larger than that of the bulk solution (Posner, 2009).

In fact, the observed enhancement in electrical conductivity of the suspension with respect to the base fluid is a consequence of net charge effect of the solid particle and the pertinent EDL interactions (Hunter, 2013; Lyklema, 2005). When particles are suspended in a polar liquid, electric charges develop on their surfaces. Ions of charge opposite to that of the particle surface are attracted, causing the development of a charged diffuse layer surrounding the particle. This layer is known as electrical double layer (Hunter, 2013) and is commonly characterized by a parameter $\kappa - 1$ (Debye length).

Apart of the physical properties of fluid as well as conductivity of particles and fluids, the effective electrical conductivity of colloidal nanosuspensions in a liquid exhibits a complex dependence on the electrical double layer, EDL characteristics, volume fraction, ionic concentrations, and other physicochemical properties. When the ionic strength of the solution is very low, the number of ions in solution is insufficient to compensate the

electric charges, and hence the net electric charge density is high on particle surfaces. The surface charge of the particles, together with ion-cloud that constitutes the EDL, actively contributes for the enhancement in conduction mechanisms through the suspension. In addition, the presence of uniformly dispersed nanoparticles is characterized with reduced equivalent particulate masses, leading to increase electrophoretic mobility, which consequently increases the effective electrical conductivity of the nanofluids. With an increase in particle volume fraction, the availability of conducting path-ways increases in the solution, which in turn increases the overall electrical conductivity of the solution.

Though the electrical conductivity of the nanoparticles and the base fluid are in the same order, the electrical conductivity of the nanofluids is much higher than that of the base fluid. This reveals that the electrical conductivity of the nanofluid is not only related to the physical properties of the base fluid and nanoparticles but is also strongly affected by other factors such as the electrochemical properties, electrical double layers, particle size, and aggregation. The higher the temperature is, the greater the electrical conductivity will be.

2.6.3.1 Theoretical models

The Maxwell model was the first model developed to determine the effective electrical or thermal conductivity of liquid–solid suspensions (Maxwell, 1954). This model is applicable to statistically homogeneous and low volume fraction liquid–solid suspensions with randomly dispersed, uniformly sized and noninteracting spherical particles.

The electrical conductivity of nanofluids in the Maxwell model, σ_M, as a function of volume fraction, ϕ, is given equation 2.13.

$$\frac{\sigma_M}{\sigma_o} = 1 + \frac{3(\alpha-1)}{(\alpha+2)-(\alpha-1)\phi} \tag{2.13}$$

where σ_0 is the electrical conductivity of base fluids, and $\alpha = \frac{\sigma_p}{\sigma_o}$ is the conductivity ratio of the nanoparticle, σ_p, to the base fluids. This model does not include the particle surface

charge effects, and motion of particles, which are important factors for the enhancement of the electrical conductivity of nanofluids.

According to the theory of colloid and surface chemistry, there is an electrical double layer around each particle surface. The surface charge of the particles, together with ion cloud that constitutes the EDL, would contribute to the enhancement in conduction through the electrophoretic transactions. Generally, the particles are positively charged when their dielectric constant is larger than that of the base fluid. And in turn, the particles will be negatively charged. The nanoparticle has a Zeta potential U_o relative to the base liquid. When an electrical field is applied, the charged particles will move towards the electrode and thus form the electrophoretic conductivity. That is to say that the nanoparticles are electric current carriers in the fluid.

The electron attachment on the particle can be expressed as:

$$q = 4\,\pi\varepsilon_r\varepsilon_o r\,U_o \tag{2.14}$$

Considering that the particle has uniform velocity under the joint function of electric force and viscous force, the electrophoretic conductivity can be expressed as:

$$\sigma_E = \frac{8\pi n_o \varepsilon_r^2 \varepsilon_0^2 U_0^2}{3\eta} \tag{2.15}$$

where n_o is the number of particles per unit volume, η is the dynamic viscosity of the liquid, ε_0 is the dielectric constant of the vacuum, and ε_r is the relatively dielectric constant of nanoparticles. If the n_o, ε_r, U_o, and r remain unchanged, the value of $\sigma_E\eta$ is a constant. The relationship indicates that though the electrical conductivity and viscosity of the base fluids change with temperature, the product of σ_E and η will remain constant in the nanofluids. This relationship is called Walden law (Bailar Jr & Auten, 1934). Hence, n_o can be expressed as.

$$n_o = \frac{1\phi}{\frac{4}{3}\pi r^3} = \frac{3\phi}{4\pi r^3} \tag{2.16}$$

Substituting this result into eq. (2.15) gives:

$$\sigma_E = \frac{2\phi\varepsilon_r^2\varepsilon_o^2 U_o^2}{\eta r^2} \tag{2.17}$$

On the other hand, the relationship of dynamic viscosity and kinematic viscosity is

$$\eta = \rho\upsilon \tag{2.18}$$

In nanofluids, both the dynamic viscosity and zeta potential will be affected by the fluctuation of the volumetric fraction of nanofluid. The variation of dynamic viscosity with respect to the volumetric fraction of nanofluid is given by Eq. (2.19) when considering the interaction of particles. When the volume fraction of nanofluid is lower than 10 %, η can be described as (Shen et al., 2012).

$$\eta = \eta_f\,(1 + 25\phi + 625\phi^2) \tag{2.19}$$

where η_f is the dynamic viscosity of pure base fluid.

In fluid mechanics, the viscosity varies with pressure and temperature. Since the pressure has a very small influence on the viscosity, it is only considering the effect of temperature. The relationship between viscosity and temperature can be expressed as (Dong et al., 2013).

$$\eta = \eta_0\, e^{-\lambda(T-To)} \tag{2.20}$$

where η_o is the dynamic viscosity of the nanofluid at temperature and λ is the decreasing rate of the viscosity when the temperature is increasing, namely, the viscosity index of the fluid.

The electrophoresis conductivity is obtained by substituting eqs. (2.18), (2.19), (2.20) into (2.17)

$$\sigma_E = \frac{2\phi\varepsilon_r^2\varepsilon_o^2 U_o^2}{\rho\upsilon(1+25\phi+625\phi^2)r^2}\, e^{\lambda(T-To)} \tag{2.21}$$

In addition to the electrophoresis of the nanoparticles in fluid, the Brownian motion of the suspended nanoparticles is also suggested to be responsible for the extra electrical conductivity enhancement. Considering nanoparticles randomly dispersed in the fluid, the Brownian motion of the nanoparticles is similar with the molecular in fluid with a mean

kinetic energy of $\frac{3}{2}$ kT. Assuming the particles are spherical, in the view of molecular motion and by Boltzmann distribution law, the average displacement of a nanoparticle in time *t* can be expressed as (Dobnikar et al., 2004).

$$x = \left(\frac{RT}{L}\frac{t}{3\pi\eta r}\right)^{1/2} \tag{2.22}$$

here *T* is the temperature in Kelvin, *L* is the Avogadro's constant, *R* is the thermodynamic constant. η is the dynamic viscosity of the nanofluid and *r* is the average radius of the monodispersed nanoparticles in fluid. Then the electrical conductivity of the nanofluid caused by the Brownian motion can be inferred as:

$$\sigma_B = \frac{3\phi\varepsilon_r\varepsilon_o U_o}{r^{3/2}}\left(\frac{RT}{L}\frac{e^{\lambda(T-To)}}{3\pi\rho\upsilon(1+25\phi+625\phi^2)}\right)^{1/2} \tag{2.23}$$

Finally, considering that in nanofluid $\frac{\sigma_p}{\sigma_o}$ >>1, the total electric conductivity is the sum of the Maxwell conductivity and dynamic electrical conductivity caused by the electrophoresis and Brownian motion of the nanoparticles. Consequently, the electric conductivity model can be defined as:

$$\begin{aligned}\sigma &= \sigma_M + \sigma_E + \sigma_B \\ &= \sigma_{o(T)}(1+3\phi) + \frac{2\phi\varepsilon_r^2\varepsilon_o^2U_o^2}{\rho\upsilon\left(1+25\phi+625\phi^2\right)r^2}e^{\lambda(T-To)} \\ &\quad + \frac{3\phi\varepsilon_r\varepsilon_o U_o}{r^{3/2}}\left(\frac{RT}{L}\frac{e^{\lambda(T-To)}}{3\pi\rho\upsilon(1+25\phi+625\phi^2)}\right)^{1/2}\end{aligned} \tag{2.24}$$

2.6.3.2 Experimental investigations

The major focus of the research work, so far, has been on the estimation of thermo-physical properties, primarily on the effective thermal conductivity. Despite the vast scientific and technological importance of electrical conductivity characteristics of nanoparticle suspensions, studies concerning the issue of the effective electrical conductivities of nano-fluids have been largely ignored. In addition, there is very few data published on the electrical properties of nanofluids. On the other hand, among the

transport properties, electrical conductivity might bring information on the state of dispersion and stability of the particulate suspension.

Despite the vast scientific and technological importance of electrical conductivity of nanofluids, studies concerning this issue have been largely ignored. Lack of electrical conductivity data is available in the literature with only a few papers about the measurement of electrical conductivity of nanofluids. Ganguly (Ganguly et al., 2009) investigated the effective electrical conductivity of aluminum oxide nanofluids as a function of particle volume fraction and temperature. The results indicate that increase of electrical conductivity of aluminum oxide with increasing of particle volume fraction and temperature. Electrical and thermal conductivities of gold nanofluids have been studied (Fang & Zhang, 2005). Few investigations dealt with numerical and analytical studies on electrical conductivity of concentrated and dilute colloidal suspensions (Cruz et al., 2005; O'brien, 1981).

A linear rise in electrical conductivity of TiO_2 suspensions with particle fraction was observed for low ionic strength and no significant impact for high ionic concentrations by Luis and Biswas (Modesto-Lopez & Biswas, 2010). Thermal and electrical conductivities of suspensions of multiwalled carbon nanotubes (MWCNT) in water were measured as a function of temperature, nanotube weight content, and nanotube length (Glory et al., 2008). The synthesis of highly stable exfoliated graphene based nanofluids with water and ethylene glycol as base fluids without any surfactant and the subsequent studies on their thermal and electrical conductivities (Baby & Ramaprabhu, 2010).

Sarojini et al. (2013) conducted an experimental evaluation of electrical conductivity of ceramic and metallic nanofluids with a different volume fraction in water and ethylene glycol base fluids. The results show that the electrical conductivity of nanofluids increases with the increasing particle volume fraction in both base fluids. Electrical conductivity of

magnetite nanofluids were investigated by Bagheli et al. (2015) at different volume fractions and temperatures. The result indicated considerable enhancement of electrical conductivity of magnetite nanofluids with increase of volume fraction and temperature. Recently, Zakaria et al. (2015) investigates the electrical conductivity of Al_2O_3 nanofluids in water-ethylene glycol mixture. The finding shows that electrical conductivity decreases as the ethylene glycol increased. However, no investigation of electrical conductivity has been carried out for maghemite nanofluids.

Previous studies also elucidated that the Maxwell model underestimated the electrical conductivity enhancement in nanofluid. This is due to the fact that the electrical conductivity is not only associated with the physical properties of nanofluid but also relates to some other physicochemical properties, such as the shape and size of the nanoparticles, agglomeration, the EDL, the electrophoresis, and the Brownian motion of nanoparticles (Dong et al., 2013; Ganguly et al., 2009; Gao et al., 2007; Minea & Luciu, 2012; Shen et al., 2012).

Several researchers have measured large increases in the electrical conductivity of nanofluids compared to the base fluid as the volume fraction (Cruz et al., 2005; Fang & Zhang, 2005; Ganguly et al., 2009; Lisunova et al., 2006; Wong & Bhshkar, 2006) and temperature (Ganguly et al., 2009) are increased.

CHAPTER 3: METHODOLOGY

This chapter describes the methodology and procedures of the synthesis, characterization, and thermophysical properties of maghemite nanofluids with and without magnetic fields effect. There are three main stages of the experiment. Figure 3.1 shows all steps and procedures of this research.

3.1 Materials

The first stage of the research is the synthesis of maghemite nanoparticles using chemical co-precipitation method. The raw materials for synthesis of maghemite nanoparticles were ferric chloride hexahydrate (Sigma-Aldrich), ferrous chloride tetrahydrate (Sigma-Aldrich), ammonium hydroxide 28 % (Merck), nitric acid 65 % (Merck), hydrochloric acid 37 % (Ajax), ferric nitrate nonahydrate (Sigma-Aldrich), and deionized water.

The second stage of this study involved the preparation of maghemite nanofluids and their stability characterizations. The raw materials used for this phase are sodium hydroxide (Merck), hydrochloric acid (Sigma-Aldrich) and deionized water.

The third stage of the research is the characterization of thermophysical properties of maghemite nanofluids. The raw materials used at this point are maghemite nanofluids and deionized water.

Deionized water with resistivity around 15 MΩ/cm was obtained using ELGA ultra analytic deionized and was used for the preparation of solution throughout the whole experiment. All chemicals were analytical grade and used as received without further purification.

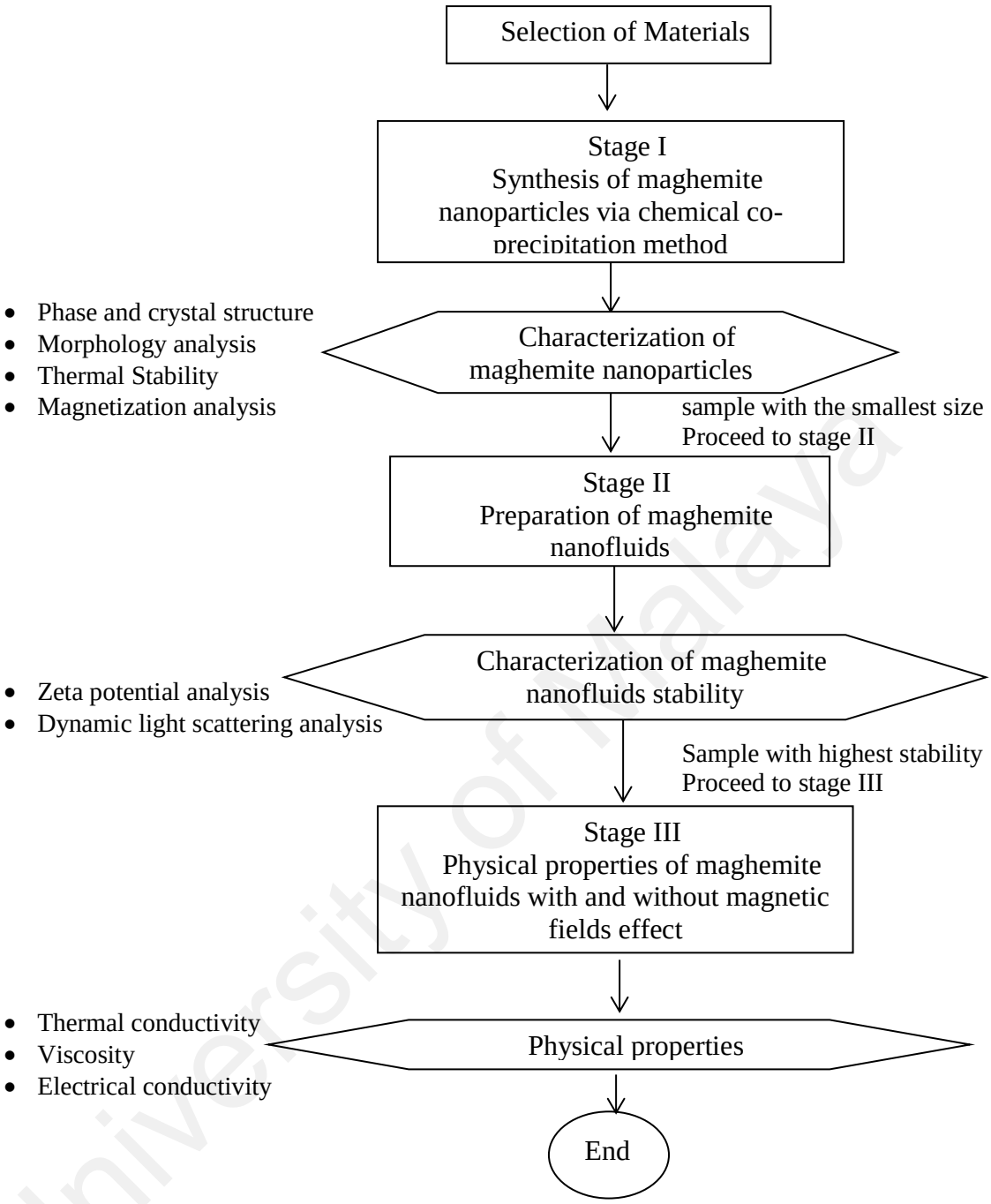

Figure 3.1: Flowchart of research methodology

3.2 Synthesis of Maghemite Nanoparticles

Maghemite nanoparticle was synthesized by a chemical co-precipitation method. In this method, ferric chloride solution (stabilized with a few drops of hydrochloric acid) and ferrous chloride solution with molar ratio 2:1 were mixed. Then ammonium hydroxide solution was added to the solution with vigorous stirring for 20 minutes at room temperature. A black precipitate produced was separated from solution using a

Gmagnet and washed several times by stirring for 5 minutes in deionized water. The precipitate is then stirred for 10 minutes in the nitric acid solution. The precipitate obtained was separated and washed several times and then oxidized to maghemite at 90 ^{o}C for 30 minutes using ferric nitrate solution. Brown precipitate was isolated from solution and then washed thoroughly with deionized water. Powder samples were obtained by drying the suspension in the oven at a slightly elevated temperature. The flow chart of the process is shown in Fig. 3.2. Characterization of maghemite nanoparticles conducted by several methods including X-Ray Diffraction (XRD), Transmission Electron Spectroscopy (TEM), Alternating Gradient magnetometer (AGM), Thermogravimetry Analysis (TGA), Dynamic Light Scattering (DLS) and Zeta Potential Analysis.

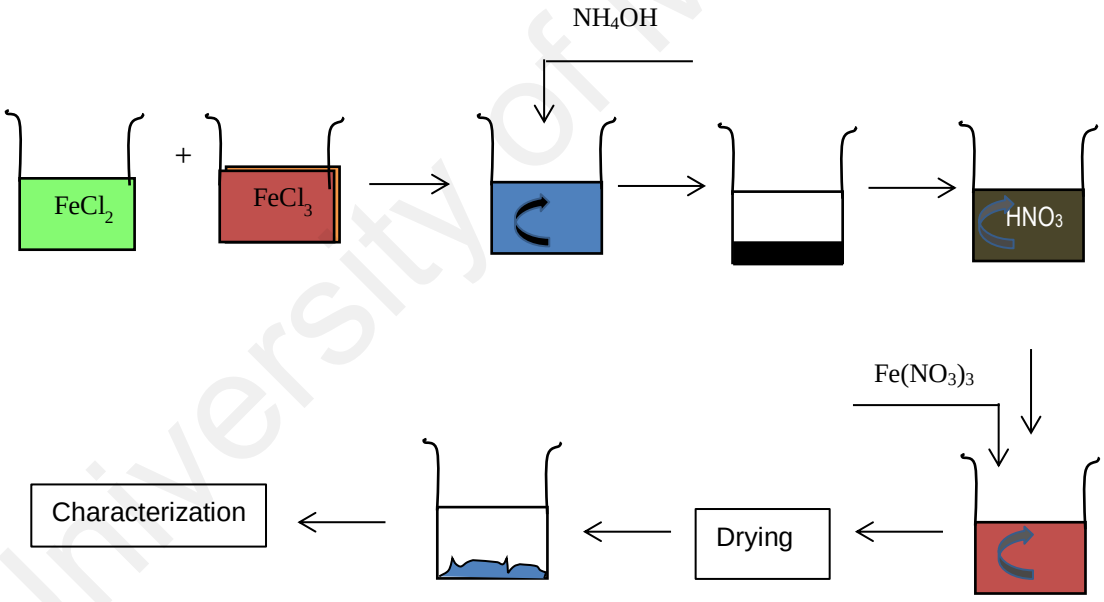

Figure 3.2: Schematic of synthesis of maghemite nanoparticles

3.3 Preparation of Maghemite Nanofluids

The stability analysis was performed at various pHs at certain maghemite nanoparticles volume fraction by adding sodium hydroxide and hydrochloric acid to alter the pH of solutions. The pH of the solution was measured by a pH meter. The effect of time on the stability of maghemite nanofluids were measured at the different time of

storage. The characterization of maghemite nanofluids was conducted by dynamic light scattering and zeta potential analysis at 2, 4, and 8 months of storage.

3.4 Thermophysical properties Measurement

3.4.1 Preparation of Maghemite Nanofluids

Maghemite nanoparticles were synthesized using a chemical co-precipitation method (Nurdin et al., 2014). Maghemite nanofluids were prepared by dilution of a known concentration of a stock solution in deionized water at a different percent of the particle volume fraction of 0.1, 0.2, 0.3, 0.4, 0.5, and 0.6 %.

The concentration of the nanofluids in percent volume fraction can be estimated by Eq. (3.1).

$$\phi = \frac{\frac{m_p}{\rho_p}}{\frac{m_p}{\rho_p}+\frac{m_f}{\rho_f}} \text{ x } 100\ \% \qquad (3.1)$$

where: ϕ : particle volume fraction

m_p : mass of nanoparticles

ρ_p : density of nanoparticles

m_f : mass of base fluids

ρ_p : density of base fluids

3.4.2 Procedure

Thermophysical properties of maghemite nanofluids were studied at various temperature and nanoparticle volume fractions, without and with using external magnetic fields. The suspensions placed in a glass jacketed vessel in which temperature keep constant with a Refrigerated JEIO Tech temperature control circulator. Different magnetic fields strengths were provided by using a pair of an electromagnet which was measured by a magnetometer. Thermophysical properties measured were thermal conductivity, viscosity, and electrical conductivity. Measurements conducted at various

parameters including the effect of temperature, the effect of the particle volume fraction, and effect magnetic fields strength. Schematic of the experimental set up are shown in Figs. 3.3, 3.4, and 3.5, respectively.

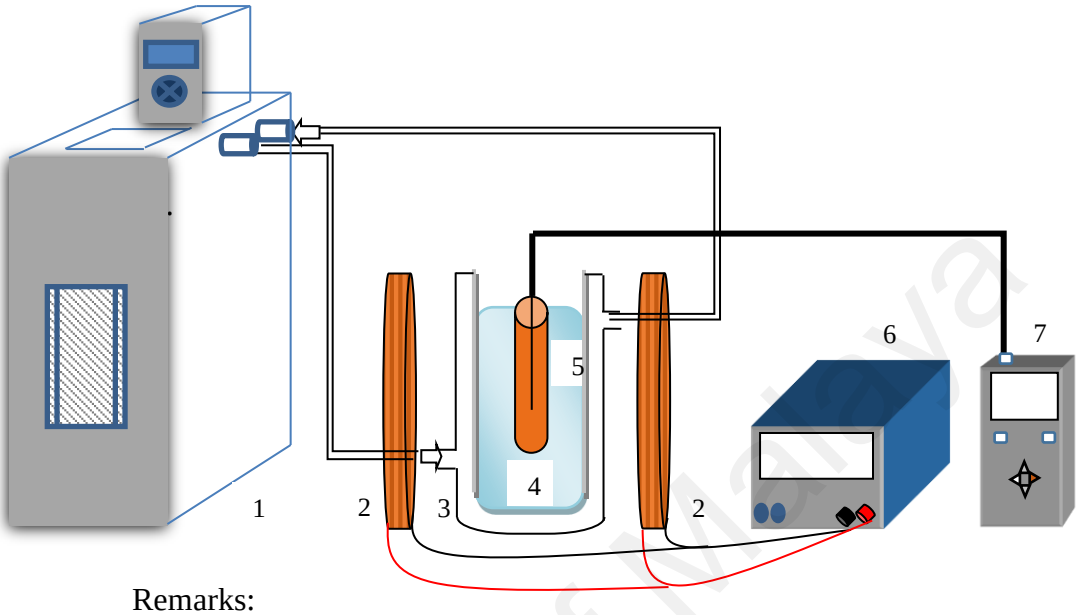

Remarks:
1. Temperature control circulator
2. Electromagnetic coil
3. Jacketed beaker glass
4. Sample
5. Sensor
6. Power supply
7. Thermal conductivity meter

Figure 3.3: Schematic of experimental set up for thermal conductivity measurement

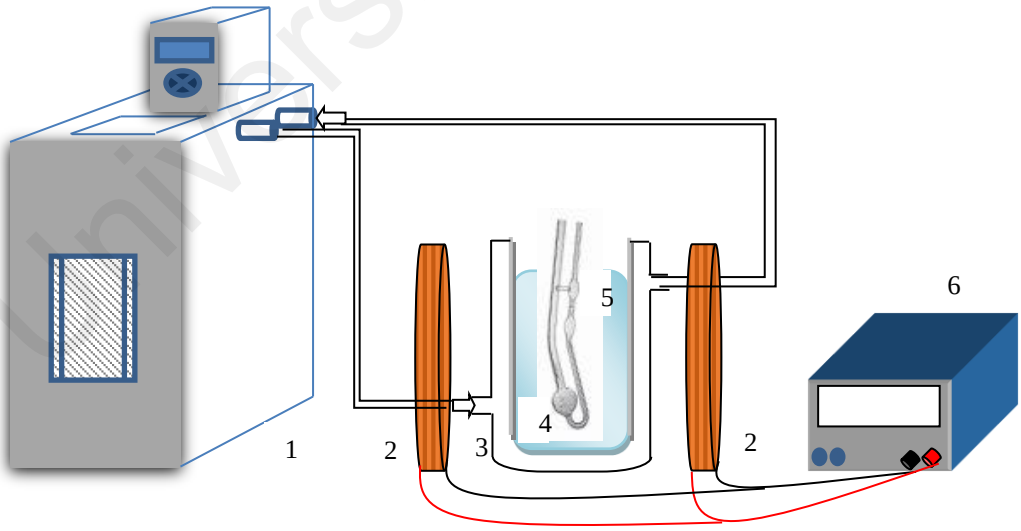

Remarks:
1. Temperature control circulator
2. Electromagnetic coil
3. Jacketed beaker glass
4. Sample
5. Glass capillary viscometer
6. Power supply

Figure 3.4: Schematic of experimental set up for viscosity measurement

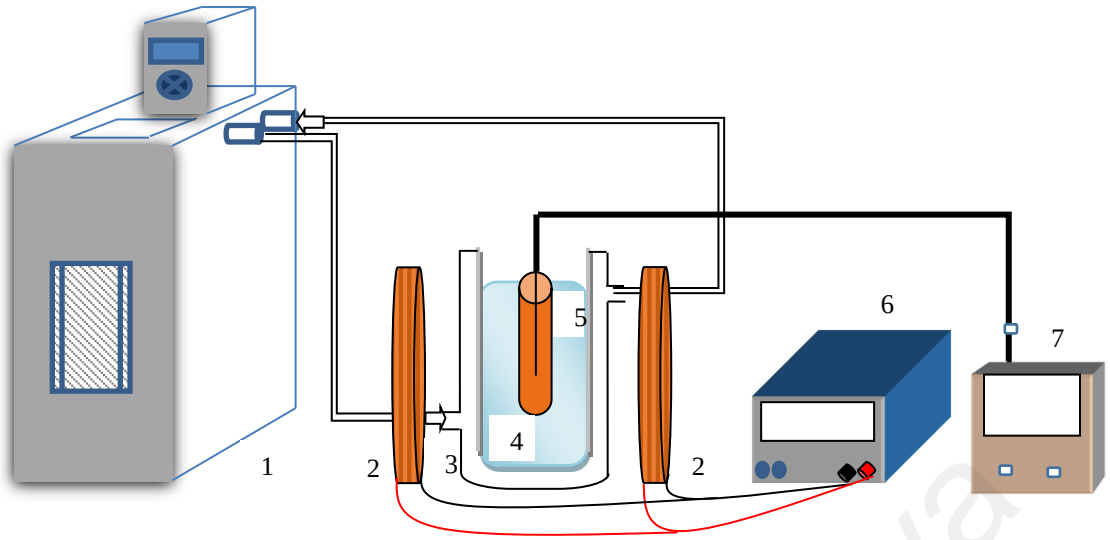

Remarks:

1. Temperature control circulator
2. Electromagnetic coil
3. Jacketed beaker glass
4. Sample
5. Sensor
6. Power supply
7. Conductivity meter

Figure 3.5: Schematic of experimental set up for electrical conductivity measurement

3.4.3 Measurement

Thermal conductivity measurements were conducted by KD2 pro thermal property analyzer equipment by Decagon Devices Company, USA, which is based on the transient hot wire method. The KD2 Pro consists of a handheld controller and sensors that should be inserted into the medium. The single-needle sensor with 1.3 mm diameter and 60 mm length was used (KS-1). The sensor integrates with its interior a heating element and a thermo-resistor, and it is connected to a microprocessor for controlling and conducting the measurements. The measurements were performed using 30 ml sample in a cylindrical glass tube bottle. The needle probe inserted in the sample bottle, then placed and exposed to the water jacketed vessel that the temperature kept constant with a JEO circulating and refrigerating water bath. The samples were allowed in the bath for 30 minutes to get desired temperature. The measurements were conducted at a different temperature, particle volume fraction, and magnetic fields strength. Prior to measurement, the meter was calibrated using the buffer solutions of known thermal conductivities. Moreover, the

measurement of thermal conductivity of water were compared with the thermal conductivity value of water in the literature. The measured value of thermal conductivity value of water was 0.595 W/mK at 20 ^{o}C compared to 0.598 W/mK at 20 ^{o}C (Haynes, 2013). Thermal conductivity data were recorded five times with an interval of 15 minutes at each parameter measurement. The average of data measurements was reported.

The viscosity of the maghemite nanofluids was measured by calibrated glass capillary viscometer as shown in Fig. 3.6. The maghemite nanofluids sample of 7 mL charged into the viscometer from L tube. Place the viscometer into the holder, and insert it into the constant temperature bath and turn the instrument to its normal vertical position. Allow about 10 minutes for the sample to get to the bath temperature desired. Apply suction to N tube in order to draw sample slightly above E mark. To measure the efflux time, let the liquid sample run freely down past F mark. Measuring the time for the meniscus to pass from E mark to F mark. Calculate the kinematic viscosity in mm^2/s (cSt) of the sample by multiplying the efflux time in seconds by the viscometer constant. The measurements were recorded five times at each parameter measurement. The average of data measurements was reported.

Electrical conductivity was measured by a 4-cell conductivity electrode meter (Eutech instrument PC 2700) with inbuilt automatic temperature compensation. Prior to measurement, the meter was calibrated using the buffer solutions of known electrical conductivities. Measurements were performed in 30 ml of the sample in a cylindrical glass tube with the conductivity probe immersed in it. Samples were placed and exposed to water jacketed vessel. The temperature kept constant with a JEO circulating and refrigerating water bath, and allowed in the bath for 30 minutes to get desired temperature. Measurements were conducted at different temperature and particle volume fractions and repeated five times for each parameter.

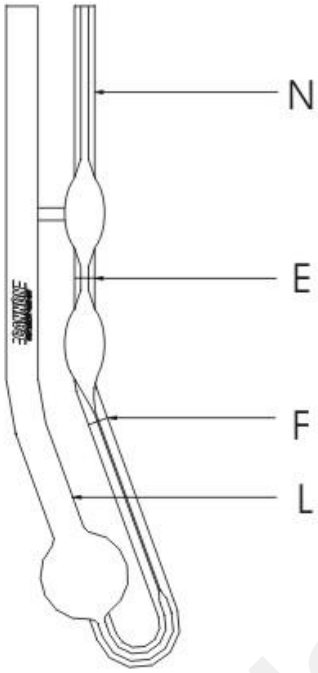

Figure 3.6: Schematic of calibrated glass capillary viscometer (https://www.cannoninstrument.com/Image/GetDocument/437?language=en)

3.5 Characterization Technique

In this section, several characterization techniques performed to characterize the samples have been explained in term of their theory, principles and sample preparations.

3.5.1 X-Ray Diffraction (XRD)

X-Ray powder diffraction (XRD) is one of the most powerful techniques for qualitative and quantitative analysis of crystalline compounds such as a pattern-fitting procedure for quantitative analysis of crystalline pharmaceuticals in solid dosage and a quantitative analysis of binary system of crystalline pharmaceuticals in tablets (Takehira et al., 2010; Yamamura & Momose, 2001). The technique provides information that cannot be obtained any other way. The information obtained includes types and nature of crystalline phase's present, structural makeup of phases, degree of crystallinity, and amount of amorphous content, microstrain and size and orientation of crystallites.

X-Ray diffraction is used to obtain information about the structure, composition and state of polycrystalline materials. Some typical applications are the identification of

unknowns based on the crystalline peaks, precise measurements of lattice constants and residual strains, and refinement of atomic coordinates.

The samples may be powders, solids, films or ribbons. The minimum amount of material required is a few milligrams. Greater accuracy can be achieved if up to a gram of sample is available. For the bulk sample, its surface is usually cleaned with alcohol and placed onto a glass slide before it is put into the sample chamber of the diffractometer. The investigations were performed using continuous scanning method at angles of 2θ within the range of 20^o to 80^o with a step size of 0.05^o and a count time of 1.5 s at each step.

When a material (sample) is irradiated with a parallel beam of monochromatic X-rays, the atomic lattice of the sample acts as a three-dimensional diffraction grating causing the X-ray beam to be diffracted at particular angles. The diffraction pattern that includes position (angles) and intensities of the diffracted beam provides the types of information about the sample. Diffraction of X-rays scattering from the cubic crystal is presented in Fig. 3.7.

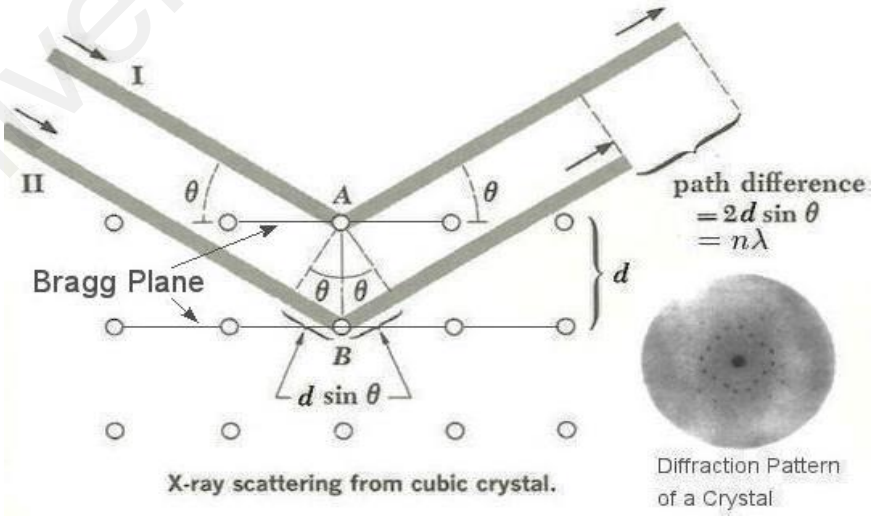

Figure 3.7: Diffraction of x-rays by atoms from two parallel planes (https://universe-review.ca/I13-04-Xdiffraction.jpg).

The phase, structure and crystallite size of the synthesized maghemite nanoparticles were determined using Philips X'Pert MPD PW3040 XRD with CuKα radiation (wavelength of 1.54056 Å). A few milligrams of samples were placed onto a silica slide. The slide was placed into the sample chamber of the diffractometer for XRD measurements. The investigations were performed using continuous scanning method at angles of 2θ within the range of 20° to 80° with a step size of 0.05° and a count time of 1.5 s at each step.

The average crystallite size of sample was calculated from the XRD line broadening using Scherrer's equation:

$$d_{XRD} = \frac{0.9\ \lambda\ (57.3)}{\beta \cos \theta} \qquad (3.2)$$

where, d_{XRD} = calculated crystallite size,

λ = wavelength, 1.54056 Å

β = full width at half maximum (FWHM) of the peaks

θ = diffraction angle

3.5.2 Transmission Electron Spectroscopy (TEM)

Microscopy is often used as a method of particle size analysis in which the individual particles are directly observed and measured. Transmission electron microscopy (TEM) can be used for the direct examination of particles in the size range 0.001 to 5 pm. An electron microscopy uses a series of magnetic lenses to focus an electron beam that is accelerated, by a high potential, through the specimen in a vacuum. The electrons emitted by the filament are accelerated to earth and are focused, via a double condenser lens system. An image from the specimen is obtained on a fluorescent screen via a three- or a four -lens magnification system. An image from electron microscopy is a result of the interaction between the electrons of the beam and the atoms of a solid specimen. The contrasts are formed in TEM by two important mechanisms, namely, diffraction contrast

and phase contrast. The image is focused by the objective lens and magnification is controlled by the excitation of the intermediate lens.

Transmission electron microscopy (TEM) is a microscopy technique in which a beam of electrons is transmitted through an ultra-thin specimen, interacting with the specimen as it passes through. An image is formed from the interaction of the electrons transmitted through the specimen. The image is magnified and focused onto an imaging device, such as a fluorescent screen, on a layer of photographic film, or to be detected by a sensor such as a CCD camera.

The TEM uses a high energy electron beam transmitted through a very thin sample to image and analyze the microstructure of materials with atomic-scale resolution. The electrons are focused with electromagnetic lenses, and the image is observed on a fluorescent screen, or recorded on film or digital camera. The electrons are augmented at several hundred kV, giving a wavelength of 0.025Å. However, the resolution of the optical microscope is limited by the wavelength of light 60 and the aberrations inherent in electromagnetic lenses to about 1-2Å (Fultz & Howe, 2012).

The bright field/dark field imaging modes of the microscope that operate at intermediate magnification, combined with electron diffraction. They are also invaluable for giving information about the morphology, crystal phases and defects in a material. The microscope is also equipped with a special imaging lens, which allows for the observation of micro magnetic domain structures in a field-free environment (Fultz & Howe, 2012). Schematic diagram of TEM is shown in Fig. 3.8.

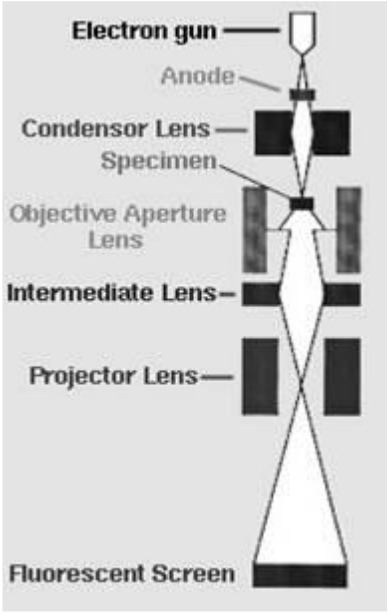

Figure 3.8: Schematic Diagram of TEM (http://www.gitam.edu/eresource/nano/nanotechnology/tem.htm)

Materials have to prepare and processes for suitable samples to view in an electron microscope. This procedure is mainly because the whole of the inside of an electron microscope is under high vacuum to enable the electron beam to travel in straight lines. The technique required varies depending on the specimen, the analysis required and the type of microscope.

Preparation of TEM specimens is particular to the material under analysis and the desired information to obtain from the sample. Many techniques have been used for the preparation of the required thin sections.

In material science and metallurgy, the specimens should be naturally resistant to vacuum, but still must be set as a thin foil, or etched. Moreover, some portion of the sample is thin enough for the beam to infiltrate. Limitations on the thickness of the material may be limited by the scattering cross-section of the atoms from which the material is comprised.

In this study, one drop of low concentration of maghemite nanoparticles suspensions was poured into a 200 mesh copper grip and dried for a night. The morphology and

physical size of the particle were studied using transmission electron microscopy (TEM). The images were taken using a Leo LIBRA transmission electron microscope operated at 120 kV.

3.5.3 Alternating Gradient Magnetometer (AGM)

Magnetic responses of the samples to an applied magnetic field were investigated using a MicroMag™ 2900 AGM with an applied field of ± 10 kOe. AGM is highly sensitive and capable of measuring the magnetic strength and types for wide of materials. Parameters such as saturation magnetization (Ms) value, coercivity, and remnants can be measured.

The system uses an alternating gradient magnetic field to produce a periodic force on a sample in a variable or static D.C. field. If the gradient produced by the coils in the magnetic gap is made AC instead of DC, i.e. the sample is subjected to an alternating force. The alternating force is proportional to the magnitude of the gradient and the magnetic moment of the sample.

The electromagnet produces a uniform magnetic field whereas the pair of gradient coils which are mounted to the electromagnet produces an alternating magnetic field. It means that during the measurement, the sample is magnetized by the uniform field from the electromagnet and simultaneously subjected to an alternating field gradient, which produces an alternating force.

The sample is mounted on an extension rod attached to a piezoelectric element as shown in Fig. 3.9. The resulting deflection of the rod is measured by piezoelectric sensing element mounted on the probe arm. The electrical signals are processed, and a build in software package performs analysis of the magnetic properties.

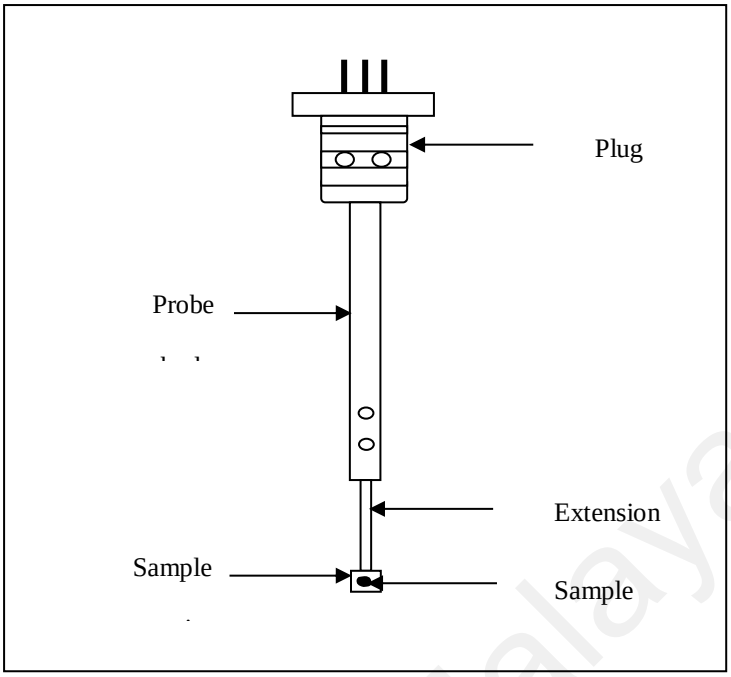

Figure 3.9: Schematic of sample in AGM analysis

The sample was weighted by a microanalytical balance and prepared in a square form of isolation to fit the sample holder of the probe. The sample was inserted into sample carrier at the edge of extension of the probe body. The magnetic properties of the maghemite nanoparticles measured by an Alternating Gradient Magnetometer (AGM) (MicroMag, model 2900) using applied fields of ± 10 kOe at room temperature.

3.5.4 Thermogravimetry Analysis (TGA)

Thermogravimetry analysis (TGA) is a technique that involves continuously measuring the mass of a sample as a function of temperature. This method can be purposed to determine the stabilities of compounds, rates of reaction, decomposition, and composition of samples qualitatively. TGA measurement was using a Metler Toledo Thermogravimetry Analyzer.

The TGA measuring cell may be used for making content determinations or to characterize evaporation and drying, decomposition, oxidation, and oxidative stability. However, some thermal events do not bring about a change in the mass of the sample, such as melting crystallization and glass transition. The measurement is carried out in the

air, or an inert atmosphere, such as Helium or Argon, and the weight is documented as a function of increasing temperature. Occasionally, the measurement is performed in a lean oxygen atmosphere (1 to 5% O_2 in N_2 or He) to slow down oxidation.

A sample is placed into a tared TGA sample pan (crucible) which is attached to a sensitive microbalance assembly. The sample holder portion of the TGA balance assembly is subsequently placed into a high-temperature furnace. The balance assembly measures the initial sample weight at room temperature and then continuously monitors changes in sample weight (losses or gains) as heat is applied to the sample. TGA tests may be run in a heating mode at some controlled heating rate, or isothermally. Typical weight loss profiles are analyzed for the amount or percent of weight loss at any given temperature. The number or percentage of non-combusted residue at some final temperature, and the temperatures of various sample degradation processes, as well as indications of thermal stability.

A few milligrams of powder samples were placed into a crucible and weighed using an electronic microbalance. The crucible was placed in the furnace of the TGA. The weight loss data for each material was collected from ambient temperature to 1000 ^{o}C with a heating rate of 10 ^{o}C/min in the air.

3.5.5 Dynamic Light Scattering (DLS)

Dynamic light scattering (DLS) is also known as photon correlation spectroscopy. This technique is one of the most popular methods used to determine the size of particles. DLS measures Brownian motion and corresponds to the particles size. The Brownian motion is the random movement of particles due to the bombardment by the molecules solvent that surround them. Usually, DLS is concerned with the particles measurement suspended in the liquid. The Brownian motion will be faster if the particles in the liquid are smaller. A knowledge of viscosity is compulsory in the measurement of DLS so known temperature is necessary for DLS. Constant and stable temperature are also the most

important factors. Otherwise, convection currents in the sample will cause non-random movements that will ruin the correct interpretation of size.

The velocity of the Brownian motion is defined by a property known as the translational diffusion coefficient, D. The size of a particle is calculated from the translational diffusion coefficient by using the Stokes-Einstein equation

$$d\,(H) = \frac{kT}{3\pi\eta D} \tag{3.3}$$

where: *d(H)* = hydrodynamic diameter

D = translational diffusion coefficient

k = Boltzmann's constant

T = absolute temperature

η = viscosity

The diameter measured in DLS is a value that denotes to how a particle diffuses within a fluid, so it is stated to a hydrodynamic diameter. The diameter that is obtained by this technique is the diameter of a sphere that has the same translational diffusion coefficient as the particle. The translational diffusion coefficient will depend not only on the size of the particle "core", but also on any surface structure, as well as the concentration and type of ions in the medium.

The advantage of using dynamic light scattering is the possibility to analyze samples containing broad distributions of species of widely differing molecular masses. They include a native protein and numerous sizes of aggregates, and to detect a very small quantity of mass species (<0.01% in many cases). Furthermore, one does not have to worry that protein aggregates are being lost within a chromatographic column because there is no chromatographic separation involved. Moreover, with this technique it is also possible to obtain absolute measurements of several parameters of interest, like molecular weight, the radius of gyration, translational diffusion constant and so on. However, the analysis might be difficult for non-rigid macromolecules. Another limit is that above zero

Kelvin molecules fluctuates (i.e. molecules deviate from their average position). The DLS measurements were using Malvern Zetasizer 3000HS Dynamic Light Scattering.

The Brownian motion occurs in particles or molecules system in the liquids. This motion caused by the movement of particles in the solution by bombardment of particles by the solvent. The intensity of light fluctuates at the rate that depends on the size of particles when the particles or molecules are irradiated with a laser. Smaller particles move rapidly. Analysis of these intensity fluctuations yields the velocity of the Brownian motion and hence the particle size using the Stokes-Einstein relationship.

The speed of particles diffusing due to Brownian motion is measured by dynamic light scattering. This procedure is done by determining the rate at which the intensity of the scattered light fluctuates when identified using a suitable optical arrangement.

If a cuvette, containing particles which are stationary, is illuminated by a laser and a frosted glass screen is used to view the sample cell. The speckle pattern will be stationary both in speckle size and position because the whole system is stationary. For a system of particles undergoing Brownian motion, a speckle pattern is observed where the position of each speckle is seen to be in constant motion. This is because the phase addition from the moving particles is constantly evolving and forming new patterns. The rate at which these intensity fluctuations occur will depend on the size of the particles. The small particles cause the intensity to fluctuate more rapidly than the large ones.

Size is obtained from the correlation function by using various algorithms. Two approaches can be taken. First, fit a single exponential to the correlation function to obtain the mean size (z-average diameter), and an estimate of the width of the distribution (polydispersity index) (this is called the Cumulants analysis and is defined in ISO13321 Part 8). Second, fit a multiple exponential to the correlation function to obtain the distribution of particle sizes (such as Non-negative least squares (NNLS) or CONTIN.

The size distribution obtained is a plot of the relative intensity of light scattered by particles in various size classes and is therefore known as an intensity size distribution.

The sample was pour in the cuvette and inserted into the sample cell. The analysis was conducted at 25 ^{o}C.

3.5.6 Zeta Potential Analysis

Zeta potential is a scientific term for electrokinetic potential in colloidal dispersions. It is usually denoted using the Greek letter zeta (ζ), hence ζ-potential. The electric potential at the boundary of the double layer is known as the Zeta potential of the particles and has values that typically range from +100 mV to -100 mV.

The zeta potential is the potential at the slipping plane, which is the outer boundary within which all ions diffuse with the particle. The zeta potential is the influence of the surface charge density, and as such, any change in the surface charge, either valence or ion condensation, will lead to changes in the measured zeta potential.

Most of the particles dispersed in a liquids system will gain a surface charge, primarily by ionization of surface molecules or adsorption of charged species. These surface charges alter the distribution of the surrounding ions, causing in a layer nearby the particle that is dissimilar to the bulk solution. This layer moves as part of the particle if the particle moves under Brownian motion, for example. The zeta potential is the potential at the point in this layer where it transfers past the bulk solution. This point is usually called the slipping plane. The charge at this plane will be very sensitive to the concentration and nature of ions in solution. The schematic representation of zeta potential is presented in Fig. 3.10.

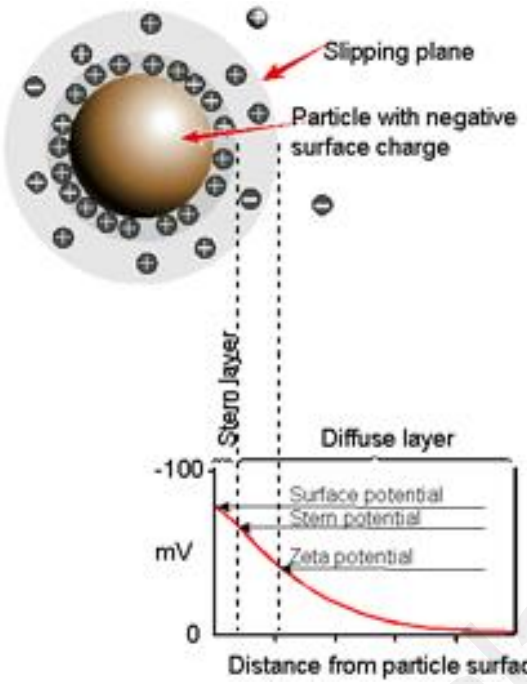

Figure 3.10: Schematic representation of zeta potential (http://www.malvern.com/en/support/resource-center/technical-notes/TN101104ZetaPotentialIntroduction.aspx?)

The level of the zeta potential gives an indication of the potential stability of the colloidal system. Zeta potential is one of the key power that facilitate interparticle interactions. Particles with a higher zeta potential of the similar charge sign, either positive or negative, will repel each other. Usually, a high zeta potential can be high in a positive or negative sense, i.e. < −30 mV and > +30 mV would both be considered as high zeta potentials. The high zeta potential will confer the stability of the solution, which means that the dispersion will resist aggregation.

Several factors affecting zeta potential are:

1. pHs, the pH of the sample is one of the most important factors that affects zeta potential. Zeta potential versus pH curve will be positive at low pH and negative at high pH. There may be a point where the plot passes through zero zeta potential. This point is called the isoelectric point and is very important from a practical consideration.
2. Thickness of double layer, the thickness of the double layer depends upon the concentration of ions in solution and can be calculated from the ionic strength of the

medium. The higher the ionic strength, the more compressed the double layer becomes. The valence of the ions will also influence double layer thickness.

3. Concentration of a formulation component, the effect of the concentration of a formulation component on the zeta potential can give information to assist in formulating a product to give maximum stability.

Zeta potential is determined by applying an electric field through the dispersion. Particles in the dispersion will migrate toward the electrode of reverse charge with a velocity relational to the level of the zeta potential.

The velocity is measured using the technique of laser Doppler anemometry. The frequency shifts or phase shift of an incident laser beam caused by these mobile particles is measured as the particle mobility. This movement is converted to the zeta potential by entering the dispersant viscosity, and the utilization of the Smoluchowski or Huckel theories. These theories are approximations suitable for most applications. More recent models are available which can give a more exact conversion, but require more knowledge of the chemistry of the dispersion.

In electrolyte containing media, ions from dispersion medium adsorb onto the particle surface. In general, the first adsorbed monolayer of ions consists of negatively charged, fixed, and dehydrated ions which is called the inner Helmholtz layer. The second monolayer adsorbed consists of positively charged, fixed but hydrate ions, which is called outer Helmholtz layer. Both Helmholtz layer together are called the Stern layer. The not yet compensated negative charge of the surface is compensated by freely diffusing counter ions, which is called diffuse layer. The border of diffuse layer is defined where the particle surface charge is fully compensated as shown in Fig.3.11.

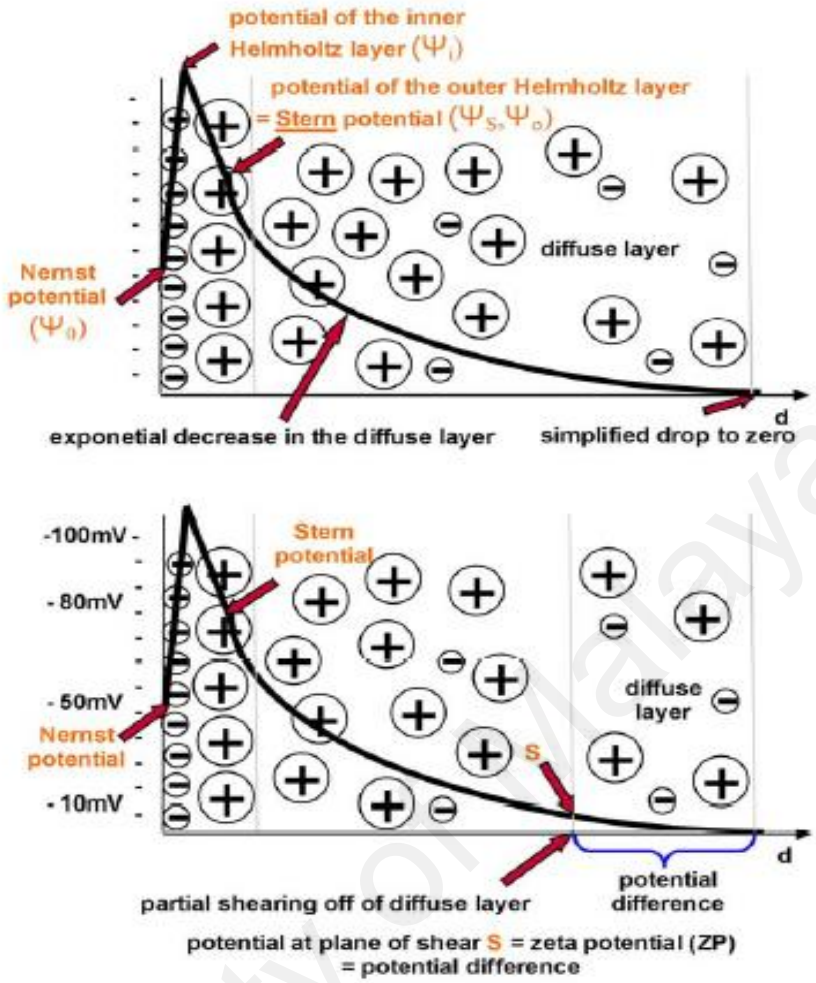

Figure 3.11: Stern model of zeta potential theory (http://www.diss.fu-berlin.de/diss/servlets/MCRFileNodeServlet/FUDISS_derivate_000000002344/06_7Chapter7.pdf?hosts)

The negative Nernst potential increases further in the inner Helmholtz layer due to the adsorption of negative ions, followed by a slight decrease in the outer Helmholtz layer. Increase and decrease are linear. In the diffuse layer decays exponentially towards zero due to the positively charged counter ions.

The zeta potential is determined by measuring the electrophoretic particle velocity in an electrical field. During the particle movement the diffuse layer is shorn off, hence the particle obtains a charge due to the loss of the counter ions in the diffuse layer this potential at the plane of shear is called the zeta potential.

With increasing electrolyte concentration, the surface charge will be compensated at a lower distance from the particle surface, which means the potential drops faster and the diffuse layer is thinner. Consequently, the measured zeta potential decreases with an increasing electrolyte concentration, whereas it decreases faster with increasing the valence of the counter ions, that means increasing from sodium to e.g. calcium and aluminum. Consequently, the stability of the suspensions is reduced.

The sample was injected by syringe into the sample cell and measured at the same temperature as DLS measurement.

CHAPTER 4: RESULTS AND DISCUSSIONS

This chapter describes the results and discussion of the synthesis, characterization and thermophysical properties of maghemite nanofluids with and without the effect of external magnetic fields.

4.1 Synthesis of Maghemite Nanoparticles

4.1.1 Effect of Nitric Acid Concentration

Synthesis of maghemite nanoparticles was conducted by chemical co-precipitation method. In this stage, the effects of nitric acid concentration on the synthesis of maghemite nanoparticles were studied. Five samples were prepared with different nitric acid concentrations of 2 M (MNA2), 4 M (MNA4), 6 M (MNA6), 8 M (MNA8) and 10 M (MNA10). The particles were characterized by XRD, TEM, AGM, TGA, DLS, and Zeta Potential. The summary of measurements for all samples are listed in Table. 4.1.

Table 4.1: Particles size, magnetic property, zeta potential and temperature stability of maghemite nanoparticles

Samples	XRD (nm)	TEM (nm)	AGM (emu/g)	DLS (nm)	Zeta Potential (mV)	T_S (^oC)
MNA2	14.2 ± 1.20	16.2 ± 2.79	42.4	247.7	36.0	525
MNA4	13.9 ± 1.15	15.6 ± 2.68	38.6	118.1	37.6	485
MNA6	12.8 ± 0.80	14.7± 2.16	36.6	93.1	39.7	475
MNA8	11.4 ± 0.80	10.9 ± 2.28	34.2	73.6	41.7	460
MNA10	10.6 ± 0.81	9.3 ± 2.74	32.1	45.3	44.6	450

The XRD patterns of the nanoparticles are shown in Fig. 4.1. The patterns show well-defined peaks that clearly indicate that the sample is crystalline. The peaks also show broadening that indicate the crystallite sizes of the sample are in nanometer dimensions. The peaks corresponding to (220), (311), (400), (511), and (440) planes are clearly observed. and located at angle of 2θ = 30.33, 35.71, 43.39, 57.43, and 62.97, respectively.

The pattern is very close to the ICDD PDF card Number 39-1346 which confirm that the particles are maghemite as shown in Table 4.2.

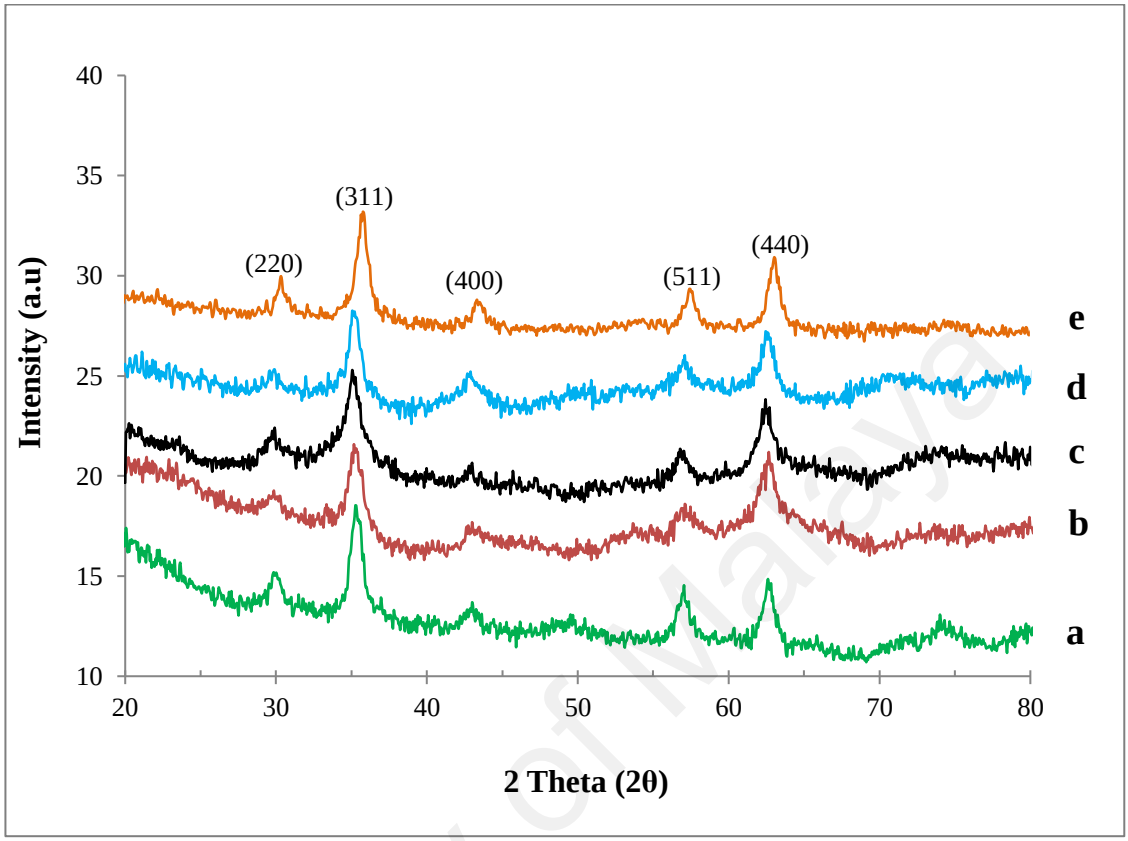

Figure 4.1: XRD patterns of maghemite nanoparticles for samples: (a) MNA2, (b) MNA4, (c) MNA6, (d) MNA8, and (e) MNA10

Table 4.2: Comparison between XRD characteristic peaks of the sample and standard

As-prepared ϒ-Fe_2O_3		**ICDD PDF 39-1346**	
Angle (2θ)	Miller indices (*hkl*)	Angle (2θ)	Miller indices (*hkl*)
30.331	220	30.266	220
35.710	311	35.661	311
43.390	400	43.321	400
57.429	511	57.323	511
62.967	440	62.983	440

The crystal structure and actual lattice parameter of the samples are also determined using data extracted from the XRD pattern. The crystal structure (Bravais lattice) is identified by indexing the Miller indices (*hkl*) of the samples, which is determined by observation the values of $\sin^2\theta$ and lattice parameter as shown in Tables 4.3 and 4.4. The reflection peaks in the pattern can be indexed to face center cubic phase with lattice parameter of a = 8.334 Å. This is in agreement with the bulk lattice parameter of maghemite (a = 8.3474 Å) (Teja & Koh, 2009). The lattice parameter and particle size from XRD calculations are shown in Fig. 4. 2.

Table 4.3: Indexing of the Miller indices of maghemite sample

2θ	**$\sin^2\theta$**	**1x $\frac{\sin^2\theta}{\sin^2\theta_{min}}$**	**2x $\frac{\sin^2\theta}{\sin^2\theta_{min}}$**	**8x $\frac{\sin^2\theta}{\sin^2\theta_{min}}$**	***$h^2 + k^2 + l^2$***	***hkl***
30.3307	0.0684	1.0000	2.0000	8.0000	8	220
35.7096	0.0940	1.3736	2.7472	10.9890	11	311
43.3899	0.1366	1.9968	3.9935	15.9740	16	400
57.4285	0.2308	3.3728	6.7456	26.9824	27	511
62.9668	0.2727	3.9708	7.9708	31.8831	32	440

Table 4.4 : Lattice parameter calculation

2θ (º)	**d-spacing (Å)**	**Miller Indices (hkl)**	**Lattice Constant (Å)**
30.3307	0.0684	220	8.329
35.7096	0.0940	311	8.333
43.3899	0.1366	400	8.335
57.4285	0.2308	511	8.331
62.9668	0.2727	440	8.344
		$a_{average}$	**8.334**

To determined the value of FWHM and β, a Profile Fitting software, *Profit* is used. This program decomposes a powder diffraction pattern into its constituent Bragg reflections and yields defining parameters of each reflection. Lanthanum hexaboride (LaB_6) is purposed as a standard calibration material for instrumental broadening measurement. The calculated average crystallite sizes are presented in Table 4.1. It is shown that the crystallite size of nanoparticles is gradually reduced if the concentration of nitric acid is increased.

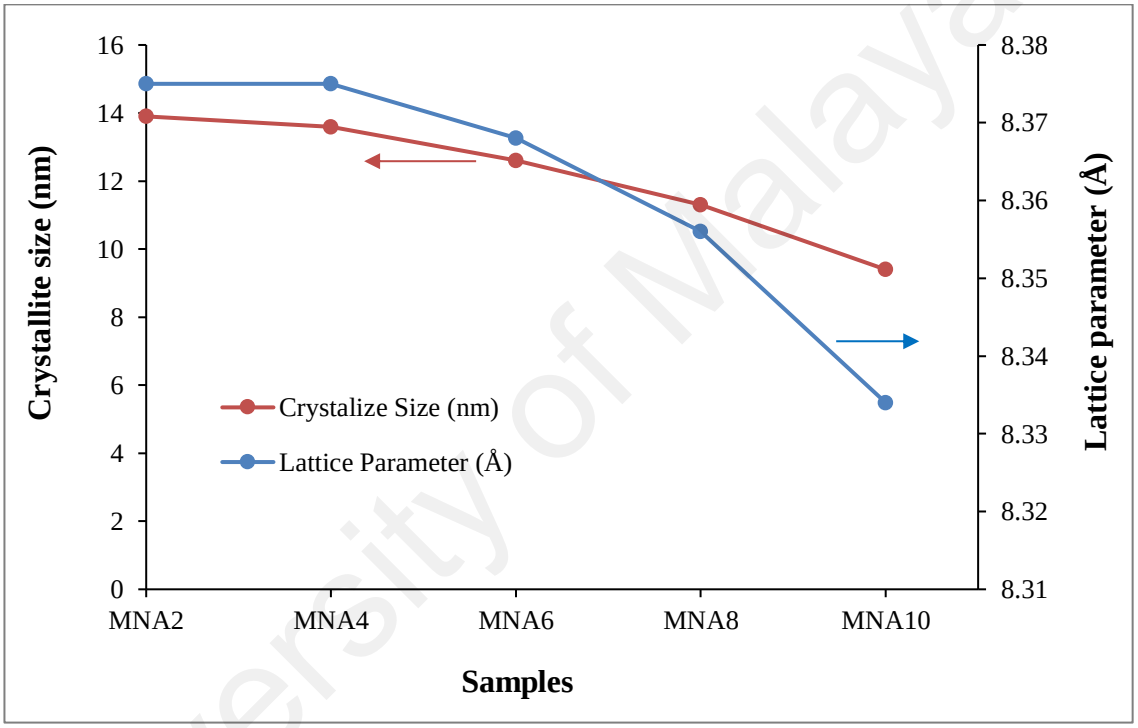

Figure 4.2: Particle size and lattice parameters

The shape and size distribution of maghemite nanoparticles were examined by transmission electron microscopy (TEM) as shown in Figs. 4.3 – 4.12. It is evidently observed that the maghemite particles have the spherical morphology and small particle size. The sizes of the particles were determined from about 100 particles and listed in Table 4.1. There are a few larger 'particles' which are found to be aggregates, which may be due to long-range magnetic dipole-dipole interaction between the particles. This average physical size is in a good agreement with the crystallite size obtained from XRD

measurement indicating that the particles are mostly monocrystals. It can also be seen that the particles show normal size distribution.

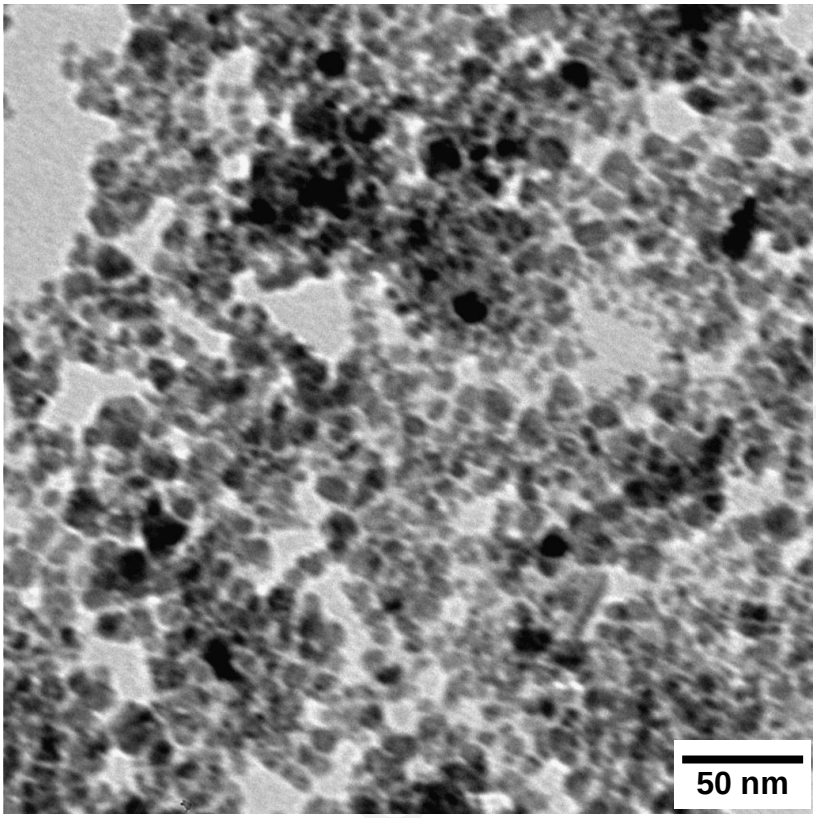

Figure 4.3: TEM images of maghemite nanoparticles for samples MNA2

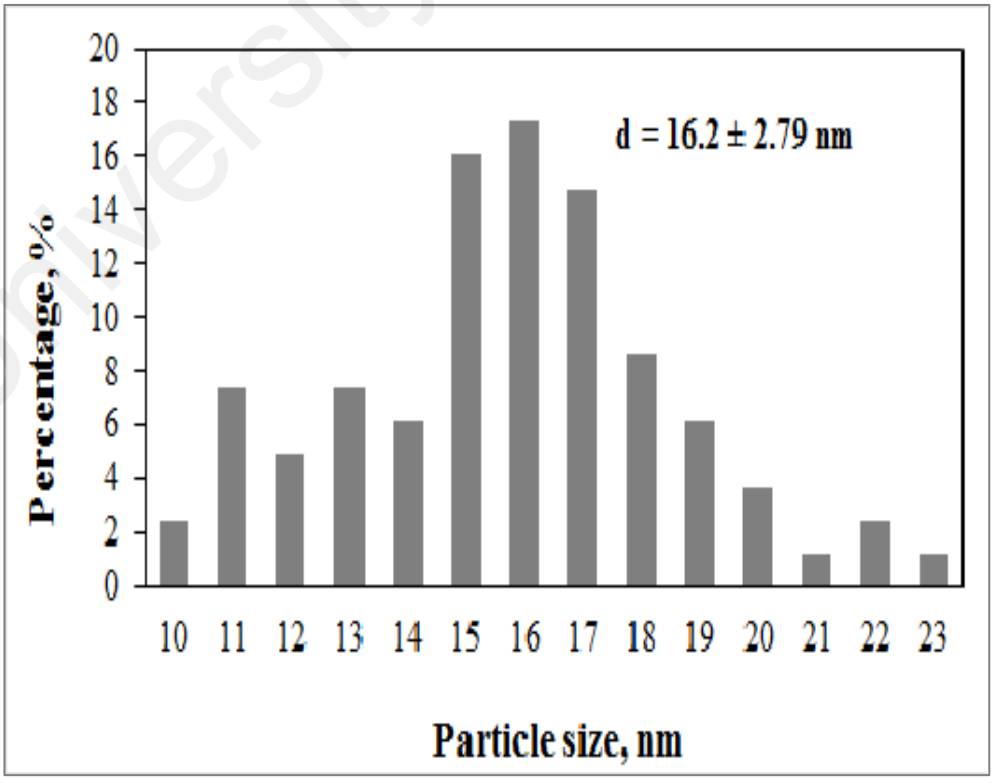

Figure 4.4: Particle distribution for maghemite nanoparticles for samples MNA2

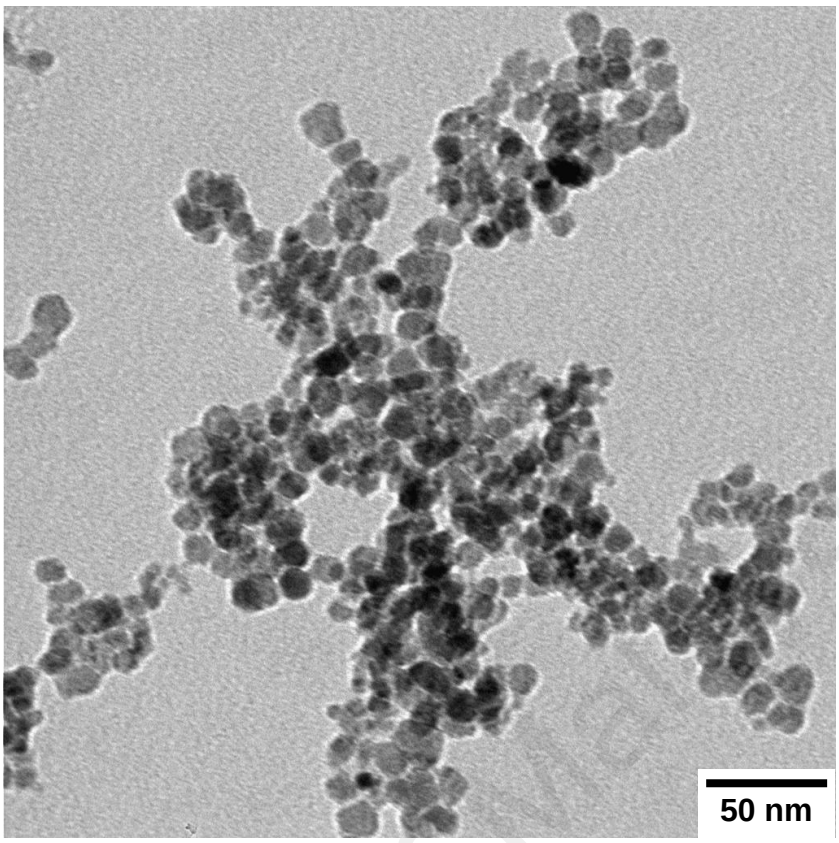

Figure 4.5: TEM images of maghemite nanoparticles for samples MNA4

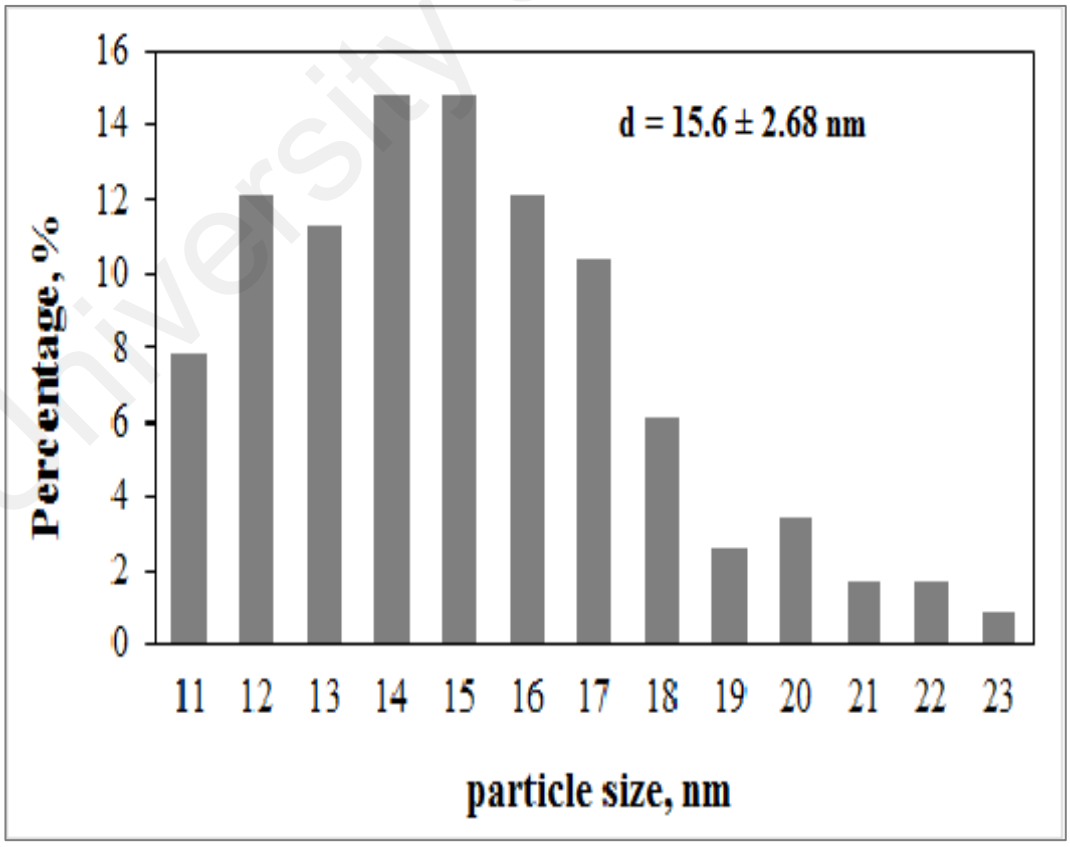

Figure 4.6: Particle distribution for maghemite nanoparticles for samples MNA4

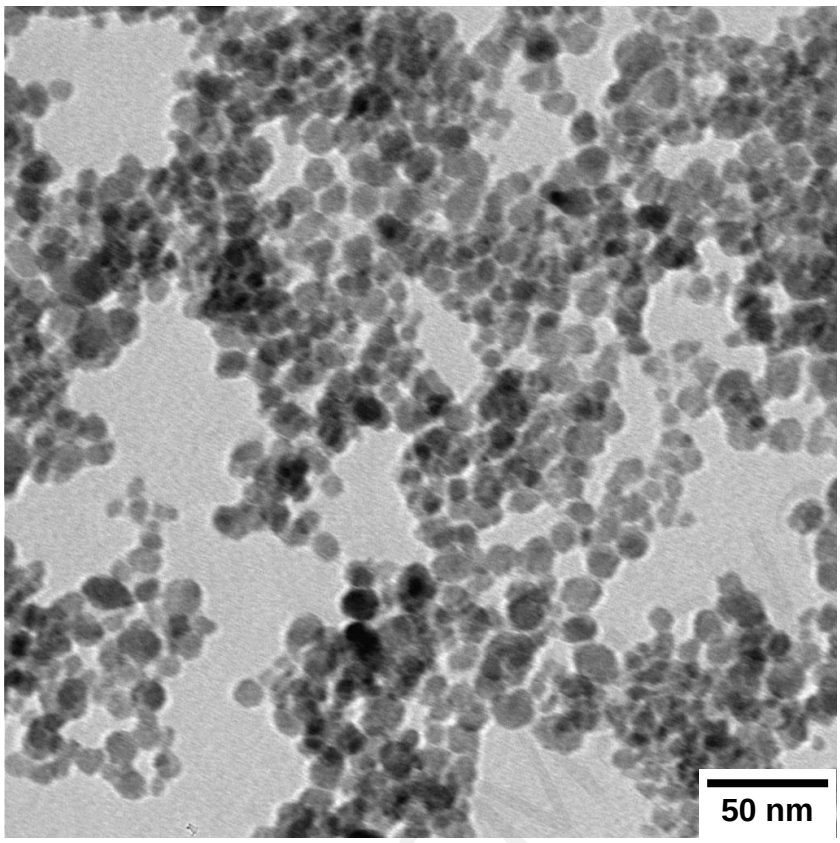

Figure 4.7: TEM images of maghemite nanoparticles for samples MNA6

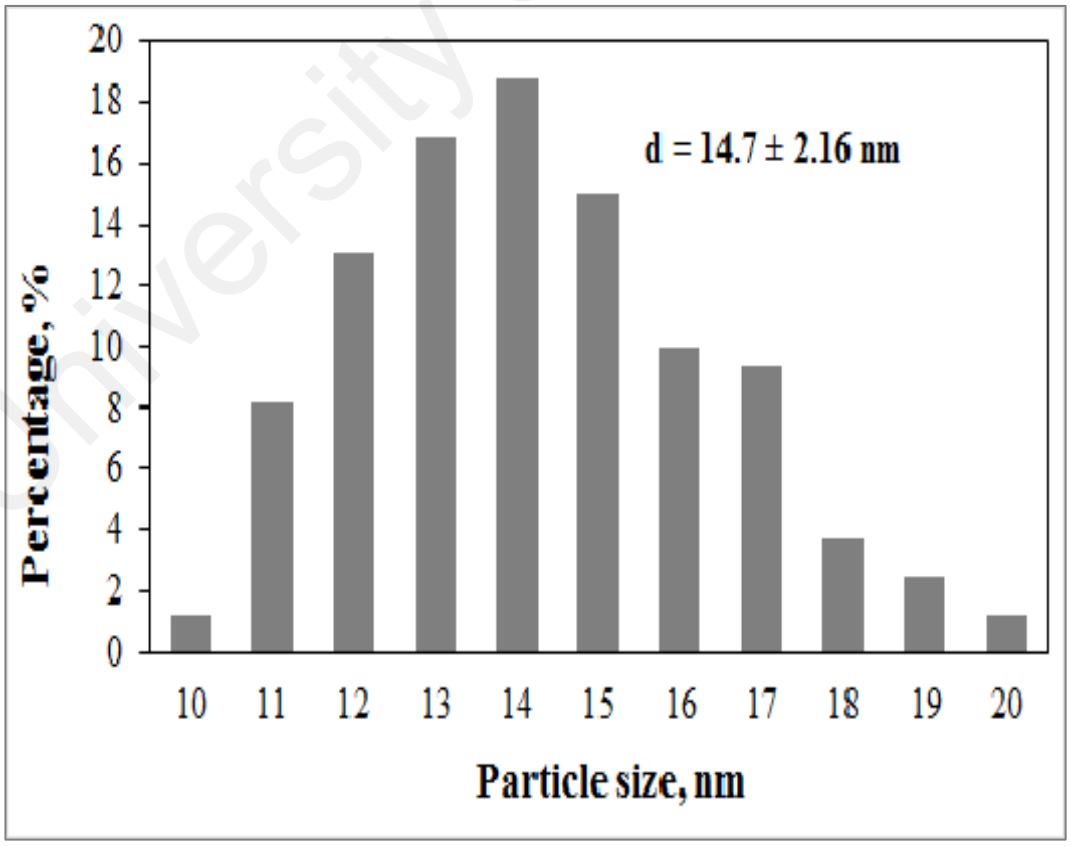

Figure 4.8: Particle distribution for maghemite nanoparticles for samples MNA6

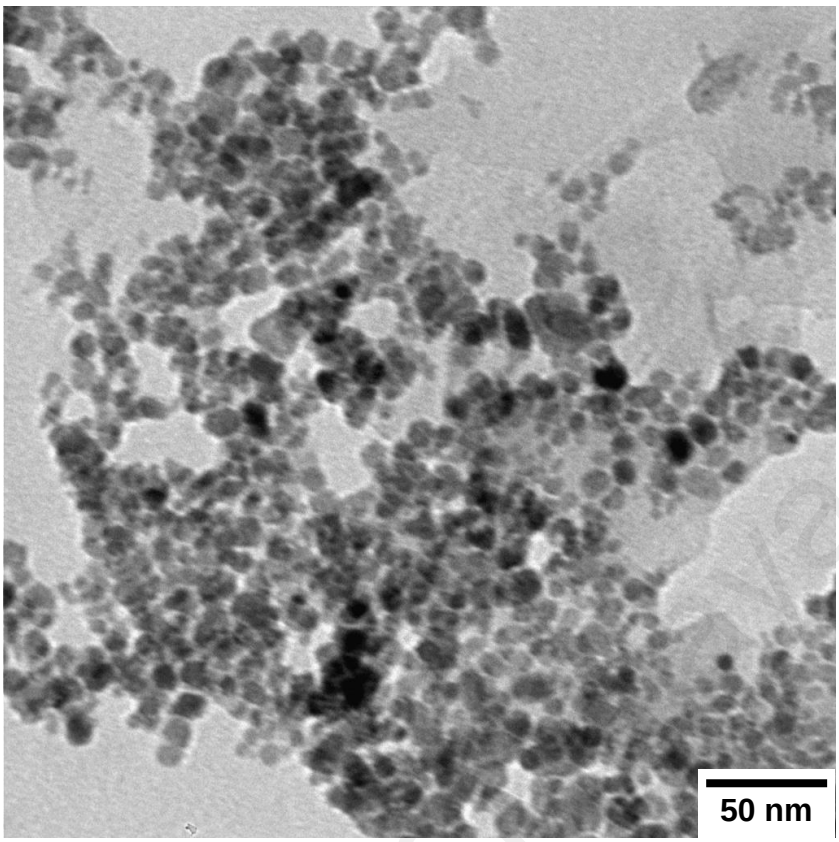

Figure 4.9: TEM images of maghemite nanoparticles for samples MNA8

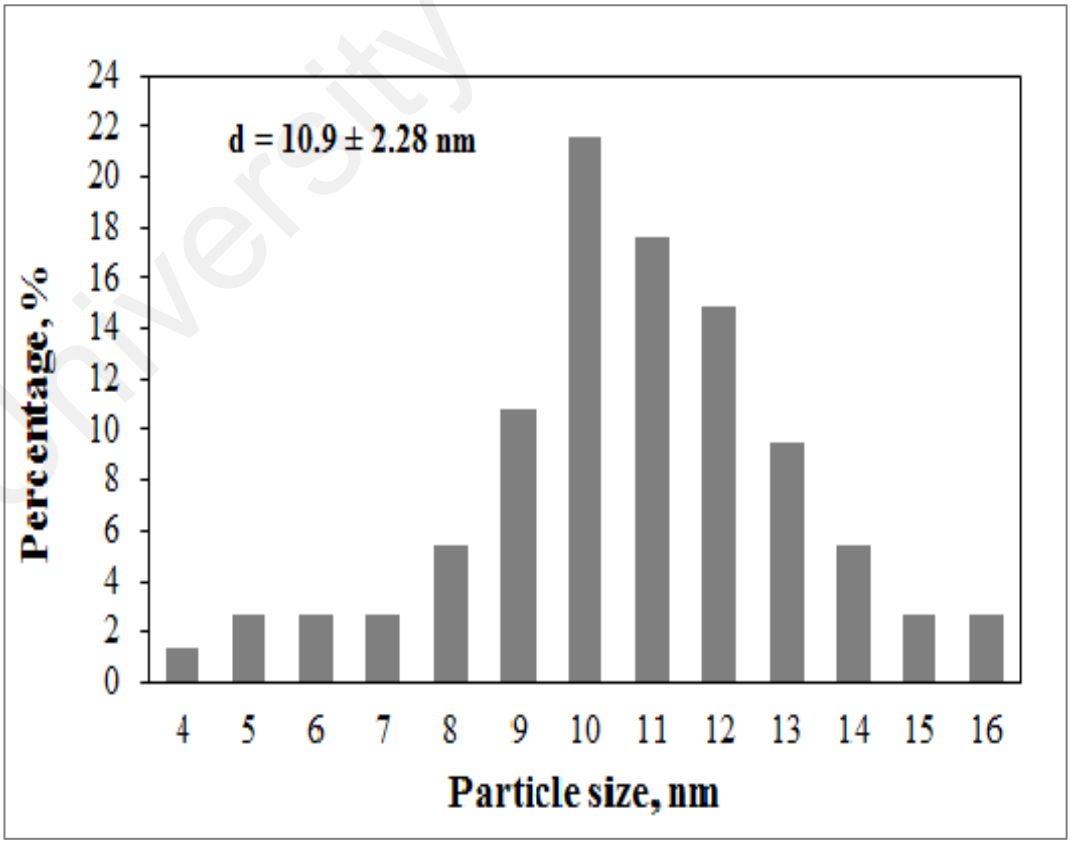

Figure 4.10: Particle distribution for maghemite nanoparticles for samples MNA8

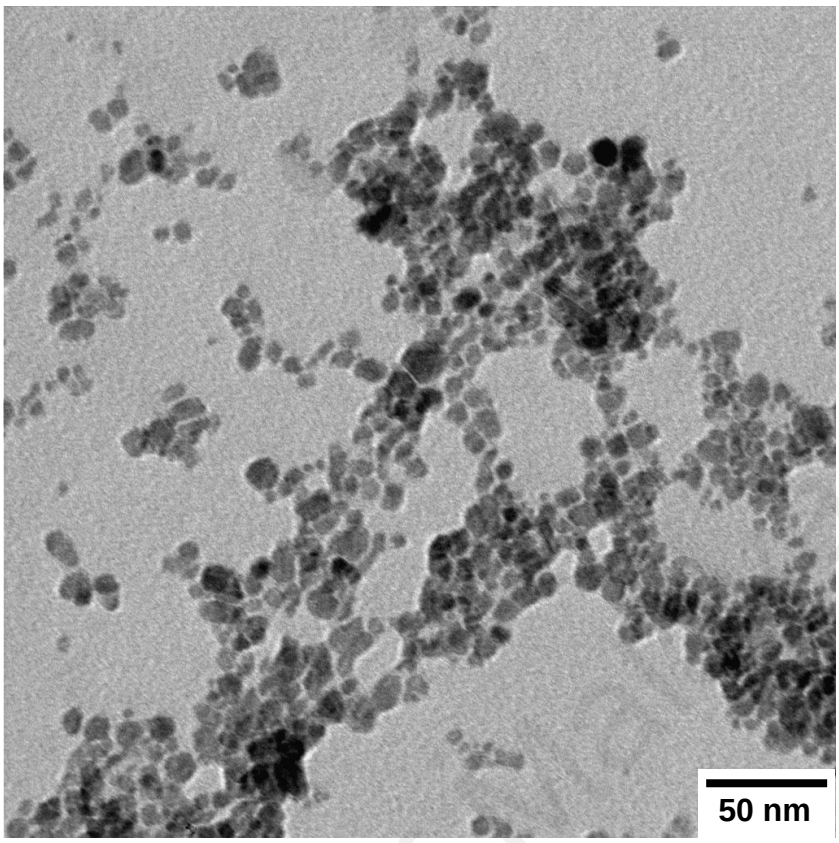

Figure 4.11: TEM images of maghemite nanoparticles for samples MNA10

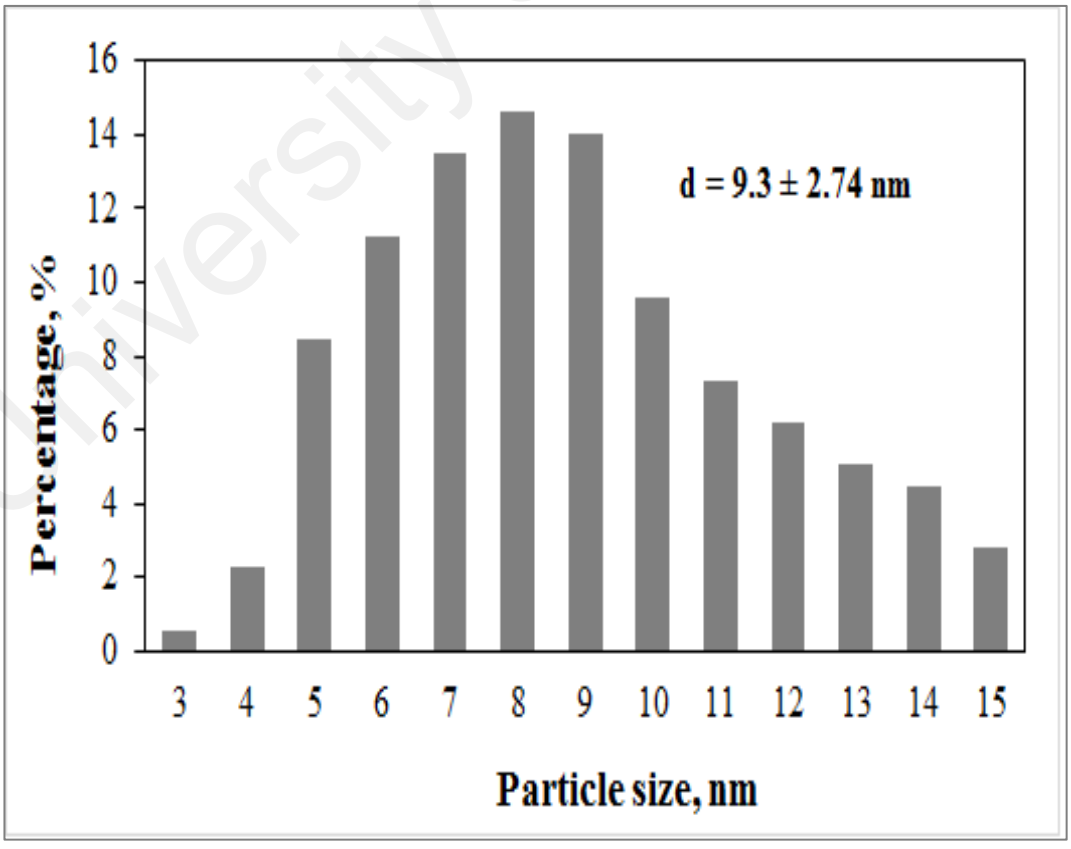

Figure 4.12: Particle distribution for maghemite nanoparticles for samples MNA10

The magnetization curve of the maghemite nanoparticle is shown in Fig. 4.13. It is clear that the curves do not exhibit hysteresis and passes through the origin, which indicates that the samples are superparamagnetic. The saturation magnetization values of maghemite nanoparticle at room temperature for samples MNA2, MNA4, MNA6, MNA8, and MNA10 are 42.4, 38.6, 36.6, 34.2, and 32.1 emu/g, respectively and the data are presented in Table 4.1. These values are smaller than that of bulk maghemite (74 emu/g). This condition is related to the crystallite size of maghemite particles that are in nanosize range. This phenomenon is usually observed in nanoparticle interacting systems. Such a decreasing of magnetization can be ascribed to surface effects arising from broken symmetry and reduced coordination of atoms lying at the surface of maghemite nanoparticles. It is also caused by a high degree of interparticle interactions (Kluchova et al., 2009).

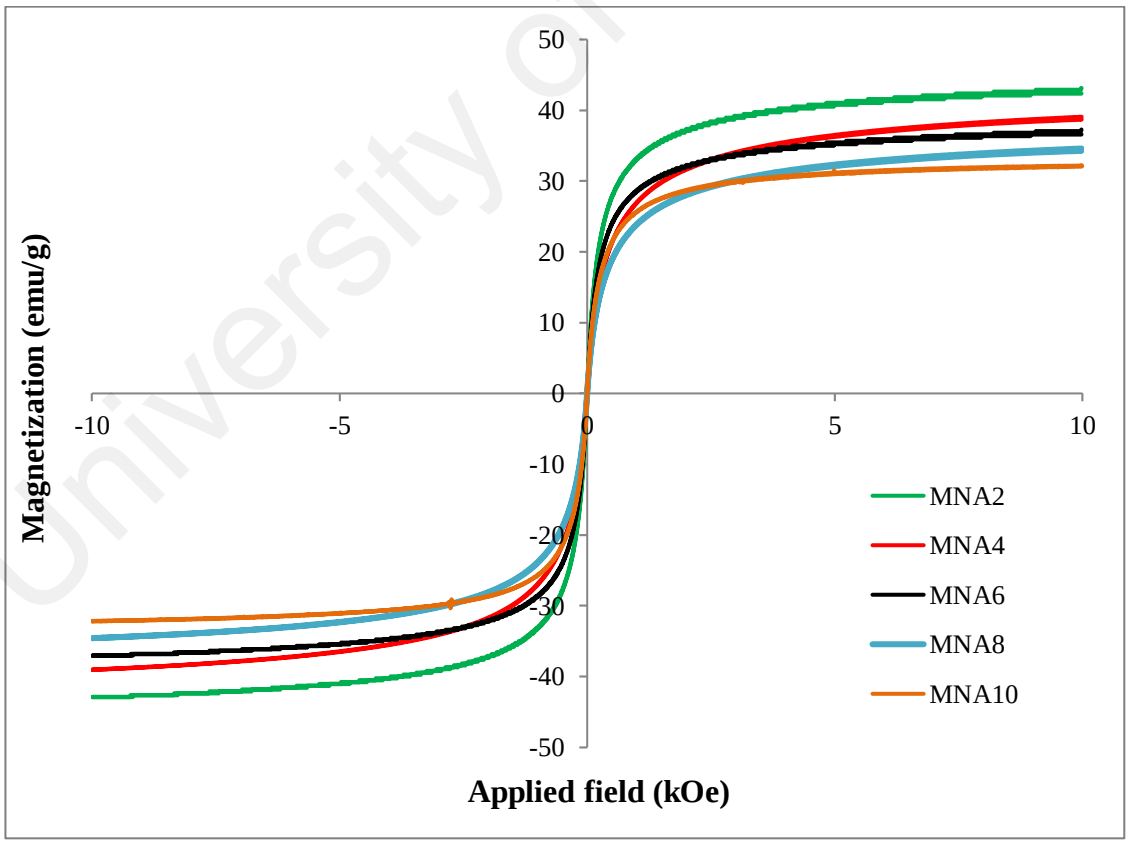

Figure 4.13: Magnetization curve of maghemite nanoparticles for all samples

TGA curves of the maghemite nanoparticle at different nitric acid concentration are shown in Fig. 4.14. It can be seen that the curves reveal similar weight loss behavior and display two weight loss steps. The first weight loss is associated with the evaporation of absorbed water and crystalline water from the sample. The final weight loss might be attributed to the volatilization of the remainder bonding water in the sample which evaporated at the critical temperature of 374 ^{o}C. No further significant weight loss or gain is found in the temperature range of 400 to 1000 ^{o}C, indicating crystalline of maghemite has been formed completely. The temperature stability (T_s) for all samples when maghemite entirely formed is presented in Table 4.1. It was displayed that the temperature stability reduces with increasing concentration of nitric acid. This phenomenon indicates that sample with the most concentrated nitric acid is stabilized earlier than other samples.

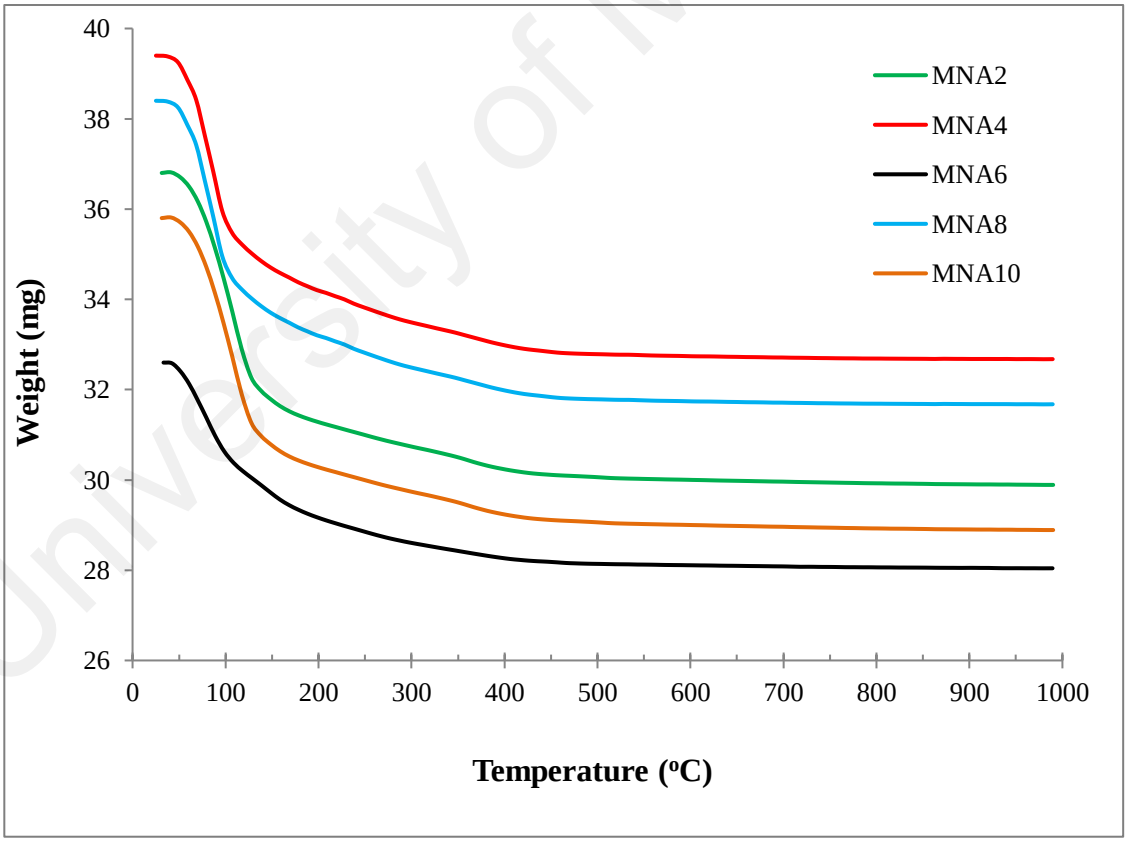

Figure 4.14: TGA thermogram of maghemite nanoparticles for all samples

The particle size distributions of maghemite nanofluids obtained from dynamic light scattering (DLS) measurement are shown in Fig. 4.15. The averaged particle size of maghemite nanoparticles for all samples are listed in Table 4.1, indicates that the increase of nitric acid concentration maghemite nanoparticles with decreasing diameter. High concentration of nitric acid will suppress double layer of ions around the particles, enhancing the diffusion speed and resulting smaller hydrodynamic diameter. It is also displayed that the particle sizes obtained are larger than the TEM results due to the hydrodynamic diameter of particles and its surrounding solvent layers.

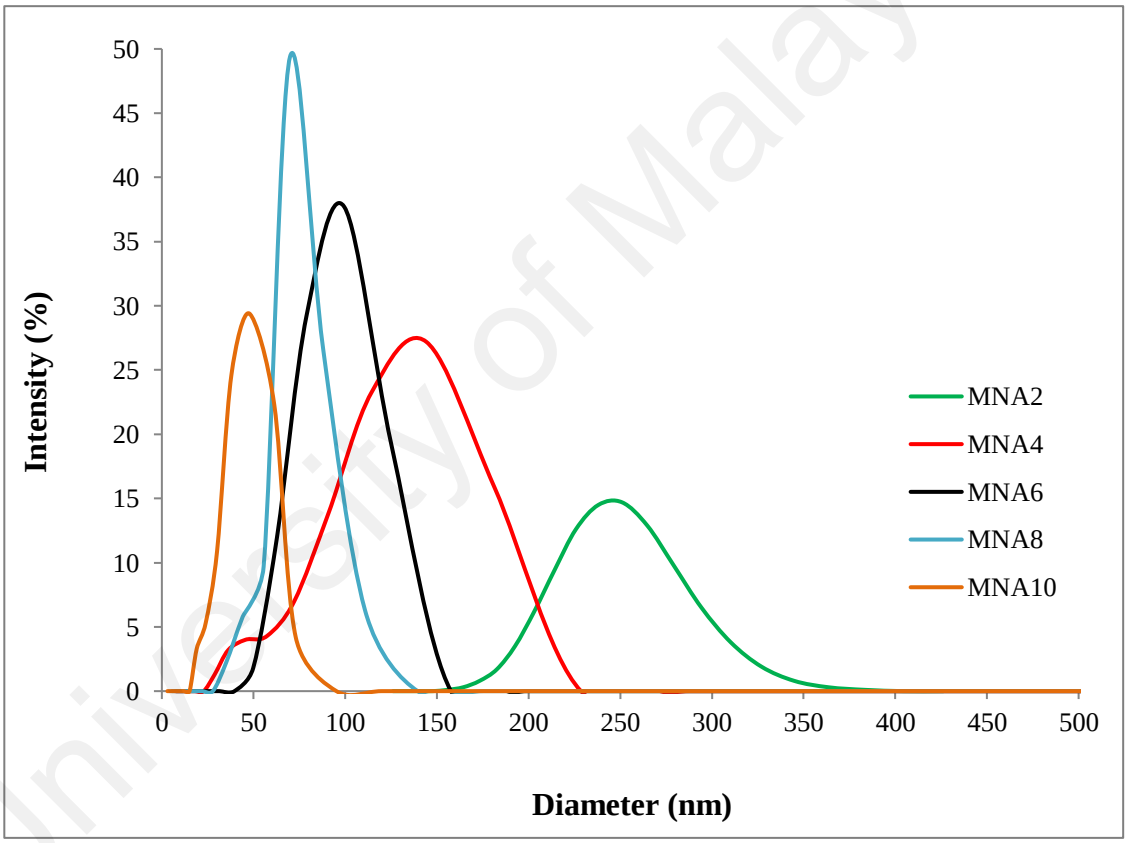

Figure 4.15: DLS measurement of maghemite nanoparticles for all samples

The stability of the suspension is related to its electrokinetics properties. Therefore, the study of electrophoretic behavior through measurement of zeta potential becomes necessary for understanding the stability of suspension (Singh et al., 2005). It is recognized that nanoparticles suspension become stable with a zeta potential value higher than ± 30 mV. The zeta potential of maghemite nanofluids is shown in Fig. 4.16 and their

values are listed in Table 4.1. These values indicate that the maghemite nanofluids are stable. Increasing concentration of nitric acid will compress the thickness of the double layer, hence increasing the particle charge. As a result, it will increase the zeta potential value.

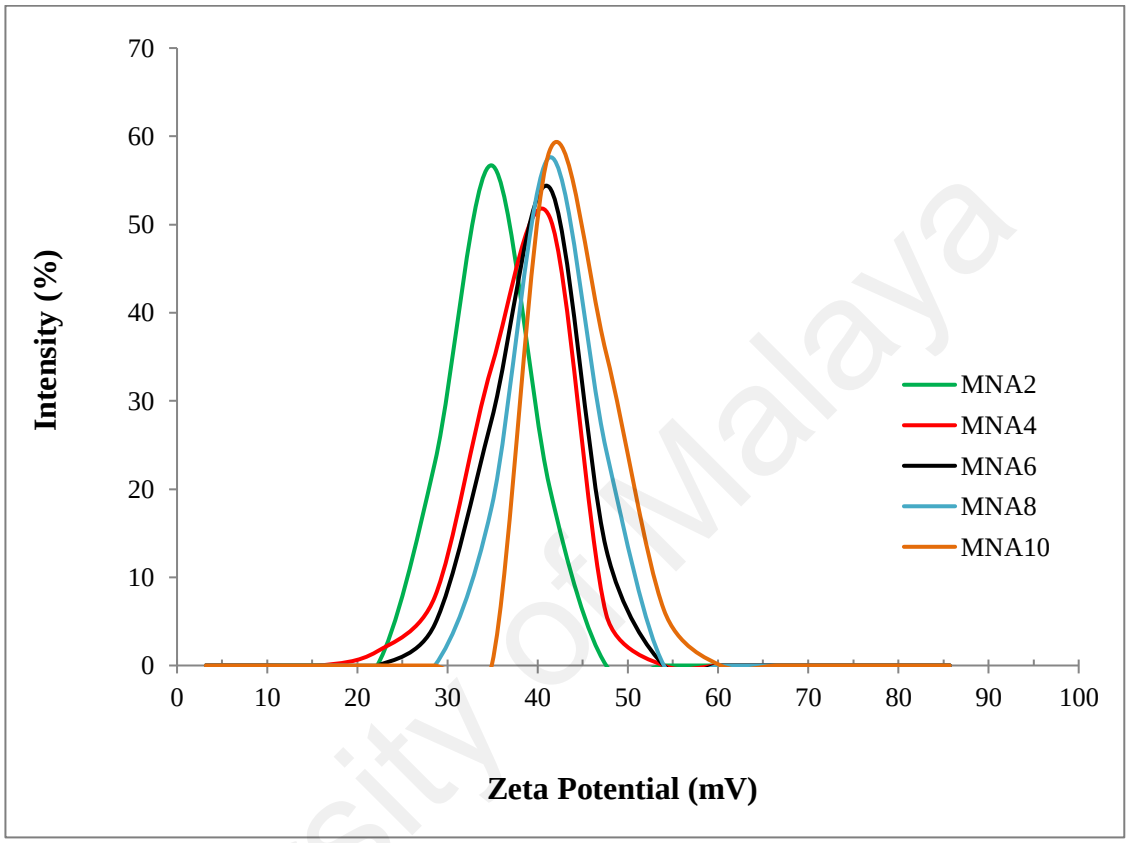

Figure 4.16: Zeta potential measurement of maghemite nanoparticles for all samples

4.2 Stability Monitoring of Maghemite Nanoparticles Suspensions

4.2.1 Effect of pH

Electrostatic stabilization is a simple way for imparting high stability to maghemite suspensions, which are sensitive to the changes in the pHs. The response of the maghemite nanofluids at different pHs values was determined by measuring electrophoretic mobility (zeta potential) as a function of pHs.

The zeta potential value of maghemite nanofluids at different pH is shown in Fig. 4.17. It can be seen that the value of zeta potential is zero when the pH of maghemite nanofluids is 6.7, which is the iso electric point (iep). When the pH is greater than 6.7, the particle

surface begins to have a negative charge. On the other hand, if suspension's pH is lower than 6.7, the particle surface has a positive charge. The value of zeta potential is higher when the pH of the suspension is far from the IEP.

It is shown that the highest value of zeta potential is 44.6 mV at pH 3.60 at the acidic condition and -46.2 mV at pH 10.50 at the alkaline condition. It is related to the smaller particle size at a higher zeta potential value. The particle size is 45.3 nm at zeta potential of 44.6 mV while, at the iso electric point, the particle size is 6560 nm. This phenomenon is due to the particles surface charge is lower at the IEP. Hence, the particles are become greater because of the agglomeration and aggregation of the particles in fluids. On the other hand, as the pH of the fluids far from IEP, the particles surface charge become higher. Hence, there is a resistance of the particles to agglomerate that give the particles in suspension is become smaller.

The suspension has electrostatic stability due to the strong repulsive force between charged particles. At the lower pH (acidic condition) and higher pH (alkaline condition), the particles create high surface charge that result in higher zeta potential values. This condition provides enough electrostatic repulsion force between particles to prevent attraction and collision caused by Brownian motion.

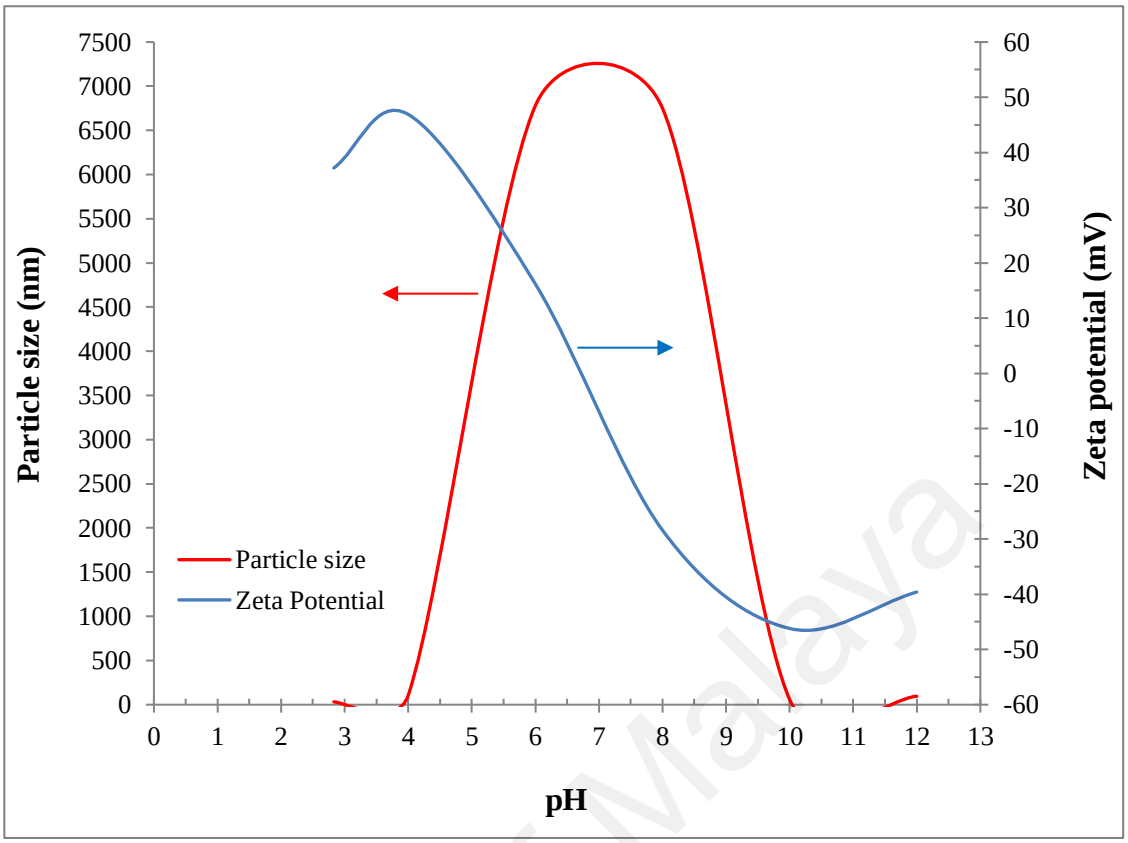

Figure 4.17: Particle size and zeta potential measurement of maghemite nanofluids at different pH

4.2.2 Effect of Time

Dynamic light scattering (DLS) and zeta potential characterizations were performed to investigate the stability of maghemite nanofluids. The characterization was conducted on the as-synthesized suspension and for the same suspension after two, four, and eight months of storage at ambient conditioned. The results are shown in Figs. 4.18 and 4.19.

The averaged particle size of the maghemite nanoparticles is 45.3 nm. The average sizes for sample after two, four, and eight months of storage are 47.1, 50.5, and 52.1 nm, respectively. Table 4.5 summarize the results. The rise in the average particle size after prolonged of storage indicates that a small degree of agglomeration was occurred. It can be stated that although the nanofluids are very stable, the particle still grows due to the growth of the particle nucleaus. Hence, the particles rise in a small degree with elapsed time. However, there is no significant agglomeration and sedimentation was visually observed on the maghemite nanofluids even after eight months of storage.

The sizes of maghemite nanoparticles obtained from DLS measurements are larger than those obtained from other characterizations such as TEM and XRD. It can be explained that the measured size from DLS are the hydrodynamic size which the size of particles and their surrounding diffuse layers while other characterizations are the size of maghemite nanoparticles themselves.

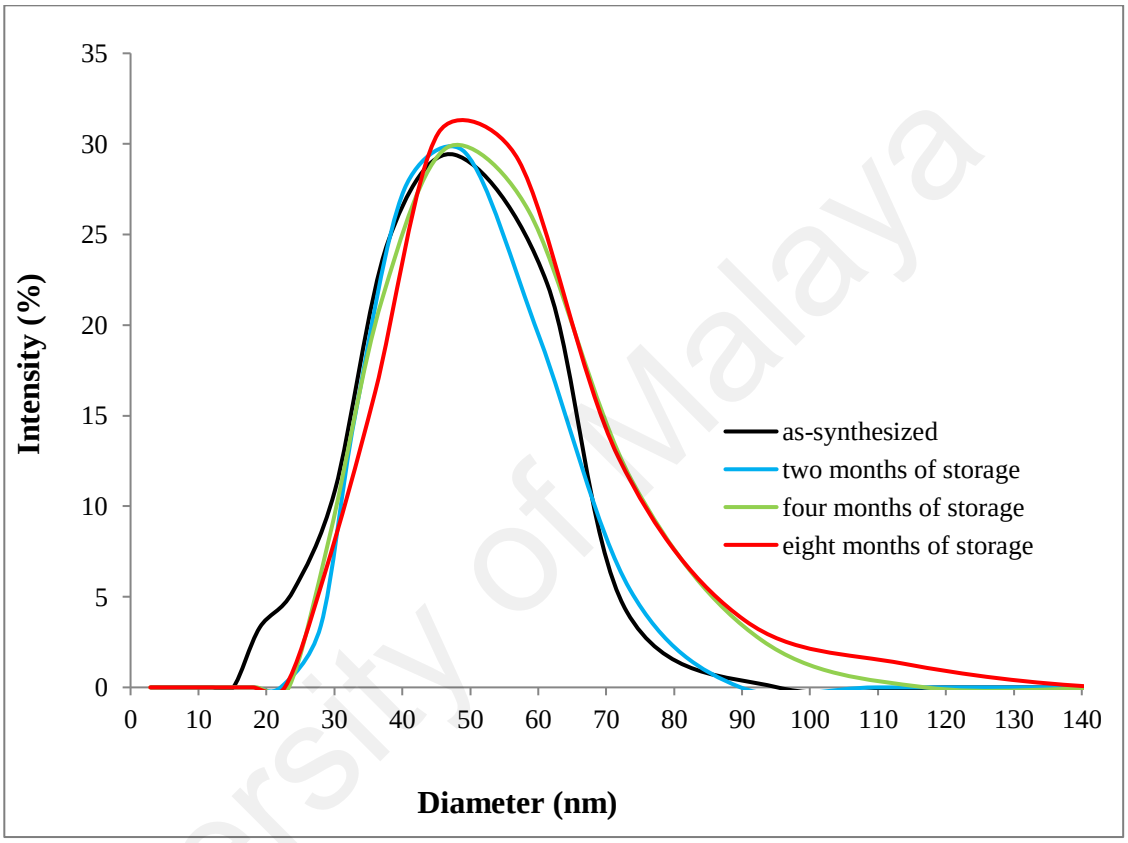

Figure 4.18: Particle size distribution of maghemite nanoparticle from DLS measurement

To further understand the stability of the suspension, the study of electrophoretic behavior through measurement of zeta potential is crucial (Singh et al., 2005). It is well known that nanofluids become stable with zeta potential value higher than ± 30 mV. The zeta potential values depend on the pH of the suspensions. The pH of these maghemite nanofluids is 3.60. The value of zeta potential for as-synthesized maghemite nanofluids is 44.6 mV. Zeta potential values of the suspension after two, four, and eight months of storage are 43.3, 42.7, and 41.8 mV, respectively, as presented in Table 4.5. These values offer enough electrostatic repulsion force between particles to avoid attraction and

collision caused by Brownian motion. This situation causes the maghemite nanofluids to remain stable even after eight months of storage.

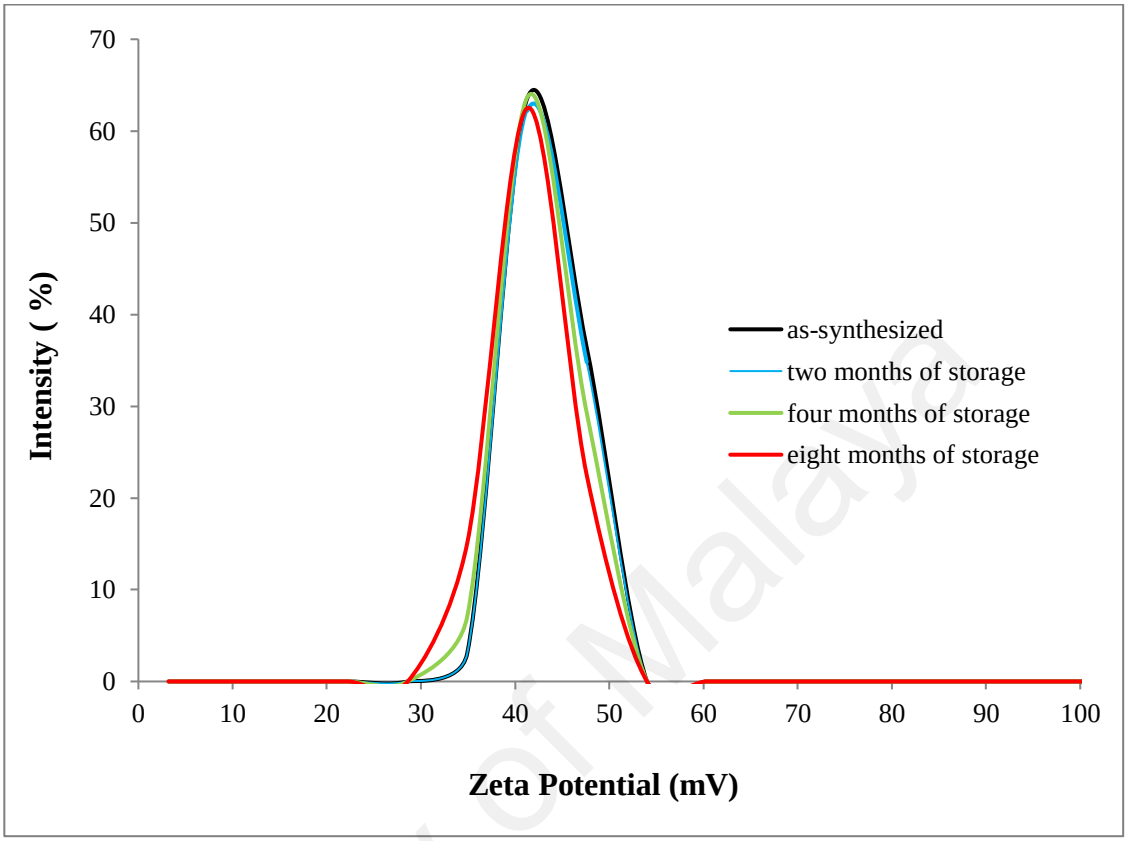

Figure 4.19: Zeta potential curves of maghemite nanofluids

Table 4.5 : Particle size and zeta potential measurement at various time of storage

Samples	Particle size (nm)	Zeta Potential (mV)
As-synthesized	45.3	44.6
Two months	47.1	43.3
Four months	50.5	42.7
Eight months	52.1	41.8

4.3 Thermophysical Properties of Maghemite Nanofluids

4.3.1 Effect of Particle Volume Fraction

4.3.1.1 Thermal Conductivity of maghemite nanofluids

The thermal conductivity of maghemite nanofluids at a various particle volume fraction and their standard deviations are presented in Table 4.6, while the graphs of thermal conductivity measurement and their regression line are shown in Fig. 4.20. The regression line and their degree of determination are tabulated in Table 4.7.

Overall, the thermal conductivities of the maghemite nanofluids increase linearly with particles volume fraction and significantly higher than that of the corresponding base fluids. This phenomenon is due to the particles have larger thermal conductivity than base liquid. The suspended of a particle into base liquids improve the thermal conductivity of suspensions that effect the maghemite nanofluids having larger thermal conductivity than pure base liquid. The mixture of the nanofluids contains of three components, namely nanoparticle, interfacial layer and liquids (Fu & Gao, 2012; Murshed et al., 2008; Tillman & Hill, 2007). When the nanoparticles are suspended in the base fluids, interaction was occurred between nanoparticles, interfacial layer and base fluids. These interactions are caused by random movement of the particles in the base fluids due to collisions with the molecules of base fluids (Godson et al., 2010). Besides that, there is also consideration towards the effect of the interfacial layer between fluids and particles as the increase of layer thickness increases the thermal conductivity of nanofluids. (Mintsa et al., 2009).

It can also be observed that the thermal conductivity of maghemite nanofluids is linearly increased with increasing particle volume fraction at a certain temperature. This condition is due to higher particle volume fraction, there are more particles suspended in the base liquid. At the same time, the conductivity was increased as the temperature increases due to the increase of maghemite nanoparticles Brownian motion. Hence, maghemite nanofluids have higher thermal conductivity.

Table 4.6: Thermal conductivity of maghemite nanofluids at different particle volume fractions

Particle volume fraction (%)	Thermal conductivity (W/mK)		
	T : 10 ºC	**T : 15 ºC**	**T : 20 ºC**
0.0	0.578 ± 0.0007	0.586 ± 0.0008	0.595 ± 0.0010
0.1	0.580 ± 0.0015	0.589 ± 0.0015	0.599 ± 0.0013
0.2	0.583 ± 0.0011	0.592 ± 0.0013	0.603 ± 0.0011
0.3	0.588 ± 0.0017	0.597 ± 0.0016	0.606 ± 0.0011
0.4	0.593 ± 0.0015	0.602 ± 0.0019	0.611 ± 0.0015
0.5	0.596 ± 0.0019	0.605 ± 0.0011	0.616 ± 0.0013
0.6	0.599 ± 0.0015	0.612 ± 0.0016	0.621 ± 0.0018
Particle volume fraction (%)	**Thermal conductivity (W/mK)**		
	T : 25 ºC	**T : 30 ºC**	**T : 35 ºC**
0.0	0.602 ± 0.0013	0.614 ± 0.0016	0.621 ± 0.0008
0.1	0.607 ± 0.0016	0.620 ± 0.0017	0.634 ± 0.0022
0.2	0.617 ± 0.0010	0.634 ± 0.0013	0.651± 0.0017
0.3	0.622 ± 0.0019	0.645 ± 0.0018	0.672 ± 0.0016
0.4	0.627 ± 0.0015	0.657 ± 0.0013	0.685 ± 0.0019
0.5	0.631 ± 0.0018	0.668 ± 0.0019	0.704 ± 0.0018
0.6	0.642 ± 0.0011	0.689 ± 0.0016	0.738 ± 0.0015

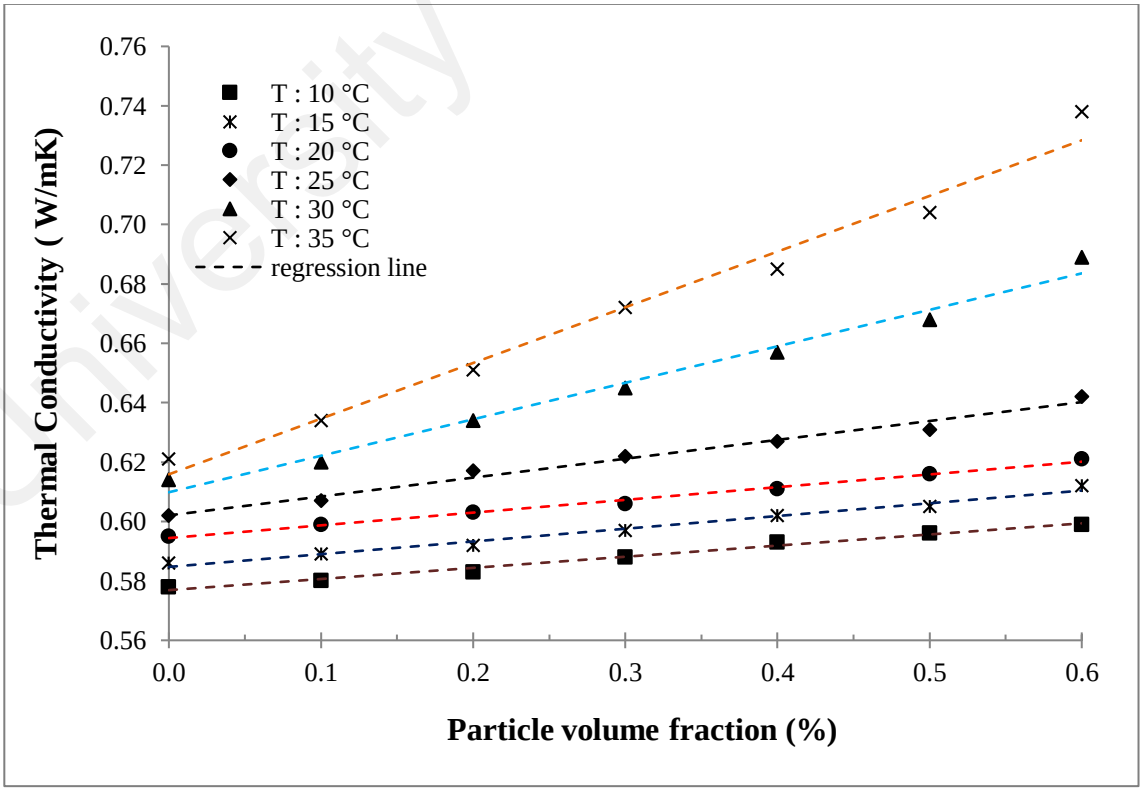

Figure 4.20: Thermal conductivity of maghemite nanofluids as a function of particle volume fraction at different temperatures.

Table 4.7: Regression line equation of thermal conductivity of maghemite nanofluids as a function of particle volume fraction at different temperatures.

Temperature (^oC)	Equation line	R^2
10	Y = 0.0038X + 0.5731	0.9872
15	Y = 0.0043X + 0.5804	0.9858
20	Y = 0.0043X + 0.5901	0.9939
25	Y = 0.0065X + 0.5954	0.9804
30	Y = 0.0123X + 0.5976	0.9839
35	Y = 0.0187X + 0.5971	0.9810

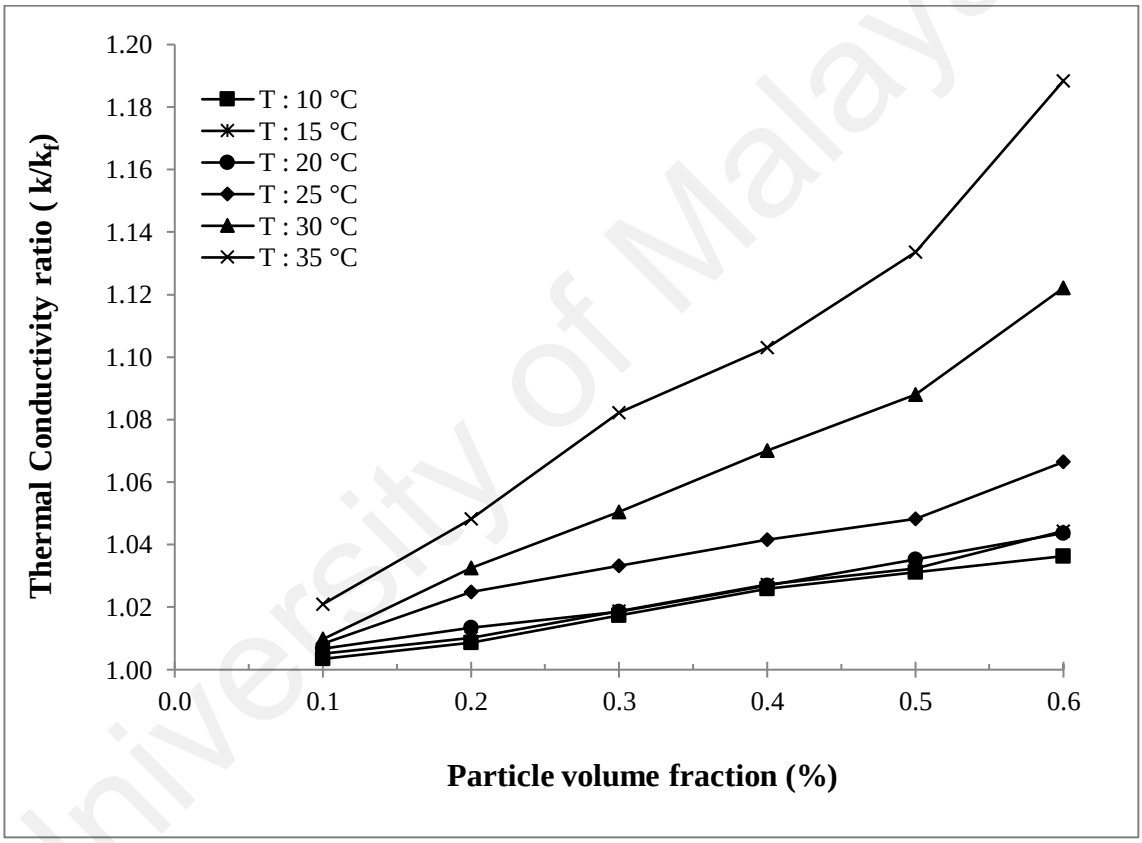

Figure 4.21: Thermal conductivity ratio of maghemite nanofluids as a function of particle volume fraction at different temperatures.

The increasing thermal conductivity of particle in the base fluids is caused by the higher thermal conductivity of particles. Hence, increasing maghemite particle volume fraction in the base fluids enhance thermal conductivity of maghemite nanofluids. The ratio of thermal conductivity and enhancement of thermal conductivity of maghemite nanofluids at various particles volume fraction are shown in Figs. 4.21 and 4.22. It can be

seen that the increased thermal conductivity is higher at a higher particle volume fraction of maghemite nanoparticles. This phenomenon is due to more particles were involved in base fluids that have higher thermal conductivity compared to base fluids. This result is in conformity with others (Abareshi et al., 2010; Gavili et al., 2012; Pastoriza-Gallego et al., 2011; Phuoc et al., 2011). Hence, at a higher particle volume fraction, the thermal conductivity of maghemite nanofluids is larger than that of lower particles volume fractions. The highest enhancement of thermal conductivity of maghemite nanoparticles suspensions is 18.84 % achieved at a particle volume fraction of 0.6 % at a temperature of 35 ºC.

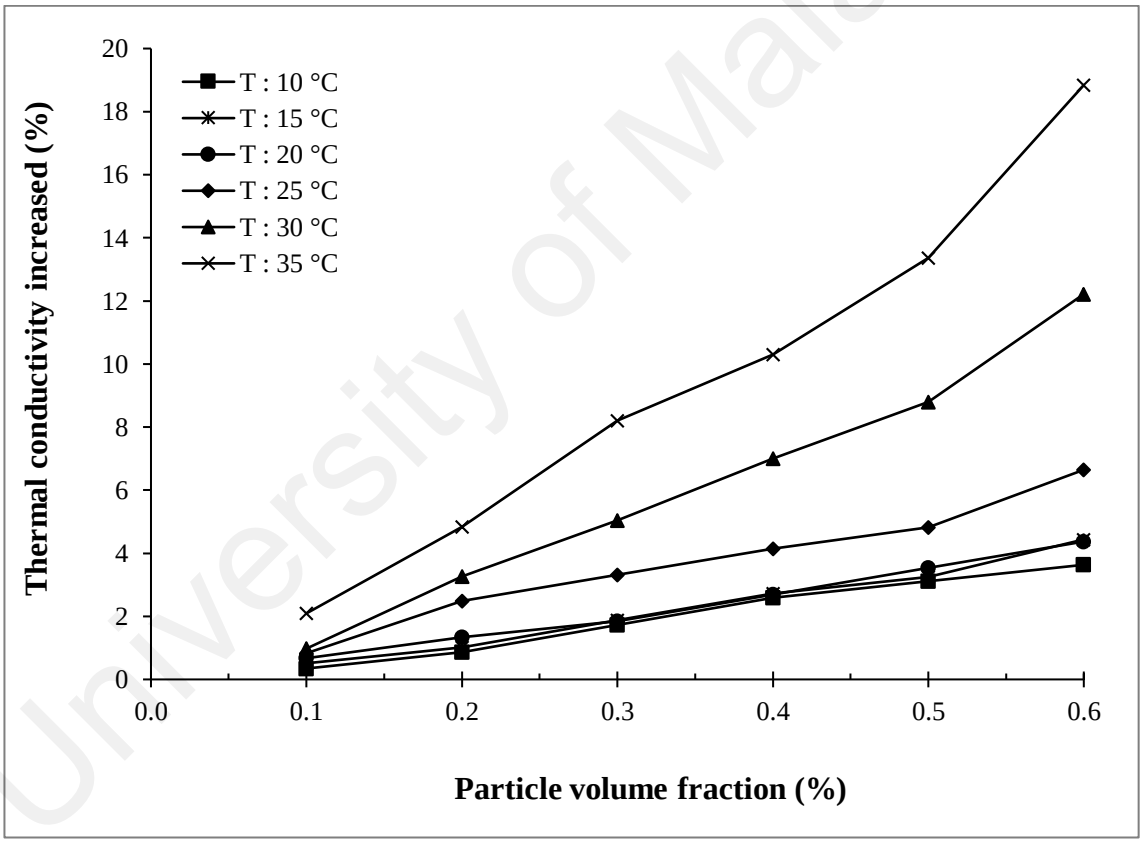

Figure 4.22: Enhancement of thermal conductivity of maghemite nanofluids as a function of particle volume fraction at different temperatures.

4.3.1.2 Kinematic viscosity of maghemite nanofluids

Kinematic viscosity of maghemite nanofluids at a various particle volume fraction and their standard deviation of measurements are tabulated in Table 4.8. The graphs of the trend of the kinematic viscosity of maghemite nanofluids are shown in Fig. 4.23. The

regression line equations and their coefficient of determinations are tabulated in Table 4.9. The kinematic viscosity ratio and percentage of kinematic viscosity enhancement are given in Figs. 4.24 and 4.25. The viscosity depends on the particles volume fraction of maghemite nanoparticle. Increasing particle concentration will enhance the viscosity of maghemite nanofluids. Once the nanoparticles are dispersed in the solution, there is possibility of enhancement in resistance between the two layers of liquid.

As a nanofluid is a mixture of nanoparticles and base fluids, there is an interaction between particles and its surrounding. The flow of nanofluids created a friction between nanofluids and its surrounding that resist the flow of nanofluids. The more concentrated of nanoparticles in the fluids will enhance the resistance of nanofluids flow, and this will enhance the viscosity of nanofluids. The highest enhancement of the kinematic viscosity of maghemite nanofluids is 13.66 % for a particle volume fraction of 0.6 % and temperature of 35 ^{o}C.

Table 4.8: Kinematic viscosity of maghemite nanofluids at different particle volume fractions

Particle volume fraction (%)	**Kinematic viscosity (cst)**		
	T : 10 ^{o}C	**T : 15 ^{o}C**	**T : 20 ^{o}C**
0.0	1.307 ± 0.0019	1.144 ± 0.0015	0.997 ± 0.0023
0.1	1.316 ± 0.0016	1.148 ± 0.0023	1.010 ± 0.0023
0.2	1.319 ± 0.0018	1.151 ± 0.0028	1.018 ± 0.0013
0.3	1.323 ± 0.0017	1.155 ± 0.0020	1.032 ± 0.0016
0.4	1.328 ± 0.0019	1.160 ± 0.0020	1.036 ± 0.0017
0.5	1.332 ± 0.0019	1.166 ± 0.0018	1.041 ± 0.0016
0.6	1.337 ± 0.0012	1.172 ± 0.0016	1.053 ± 0.0019
Particle volume fraction (%)	**Kinematic viscosity (cst)**		
	T : 25 ^{o}C	**T : 30 ^{o}C**	**T : 35 ^{o}C**
0.0	0.889 ± 0.0019	0.799 ± 0.0011	0.732 ± 0.0012
0.1	0.901 ± 0.0026	0.812 ± 0.0017	0.748 ± 0.0018
0.2	0.922 ± 0.0018	0.835 ± 0.0015	0.767 ± 0.0018
0.3	0.945 ± 0.0020	0.856 ± 0.0020	0.789 ± 0.0017
0.4	0.957 ± 0.0012	0.868 ± 0.0014	0.805 ± 0.0019
0.5	0.968 ± 0.0022	0.881 ± 0.0017	0.816 ± 0.0009
0.6	0.976 ± 0.0014	0.893 ± 0.0020	0.832 ± 0.0017

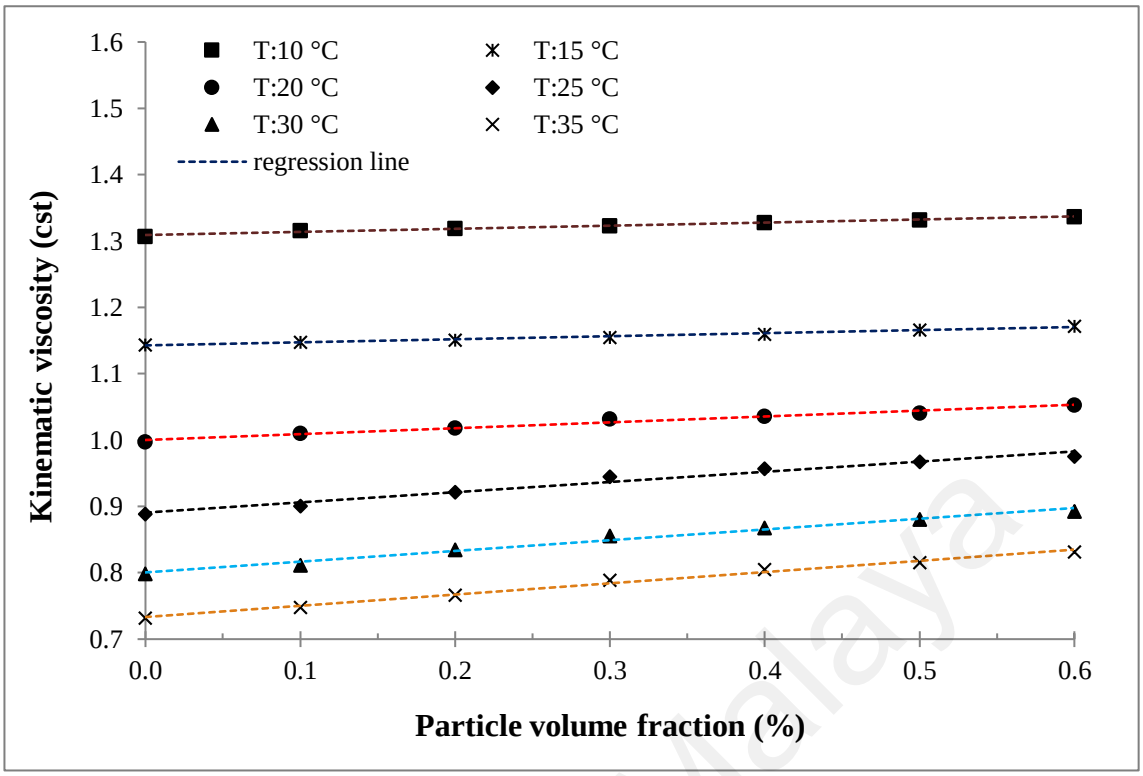

Figure 4.23: Viscosity of maghemite nanofluids as a function of particle volume fraction at different temperatures.

Table 4.9: Regression line equation of kinematic viscosity of maghemite nanofluids as a function of particle volume fraction.

Temperature (^oC)	Equation line	R^2
10	Y = 0.0047X + 1.3044	0.9840
15	Y = 0.0046X + 1.1381	0.9844
20	Y = 0.0089X + 0.9913	0.9774
25	Y = 0.0154X + 0.8754	0.9753
30	Y = 0.0162X + 0.7844	0.9857
35	Y = 0.0169X + 0.7164	0.9927

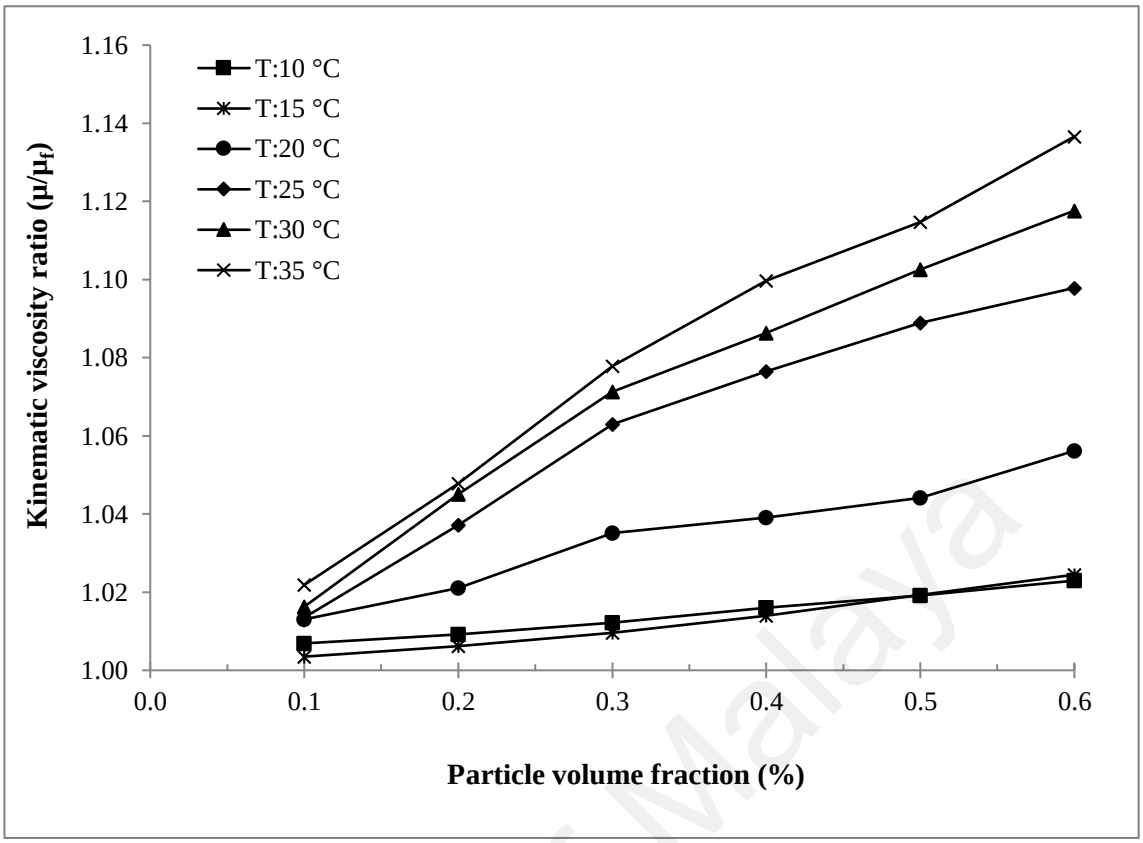

Figure 4.24: Kinematic viscosity ratio of maghemite nanofluids as a function particle volume fraction at different temperatures.

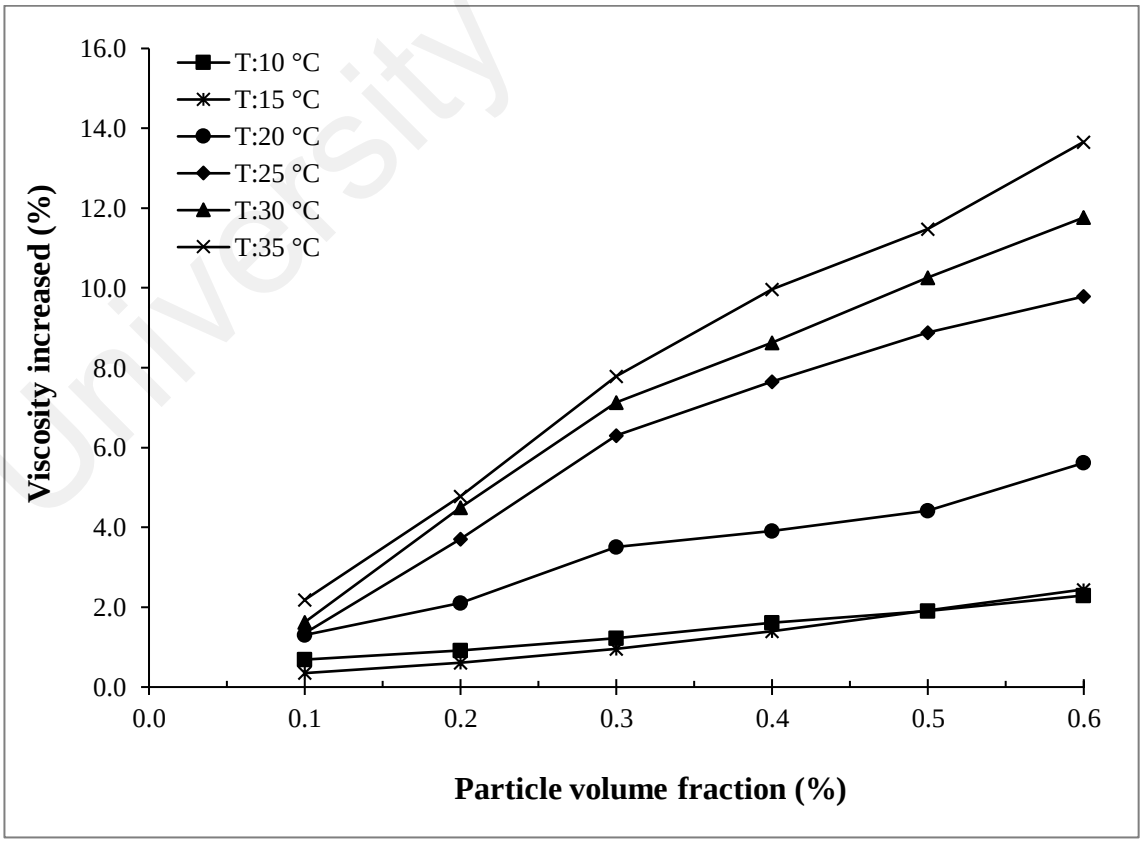

Figure 4.25: Enhancement of kinematic viscosity of maghemite nanofluids as a function of particle volume fraction at different temperatures.

4.3.1.3 Electrical Conductivity

Electrical conductivity of maghemite nanofluids and their standard deviation of measurements are tabulated in Table 4.10. The electrical conductivity of maghemite nanofluids are shown in Fig. 4.26. The regression line and their degree of conformity are presented in Table 4.11. The percentage of enhancement of maghemite nanofluids at various particle volume fractions is given in Fig. 4.27.

It can be seen from Fig. 4.26 that the electrical conductivity of maghemite nanofluids increases almost linearly with increase in volume fraction of the maghemite nanoparticles. The experimental data also indicates that for a given volume fraction, the electrical conductivity of the suspension increases with the temperature. The highest value of electrical conductivity was 7.348 mS/cm recorded for a volume fraction of 0.6 % at a temperature of 35 ^{o}C. The corresponding values at room temperature (25 ^{o}C) was 6.617 mS/cm and the lowest temperature (10 ^{o}C) was 4.046 mS/cm. These conductivity values are much higher (with ordering of 3) when compared with the electrical conductivity values of magnetite nanoparticles obtained by Bagheli (Bagheli et al., 2015).

This phenomenon is due to the electrical conductivity of colloidal nano suspensions in a fluid exhibits a complicated dependence on the electrical double layers. It also depends on characteristics, volume fraction, ionic concentrations and other physicochemical properties (Modesto-Lopez & Biswas, 2010).

When maghemite nanoparticles are suspended in a polar liquid like water, electrical charges are developing on the surfaces. Ions opposite to that relating to the particle surface are attracted, causing the creation of a charged diffuse layer all around the particle. The surface charge of the particles, as well as ion-cloud that constitutes the EDL actively plays a part in the enhancement of conduction mechanisms through the suspension. Furthermore, the existence of uniformly dispersed nanoparticles is considered by reduced equivalent particulate masses, leading to increased electrophoretic mobility, which

consequently enhance the electrical conductivity of the maghemite nanofluids. With increasing of particle volume fraction in the solution, more conducting pathway in the solutions are formed, that in turn enhances the overall electrical conductivity of the solution.

The enhancement of electrical conductivity of maghemite nanofluids is presented in Fig. 4.27. For those purpose, the rate of enhancement of the electrical conductivity desired as the different between the electrical conductivity of the nanoparticle suspension and the electrical conductivity of the base fluids divided by the electrical conductivity of the base fluids. As shown in Fig. 4.27, the enhancement increases with respect to increase in nanoparticle volume fraction, which indicate a dependence on volume fraction. This variation also depends on the temperature, where the higher the temperature, the greater is the enhancement. A 100.3 % increase in the electrical conductivity was observed for 0.2 % volume concentration of maghemite nanoparticles in water at temperature 35 ^{o}C. With rise in volume fraction (0.6 %), a 567 % increase in the electrical conductivity was measured for the same temperature of 35 ^{o}C.

Table 4.10 : Electrical conductivity of maghemite nanofluids as a function of particle volume fraction at different temperatures.

Particle volume fraction (%)	**Electrical conductivity (mS/cm)**		
	T : 10 ºC	**T : 15 ºC**	**T : 20 ºC**
0.1	0.868± 0.0011	0.947± 0.0010	0.990 ± 0.0016
0.2	1.461± 0.0013	1.645± 0.0018	1.814 ± 0.0016
0.3	2.165± 0.0016	2.561± 0.0013	2.819 ± 0.0013
0.4	2.754± 0.0015	3.318± 0.0011	3.688 ± 0.0014
0.5	3.378± 0.0003	4.204± 0.0019	4.643 ± 0.0010
0.6	4.046± 0.0011	5.194± 0.0016	5.673 ± 0.0013
Particle volume fraction (%)	**Electrical conductivity (mS/cm)**		
	T : 25 ºC	**T : 30 ºC**	**T : 35 ºC**
0.1	1.010 ± 0.0013	1.051 ± 0.0016	1.102 ± 0.0011
0.2	1.986 ± 0.0012	2.168 ± 0.0011	2.376 ± 0.0007
0.3	3.109 ± 0.0016	3.375 ± 0.0016	3.644 ± 0.0011
0.4	4.017 ± 0.0019	4.367 ± 0.0008	4.745 ± 0.0007
0.5	4.991 ± 0.0016	5.456 ± 0.0013	5.998 ± 0.0009
0.6	6.617 ± 0.0020	6.681 ± 0.0010	7.348 ± 0.0018

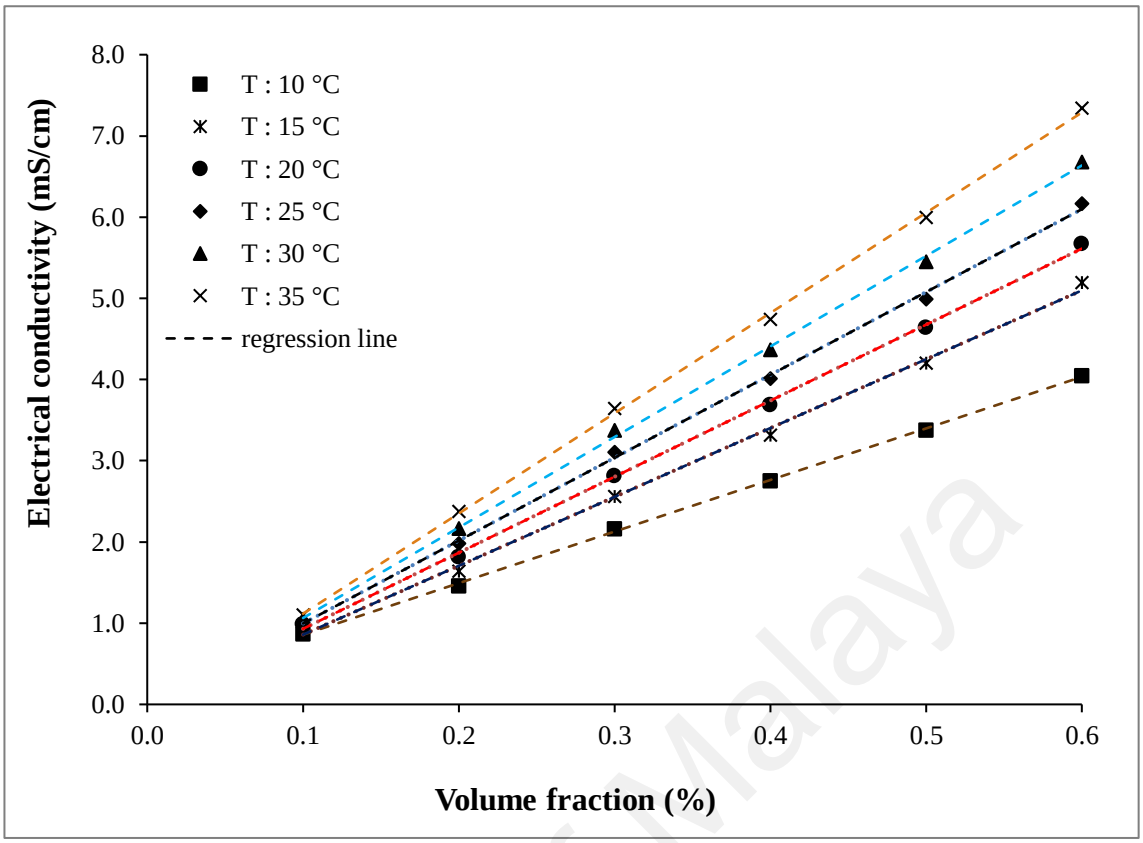

Figure 4.26: Electrical conductivity of maghemite nanofluids as a function of particle volume fraction at different temperatures**.**

Table 4.11: Regression line equation of electrical conductivity of Maghemite nanofluids at various particle volume fractions.

Temperature (ºC)	Equation line	R^2
10	Y = 6.3514X + 0.2223	0.9996
15	Y = 8.4769X + 0.0113	0.9976
20	Y = 9.3631X – 0.0059	0.9991
25	Y = 10.202X – 0.0241	0.9989
30	Y = 11.145X – 0.0509	0.9993
35	Y = 12.342X – 0.1175	0.9994

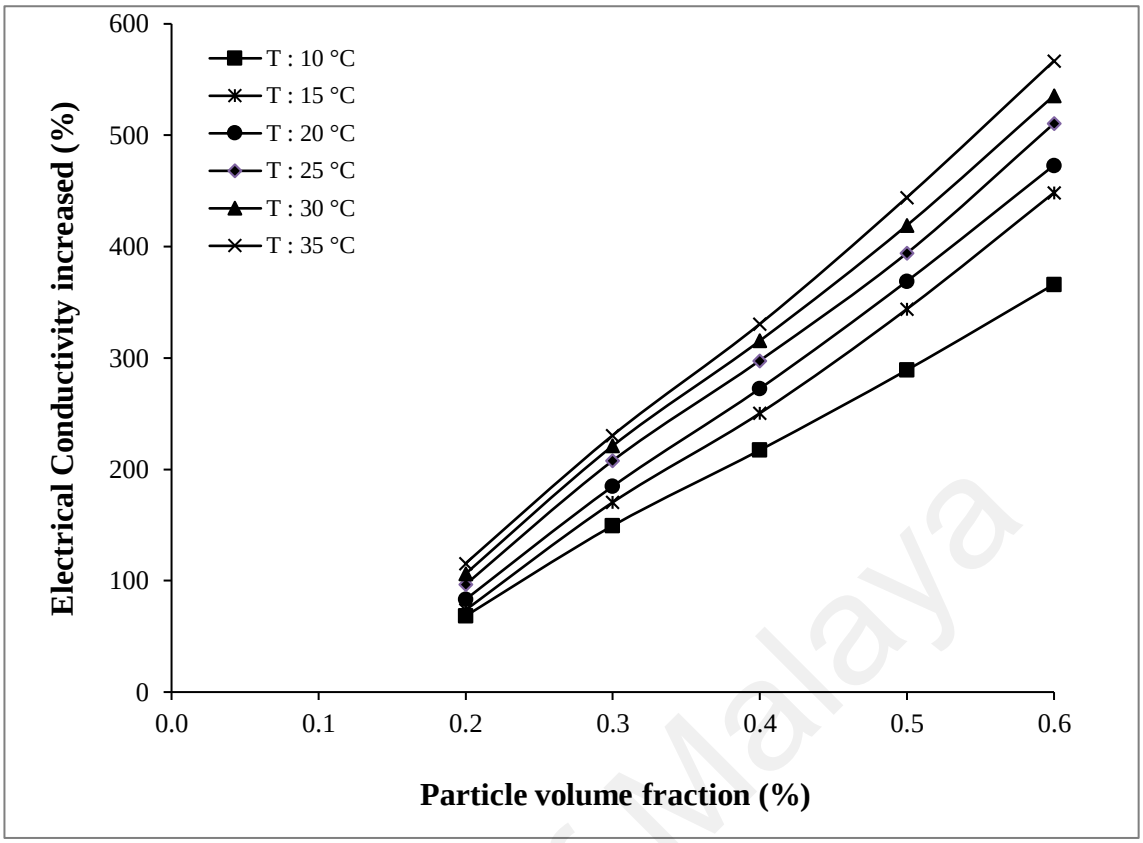

Figure 4.27: Enhancement of electrical conductivity of maghemite nanofluids as a function of particle volume fraction at different temperatures.

4.3.2 Effect of Temperature

4.3.2.1 Thermal Conductivity

The thermal conductivities of maghemite nanofluids and their standard deviation of measurements are tabulated in Table 4.12. The effect of temperature on thermal conductivity of maghemite nanofluids is shown in Fig. 4.28. The regression line and degree of conformity of measurement are tabulated in Table 4.13. The thermal conductivity ratio and percentage of enhancement of maghemite nanofluids at various temperatures are shown in Figs. 4.29 and 4.30.

The thermal conductivities are nonlinearly increases with the increase of temperature. When the temperature rises, the intensity of Brownian motion augments greatly, which leads to a corresponding enhancement of thermal conductivity. The thermal conductivity of high volume fraction of maghemite become larger than that with lower volume fraction

due to the difference in intensity of Brownian motion at elevated temperature (Murshed et al., 2008).

Table 4.12: Thermal conductivity of maghemite nanofluids at different temperatures

Temperature (°C)	Thermal conductivity (W/mK)			
	DI water	ϕ : 0.1 %	ϕ : 0.2 %	ϕ : 0.3 %
10	0.578 ± 0.0007	0.580 ± 0.0015	0.583 ± 0.0011	0.588 ± 0.0017
15	0.586 ± 0.0008	0.589 ± 0.0015	0.592 ± 0.0013	0.597 ± 0.0016
20	0.595 ± 0.0010	0.599 ± 0.0013	0.603 ± 0.0011	0.606 ± 0.0011
25	0.602 ± 0.0013	0.607 ± 0.0016	0.617 ± 0.0010	0.622 ± 0.0019
30	0.614 ± 0.0016	0.620 ± 0.0017	0.634 ± 0.0013	0.645 ± 0.0018
35	0.621 ± 0.0008	0.634 ± 0.0022	0.651± 0.0017	0.672 ± 0.0016

Temperature (°C)	Thermal conductivity (W/mK)		
	ϕ : 0.4 %	ϕ : 0.5 %	ϕ : 0.6 %
10	0.593 ± 0.0015	0.596 ± 0.0019	0.599 ± 0.0015
15	0.602 ± 0.0019	0.605 ± 0.0011	0.612 ± 0.0016
20	0.611 ± 0.0015	0.616 ± 0.0013	0.621 ± 0.0018
25	0.627 ± 0.0015	0.631 ± 0.0018	0.642 ± 0.0011
30	0.657 ± 0.0013	0.668 ± 0.0019	0.689 ± 0.0016
35	0.685 ± 0.0019	0.704 ± 0.0018	0.738 ± 0.0015

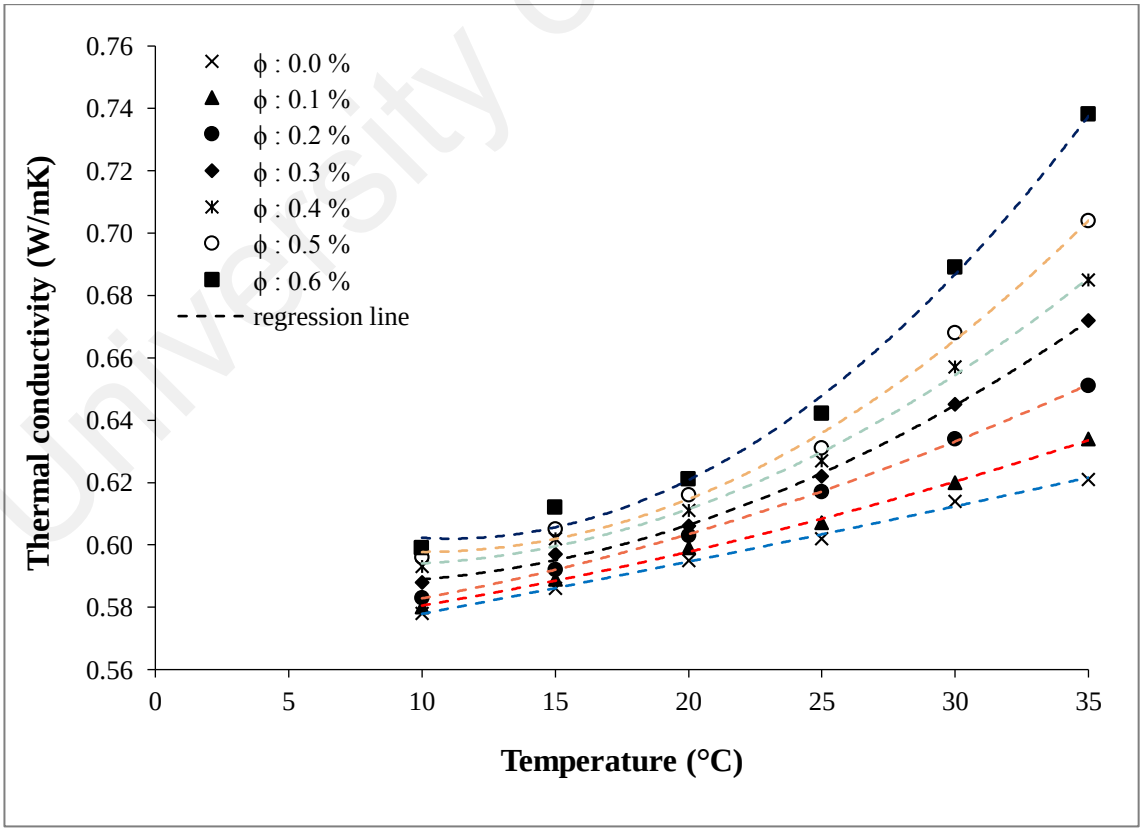

Figure 4.28: Thermal conductivity of maghemite nanofluids as a function of temperature at different particle volume fractions.

Table 4.13: Regression line equation of thermal conductivity of maghemite nanofluids as a function of temperature.

Particle volume fraction (%)	Equation line	R^2
0.0	$Y = 5E\text{-}06X^2+0.0015X+0.5622$	0.9962
0.1	$Y = 3E\text{-}05X^2+0.0009X+0.5686$	0.9979
0.2	$Y = 5E\text{-}05X^2+0.0007X+0.5714$	0.9962
0.3	$Y = 1E\text{-}04X^2-0.0014X+0.5923$	0.9988
0.4	$Y = 1E\text{-}04X^2-0.0021X+0.6022$	0.9965
0.5	$Y = 2E\text{-}04X^2-0.0034X+0.6150$	0.9949
0.6	$Y = 2E\text{-}04X^2-0.0051X+0.6300$	0.9944

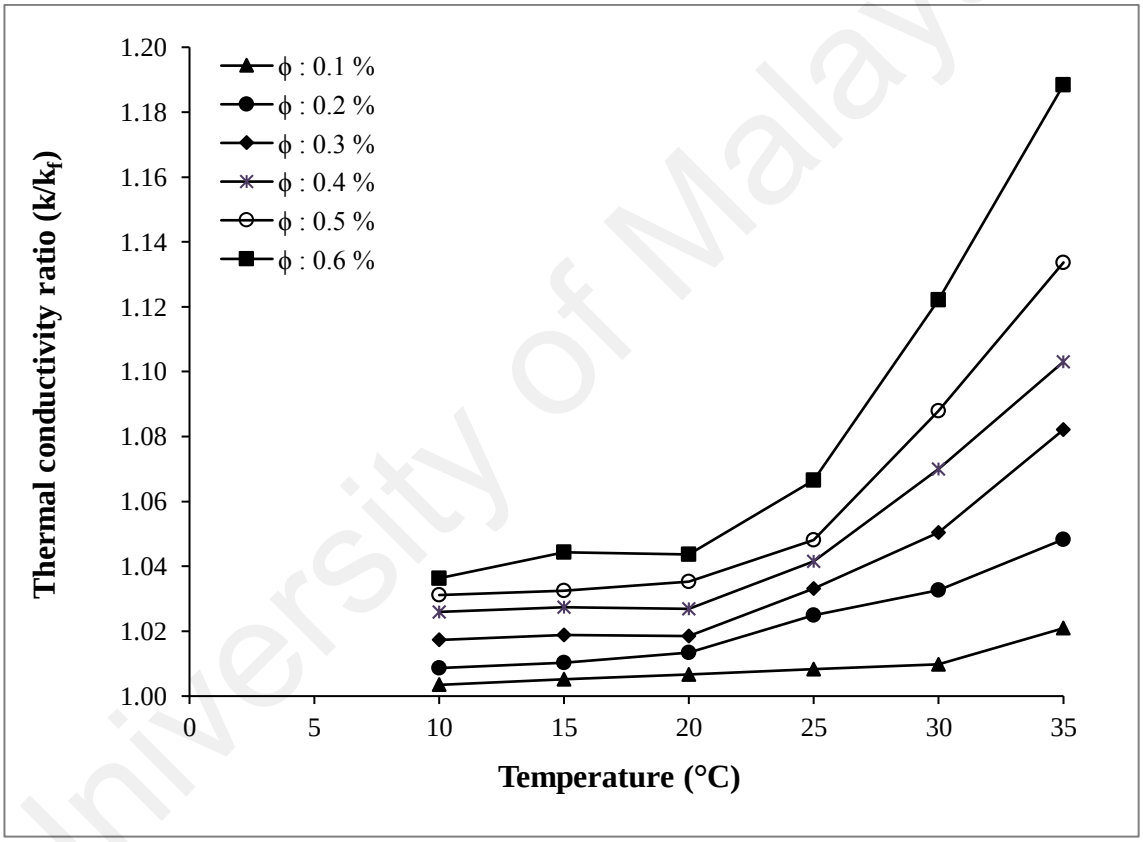

Figure 4.29: Thermal conductivity ratio of maghemite nanofluids as a function of temperature at different particle volume fractions.

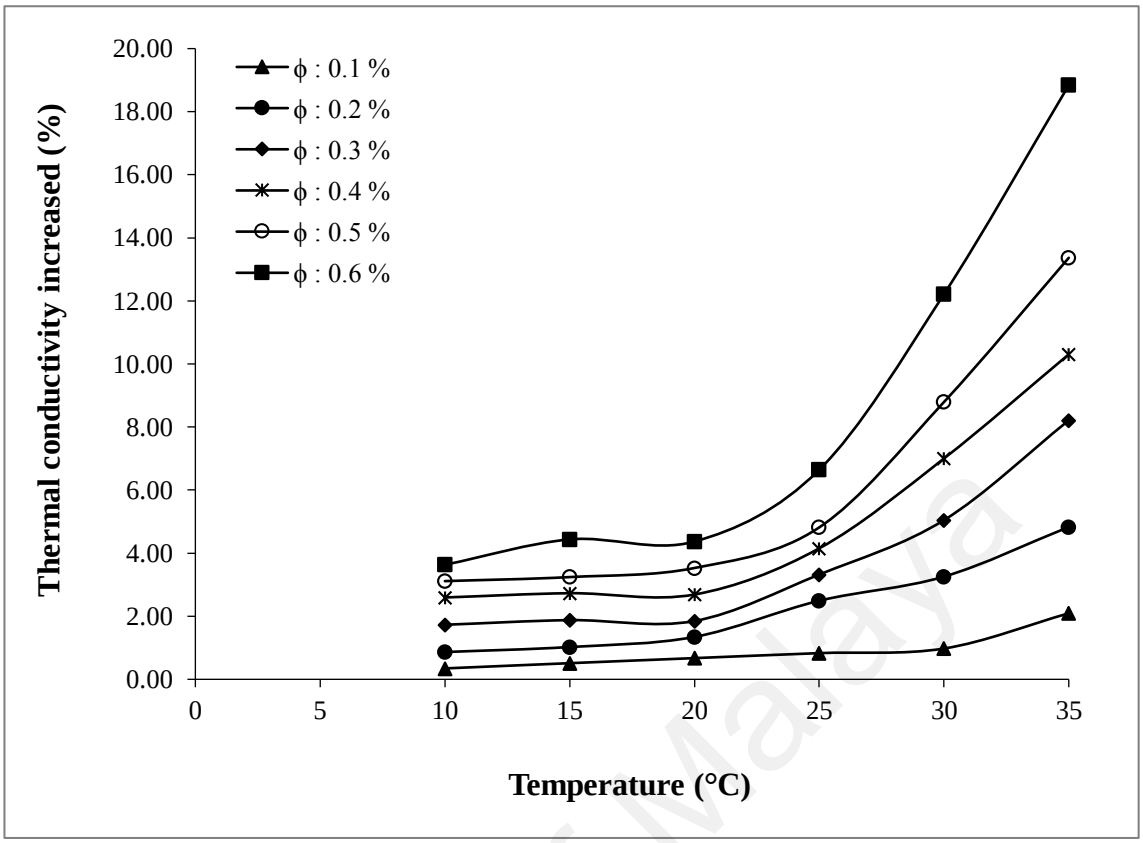

Figure 4.30: Enhancement of thermal conductivity of maghemite as a function of temperature at different particle volume fractions.

From Fig 4.30, it can be seen that high degree of enhancement of thermal conductivity of maghemite nanofluids at higher temperature. At lower temperature, the particles are tightly bound within suspension, hence slower movement of the particles in the solution. On the other hand, at higher temperature, there are more mobile particles movement rapidly in the solution. Increasing temperature of suspensions will increase nonlinearly the thermal conductivity of suspensions. Since temperature are significantly effects thermal conductivity by randomly increasing of the molecular movement in the suspension.

4.3.2.2 Kinematic Viscosity

Kinematic viscosity of maghemite nanofluids at different temperatures and their standard deviation measurements are tabulated in Table 4.14. The graphs of kinematic viscosity of maghemite nanofluids at different temperatures are presented in Fig. 4.31. The regression line equations and their coefficient of determinations are tabulated in

Table 4.15. The kinematic viscosity ratio and percentage of kinematic viscosity decreased with the effect of temperature are displayed in Figs. 4.32 and 4.33.

Table 4.14: Kinematic viscosity of maghemite nanofluids as a function of temperature at different particle volume fractions.

Temperature (°C)	Kinematic viscosity (cst)			
	ϕ : 0.0 %	**ϕ : 0.1 %**	**ϕ : 0.2 %**	**ϕ : 0.3 %**
10	1.307 ± 0.0019	1.316 ± 0.0016	1.319 ± 0.0018	1.323 ± 0.0017
15	1.144 ± 0.0015	1.148 ± 0.0023	1.151 ± 0.0028	1.155 ± 0.0020
20	0.997 ± 0.0023	1.010 ± 0.0023	1.018 ± 0.0013	1.032 ± 0.0016
25	0.889 ± 0.0019	0.901 ± 0.0026	0.922 ± 0.0018	0.945 ± 0.0020
30	0.799 ± 0.0011	0.812 ± 0.0017	0.835 ± 0.0015	0.856 ± 0.0020
35	0.732 ± 0.0012	0.748 ± 0.0018	0.767 ± 0.0018	0.789 ± 0.0017

Temperature (°C)	Kinematic viscosity (cst)		
	ϕ : 0.4 %	**ϕ : 0.5 %**	**ϕ : 0.6 %**
10	1.328 ± 0.0019	1.332 ± 0.0019	1.337 ± 0.0012
15	1.160 ± 0.0020	1.166 ± 0.0018	1.172 ± 0.0016
20	1.036 ± 0.0017	1.041 ± 0.0016	1.053 ± 0.0019
25	0.957 ± 0.0012	0.968 ± 0.0022	0.976 ± 0.0014
30	0.868 ± 0.0014	0.881 ± 0.0017	0.893 ± 0.0020
35	0.805 ± 0.0019	0.816 ± 0.0009	0.832 ± 0.0017

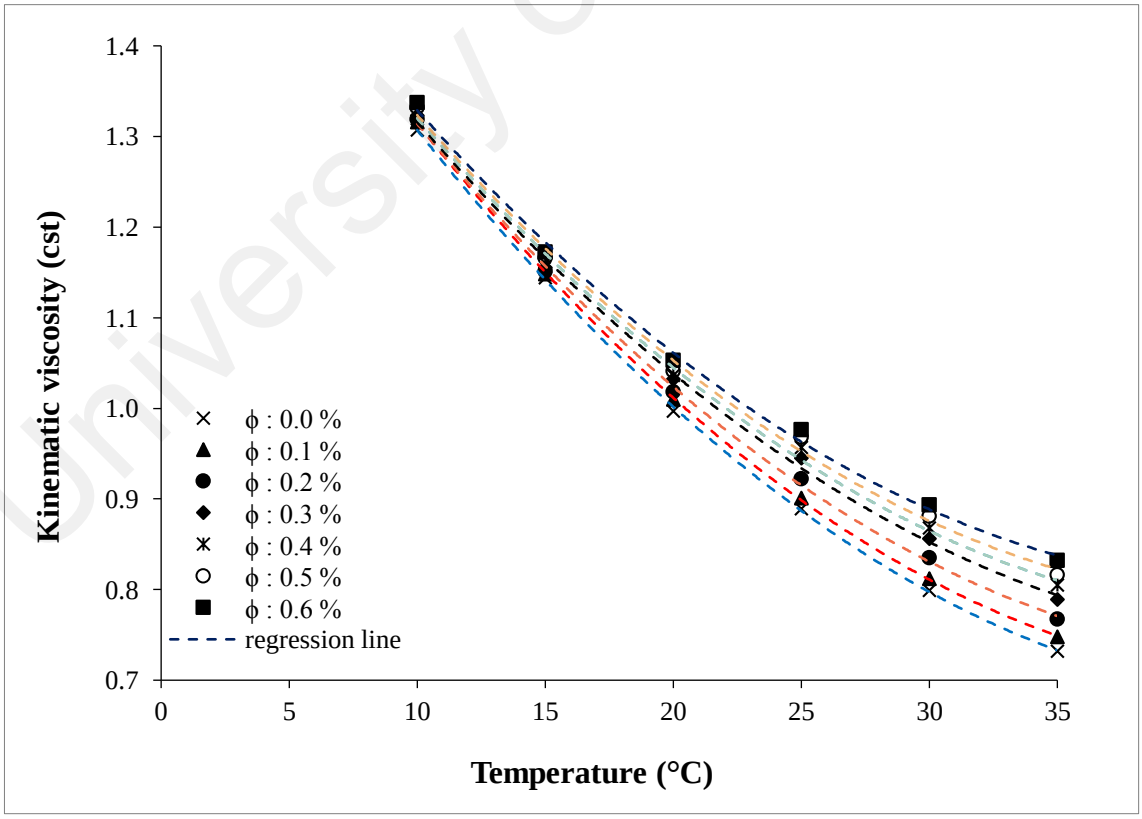

Figure 4.31: Kinematic viscosity of maghemite nanofluids as a function of temperature at different particle volume fractions.

Table 4.15: Regression line equation of kinematic viscosity of maghemite nanofluids as a function of temperature at different particle volume fractions.

Particle volume fraction (%)	Equation line	R^2
0.0	$Y = 0.0005X^2 - 0.0457X + 1.7137$	0.9999
0.1	$Y = 0.0005X^2 - 0.0456X + 1.7195$	0.9999
0.2	$Y = 0.0005X^2 - 0.0437X + 1.7028$	0.9992
0.3	$Y = 0.0005X^2 - 0.0415X + 1.6849$	0.9981
0.4	$Y = 0.0005X^2 - 0.0418X + 1.6905$	0.9974
0.5	$Y = 0.0005X^2 - 0.0412X + 1.6884$	0.9965
0.6	$Y = 0.0005X^2 - 0.0410X + 1.6915$	0.9972

It can be seen that the kinematic viscosity ratio of maghemite nanofluids are decreased nonlinearly with the temperature. The liquid molecules are tightly bounded by attractive inter-molecular forces (e.g. Van der Waal forces) at low temperature. These attractive forces are responsible for the viscosity since the individual molecule is difficult to move due to it tightly bounded to its neighbors. Therefore, the kinematic viscosity is larger at low temperature.

The impact of increasing temperature weakened the inter-particle and inter-molecular adhesion forces hence accelerate the movement of the particles in liquids (Nguyen et al., 2007). The increase in temperature causes the increase of kinetic or thermal energy and the molecules become more mobile. As a result, the viscosity is reduced. From Fig. 4.33, it can also be seen that kinematic viscosity of maghemite nanofluids is linearly decreased with increasing of temperature.

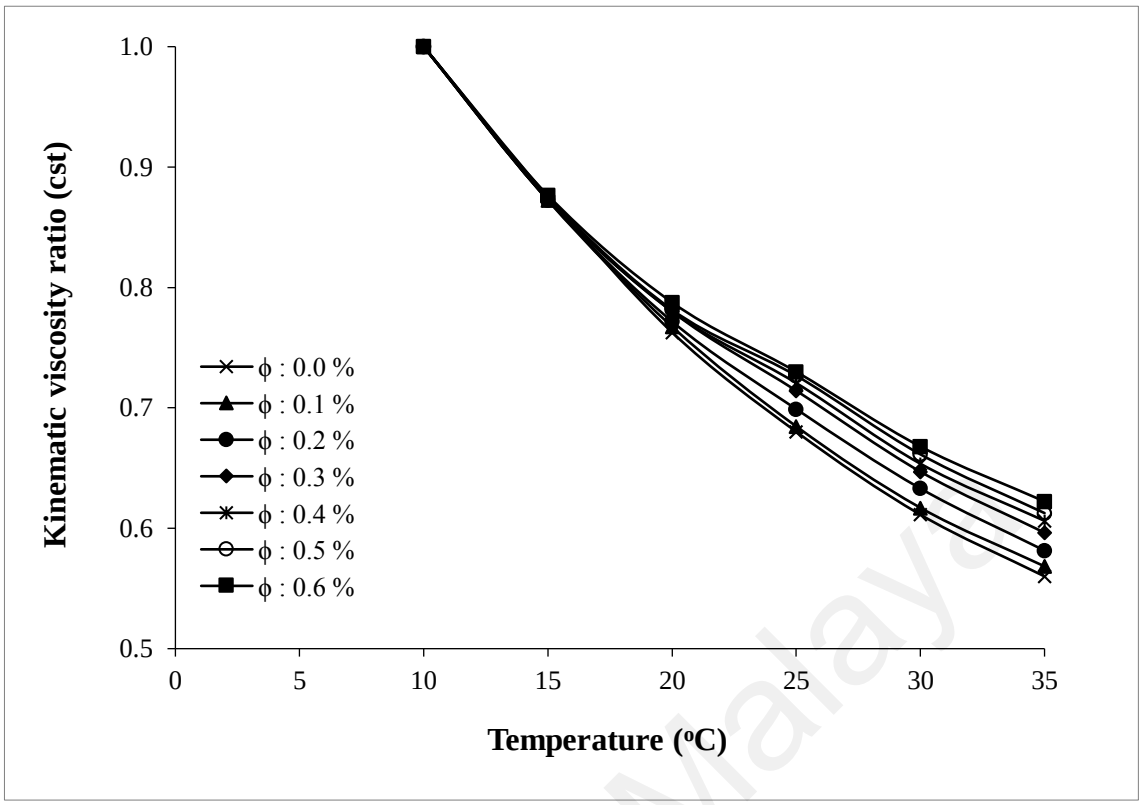

Figure 4.32: Kinematic viscosity ratio of maghemite nanofluids as a function of temperature at different particle volume fractions.

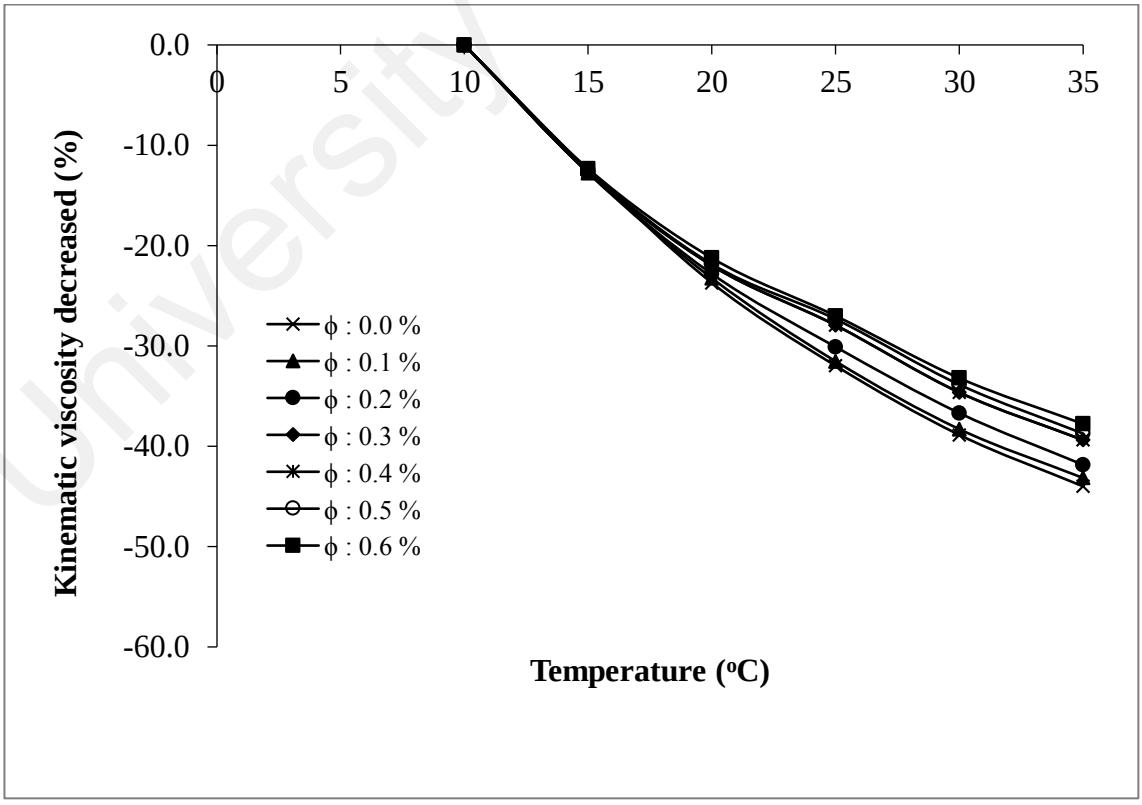

Figure 4.33: Decreasing of kinematic viscosity of maghemite nanofluids as a function of temperature at different particle volume fractions.

4.3.2.3 Electrical conductivity

Electrical conductivity of maghemite nanofluids at different temperature and their standard deviation measurement are tabulated in Table 4.16. The graphs of electrical conductivity of maghemite nanofluids at different temperatures are presented in Fig. 4.34. The regression line equations and their coefficient of determinations are tabulated in Table 4.17. The percentage of increasing of electrical conductivity of maghemite nanofluids at various temperatures are presented in Fig. 4.35.

Table 4.16: Electrical conductivity of maghemite nanofluids as a function of temperature at different particle volume fractions.

Temperature (^oC)	**Electrical conductivity (mS/cm)**		
	ϕ : 0.1 %	**ϕ : 0.2 %**	**ϕ : 0.3 %**
10	0.868± 0.0011	1.461± 0.0013	2.165± 0.0016
15	0.947± 0.0010	1.645± 0.0018	2.561± 0.0013
20	0.990 ± 0.0016	1.814 ± 0.0016	2.819 ± 0.0013
25	1.010 ± 0.0013	1.986 ± 0.0012	3.109 ± 0.0016
30	1.051 ± 0.0016	2.168 ± 0.0011	3.375 ± 0.0016
35	1.102 ± 0.0011	2.376 ± 0.0007	3.644 ± 0.0011
Temperature (^oC)	**Electrical conductivity (mS/cm)**		
	ϕ : 0.4 %	**ϕ : 0.5 %**	**ϕ : 0.6 %**
10	2.754± 0.0015	3.378± 0.0013	4.046± 0.0011
15	3.318± 0.0011	4.204± 0.0019	5.194± 0.0016
20	3.688 ± 0.0014	4.643 ± 0.0010	5.673 ± 0.0013
25	4.017 ± 0.0019	4.991 ± 0.0016	6.617 ± 0.0020
30	4.367 ± 0.0008	5.456 ± 0.0013	6.681 ± 0.0010
35	4.745 ± 0.0007	5.998 ± 0.0009	7.348 ± 0.0018

The experimental data indicate that for a given particle volume fraction, the electrical conductivity of the maghemite nanofluids increases with the temperature. The increasing of maghemite nanofluids is slower at lower temperature. As the temperature of the maghemite nanofluids increase, it will decrease the viscosity and enhance the ions mobility. Furthermore, it could also increase the number of ions in the solution due to molecular dissociation. As a result, this will lead to an increase in its conductivity.

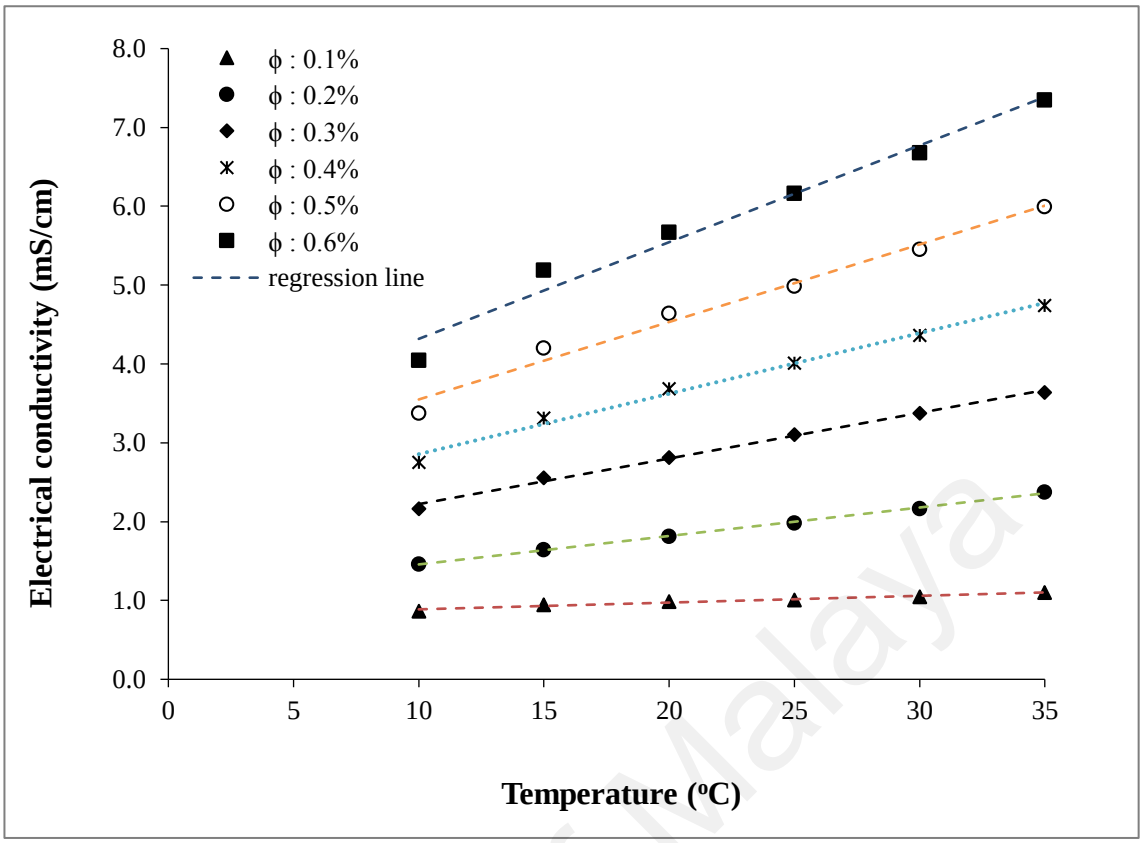

Figure 4.34: Electrical conductivity of maghemite nanofluids as a function of temperature at different particle volume fractions.

Table 4.17: Regression line equation of electrical conductivity of maghemite nanofluids as a function of temperature at different particle volume fractions.

Particle volume fraction (%)	Equation line	R^2
0.0		
0.1	Y = 0.0086X + 0.8016	0.9688
0.2	Y = 0.0361X + 1.0963	0.9989
0.3	Y = 0.0579X + 1.6435	0.9952
0.4	Y = 0.0767X + 2.088	0.9914
0.5	Y = 0.0983X + 2.5664	0.9952
0.6	Y = 0.1227X + 3.0917	0.975

From Fig. 4.35, it is shown that the enhancement of electrical conductivity of maghemite nanofluids increases almost linearly with temperature. This enhancement also depends on the volume fraction as the higher the volume fraction, the greater its enhancement. 52 % of enhancement in the electrical conductivity was recorded at room temperature (25 ºC) for 0.6 % of volume fraction. Meanwhile, 82 % of enhancement in the electrical conductivity was recorded for the same volume fraction (0.6 %) at higher

temperature of 35 ºC. The electrical conductivity enhancement of maghemite nanofluids due to temperature effect is lowered by first order compared to volume fraction effect.

These results are in good agreement with published data on other nanofluids (Dong et al., 2013; Ganguly et al., 2009; Minea & Luciu, 2012; Sarojini et al., 2013; Shen et al., 2012; Sikdar et al., 2011; Steven et al., 2011). However, the findings do not correlated with the Maxwell (Maxwell, 1954) and Bruggeman models (Bruggeman, 1935) due to these models do not take into account the temperature factor. This observation is also supported by Sundar et al. (2014).

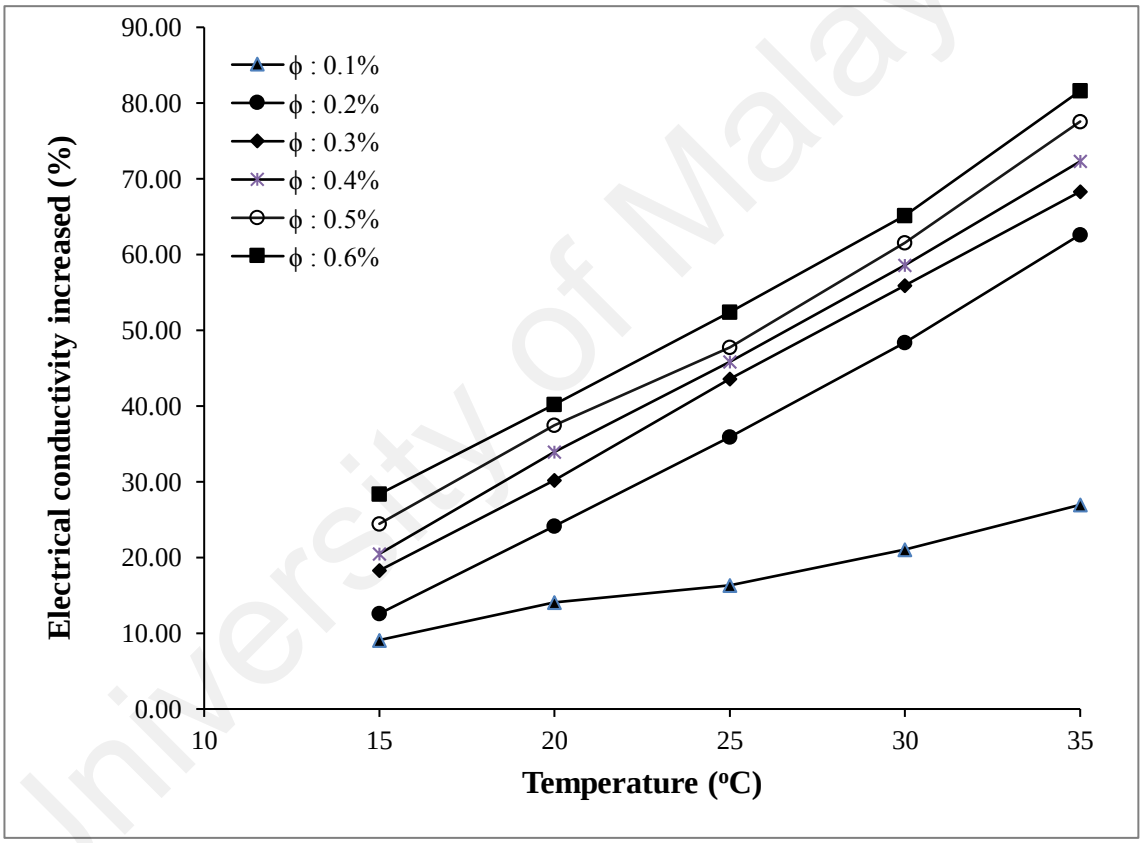

Figure 4.35: Enhancement of electrical conductivity of maghemite nanofluids as a function of temperature at different particle volume fractions.

4.3.3 Effect of Magnetic Fields

The effect of magnetic fields on the properties of maghemite nanofluids was conducted in a pair of Helmholtz coils, which arrange in perpendicular and parallel to the samples. The measurements of the properties were performed with the effect of both arrangements of the magnetic fields.

The advantage of this system was one can control the particles aggregation with different chain lengths. Due to the superparamagnetic nature of particles, the aggregation phenomenon was perfectly reversible.

4.3.3.1 Thermal Conductivity

Data measurements and their standard deviation of thermal conductivity of maghemite nanofluids under parallel magnetic fields arrangements is presented in Table 4.18. The effect of magnetic fields strength on thermal conductivity of maghemite nanofluids for parallel magnetic fields arrangements is shown in Fig. 4.36. The regression line equations and their coefficient of determinations are tabulated in Table 4.19. Thermal conductivity ratio of maghemite nanofluids and their percentage of enhancement are presented in Figs. 4.37 and 4.38.

Table 4.18: Thermal conductivity of maghemite nanofluids at different parallel magnetic fields strength

Magnetic fields strength (Gauss)	**Thermal conductivity (W/mK)**		
	ϕ : 0.1 %	**ϕ : 0.2 %**	**ϕ : 0.3 %**
0	0.607 ± 0.0016	0.617 ± 0.0013	0.622± 0.0016
50	0.612 ± 0.0015	0.620 ± 0.0015	0.624 ± 0.0011
100	0.615 ± 0.0013	0.623 ± 0.0016	0.632 ± 0.0013
150	0.628 ± 0.0016	0.635 ± 0.0018	0.642 ± 0.0015
200	0.640 ± 0.0017	0.654 ± 0.0016	0.663 ± 0.0013
250	0.650 ± 0.0016	0.667 ± 0.0018	0.682 ± 0.0011
300	0.662 ± 0.0013	0.681 ± 0.0017	0.711 ± 0.0015
Magnetic fields strength (Gauss)	**Thermal conductivity (W/mK)**		
	ϕ : 0.4 %	**ϕ : 0.5 %**	**ϕ : 0.6 %**
0	0.627 ± 0.0012	0.632 ± 0.0016	0.643 ± 0.0011
50	0.631 ± 0.0013	0.635 ± 0.0016	0.647 ± 0.0012
100	0.636 ± 0.0011	0.639 ± 0.0016	0.652 ± 0.0011
150	0.647 ± 0.0013	0.651 ± 0.0016	0.661± 0.0017
200	0.672 ± 0.0015	0.680 ± 0.0016	0.696 ± 0.0011
250	0.698 ± 0.0017	0.724 ± 0.0016	0.743 ± 0.0015
300	0.738 ± 0.0016	0.766 ± 0.0016	0.793 ± 0.0011

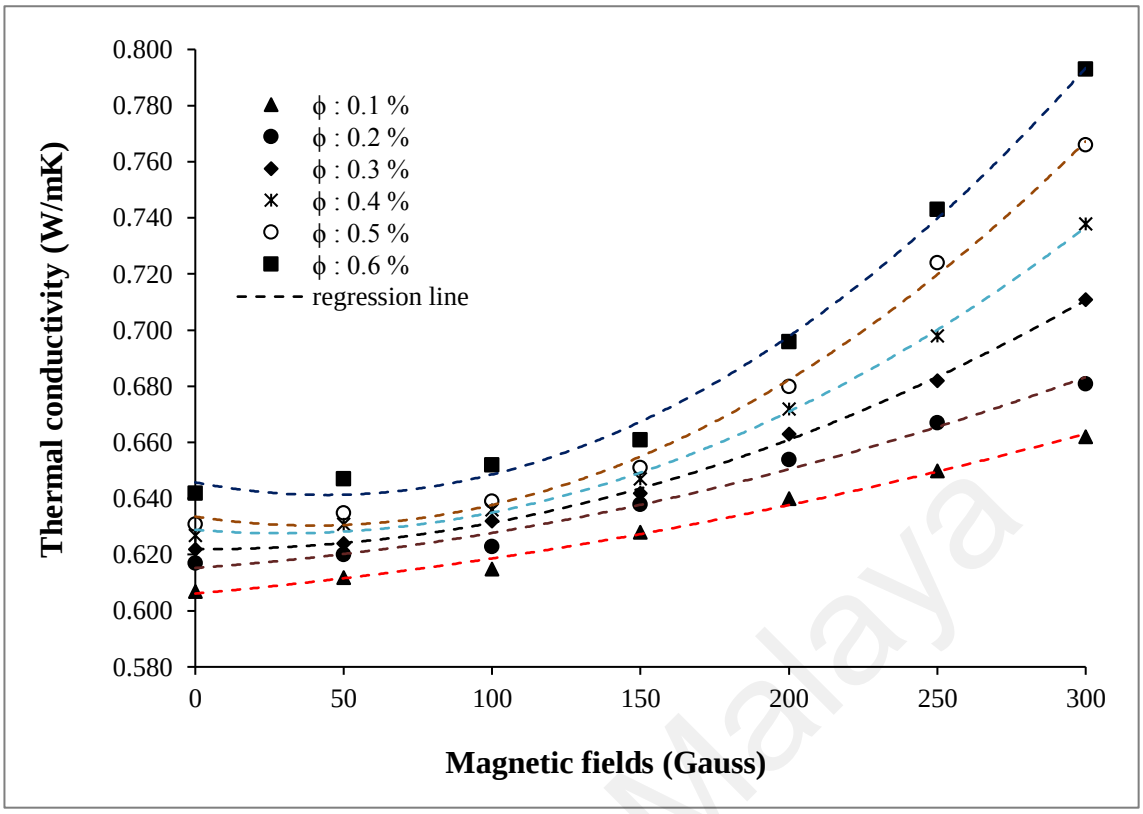

Figure 4.36: Thermal conductivity of maghemite nanofluids at different parallel magnetic fields strength

Table 4.19: Regression line equation of thermal conductivity of maghemite nanofluids at different parallel magnetic fields strength.

Particle volume fraction (%)	Equation line	R^2
0.1	$Y = 3E\text{-}07X^2 + 9E\text{-}05X + 0.6061$	0.9917
0.2	$Y = 5E\text{-}07X^2 + 7E\text{-}05X + 0.6153$	0.9879
0.3	$Y = 1E\text{-}06X^2 - 7E\text{-}06X + 0.6220$	0.9986
0.4	$Y = 1E\text{-}06X^2 - 9E\text{-}05X + 0.6289$	0.9976
0.5	$Y = 2E\text{-}06X^2 - 2E\text{-}04X + 0.6335$	0.9958
0.6	$Y = 2E\text{-}06X^2 - 2E\text{-}04X + 0.6465$	0.9947

It can be observed from Figs. 4.37 and 4.38 that the thermal conductivity of maghemite nanofluids increases with increase in applied magnetic field strength. With increasing concentration of maghemite, the enhancement in the thermal conductivity was significant. At the lower magnetic field strength (< 150 G), the thermal conductivity ratio (k/k_f) values are slightly changed for all concentrations of nanofluids. However, above the magnetic field strength of 150 G, the k/k_f values are significantly increased. Further increase in the

magnetic field strength leads to a drastic increase in k/k_f. The higher the concentration of maghemite nanoparticles, the larger of the increment was. For external magnetic field strength of 300 G, the k/k_f increases from 1.09 to 1.235 when the volume fraction of the particles changes from 0.1 to 0.6 %. The highest enhancement of thermal conductivity was observed as 23.5 % at nanofluids of 0.6 % volume fraction of particles and magnetic field strength of 300 G. A similar enhancement trend is observed by Li and Gavili by considering magnetite nanofluids (Gavili et al., 2012; Li et al., 2005). When the magnetic field was parallel to the temperature gradient, the formed particles chains provided more effectively bridges for energy transport inside the magnetic nanofluids along the direction of temperature gradient (Li et al., 2005).

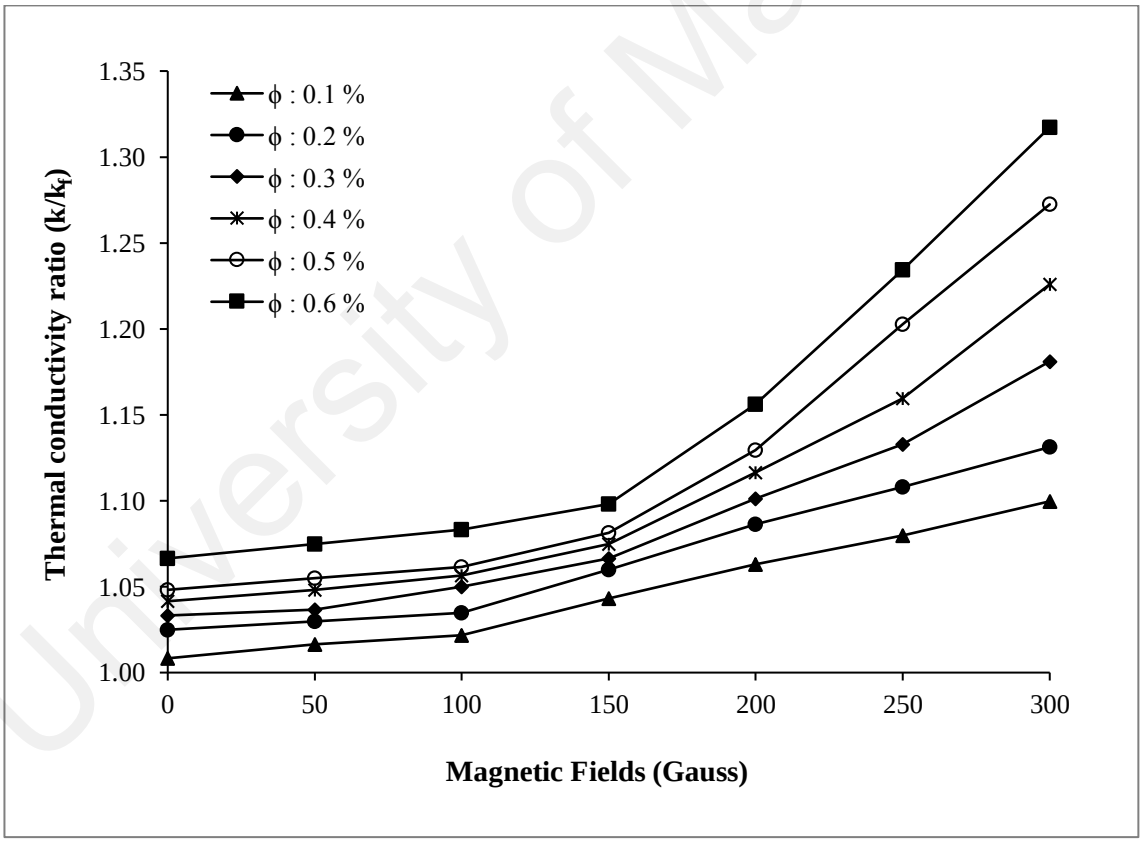

Figure 4.37: Thermal conductivity ratio of maghemite nanofluids as a function of magnetic field parallel to the temperature gradient at different volume fractions.

By applying the external magnetic fields, the magnetic dipolar interaction energy become strong enough to dominate the thermal energy so that the magnetic moments of the nanoparticles start aligning in the direction of magnetic fields. As the magnetic fields

increase, the particles start forming doublets, triplets and short chains along the direction of the magnetic fields. The lengths of the chains increase with increasing the magnetic fields.

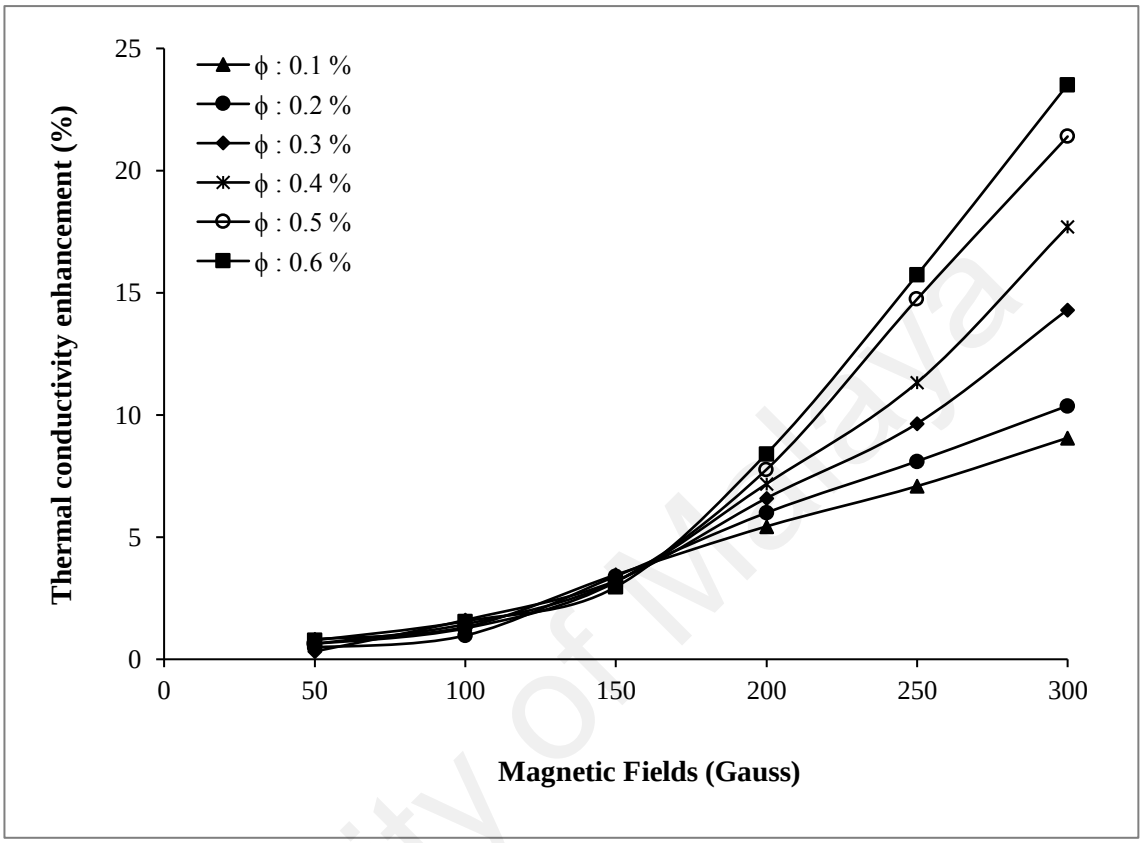

Figure 4.38: Thermal conductivity enhancement of maghemite nanofluids as a function of magnetic field parallel to the temperature gradient at different volume fractions.

Data measurements and their standard deviation of thermal conductivity of maghemite nanofluids under perpendicular magnetic fields arrangements is presented in Table 4.20. Meanwhile, the effect of magnetic fields strength on thermal conductivity of maghemite nanofluids for perpendicular magnetic fields arrangements was shown in Fig. 4.39. The regression line equations and their coefficient of determinations are tabulated in Table 4.21. Thermal conductivity ratio of maghemite nanofluids and their percentage of enhancement are presented in Figs. 4.40 and 4.41.

Table 4.20: Thermal conductivity of maghemite nanofluids at different perpendicular magnetic fields strength

Magnetic fields strength (Gauss)	**Thermal conductivity (W/mK)**		
	ϕ : 0.1 %	**ϕ : 0.2 %**	**ϕ : 0.3 %**
0	0.607 ± 0.0016	0.617 ± 0.0013	0.622 ± 0.0013
50	0.608 ± 0.0013	0.617 ± 0.0015	0.622 ± 0.0017
100	0.609 ± 0.0011	0.619 ± 0.0011	0.625 ± 0.0015
150	0.611 ± 0.0013	0.622 ± 0.0014	0.627 ± 0.0013
200	0.612 ± 0.0010	0.624 ± 0.0013	0.630 ± 0.0013
250	0.614 ± 0.0011	0.625 ± 0.0011	0.632 ± 0.0011
300	0.614 ± 0.0014	0.627 ± 0.0011	0.633 ± 0.0013
Magnetic fields strength (Gauss)	**Thermal conductivity (W/mK)**		
	ϕ : 0.4 %	**ϕ : 0.5 %**	**ϕ : 0.6 %**
0	0.627 ± 0.0016	0.631 ± 0.0016	0.643 ± 0.0016
50	0.629 ± 0.0015	0.633 ± 0.0015	0.644 ± 0.0013
100	0.632 ± 0.0016	0.636 ± 0.0013	0.645 ± 0.0011
150	0.635 ± 0.0013	0.639 ± 0.0011	0.648 ± 0.0013
200	0.637 ± 0.0015	0.641 ± 0.0015	0.651 ± 0.0014
250	0.641 ± 0.0018	0.645 ± 0.0016	0.654 ± 0.0016
300	0.643 ± 0.0014	0.650 ± 0.0011	0.656 ± 0.0013

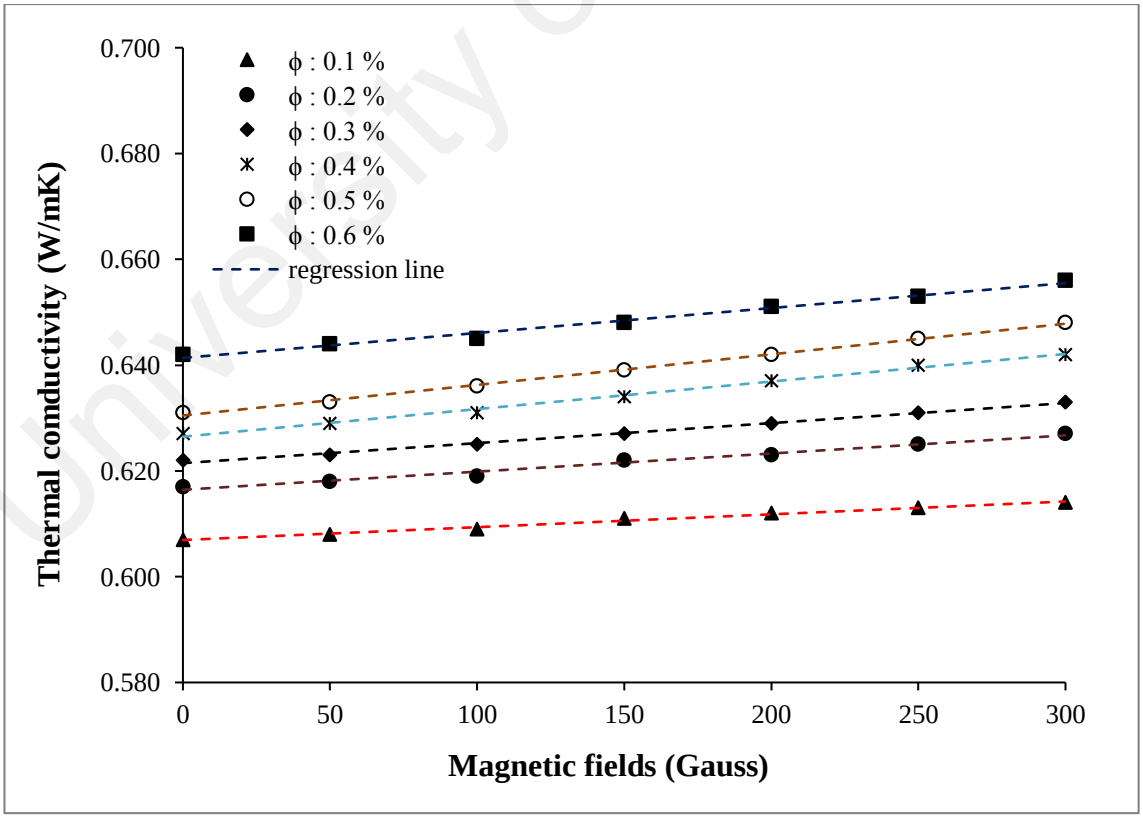

Figure 4.39: Thermal conductivity of maghemite nanofluids at different perpendicular magnetic fields strength

Table 4.21: Regression line equation of thermal conductivity of maghemite nanofluids at different perpendicular magnetic fields strength.

Particle volume fraction (%)	Equation line	R^2
0.1	Y = 3E-05X+0.6069	0.9759
0.2	Y = 4E-05X+0.6161	0.9705
0.3	Y = 4E-05X+0.6214	0.9849
0.4	Y = 6E-05X+0.6266	0.9948
0.5	Y = 6E-05X+0.6301	0.9804
0.6	Y = 5E-05X+0.6417	0.9708

It can be seen that the thermal conductivity of maghemite nanofluids is slightly dependent on perpendicular magnetic fields. There is little epffect if the magnetic fields are in position of a perpendicular direction to the samples. This can be explained that the maghemite nanoparticles suspended in the solution will be aligning to the direction of the magnetic fields. There has been very minor change in the thermal conductivity values, irrespective the applied magnetic field strength and the volume fraction of the particles as shown in Figs. 4.39 and 4.40. This can be explained that maghemite nanoparticles suspended in the solution form chain-like aggregation structure were aligned to the direction of magnetic fields (Shima et al., 2009). As a result, no chain alignment emerges on the particles along the temperature gradient. Therefore, thermal conductivity of nanofluids is weakly affected by perpendicular mode with maximum enhancement is only 2.69 %.

Without any external magnetic field, the magnetic moments of the scatterers are oriented in the random direction. With the increase in magnetic field, the moments of the magnetic particles start to align themselves along the direction of the magnetic fields.

Therefore, the observed enhancement of thermal conductivity is due to the effective heat transport through chain-like aggregates of nanoparticles. Though the particle aggregates in dispersions are fracted in nature, the aggregates formed are highly ordered under an external magnetic field. This enhanced the conduction through percolation paths that form parallel modes of conduction (Eapen et al., 2007).

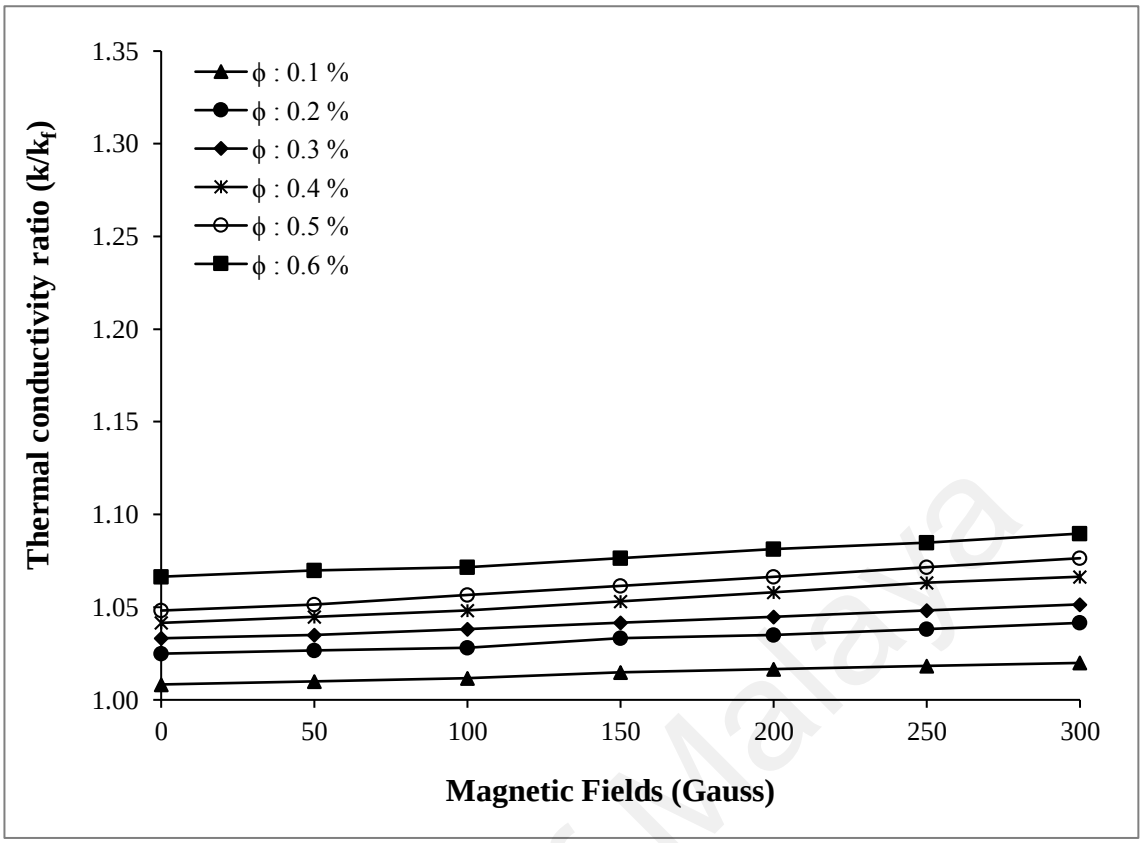

Figure 4.40: Thermal conductivity ratio of maghemite nanofluids as a function of magnetic field perpendicular to the temperature gradient at different volume fractions.

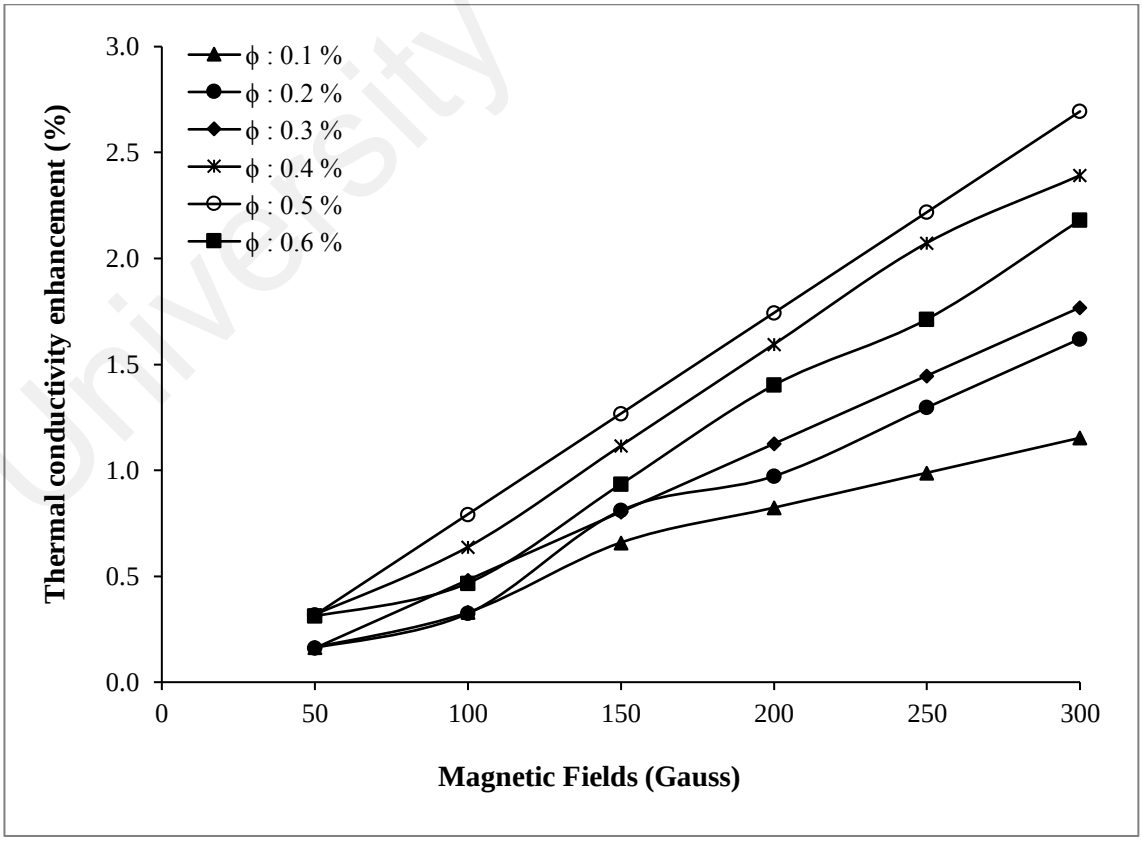

Figure 4.41: Thermal conductivity enhancement of maghemite nanofluids as a function of magnetic field perpendicular to the temperature gradient at different volume fractions

4.3.3.2 Kinematic Viscosity

Measurements and their standard deviation of kinematic viscosity of maghemite nanofluids under parallel magnetic fields arrangements is presented in Table 4.22. The effect of magnetic fields strength on kinematic viscosity of maghemite nanofluids for parallel magnetic fields arrangements is shown in Fig. 4.42. The regression line equations and their coefficient of determinations are tabulated in Table 4.23. Kinematic viscosity ratio of maghemite nanofluids and their percentage of enhancement are presented in Figs. 4.43 and 4.44.

Table 4.22: Kinematic viscosity of maghemite nanofluids as a function of different parallel magnetic fields strength at 25 ^{o}C for different particle volume fraction.

Magnetic fields strength (Gauss)	**Kinematic viscosity (cst)**		
	ϕ : 0.1 %	**ϕ : 0.2 %**	**ϕ : 0.3 %**
0	0.901 ± 0.0014	0.922 ± 0.0012	0.945 ± 0.0013
50	0.905 ± 0.0017	0.927 ± 0.0011	0.951 ± 0.0017
100	0.914 ± 0.0020	0.937 ± 0.0013	0.964 ± 0.0015
150	0.927 ± 0.0016	0.951 ± 0.0018	0.976 ± 0.0014
200	0.941 ± 0.0015	0.971 ± 0.0016	0.999 ± 0.0012
250	0.952 ± 0.0016	0.989 ± 0.0014	1.018 ± 0.0011
300	0.969 ± 0.0012	1.006 ± 0.0013	1.041 ± 0.0010
Magnetic fields strength (Gauss)	**Kinematic viscosity (cst)**		
	ϕ : 0.4 %	**ϕ : 0.5 %**	**ϕ : 0.6 %**
0	0.957 ± 0.0018	0.968 ± 0.0010	0.976 ± 0.0019
50	0.964 ± 0.0020	0.977 ± 0.0014	0.993 ± 0.0019
100	0.978 ± 0.0012	0.993 ± 0.0016	1.007 ± 0.0009
150	0.996 ± 0.0017	1.011 ± 0.0015	1.038 ± 0.0013
200	1.019 ± 0.0012	1.045 ± 0.0012	1.070 ± 0.0017
250	1.053 ± 0.0015	1.086 ± 0.0016	1.117 ± 0.0018
300	1.087 ± 0.0013	1.127 ± 0.0016	1.156 ± 0.0015

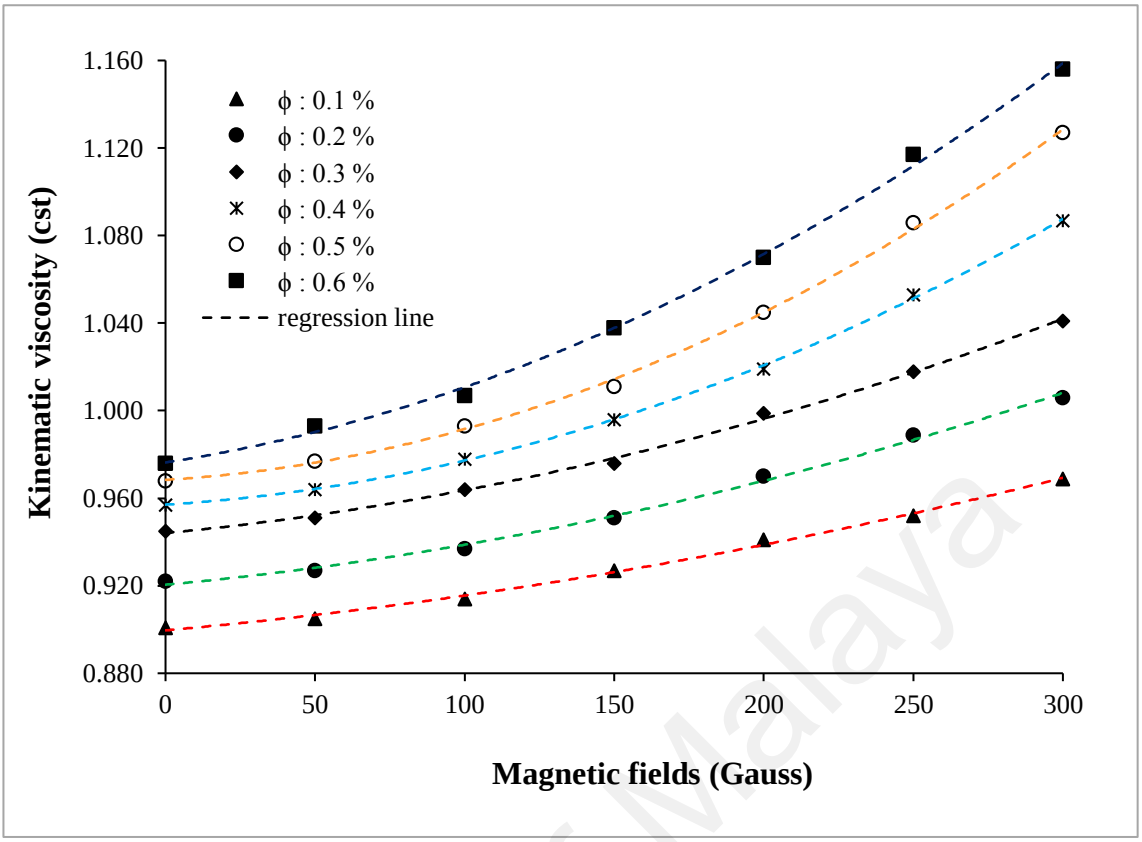

Figure 4.42: Kinematic viscosity of maghemite nanofluids as a function of different parallel magnetic fields strength at 25 ºC for different particle volume fractions.

Table 4.23: Regression line equation of kinematic viscosity of maghemite nanofluids at different parallel magnetic fields strength

Particle volume fraction (%)	Equation line	R^2
0.1	$Y = 4E\text{-}07X^2 + 0.0001X + 0.8996$	0.9964
0.2	$Y = 5E\text{-}07X^2 + 1E\text{-}04X + 0.9205$	0.9964
0.3	$Y = 7E\text{-}06X^2 + 0.0001X + 0.9440$	0.9979
0.4	$Y = 1E\text{-}06X^2 + 8E\text{-}05X + 0.9570$	0.9995
0.5	$Y = 2E\text{-}06X^2 + 8E\text{-}05X + 0.9684$	0.9987
0.6	$Y = 1E\text{-}06X^2 + 0.0002X + 0.9763$	0.9978

It can be seen that the kinematic viscosity of maghemite nanofluids is increased with increasing of magnetic fields strength at any particle volume fraction. In the presence of magnetic field, the viscosity of the nanofluid become strongly anisotropic due to nanoparticle structure that alter the transport properties.

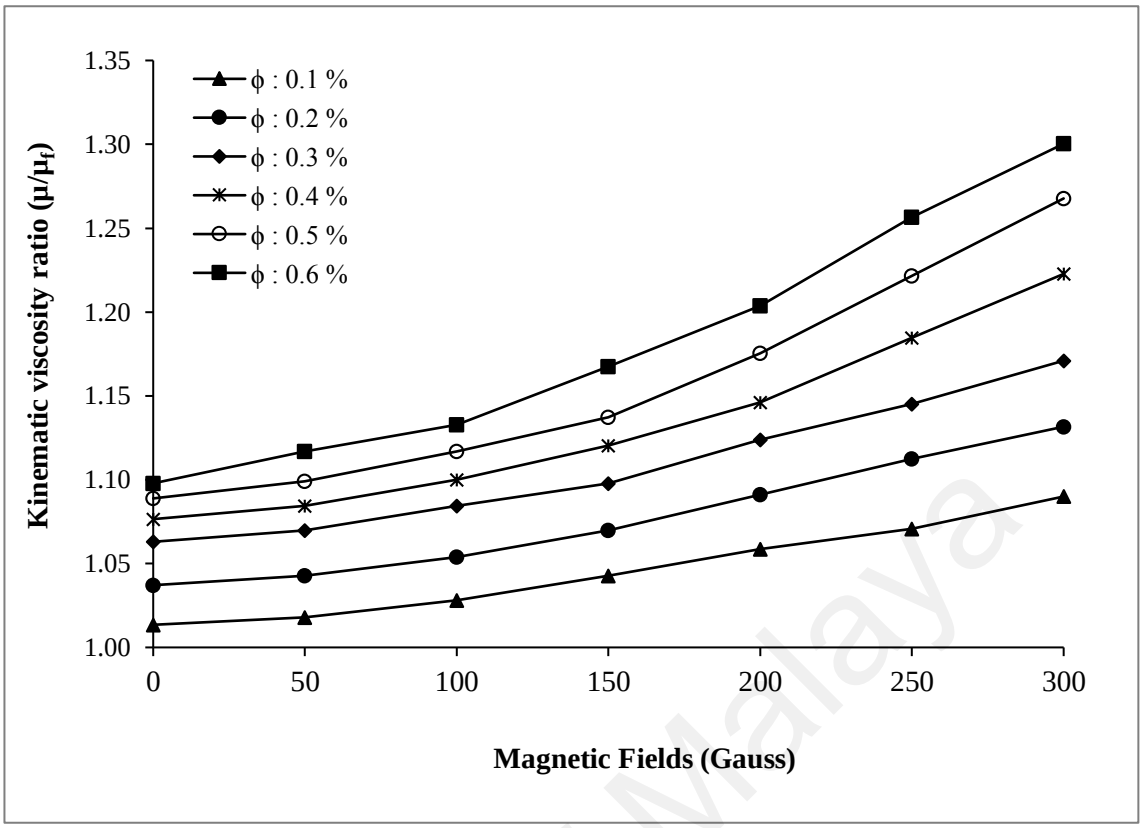

Figure 4.43: Kinematic viscosity ratio of maghemite nanofluids as a function of different parallel magnetic fields strength at 25 ºC for different particle volume fractions

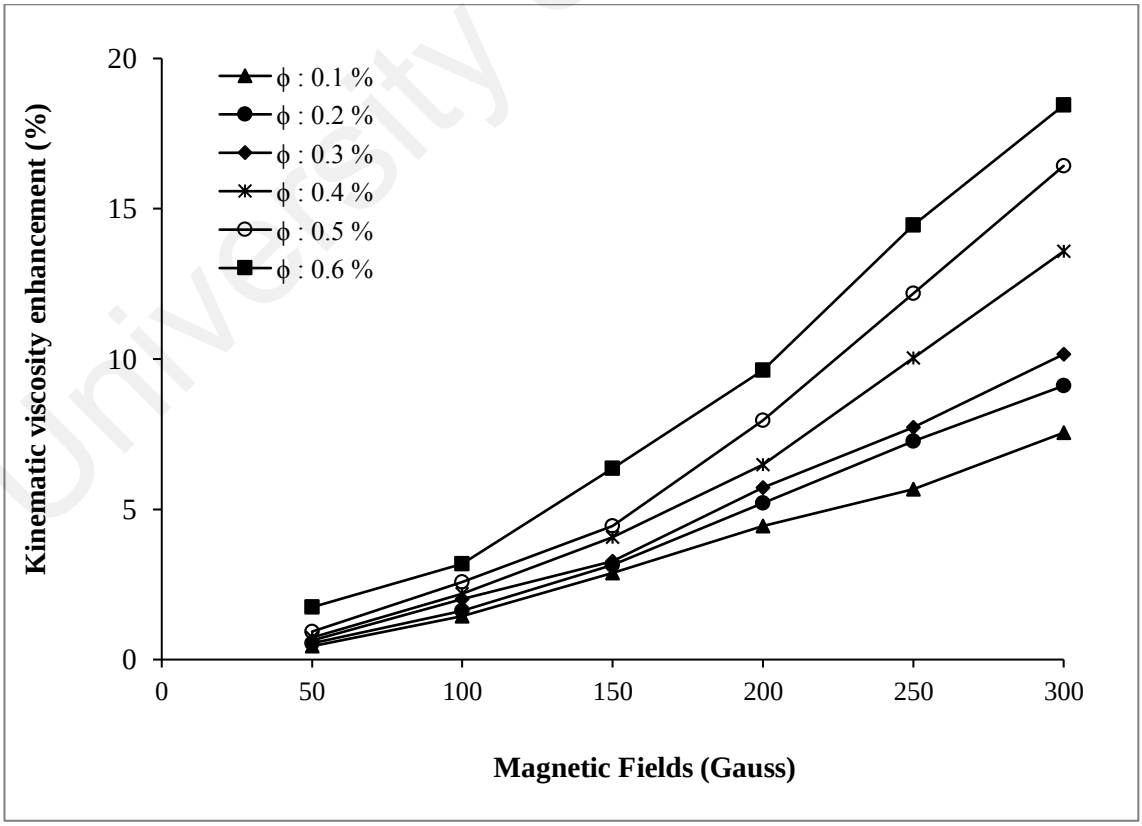

Figure 4.44: Kinematic viscosity enhancement of maghemite nanofluids as a function of different parallel magnetic fields strength at 25 ºC for different particle volume fractions.

Measurements and their standard deviation of kinematic viscosity of maghemite nanofluids under perpendicular magnetic fields arrangements is presented in Table 4.24. The effect of magnetic fields strength on kinematic viscosity of maghemite nanofluids for parallel magnetic fields arrangements is shown in Fig. 4.45. The regression line equations and their coefficient of determinations are tabulated in Table 4.25. Kinematic viscosity ratio of maghemite nanofluids and their percentage of enhancement are presented in Figs. 4.46 and 4.47.

Table 4.24: Kinematic viscosity of maghemite nanofluids at different perpendicular magnetic fields strength

Magnetic fields strength (Gauss)	**Kinematic viscosity (cst)**		
	ϕ : 0.1 %	**ϕ : 0.2 %**	**ϕ : 0.3 %**
0	0.901 ± 0.0014	0.922 ± 0.0012	0.945 ± 0.0013
50	0.906 ± 0.0015	0.926 ± 0.0013	0.952 ± 0.0015
100	0.912 ± 0.0013	0.934 ± 0.0017	0.961 ± 0.0010
150	0.920 ± 0.0012	0.942 ± 0.0018	0.969 ± 0.0016
200	0.928 ± 0.0022	0.957 ± 0.0017	0.978 ± 0.0010
250	0.938 ± 0.0021	0.972 ± 0.0012	0.989 ± 0.0014
300	0.955 ± 0.0021	0.988 ± 0.0014	1.010 ± 0.0014
Magnetic fields strength (Gauss)	**Kinematic viscosity (cst)**		
	ϕ : 0.4 %	**ϕ : 0.5 %**	**ϕ : 0.6 %**
0	0.957 ± 0.0018	0.968 ± 0.0010	0.976 ± 0.0019
50	0.964 ± 0.0015	0.975 ± 0.0015	0.985 ± 0.0021
100	0.972 ± 0.0011	0.983 ± 0.0020	0.997 ± 0.0013
150	0.984 ± 0.0010	0.998 ± 0.0016	1.014 ± 0.0015
200	1.002 ± 0.0016	1.021 ± 0.0019	1.036 ± 0.0017
250	1.022 ± 0.0012	1.051 ± 0.0018	1.073 ± 0.0013
300	1.045 ± 0.0021	1.078 ± 0.0014	1.102 ± 0.0014

It can be seen that the kinematic viscosity of maghemite nanofluids at any particle volume fraction is increased with magnetic fields strength. For diluted maghemite nanofluids with noninteracting particles, the Brownian motion of particles is hindered by magnetic fields, resulting in the increase of kinematic viscosity. In the other case, the interactions between particles and particularly the cluster formation will further increase the viscosity.

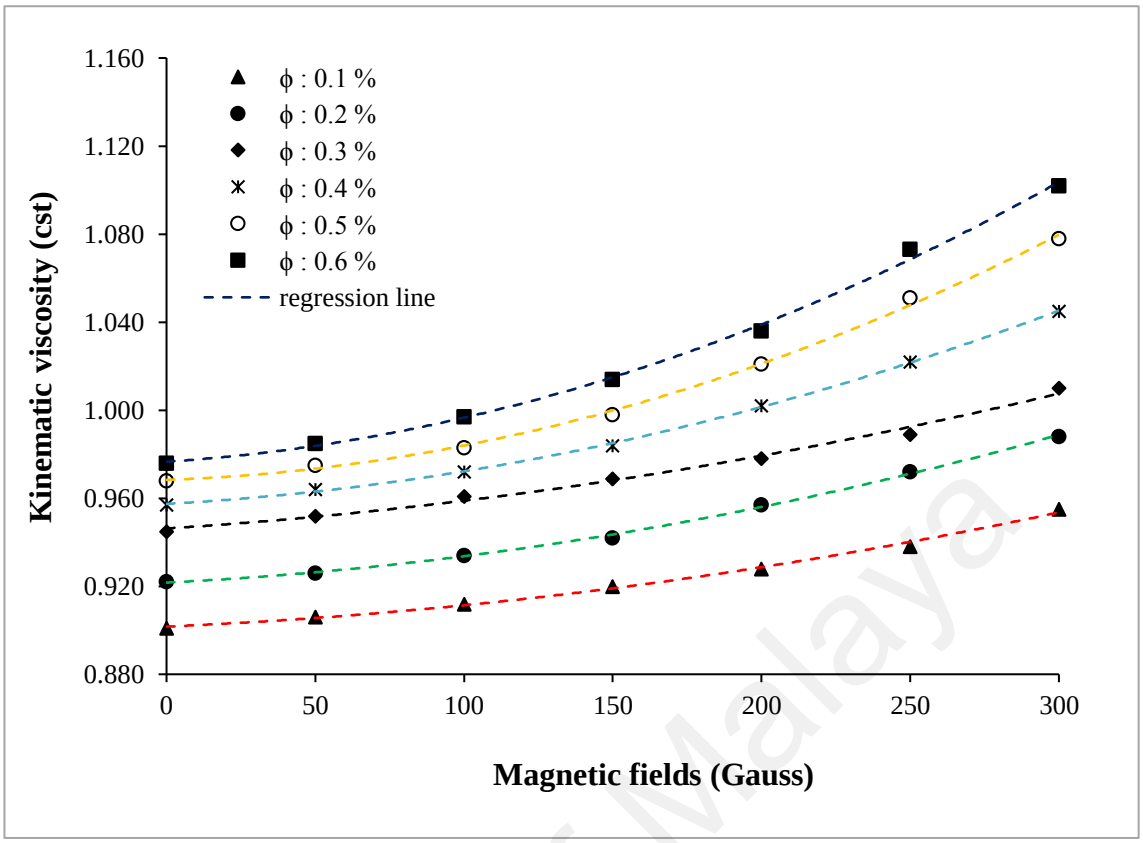

Figure 4.45: Kinematic viscosity of maghemite nanofluids at different perpendicular magnetic fields strength at 25 ^{o}C.

Table 4.25: Regression line equation of kinematic viscosity of maghemite nanofluids at different perpendicular magnetic fields strength.

Particle volume fraction (%)	Equation line	R^2
0.1	$Y = 4E\text{-}07X^2 + 1E\text{-}04X + 0.9017$	0.9958
0.2	$Y = 5E\text{-}07X^2 + 7E\text{-}05X + 0.9217$	0.9986
0.3	$Y = 4E\text{-}07X^2 + 9E\text{-}05X + 0.9462$	0.9912
0.4	$Y = 7E\text{-}07X^2 + 8E\text{-}05X + 0.9574$	0.9996
0.5	$Y = 1E\text{-}06X^2 + 5E\text{-}05X + 0.9683$	0.9980
0.6	$Y = 1E\text{-}06X^2 + 9E\text{-}05X + 0.9766$	0.9974

When maghemite nanofluids were subjected to both perpendicular and parallel magnetic fields arrangement, the particle chains along the direction of magnetic fields blocks the flow channel of the maghemite nanofluids, resulted in higher friction force along the flow of maghemite nanofluids. This phenomenon enhances the kinematic viscosity of maghemite nanofluids.

It can also be seen that the kinematic viscosity of maghemite nanofluids are slightly higher in parallel magnetic fields arrangement compared to perpendicular magnetic fields arrangement.

The highest enhancement of kinematic viscosity of maghemite nanofluids at perpendicular and parallel arrangement are 12.91 % and 18.44 %, respectively which obtained at magnetic fields strength of 300 Gauss and particle volume fraction of 0.6 %.

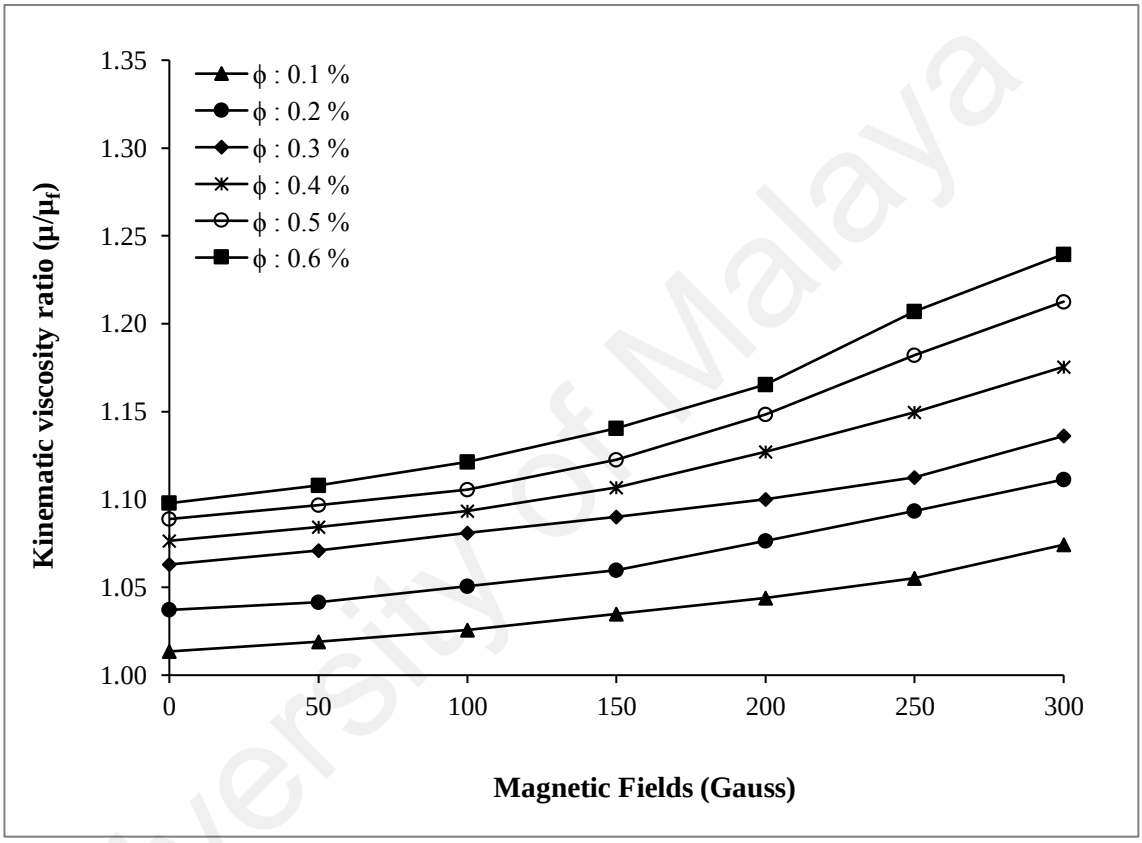

Figure 4.46: Kinematic viscosity ratio of maghemite nanofluids as a function of magnetic field perpendicular to the temperature gradient at different volume fractions.

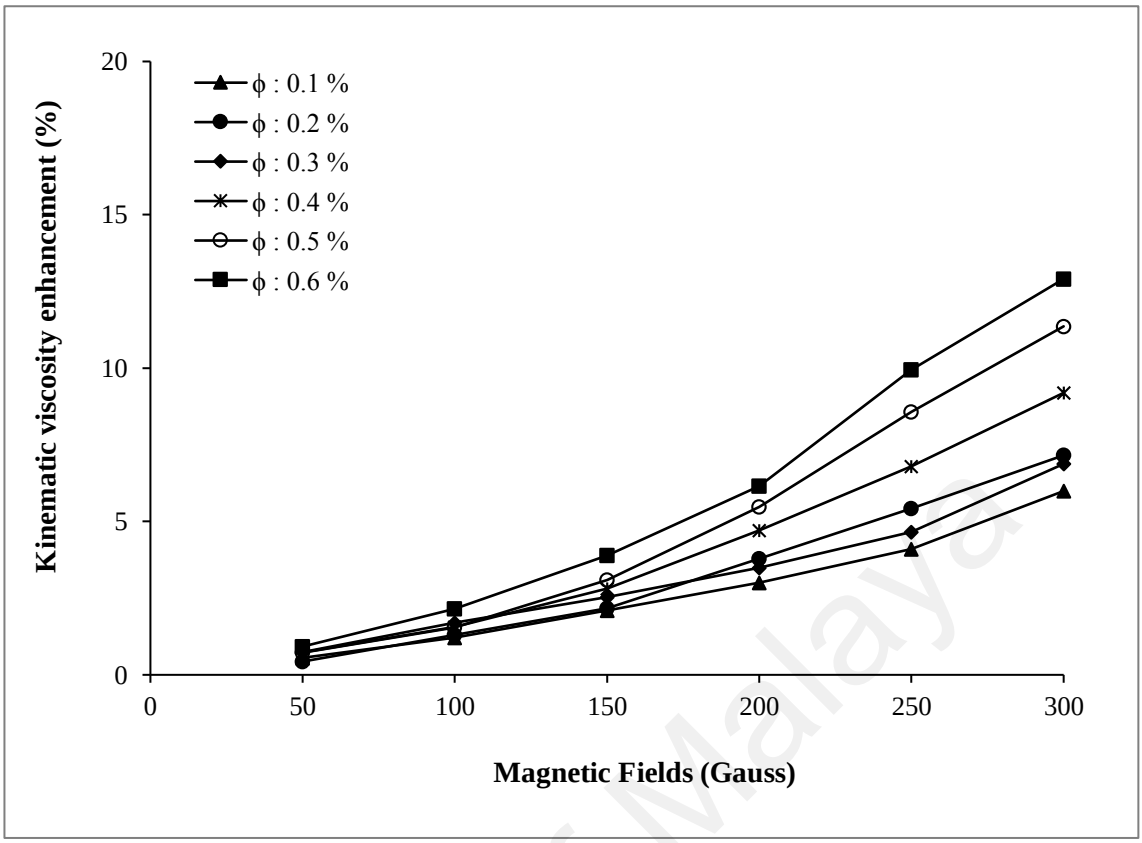

Figure 4.47: Kinematic viscosity enhancement of maghemite nanofluids as a function of magnetic field perpendicular to the temperature gradient at different volume fractions

4.3.3.3 Electrical Conductivity

Measurements data and their standard deviation of electrical conductivity of maghemite nanofluids under parallel magnetic fields arrangements is presented in Table 4.26. The effect of magnetic fields strength on electrical conductivity of maghemite nanofluids for parallel magnetic fields arrangements is shown in Fig. 4.48. The regression line equations and their coefficient of determinations are tabulated in Table 4.27.

Table 4.26: Electrical conductivity of maghemite nanofluids at different parallel magnetic fields strength

Magnetic fields strength (Gauss)	Electrical Conductivity (mS/cm)		
	ϕ : 0.1 %	**ϕ : 0.2 %**	**ϕ : 0.3 %**
0	1.011 ± 0.0013	2.019 ± 0.0013	3.160 ± 0.0014
50	1.011 ± 0.0009	2.020 ± 0.0013	3.161 ± 0.0009
100	1.012 ± 0.0014	2.020 ± 0.0015	3.161 ± 0.0010
150	1.013 ± 0.0011	2.021 ± 0.0009	3.162 ± 0.0013
200	1.013 ± 0.0011	2.021 ± 0.0013	3.162 ± 0.0011
250	1.014 ± 0.0016	2.022 ± 0.0013	3.163 ± 0.0014
300	1.015 ± 0.0008	2.023 ± 0.0009	3.164 ± 0.0012
Magnetic fields strength (Gauss)	Electrical Conductivity (mS/cm)		
	ϕ : 0.4 %	**ϕ : 0.5 %**	**ϕ : 0.6 %**
0	4.109 ± 0.0010	4.994 ± 0.0013	6.624 ± 0.0013
50	4.113 ± 0.0013	4.996 ± 0.0013	6.627 ± 0.0010
100	4.113 ± 0.0008	4.998 ± 0.0010	6.630 ± 0.0009
150	4.115 ± 0.0011	5.002 ± 0.0009	6.631 ± 0.0013
200	4.116 ± 0.0013	5.003 ± 0.0015	6.632 ± 0.0013
250	4.117 ± 0.0009	5.004 ± 0.0014	6.634 ± 0.0013
300	4.119 ± 0.0008	5.005 ± 0.0009	6.635 ± 0.0010

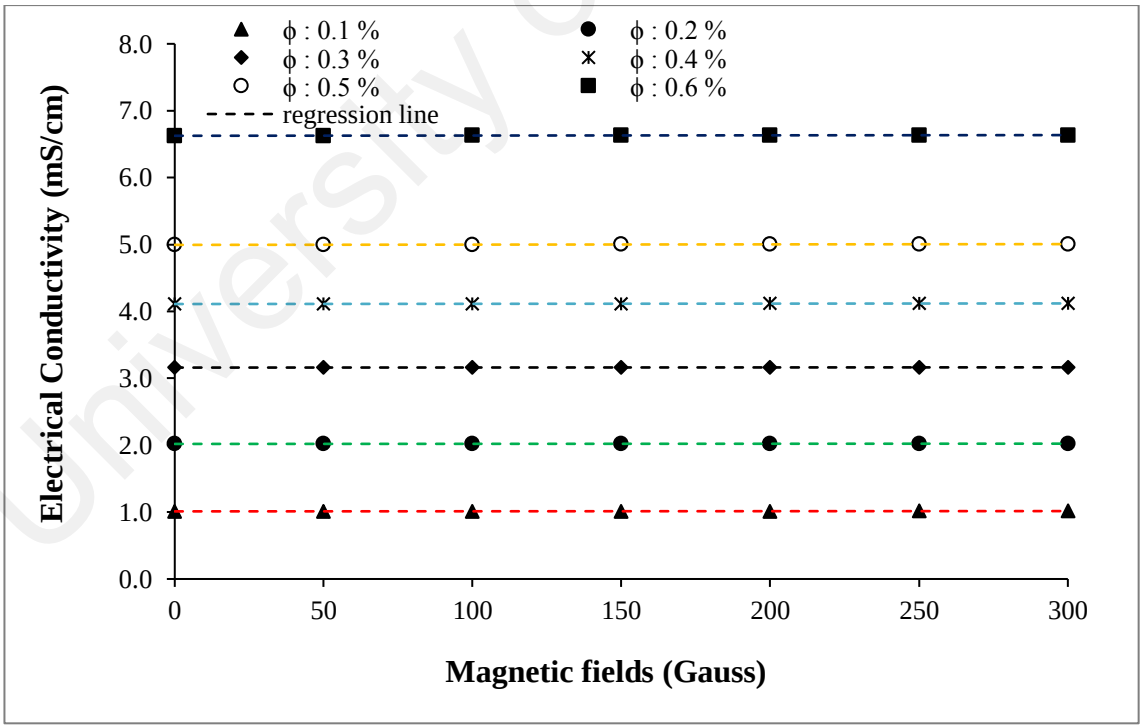

Figure 4.48: Electrical conductivity of maghemite nanofluids as a function of magnetic field parallel to the temperature gradient at different volume fractions.

Table 4.27: Regression line equation of electrical conductivity of maghemite nanofluids at different parallel magnetic fields strength.

Particle volume fraction (%)	Equation line	R^2
0.1	Y = 1E-5X+1.0107	0.9601
0.2	Y = 1E-5X+2.019	0.9507
0.3	Y = 1E-5X+3.16	0.9507
0.4	Y = 3E-5X+4.1102	0.9423
0.5	Y = 4E-5X+4.9945	0.9517
0.6	Y = 4E-5X+6.6252	0.9558

It can be seen that the electrical conductivity of maghemite nanofluids are independent of the magnetic fields strength at any particle volume fraction. This can be explained that the electrical conductivity of nanofluids is related to the ability of charged particles (ions) in the suspensions to carry the charges (electrons) towards respective electrode when the electrical potential is applied. In nanofluids, the dispersed nanoparticles in a base fluids get charged due to the formation of electrical double layers around the particle surface. These nanoparticles along with EDL move towards oppositely charged electrode when the potential is applied. This EDL formation depends on the surface charge (pH), size and particle volume fraction and ionic concentration in base fluids. Thus the electrophoretic mobility of charged particles determines the electrical conductivity of nanofluids (Sarojini et al., 2013).

Without any external magnetic field, the magnetic moments of the scatterers are oriented in the random direction. With the increase in magnetic field, the moments of the magnetic particles start to align themselves along the direction of the magnetic fields. However, the surface charge of the particles is remained with the effect of magnetic fields. Hence, the electrical conductivity of maghemite nanofluids remain stable at any particular concentrations.

Measurements data and their standard deviation of electrical conductivity of maghemite nanofluids under perpendicular magnetic fields arrangements is presented in Table 4.28. The effect of magnetic fields strength on electrical conductivity of maghemite

nanofluids for perpendicular magnetic fields arrangements was shown in Fig. 4.49. The regression line equations and their coefficient of determinations are tabulated in Table 4.29.

Table 4.28: Electrical conductivity of maghemite nanofluids at different perpendicular magnetic fields strength

Magnetic fields strength (Gauss)	**Electrical Conductivity (mS/cm)**		
	ϕ : 0.1 %	**ϕ : 0.2 %**	**ϕ : 0.3 %**
0	1.013 ± 0.0011	2.019 ± 0.0008	3.130 ± 0.0011
50	1.016 ± 0.0010	2.022 ± 0.0009	3.133 ± 0.0010
100	1.018 ± 0.0013	2.023 ± 0.0010	3.135 ± 0.0013
150	1.020 ± 0.0010	2.024 ± 0.0008	3.137 ± 0.0015
200	1.021 ± 0.0011	2.025 ± 0.0010	3.139 ± 0.0013
250	1.022 ± 0.0013	2.027 ± 0.0009	3.139 ± 0.0010
300	1.023 ± 0.0011	2.028 ± 0.0009	3.140 ± 0.0011
Magnetic fields strength (Gauss)	**Electrical Conductivity (mS/cm)**		
	ϕ : 0.4 %	**ϕ : 0.5 %**	**ϕ : 0.6 %**
0	4.118 ± 0.0011	5.008 ± 0.0011	6.628 ± 0.0009
50	4.120 ± 0.0010	5.011 ± 0.0010	6.630 ± 0.0011
100	4.121 ± 0.0008	5.012 ± 0.0013	6.631 ± 0.0013
150	4.123 ± 0.0010	5.014 ± 0.0010	6.633 ± 0.0011
200	4.123 ± 0.0015	5.015 ± 0.0008	6.633 ± 0.0013
250	4.124 ± 0.0009	5.016 ± 0.0011	6.634 ± 0.0008
300	4.125 ± 0.0010	5.017 ± 0.0008	6.635 ± 0.0009

It can also be observed that the magnetic fields strength does not affect the electrical conductivity of maghemite nanofluids at perpendicular arrangement of magnetic fields. According to EDL theory, since the charged nanoparticles are electrically conducting material, the electrical conductivity may still increase due to establishment of short conducting paths by aggregate contact of the solid materials. According to this assumption, the EDL effects are very small and insignificant, and, therefore, the electrophoretic effects may be also unimportant (Washabaugh et al., 1996).

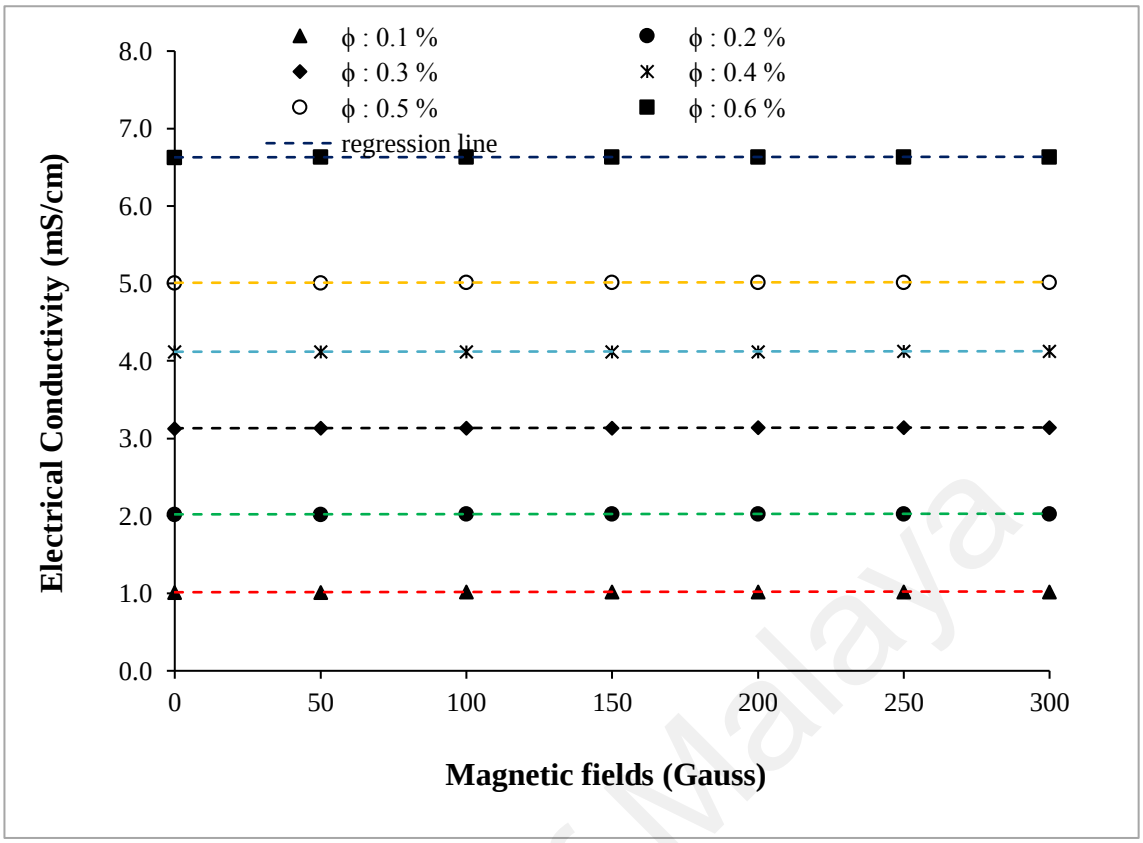

Figure 4.49: Electrical conductivity enhancement of maghemite nanofluids as a function of magnetic field perpendicular to the temperature gradient at different volume fractions.

Table 4.29: Regression line equation of electrical conductivity of maghemite nanofluids at different parallel magnetic fields strength.

Particle volume fraction (%)	Equation line	R^2
0.1	Y = 3E-5X+1.0142	0.9516
0.2	Y = 3E-5X+2.0198	0.9700
0.3	Y = 3E-5X+3.1312	0.9346
0.4	Y = 2E-5X+4.1187	0.9534
0.5	Y = 3E-5X+5.009	0.9615
0.6	Y = 2E-5X+6.6287	0.9534

CHAPTER 5: CONCLUSIONS AND RECOMENDATIONS

This chapter describes the conclusions of the synthesis, characterization and thermophysical properties of maghemite nanofluids with and without magnetic fields effect and recommendations for future research.

5.1 Conclusions

Stable maghemite nanoparticles have been successfully synthesized using a chemical coprecipitation method with the effect of nitric acid concentrations as an oxidizing agent. The pattern obtained from XRD results confirm that the particles are maghemite. The morphology of maghemite nanoparticles are spherical. The maghemite nanoparticles show superparamagnetic behavior with decreased magnetization values at the increasing concentration of nitric acid concentration. With this behavior, the maghemite nanoparticles can be controlled with external magnetic fields. Thermal stability of maghemite nanoparticles show a two steps weight loss behavior. TGA measurement showed that the stability temperature decreases with the increasing concentration of nitric acid. The temperature stability is achieved earlier at the smaller particle size. DLS measurement showed that the hydrodynamic particle sizes decrease with the increasing concentration of nitric acid. The zeta potential values decrease with the increasing concentration of nitric acid. The increasing concentration of nitric acid in synthesis of maghemite nanoparticles produced smaller size particles, lower magnetization, better thermal stability and more stable maghemite nanofluids. It can be concluded that the best result from synthesis parameter is using 10 M nitric acid concentration.

The environmental play a significant role in the stability of the suspension. The maghemite nanofluids are remain stable with the effect of time of storage. The suspensions remain stable after eight months of storage.

The particle volume fraction has significant effect to the enhancement of the thermophysical properties of maghemite nanofluids. The thermal conductivity of maghemite nanofluids linearly increases with the increasing of particle volume fraction. The kinematic viscosity of maghemite nanofluids linearly increases with increasing of particle volume fraction. The electrical conductivity of maghemite nanofluids is signicantly increase with the increasing of particle volume fraction.

The temperature of the solution also effects the properties of thermophysical properties of maghemite nanofluids. The temperature is significantly effects of thermal conductivity by randomly increase the molecule movement in the suspension. Hence, thermal conductivity of maghemite nanofluids nonlinearly increase with the increasing of temperature. The kinematic viscosity of maghemite nanofluids nonlinearly decrease with the increasing of temperature of solutions due to weakening of inter-particle and inter-molecular adhesion forces hence accelerate the movement of the particles in liquids. The electrical conductivity of maghemite nanofluids linearly increases with the increasing of temperature.

The effect of external magnetic fields on the thermophysical properties of maghemite nanofluids is significant. The data show that thermal conductivity of maghemite nanofluids increases with the increasing of the strength of magnetic fields for parallel and perpendicular magnetic fields arrangements. The parallel arrangement has significant enhancement compared to perpendicular arrangement. The kinematic viscosity of maghemite nanofluids also increase with increasing of magnetic fields strength for both parallel and perpendicular arrangements. The enhancement of kinematic viscosity of maghemite nanofluids for parallel arrangement is higher than perpendicular arrangement. The electrical conductivity of maghemite nanofluids are not influenced by the increasing of magnetic fields strength for both parallel and perpendicular arrangements.

5.2 Recommendations

In this study maghemite nanoparticles have been synthesized using chemical co-precipitation method. Preparation of maghemite nanofluids is conducted by disperse a certain amount of maghemite nanoparticles in water as base fluids. The thermophysical properties is studied at the effect of particle volume fraction, temperatures and magnetic fields. Some considerations and recommendations can be suggested to further investigated of the unique maghemite nanofluids.

1. The maghemite nanoparticles were synthesized at different nitric acid concentration. The results show that stable maghemite nanoparticle have been synthesized. There are several factors that influenced the synthesis of maghemite nanoparticles by co-precipitation methods, such as temperature, concentration ratio, and reaction time. It is suggested to further investigate those effect to get more detail results.
2. The stability of nanofluids is strongly depend on the pH of the solution. In this study, the pH of maghemite nanofluids is 3.60. We did not put any surfactant for the stability study to these nanofluids. Therefore, in order to further investigate the stability of maghemite nanofluids in various pHs, it suggested to evaluate the effect of surfactant on the stability of maghemite nanofluids.
3. The thermophysical properties are important parameters in the application of maghemite nanofluids. Several parameters such as thermal conductivity, viscosity, and electrical conductivity have been studied in various effect such as particle volume fraction, temperature, and magnetic fields strength. However, there are many other parameters and effects which are not yet been explored. Hence, further investigations are required to enrich physical properties data for maghemite nanofluids.
4. This study has not been considered the model development for the formulation of thermophysical properties of maghemite nanofluids. This is needed in order to predict

the properties of maghemite nanofluids in the application processes. So, the development of the model is required in the further study.

REFERENCES

Abareshi, M., Goharshadi, E. K., Zebarjad, S. M., Fadafan, H. K., & Youssefi, A. (2010). Fabrication, characterization and measurement of thermal conductivity of Fe_3O_4 nanofluids. *Journal of Magnetism and Magnetic Materials, 322*(24), 3895-3901.

Abbas, M., Islam, M. N., Rao, B. P., Abdel-Hamed, M. O., & Kim, C. (2015). Facile one-pot chemical approach for synthesis of monodisperse chain-like superparamagnetic maghemite (γ-Fe_2O_3) nanoparticles. *Journal of Industrial and Engineering Chemistry, 31*, 43-46.

Ali, K., Sarfraz, A. K., Mirza, I. M., Bahadur, A., Iqbal, S., & ul Haq, A. (2015). Preparation of superparamagnetic maghemite (γ-Fe_2O_3) nanoparticles by wet chemical route and investigation of their magnetic and dielectric properties. *Current Applied Physics, 15*(8), 925-929.

Alsaady, M., Fu, R., Li, B., Boukhanouf, R., & Yan, Y. (2015). Thermo-physical properties and thermo-magnetic convection of ferrofluid. *Applied Thermal Engineering, 88*, 14-21.

Asuha, S., Suyala, B., Siqintana, X., & Zhao, S. (2011). Direct synthesis of Fe_3O_4 nanopowder by thermal decomposition of Fe-urea complex and its properties. *Journal of Alloys and Compounds, 509*(6), 2870-2873.

Azmi, W. H., Sharma, K. V., Mamat, R., Najafi, G., & Mohamad, M. S. (2016). The enhancement of effective thermal conductivity and effective dynamic viscosity of nanofluids – A review. *Renewable and Sustainable Energy Reviews, 53*, 1046-1058.

Babita, Sharma, S. K., & Gupta, S. M. (2016). Preparation and evaluation of stable nanofluids for heat transfer application: A review. *Experimental Thermal and Fluid Science, 79*, 202-212.

Baby, T. T., & Ramaprabhu, S. (2010). Investigation of thermal and electrical conductivity of graphene based nanofluids. *Journal of Applied Physics, 108*(12), 124308.

Bagheli, S., Fadafan, H. K., Orimi, R. L., & Ghaemi, M. (2015). Synthesis and experimental investigation of the electrical conductivity of water based magnetite nanofluids. *Powder Technology, 274*, 426-430.

Bailar Jr, J. C., & Auten, R. W. (1934). The stereochemistry of complex inorganic compounds. I. The Walden inversion as exhibited by diethylenediaminocobaltic compounds. *Journal of the American Chemical Society, 56*(4), 774-776.

Batchelor, G. (1977). The effect of Brownian motion on the bulk stress in a suspension of spherical particles. *Journal of Fluid Mechanics, 83*(01), 97-117.

Bee, A., Massart, R., & Neveu, S. (1995). Synthesis of Very Fine Maghemite Particles. *Journal of Magnetism and Magnetic Materials, 149*(1-2), 6-9.

Behdadfar, B., Kermanpur, A., Sadeghi-Aliabadi, H., Morales, M. D., & Mozaffari, M. (2012). Synthesis of aqueous ferrofluids of $ZnxFe_3$-xO_4 nanoparticles by citric

acid assisted hydrothermal-reduction route for magnetic hyperthermia applications. *Journal of Magnetism and Magnetic Materials, 324*(14), 2211-2217.

Blasiak, B., van Veggel, F. C., & Tomanek, B. (2013). Applications of nanoparticles for MRI cancer diagnosis and therapy. *Journal of Nanomaterials, 2013*, 12.

Blums, E. (2002). Heat and mass transfer phenomena. *Journal of Magnetism and Magnetic Materials, 252*(0), 189-193.

Brinkman, H. (1952). The viscosity of concentrated suspensions and solutions. *The Journal of Chemical Physics, 20*(4), 571-571.

Bruggeman, D. (1935). Dielectric constant and conductivity of mixtures of isotropic materials. *Ann Phys (Leipzig), 24*, 636-679.

Cabuil, V., Neveu, S., & Rosensweig, R. (1993). Introduction to the magnetic fluids bibliography. *Journal of Magnetism and Magnetic Materials, 122*(1), 437-438.

Caparrós, C., Benelmekki, M., Martins, P. M., Xuriguera, E., Silva, C. J. R., Martinez, L. M., & Lanceros-Méndez, S. (2012). Hydrothermal assisted synthesis of iron oxide-based magnetic silica spheres and their performance in magnetophoretic water purification. *Materials Chemistry and Physics, 135*(2–3), 510-517.

Carp, M., Müller, R., Draghiciu, L., Voicu, R., & Danila, M. (2011). Characterization of microdevices for ferrous chloride separation for biosensing applications. *Sensors and Actuators A: Physical, 171*(1), 26-33.

Casula, M. F., Corrias, A., Arosio, P., Lascialfari, A., Sen, T., Floris, P., & Bruce, I. J. (2011). Design of water-based ferrofluids as contrast agents for magnetic resonance imaging. *Journal of Colloid and Interface Science, 357*(1), 50-55.

Charles, S. W. (2002). The preparation of magnetic fluids *Ferrofluids* (pp. 3-18): Berlin, Springer.

Chaudhury, M. K. (2003). Complex fluids: Spread the word about nanofluids. *Nature, 423*(6936), 131-132.

Chin, A. B., & Yaacob, I. I. (2007). Synthesis and characterization of magnetic iron oxide nanoparticles via w/o microemulsion and Massart's procedure. *Journal of materials processing technology, 191*(1), 235-237.

Choi, S.-S. (1998). Nanofluid technology: current status and future research: Argonne National Lab., IL (US).

Choi, S. U., Xu, X., Keblinski, P., & Yu, W. (2002). *Nanofluids can take the heat.* Paper presented at the DOE/BES Symposium on Energy Engineering Sciences.

Choi, S. U., Zhang, Z. G., & Keblinski, P. (2004). Nanofluids *Encyclopedia of Nanoscience and Nanotechnology* (Vol. 6, pp. 757-773): American Scientific Publishers.

Chol, S. (1995). Enhancing thermal conductivity of fluids with nanoparticles. *ASME-Publications-Fed, 231*, 99-106.

Chopkar, M., Das, P. K., & Manna, I. (2006). Synthesis and characterization of nanofluid for advanced heat transfer applications. *Scripta Materialia, 55*(6), 549-552.

Chopkar, M., Kumar, S., Bhandari, D., Das, P. K., & Manna, I. (2007). Development and characterization of Al_2Cu and Ag_2Al nanoparticle dispersed water and ethylene glycol based nanofluid. *Materials Science and Engineering: B, 139*(2), 141-148.

Cruz, R. C., Reinshagen, J., Oberacker, R., Segadães, A. M., & Hoffmann, M. J. (2005). Electrical conductivity and stability of concentrated aqueous alumina suspensions. *Journal of Colloid and Interface Science, 286*(2), 579-588.

Cuny, L., Herrling, M. P., Guthausen, G., Horn, H., & Delay, M. (2015). Magnetic resonance imaging reveals detailed spatial and temporal distribution of iron-based nanoparticles transported through water-saturated porous media. *Journal of Contaminant Hydrology, 182*, 51-62.

Dibaji, S. A. R., Al-Rjoub, M. F., Myers, M. R., & Banerjee, R. K. (2013). Enhanced Heat Transfer and Thermal Dose Using Magnetic Nanoparticles During HIFU Thermal Ablation—An In-Vitro Study. *Journal of Nanotechnology in Engineering and Medicine, 4*(4), 040902.

Dobnikar, J., Haložan, D., Brumen, M., Von Grünberg, H.-H., & Rzehak, R. (2004). Poisson–Boltzmann Brownian dynamics of charged colloids in suspension. *Computer Physics Communications, 159*(2), 73-92.

Dong, M., Shen, L., Wang, H., Wang, H., & Miao, J. (2013). Investigation on the electrical conductivity of transformer oil-based AlN nanofluid. *Journal of Nanomaterials, 2013*, 164.

Eapen, J., Williams, W. C., Buongiorno, J., Hu, L.-w., Yip, S., Rusconi, R., & Piazza, R. (2007). Mean-field versus microconvection effects in nanofluid thermal conduction. *Physical Review Letters, 99*(9), 095901.

Eastman, J. A., Phillpot, S., Choi, S., & Keblinski, P. (2004). Thermal transport in nanofluids 1. *Annu. Rev. Mater. Res., 34*, 219-246.

Eggers, J. R., & Kabelac, S. (2016). Nanofluids revisited. *Applied Thermal Engineering, 106*, 1114-1126.

Einstein, A. (1906). Eine neue bestimmung der moleküldimensionen. *Annalen der Physik, 324*(2), 289-306.

Evans, W., Prasher, R., Fish, J., Meakin, P., Phelan, P., & Keblinski, P. (2008). Effect of aggregation and interfacial thermal resistance on thermal conductivity of nanocomposites and colloidal nanofluids. *International Journal of Heat and Mass Transfer, 51*(5), 1431-1438.

Fang, F., & Zhang, Y. (2005). DC electrical conductivity of Au nanoparticle/chloroform and toluene suspensions. *Journal of materials science, 40*(11), 2979-2980.

Fleet, M. E. (1986). The structure of magnetite: Symmetry of cubic spinels. *Journal of Solid State Chemistry, 62*(1), 75-82.

Fu, H. L., & Gao, L. (2012). Effect of interfacial nanolayer on thermophoresis in nanofluids. *International Journal of Thermal Sciences, 61*(0), 61-66.

Fultz, B., & Howe, J. M. (2012). *Transmission electron microscopy and diffractometry of materials*: Springer Science & Business Media.

Galindo, R., Dector, A., Arriaga, L., Gutiérrez, S., & Herrasti, P. (2012). Maghemite as a catalyst for glucose oxidation in a microfluidic fuel cell. *Journal of Electroanalytical Chemistry, 671*, 38-43.

Ganguly, S., Sikdar, S., & Basu, S. (2009). Experimental investigation of the effective electrical conductivity of aluminum oxide nanofluids. *Powder Technology, 196*(3), 326-330.

Gao, L., Zhou, X., & Ding, Y. (2007). Effective thermal and electrical conductivity of carbon nanotube composites. *Chemical Physics Letters, 434*(4), 297-300.

Gavili, A., Zabihi, F., Isfahani, T. D., & Sabbaghzadeh, J. (2012). The thermal conductivity of water base ferrofluids under magnetic field. *Experimental Thermal and Fluid Science, 41*, 94-98.

Genc, S., & Derin, B. (2014). Synthesis and rheology of ferrofluids: a review. *Current Opinion in Chemical Engineering, 3*, 118-124.

Ghadimi, A., Saidur, R., & Metselaar, H. (2011). A review of nanofluid stability properties and characterization in stationary conditions. *International Journal of Heat and Mass Transfer, 54*(17), 4051-4068.

Glory, J., Bonetti, M., Helezen, M., Mayne-L'Hermite, M., & Reynaud, C. (2008). Thermal and electrical conductivities of water-based nanofluids prepared with long multiwalled carbon nanotubes. *Journal of Applied Physics, 103*(9), 094309.

Godson, L., Raja, B., Mohan Lal, D., & Wongwises, S. (2010). Enhancement of heat transfer using nanofluids—An overview. *Renewable and Sustainable Energy Reviews, 14*(2), 629-641.

Gonçalves, J. R. (2016). The Soil and Groundwater Remediation with Zero Valent Iron Nanoparticles. *Procedia Engineering, 143*, 1268-1275.

Goshayeshi, H. R., Goodarzi, M., Safaei, M. R., & Dahari, M. Experimental Study on the Effect of Inclination Angle on Heat Transfer Enhancement of a Ferrofluid in a Closed Loop Oscillating Heat Pipe under Magnetic Field. *Experimental Thermal and Fluid Science*.

Gupte, S. K., Advani, S. G., & Huq, P. (1995). Role of micro-convection due to non-affine motion of particles in a mono-disperse suspension. *International Journal of Heat and Mass Transfer, 38*(16), 2945-2958.

Hamilton, R., & Crosser, O. (1962). Thermal conductivity of heterogeneous two-component systems. *Industrial & Engineering chemistry fundamentals, 1*(3), 187-191.

Haynes, W. M. (2013). *CRC handbook of chemistry and physics*: Londan, CRC press.

Herrmann, I., Schlegel, A., Graf, R., Stark, W., & Beck-Schimmer, B. (2015). Magnetic separation-based blood purification: a promising new approach for the removal of disease-causing compounds. *Journal of nanobiotechnology, 13*(1), 49.

Hong, T.-K., Yang, H.-S., & Choi, C. (2005). Study of the enhanced thermal conductivity of Fe nanofluids. *Journal of Applied Physics, 97*(6), 064311.

Hsieh, T.-H., Ho, K.-S., Bi, X., Han, Y.-K., Chen, Z.-L., Hsu, C.-H., & Chang, Y.-C. (2009). Synthesis and electromagnetic properties of polyaniline-coated silica/maghemite nanoparticles. *European Polymer Journal, 45*(3), 613-620.

Huang, C., Neoh, K. G., Wang, L., Kang, E.-T., & Shuter, B. (2010). Magnetic nanoparticles for magnetic resonance imaging: modulation of macrophage uptake by controlled PEGylation of the surface coating. *Journal of Materials Chemistry, 20*(39), 8512-8520.

Huang, J., Wang, X., Long, Q., Wen, X., Zhou, Y., & Li, L. (2009). *Influence of pH on the stability characteristics of nanofluids.* Paper presented at the Photonics and Optoelectronics, 2009. SOPO 2009. Wuhan, China.

Huminic, G., Huminic, A., Morjan, I., & Dumitrache, F. (2011). Experimental study of the thermal performance of thermosyphon heat pipe using iron oxide nanoparticles. *International Journal of Heat and Mass Transfer, 54*(1), 656-661.

Hunter, R. J. (2013). *Zeta potential in colloid science: principles and applications* (Vol. 2): London, Academic press limited.

Hwang, Y., Lee, J.-K., Lee, J.-K., Jeong, Y.-M., Cheong, S.-i., Ahn, Y.-C., & Kim, S. H. (2008). Production and dispersion stability of nanoparticles in nanofluids. *Powder Technology, 186*(2), 145-153.

Hwang, Y., Lee, J. K., Lee, C. H., Jung, Y. M., Cheong, S. I., Lee, C. G., . . . Jang, S. P. (2007). Stability and thermal conductivity characteristics of nanofluids. *Thermochimica Acta, 455*(1–2), 70-74.

İlhan, B., Kurt, M., & Ertürk, H. (2016). Experimental investigation of heat transfer enhancement and viscosity change of hBN nanofluids. *Experimental Thermal and Fluid Science, 77*, 272-283.

Jakubovics, J. P., & Jakubovics, J. (1994). *Magnetism and magnetic materials*: Institute of Materials.

Jang, S. P., & Choi, S. U. (2004). Role of Brownian motion in the enhanced thermal conductivity of nanofluids. *Applied Physics Letters, 84*(21), 4316-4318.

Johnson, G., Benveniste, H., Black, R., Hedlund, L., Maronpot, R., & Smith, B. (1993). Histology by magnetic resonance microscopy. *Magnetic resonance quarterly, 9*(1), 1-30.

Keblinski, P., Phillpot, S., Choi, S., & Eastman, J. (2002). Mechanisms of heat flow in suspensions of nano-sized particles (nanofluids). *International Journal of Heat and Mass Transfer, 45*(4), 855-863.

Kim, P., Shi, L., Majumdar, A., & McEuen, P. (2001). Thermal transport measurements of individual multiwalled nanotubes. *Physical Review Letters, 87*(21), 215502.

Kim, Y., Han, S., & Hong, S. (2011). A feasibility study of magnetic separation of magnetic nanoparticle for forward osmosis. *Water Science & Technology, 64*(2), 469-476.

Kläser, K., Graeser, M., Steinhagen, D., & Luedtke-Buzug, K. (2015). Construction of a device for magnetic separation of superparamagnetic iron oxide nanoparticles. *Current Directions in Biomedical Engineering, 1*(1), 306-309.

Kluchova, K., Zboril, R., Tucek, J., Pecova, M., Zajoncova, L., Safarik, I., . . . Sebela, M. (2009). Superparamagnetic maghemite nanoparticles from solid-state synthesis–their functionalization towards peroral MRI contrast agent and magnetic carrier for trypsin immobilization. *Biomaterials, 30*(15), 2855-2863.

Kole, M., & Dey, T. (2010). Viscosity of alumina nanoparticles dispersed in car engine coolant. *Experimental Thermal and Fluid Science, 34*(6), 677-683.

Koo, J., & Kleinstreuer, C. (2004). A new thermal conductivity model for nanofluids. *Journal of Nanoparticle Research, 6*(6), 577-588.

Kováčik, J., Emmer, Š., & Bielek, J. (2015). Thermal conductivity of Cu-graphite composites. *International Journal of Thermal Sciences, 90*, 298-302.

Krishnamurthy, S., Bhattacharya, P., Phelan, P., & Prasher, R. (2006). Enhanced mass transport in nanofluids. *Nano Letters, 6*(3), 419-423.

Kumar, D. H., Patel, H. E., Kumar, V. R., Sundararajan, T., Pradeep, T., & Das, S. K. (2004). Model for heat conduction in nanofluids. *Physical Review Letters, 93*(14), 144301.

Lee, D. (2007). Thermophysical properties of interfacial layer in nanofluids. *Langmuir, 23*(11), 6011-6018.

Lee, D., Kim, J.-W., & Kim, B. G. (2006). A new parameter to control heat transport in nanofluids: surface charge state of the particle in suspension. *The Journal of Physical Chemistry B, 110*(9), 4323-4328.

Leong, K., Yang, C., & Murshed, S. (2006). A model for the thermal conductivity of nanofluids–the effect of interfacial layer. *Journal of Nanoparticle Research, 8*(2), 245-254.

Li, Q., Lian, W., Sun, H., & Xuan, Y. (2008). Investigation on operational characteristics of a miniature automatic cooling device. *International Journal of Heat and Mass Transfer, 51*(21), 5033-5039.

Li, Q., Xuan, Y., & Wang, J. (2005). Experimental investigations on transport properties of magnetic fluids. *Experimental Thermal and Fluid Science, 30*(2), 109-116.

Li, Q., & Xuan, Y. M. (2009). Experimental investigation on heat transfer characteristics of magnetic fluid flow around a fine wire under the influence of an external magnetic field. *Experimental Thermal and Fluid Science, 33*(4), 591-596.

Li, X., Zhu, D., Wang, X., Wang, N., Gao, J., & Li, H. (2008). Thermal conductivity enhancement dependent pH and chemical surfactant for Cu-H_2O nanofluids. *Thermochimica Acta, 469*(1), 98-103.

Lisunova, M. O., Lebovka, N. I., Melezhyk, O. V., & Boiko, Y. P. (2006). Stability of the aqueous suspensions of nanotubes in the presence of nonionic surfactant. *Journal of Colloid and Interface Science, 299*(2), 740-746.

Lundgren, T. S. (1972). Slow flow through stationary random beds and suspensions of spheres. *Journal of Fluid Mechanics, 51*(02), 273-299.

Lyklema, J. (2005). *Fundamentals of interface and colloid science: soft colloids* (Vol. 5): Academic press.

Magnet, C., Akouala, M., Kuzhir, P., Bossis, G., Zubarev, A., & Wereley, N. M. (2015). Closed-loop magnetic separation of nanoparticles on a packed bed of spheres. *Journal of Applied Physics, 117*(17), 17C719.

Mahbubul, I., Saidur, R., & Amalina, M. (2012). Latest developments on the viscosity of nanofluids. *International Journal of Heat and Mass Transfer, 55*(4), 874-885.

Maleki, H., Simchi, A., Imani, M., & Costa, B. F. O. (2012). Size-controlled synthesis of superparamagnetic iron oxide nanoparticles and their surface coating by gold for biomedical applications. *Journal of Magnetism and Magnetic Materials, 324*(23), 3997-4005.

Massart, R. (1981). Preparation of aqueous magnetic liquids in alkaline and acidic media. *IEEE transactions on magnetics*, 1247-1248.

Masuda, H., Ebata, A., Teramae, K., & Hishinuma, N. (1993). Alteration of thermal conductivity and viscosity of liquid by dispersing ultra-fine particles. *Netsu Bussei, 7*(4), 227-233.

Maxwell, J. C. (1954). *A Treatise on Electricity and Magnetism: By James Clerk Maxwell*: Dover.

Minea, A. A., & Luciu, R. S. (2012). Investigations on electrical conductivity of stabilized water based Al_2O_3 nanofluids. *Microfluidics and nanofluidics, 13*(6), 977-985.

Mintsa, H. A., Roy, G., Nguyen, C. T., & Doucet, D. (2009). New temperature dependent thermal conductivity data for water-based nanofluids. *International Journal of Thermal Sciences, 48*(2), 363-371.

Modesto-Lopez, L. B., & Biswas, P. (2010). Role of the effective electrical conductivity of nanosuspensions in the generation of TiO_2 agglomerates with electrospray. *Journal of Aerosol Science, 41*(8), 790-804.

Moeen, S. J., Vaezi, M., Yousefi, A., & Ghasemi, E. (2012). Synthesis and rheological properties of nickel-zinc ferrite polymer nanocomposites. *Journal of Applied Polymer Science, 123*(4), 2534-2539.

Murshed, S., Leong, K., & Yang, C. (2006). A model for predicting the effective thermal conductivity of nanoparticle-fluid suspensions. *International Journal of Nanoscience, 5*(01), 23-33.

Murshed, S., Leong, K., & Yang, C. (2008). Investigations of thermal conductivity and viscosity of nanofluids. *International Journal of Thermal Sciences, 47*(5), 560-568.

Nalwa, H. S. (2001). *Nanostructured materials and nanotechnology: concise edition*: Gulf Professional Publishing.

Nguyen, C., Desgranges, F., Roy, G., Galanis, N., Mare, T., Boucher, S., & Angue Mintsa, H. (2007). Temperature and particle-size dependent viscosity data for water-based nanofluids–hysteresis phenomenon. *International Journal of Heat and Fluid Flow, 28*(6), 1492-1506.

Nikitin, P. I., Vetoshko, P. M., & Ksenevich, T. I. (2007). New type of biosensor based on magnetic nanoparticle detection. *Journal of Magnetism and Magnetic Materials, 311*(1), 445-449.

Nitsas, M. T., & Koronaki, I. P. (2016). Investigating the potential impact of nanofluids on the performance of condensers and evaporators – A general approach. *Applied Thermal Engineering, 100*, 577-585.

Nkurikiyimfura, I., Wang, Y., & Pan, Z. (2013). Heat transfer enhancement by magnetic nanofluids—A review. *Renewable and Sustainable Energy Reviews, 21*, 548-561.

Nkurikiyimfura, I., Wang, Y., Pan, Z., & Hu, D. (2011). *Thermal conductivity enhancement of magnetic nanofluid in magnetic field.* Paper presented at the IEEE Proceedings of the International Conference on Materials for Renewable Energy & Environment (ICMREE), IEEE, Shanghai, China.

Nowak, J., Wolf, D., & Odenbach, S. (2014). A rheological and microscopical characterization of biocompatible ferrofluids. *Journal of Magnetism and Magnetic Materials, 354*, 98-104.

Nurdin, I., Johan, M., Yaacob, I., Ang, B., & Andriyana, A. (2014). Synthesis, characterisation and stability of superparamagnetic maghemite nanoparticle suspension. *Materials Research Innovations, 18*(S6), S6-200-S206-203.

O'brien, R. (1981). The electrical conductivity of a dilute suspension of charged particles. *Journal of Colloid and Interface Science, 81*(1), 234-248.

Odenbach, S. (2003). Ferrofluids—magnetically controlled suspensions. *Colloids and Surfaces A: Physicochemical and Engineering Aspects, 217*(1–3), 171-178.

Odenbach, S. (2004). Ferrofluids: Magnetically Controllable Fluids and Their Applications. *Applied Rheology, 14*(4), 179-179.

Odenbach, S., & Thurm, S. (2002). *Magnetoviscous effects in ferrofluids*: Berlin, Springer-Verlag.

Oh, J. K., & Park, J. M. (2011). Iron oxide-based superparamagnetic polymeric nanomaterials: design, preparation, and biomedical application. *Progress in Polymer Science, 36*(1), 168-189.

Pak, B. C., & Cho, Y. I. (1998). Hydrodynamic and heat transfer study of dispersed fluids with submicron metallic oxide particles. *Experimental Heat Transfer an International Journal, 11*(2), 151-170.

Pankhurst, Q. A., Connolly, J., Jones, S., & Dobson, J. (2003). Applications of magnetic nanoparticles in biomedicine. *Journal of Physics D: Applied Physics, 36*(13), R167.

Pastoriza-Gallego, M., Lugo, L., Legido, J., & Piñeiro, M. (2011). Enhancement of thermal conductivity and volumetric behavior of Fe_xO_y nanofluids. *Journal of Applied Physics, 110*(1), 014309.

Patel, R., Upadhyay, R., & Mehta, R. (2003). Viscosity measurements of a ferrofluid: comparison with various hydrodynamic equations. *Journal of Colloid and Interface Science, 263*(2), 661-664.

Peng, S., Wang, C., Xie, J., & Sun, S. (2006). Synthesis and stabilization of monodisperse Fe nanoparticles. *Journal of the American Chemical Society, 128*(33), 10676-10677.

Philip, J., Shima, P., & Raj, B. (2007). Enhancement of thermal conductivity in magnetite based nanofluid due to chainlike structures. *Applied Physics Letters, 91*(20), 203108-203108-203103.

Phuoc, T. X., Massoudi, M., & Chen, R.-H. (2011). Viscosity and thermal conductivity of nanofluids containing multi-walled carbon nanotubes stabilized by chitosan. *International Journal of Thermal Sciences, 50*(1), 12-18.

Posner, J. D. (2009). Properties and electrokinetic behavior of non-dilute colloidal suspensions. *Mechanics Research Communications, 36*(1), 22-32.

Raja, M., Vijayan, R., Dineshkumar, P., & Venkatesan, M. (2016). Review on nanofluids characterization, heat transfer characteristics and applications. *Renewable and Sustainable Energy Reviews, 64*, 163-173.

Ramimoghadam, D., Bagheri, S., & Abd Hamid, S. B. (2015). Stable monodisperse nanomagnetic colloidal suspensions: An overview. *Colloids and Surfaces B: Biointerfaces, 133*, 388-411.

Ramirez-Rico, J., Gutierrez-Pardo, A., Martinez-Fernandez, J., Popov, V. V., & Orlova, T. S. (2016). Thermal conductivity of Fe graphitized wood derived carbon. *Materials & Design, 99*, 528-534.

Rossi, L. M., Costa, N. J., Silva, F. P., & Goncalves, R. V. (2013). Magnetic nanocatalysts: supported metal nanoparticles for catalytic applications. *Nanotechnology Reviews, 2*(5), 597-614.

Sarojini, K. G. K., Manoj, S. V., Singh, P. K., Pradeep, T., & Das, S. K. (2013). Electrical conductivity of ceramic and metallic nanofluids. *Colloids and Surfaces A: Physicochemical and Engineering Aspects, 417*(0), 39-46.

Schinteie, G., Palade, P., Vekas, L., Iacob, N., Bartha, C., & Kuncser, V. (2013). Volume fraction dependent magnetic behaviour of ferrofluids for rotating seal applications. *Journal of Physics D: Applied Physics, 46*(39), 395501.

Schwegmann, H., Feitz, A. J., & Frimmel, F. H. (2010). Influence of the zeta potential on the sorption and toxicity of iron oxide nanoparticles on S. cerevisiae and E. coli. *Journal of Colloid and Interface Science, 347*(1), 43-48.

Sekine, K., Mitamura, Y., Murabayashi, S., Nishimura, I., Yozu, R., & Kim, D. W. (2003). Development of a magnetic fluid shaft seal for an axial-flow blood pump. *Artificial organs, 27*(10), 892-896.

Shao, M., Ning, F., Zhao, J., Wei, M., Evans, D. G., & Duan, X. (2012). Preparation of $Fe_3O_4xSiO_2$ layered double hydroxide core–hell microspheres for magnetic separation of proteins. *Journal of the American Chemical Society, 134*(2), 1071-1077.

Shen, L., Wang, H., Dong, M., Ma, Z., & Wang, H. (2012). Solvothermal synthesis and electrical conductivity model for the zinc oxide-insulated oil nanofluid. *Physics Letters A, 376*(10), 1053-1057.

Shima, P., Philip, J., & Raj, B. (2009). Magnetically controllable nanofluid with tunable thermal conductivity and viscosity. *Applied Physics Letters, 95*(13), 133112-133112-133113.

Shin, K. S., Choi, J.-Y., Park, C. S., Jang, H. J., & Kim, K. (2009). Facile synthesis and catalytic application of silver-deposited magnetic nanoparticles. *Catalysis Letters, 133*(1-2), 1-7.

Sikdar, S., Basu, S., & Ganguly, S. (2011). Investigation of electrical conductivity of titanium dioxide nanofluids. *International Journal of Nanoparticles, 4*(4), 336-349.

Singh, B. P., Bhattacharjee, S., & Besra, L. (2002). Influence of surface charge on maximizing solids loading in colloidal processing of alumina. *Materials Letters, 56*(4), 475-480.

Singh, B. P., Bhattacharjee, S., & Besra, L. (2002). Optimisation of performance of dispersants in aqueous plasma dissociated zircon suspension. *Ceramics International, 28*(4), 413-417.

Singh, B. P., Bhattacharjee, S., Besra, L., & Sengupta, D. K. (2004). Evaluation of dispersibility of aqueous alumina suspension in presence of Darvan C. *Ceramics International, 30*(6), 939-946.

Singh, B. P., Menchavez, R., Takai, C., Fuji, M., & Takahashi, M. (2005). Stability of dispersions of colloidal alumina particles in aqueous suspensions. *Journal of Colloid and Interface Science, 291*(1), 181-186.

Song, X., Luo, X., Zhang, Q., Zhu, A., Ji, L., & Yan, C. (2015). Preparation and characterization of biofunctionalized chitosan/Fe_3O_4 magnetic nanoparticles for application in liver magnetic resonance imaging. *Journal of Magnetism and Magnetic Materials, 388*, 116-122.

Steven, B., Albert, J., & Kevin, P. (2011). Investigation of the electrical conductivity of propylene glycol-based ZnO nanofluids. *Nanosca. Res. Lett, 6*, 346-351.

Sun, Z.-X., Su, F.-W., Forsling, W., & Samskog, P.-O. (1998). Surface Characteristics of Magnetite in Aqueous Suspension. *Journal of Colloid and Interface Science, 197*(1), 151-159.

Sundar, L. S., Sharma, K., Naik, M., & Singh, M. K. (2013a). Empirical and theoretical correlations on viscosity of nanofluids: A review. *Renewable and Sustainable Energy Reviews, 25*, 670-686.

Sundar, L. S., Singh, M. K., & Sousa, A. C. (2013b). Investigation of thermal conductivity and viscosity of Fe_3O_4 nanofluid for heat transfer applications. *International Communications in Heat and Mass Transfer, 44*, 7-14.

Takehira, R., Momose, Y., & Yamamura, S. (2010). Quantitative analysis of crystalline pharmaceuticals in tablets by pattern-fitting procedure using X-ray diffraction pattern. *International Journal of Pharmaceutics, 398*(1–2), 33-38.

Teja, A. S., & Koh, P.-Y. (2009). Synthesis, properties, and applications of magnetic iron oxide nanoparticles. *Progress in Crystal Growth and Characterization of Materials, 55*(1–2), 22-45.

Thomas, R., Park, I.-K., & Jeong, Y. Y. (2013). Magnetic iron oxide nanoparticles for multimodal imaging and therapy of cancer. *International journal of molecular sciences, 14*(8), 15910-15930.

Tillman, P., & Hill, J. M. (2007). Determination of nanolayer thickness for a nanofluid. *International Communications in Heat and Mass Transfer, 34*(4), 399-407.

Timofeeva, E. V., Gavrilov, A. N., McCloskey, J. M., Tolmachev, Y. V., Sprunt, S., Lopatina, L. M., & Selinger, J. V. (2007). Thermal conductivity and particle agglomeration in alumina nanofluids: experiment and theory. *Physical Review E, 76*(6), 061203.

Touloukian, Y., Powell, R., Ho, C., & Klemens, P. (1970). Thermophysical Properties of Matter-The TPRC Data Series. Volume 1. Thermal Conductivity-Metallic Elements and Alloys: DTIC Document.

Tsakiroglou, C., Terzi, K., Sikinioti-Lock, A., Hajdu, K., & Aggelopoulos, C. (2016). Assessing the capacity of zero valent iron nanofluids to remediate NAPL-polluted porous media. *Science of The Total Environment, 563–564*, 866-878.

Vafaei, S., & Wen, D. (2014). Critical heat flux of nanofluids inside a single microchannel: Experiments and correlations. *Chemical Engineering Research and Design, 92*(11), 2339-2351.

Varma, R. S. (2014). Nano-catalysts with magnetic core: sustainable options for greener synthesis. *Sustainable Chemical Processes, 2*(1), 11.

Vidal-Vidal, J., Rivas, J., & López-Quintela, M. A. (2006). Synthesis of monodisperse maghemite nanoparticles by the microemulsion method. *Colloids and Surfaces A: Physicochemical and Engineering Aspects, 288*(1–3), 44-51.

Wamkam, C. T., Opoku, M. K., Hong, H., & Smith, P. (2011). Effects of pH on heat transfer nanofluids containing ZrO_2 and TiO_2 nanoparticles. *Journal of Applied Physics, 109*(2), 024305.

Wang, B.-X., Zhou, L.-P., & Peng, X.-F. (2003). A fractal model for predicting the effective thermal conductivity of liquid with suspension of nanoparticles. *International Journal of Heat and Mass Transfer, 46*(14), 2665-2672.

Wang, X., Xu, X., & S. Choi, S. U. (1999). Thermal conductivity of nanoparticle-fluid mixture. *Journal of Thermophysics and Heat Transfer, 13*(4), 474-480.

Wasan, D. T., & Nikolov, A. D. (2003). Spreading of nanofluids on solids. *Nature, 423*(6936), 156-159.

Washabaugh, A., Mamishev, A., Du, Y., & Zahn, M. (1996). *Dielectric measurements of semi-insulating liquids and solids.* Paper presented at the Conduction and Breakdown in Dielectric Liquids, 1996, ICDL'96.

White, M.A. (2012), Physical properties of materials, second edition, CRC Press, Bocaraton, FL.

Wong, K.-F., & Bhshkar, T. (2006). *Transport properties of alumina nanofluids.* Paper presented at the ASME 2006 International Mechanical Engineering Congress and Exposition.

Xie, H., Fujii, M., & Zhang, X. (2005). Effect of interfacial nanolayer on the effective thermal conductivity of nanoparticle-fluid mixture. *International Journal of Heat and Mass Transfer, 48*(14), 2926-2932.

Xu, J., Yang, H., Fu, W., Du, K., Sui, Y., Chen, J., . . . Zou, G. (2007). Preparation and magnetic properties of magnetite nanoparticles by sol–gel method. *Journal of Magnetism and Magnetic Materials, 309*(2), 307-311.

Xuan, Y., & Li, Q. (2000). Heat transfer enhancement of nanofluids. *International Journal of Heat and fluid flow, 21*(1), 58-64.

Xuan, Y., Li, Q., & Hu, W. (2003). Aggregation structure and thermal conductivity of nanofluids. *AIChE Journal, 49*(4), 1038-1043.

Xuan, Y., & Lian, W. (2011). Electronic cooling using an automatic energy transport device based on thermomagnetic effect. *Applied Thermal Engineering, 31*(8), 1487-1494.

Yamaguchi, H., Derec, C., Smerlak, M., Servais, J., & Bacri, J.-C. (2010). 12th International Conference on Magnetic Fluids (ICMF12) Anomalous diffusion in microchannel under magnetic field. *Physics Procedia, 9*, 109-112.

Yamamura, S., & Momose, Y. (2001). Quantitative analysis of crystalline pharmaceuticals in powders and tablets by a pattern-fitting procedure using X-ray powder diffraction data. *International Journal of Pharmaceutics, 212*(2), 203-212.

Yarahmadi, M., Moazami Goudarzi, H., & Shafii, M. B. (2015). Experimental investigation into laminar forced convective heat transfer of ferrofluids under constant and oscillating magnetic field with different magnetic field arrangements and oscillation modes. *Experimental Thermal and Fluid Science, 68*, 601-611.

Yavuz, C. T., Prakash, A., Mayo, J., & Colvin, V. L. (2009). Magnetic separations: from steel plants to biotechnology. *Chemical Engineering Science, 64*(10), 2510-2521.

Yu, W., & Choi, S. (2003). The role of interfacial layers in the enhanced thermal conductivity of nanofluids: a renovated Maxwell model. *Journal of Nanoparticle Research, 5*(1-2), 167-171.

Yu, W., & Choi, S. (2004). The role of interfacial layers in the enhanced thermal conductivity of nanofluids: a renovated Hamilton–Crosser model. *Journal of Nanoparticle Research, 6*(4), 355-361.

Zablotsky, D., Mezulis, A., & Blums, E. (2009). Surface cooling based on the thermomagnetic convection: Numerical simulation and experiment. *International Journal of Heat and Mass Transfer, 52*(23), 5302-5308.

Zhang, H., Zhao, Z., Xu, X., & Li, L. (2011). Study on industrial wastewater treatment using superconducting magnetic separation. *Cryogenics, 51*(6), 225-228.

Zhang, H., & Zhu, G. (2012). One-step hydrothermal synthesis of magnetic Fe_3O_4 nanoparticles immobilized on polyamide fabric. *Applied Surface Science, 258*(11), 4952-4959.

Zhao, G., Jian, Y., & Li, F. (2016). Streaming potential and heat transfer of nanofluids in parallel plate microchannels. *Colloids and Surfaces A: Physicochemical and Engineering Aspects, 498*, 239-247.

Zhao, Y., Xi, B., Li, Y., Wang, M., Zhu, Z., Xia, X., . . . Luan, Z. (2012). Removal of phosphate from wastewater by using open gradient superconducting magnetic separation as pretreatment for high gradient superconducting magnetic separation. *Separation and Purification Technology, 86*, 255-261.

Župan, J., & Renjo, M. M. (2015). Thermal and Rheological Properties of Water-based Ferrofluids and Their Applicability as Quenching Media. *Physics Procedia, 75*, 1458-1467.

Zussman, S. (1997). New nanofluids increase heat transfer capability. *Argonne National Laboratory, USA, 4*.

LIST OF PUBLICATIONS AND PAPER PRESENTED

PUBLICATIONS:

1. Irwan Nurdin, Iskandar Idris Yaacob, Mohd. Rafie Johan, & Bee Chin Ang, (2012), Characterization and Stability Monitoring of Maghemite Nanoparticle Suspensions, Advanced Materials Research, Vol. 576, 398 – 401. (SCOPUS-Cited Publication).

2. B.C. Ang, I.I. Yaacob and Irwan Nurdin (2013). Investigation of Fe_2O_3/SiO_2 Nanocomposite by FESEM and TEM, Journal of Nanomaterials, Vol. 2013, 980390 (ISI cited - Q2). IP: 1.547

3. Bee Chin Ang, Iskandar Idris Yaacob, Irwan Nurdin (2013), Effect of Fe_2O_3/SiO_2 ratio on maghemite-silica particulate nanocomposites, Journal of Central South University, Vol. 20, Issue 11, pp 2954-2959 (ISI cited - Q3). IP: 0.434

4. Irwan Nurdin, Mohd Rafie Johan, Iskandar Idris Yaacob & Bee Chin Ang, (2014), Effect of Nitric Acid Concentrations on Synthesis and Stability of Maghemite Nanoparticle Suspension, The Scientific World Journal, Vol. 2014, 589479 (ISI cited - Q1). IP: 1.730

5. I. Nurdin, M. R. Johan, I. I. Yaacob, B. C. Ang and A. Andriyana (2014), Synthesis, Characterization and Stability of Superparamagnetic Maghemite Nanoparticle Suspensions. Materials Research Innovations, vol. 18. pp (ISI cited - Q4). IP: 0.321

6. Irwan Nurdin, Iskandar Idris Yaacob, Mohd Rafie Johan, (2016), Enhancement of thermal conductivity and kinematic viscosity in magnetically controllable maghemite (γ-Fe_2O_3) nanofluids, Experimental Thermal and Fluid Science vol. 77, pp. 265–271 (ISI cited - Q1). IP: 1.990

PAPER PRESENTED:

1. International Conference on Agricultural, Food and Biological Engineering (ICAFBE) 2012, May 10-13, 2012, Guangzhou, China.

2. International Conference on Advance Manufacturing and Materials Engineering (ICAMME) 2012, July 3-5, 2012, Kuala Lumpur, Malaysia.

3. 4th International Conference on Functional Materials and Devices (ICFMD) 2013, April 8 – 11, 2013, Penang, Malaysia.

4. 1st International Conference on the Science and Engineering of Materials (ICoSEM) 2013, November 13-14, 2013, Kuala Lumpur, Malaysia.

APPENDICES

Appendix A: Profile fit for XRD analysis

Profile Fit

Report

Experiment: ***IRWAN3.PRF***

User:

General

Pattern file:	E:\XRDFIL~1\IRWAN4.RD
Background file:	
Sample identification:	
Profile shape:	Pearson VII
Start angle:	10.0264
End angle:	99.8734

Search parameters:

FWHM:	0.518
Asymmetry parameter:	5
Intensity ratio:	0.5
Refine intensity ratio:	No
Peak detection threshold:	0

Refinement parameters:

Minimum calculated psf:	16.24
$\Delta\lambda / \lambda$:	0.0024817
Number of refinements:	5

Assigment parameters:

Initial refinement flag:	1
Assignment threshold:	5

Philips Analytical X-Ray **Peak Fit parameters** Profile Fit 1.0c

Num	Group	K	&	2θ		Intensity		FWHM		Asymm	μ & ξ	a2/a1	Integr.	Breadth
1	1	1		30.3307	Y	103	Y	0.8160	Y	5.00	1.60	0.50	1613.12	1.046
2	2	1		35.7096	Y	338	Y	0.8893	Y	5.00	1.60	0.50	5746.85	1.140
3	3	1		43.3899	Y	84	Y	0.8697	Y	5.00	1.60	0.50	1400.74	1.115
4	4	1		57.4285	Y	121	Y	0.8055	Y	5.00	1.60	0.50	1859.97	1.032
5	5	1		62.9668	Y	231	Y	0.8197	Y	5.00	1.60	0.50	3613.76	1.050

Num	Ratio	Total area	Overlap	Bg Res
1	0.780	2308.68	0.00	0.00
2	0.780	8416.62	0.00	0.00
3	0.780	1986.64	0.00	0.00
4	0.780	2675.69	0.00	0.00
5	0.780	5269.89	0.00	0.00

Num	Fixed	Start angle	End angle	Offset of background	Slope of background	Rmin
1		27.7814	32.0000	0.000	0.000	0.0880
2		33.4094	38.0324	0.000	0.000	0.0123
3		41.1140	45.0674	0.000	0.000	0.1110
4		55.1170	59.2044	0.000	0.000	0.0554
5		60.7450	65.2344	0.000	0.000	0.0181

Num	Angle	Intensity
0	27.7623	412
1	31.7765	399
2	31.9225	398
3	31.9225	399
4	33.3823	396
5	37.7615	383
6	40.9729	351
7	44.9142	340
8	55.0594	360
9	59.1467	333
10	60.5334	342
11	65.2776	335

Experiment: E:\XRDFIL~1\IRWAN3.PRF 19-sep-2011 12:59

Philips Analytical X-Ray **Plot** Profile Fit 1.0c

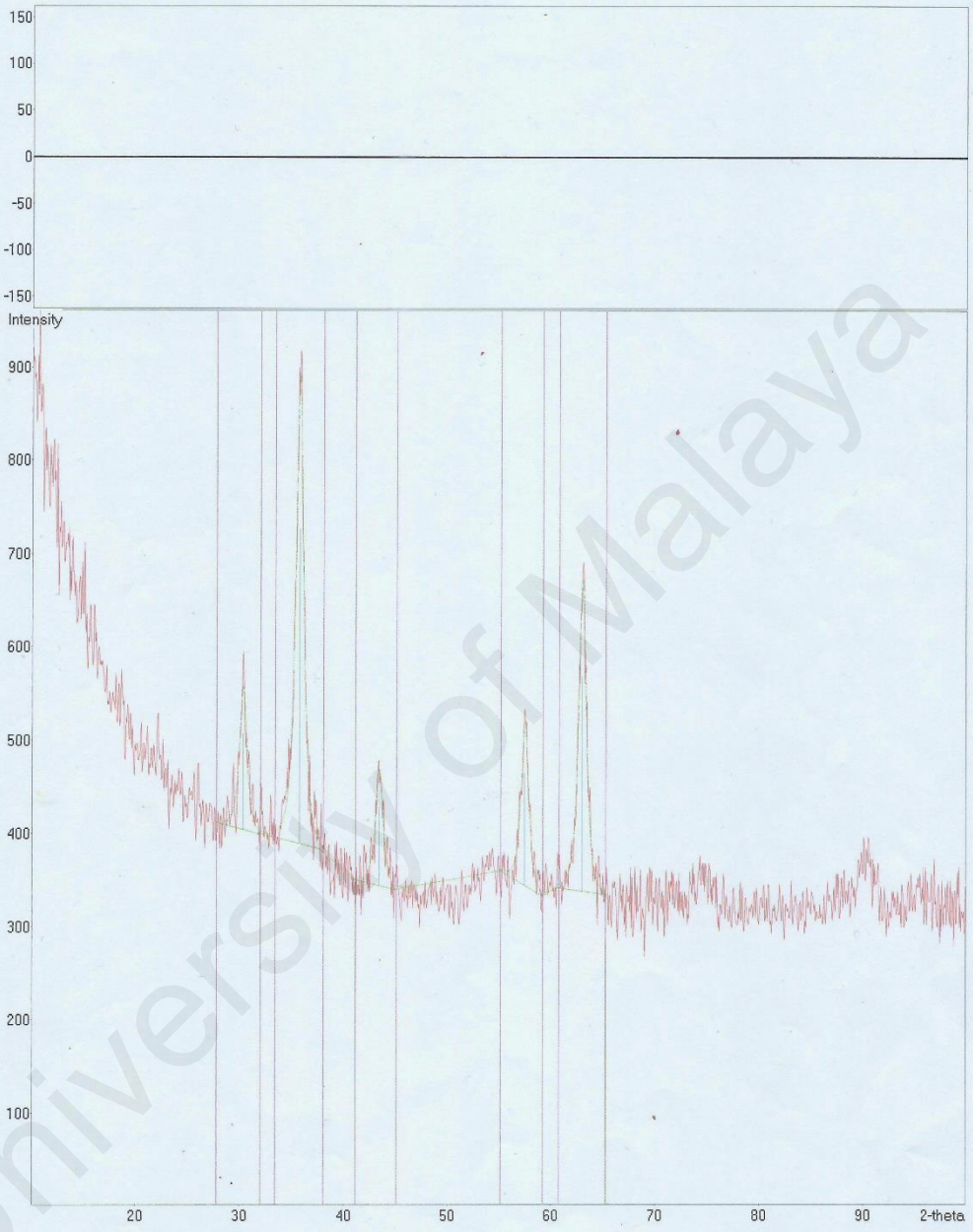

Appendix B: TEM image of maghemite nanoparticle

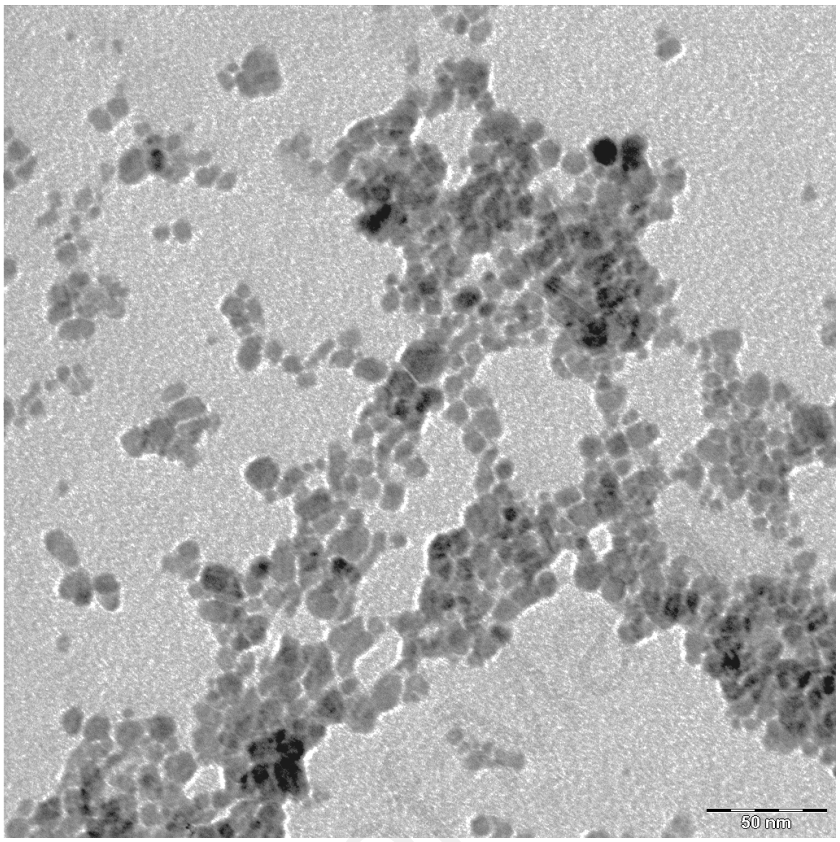

Appendix C: TGA thermogram of maghemite nanoparticle

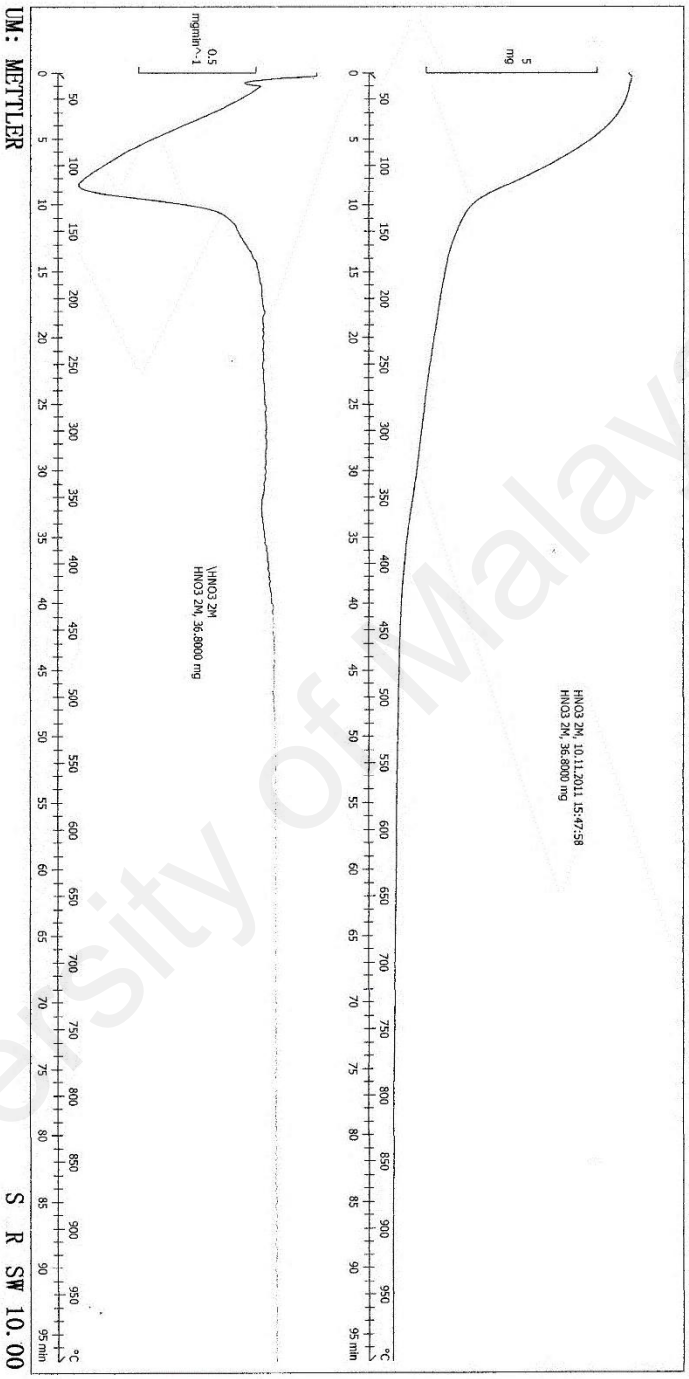

Appendix D: DLS measurement of maghemite nanoparticle

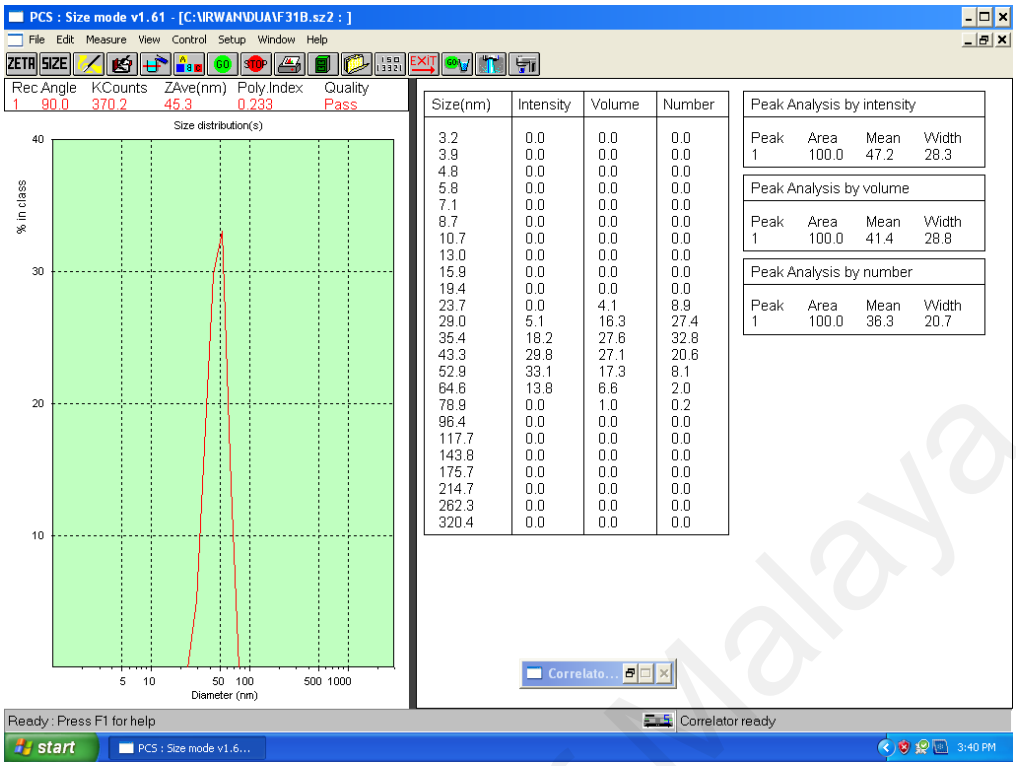

Appendix E: Zeta Potential measurement of maghemite nanoparticle

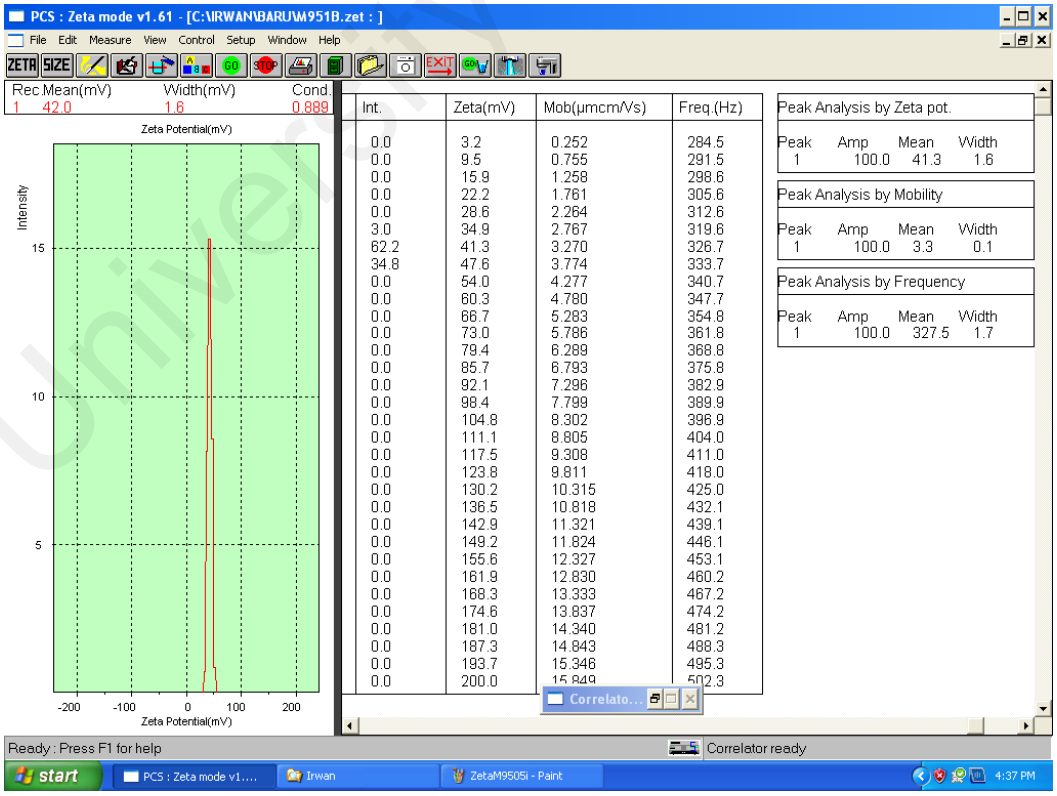

Appendix F: Thermal conductivity measurements at various particle volume fraction

Temp (°C)	ϕ (%)	Thermal conductivity (W/mK)						stdv
		k1	k2	k3	k4	k5	avg	
10	0	0.578	0.579	0.578	0.577	0.578	0.578	0.0007
	0.1	0.580	0.581	0.582	0.578	0.580	0.580	0.0015
	0.2	0.583	0.585	0.584	0.583	0.582	0.583	0.0011
	0.3	0.588	0.588	0.590	0.586	0.590	0.588	0.0017
	0.4	0.593	0.595	0.591	0.593	0.594	0.593	0.0015
	0.5	0.596	0.598	0.597	0.593	0.595	0.596	0.0019
	0.6	0.599	0.599	0.601	0.598	0.597	0.599	0.0015
15	0	0.586	0.587	0.587	0.586	0.585	0.586	0.0008
	0.1	0.588	0.588	0.589	0.591	0.591	0.589	0.0015
	0.2	0.591	0.593	0.594	0.592	0.591	0.592	0.0013
	0.3	0.597	0.598	0.599	0.595	0.596	0.597	0.0016
	0.4	0.603	0.601	0.604	0.599	0.601	0.602	0.0019
	0.5	0.605	0.606	0.607	0.604	0.605	0.605	0.0011
	0.6	0.610	0.613	0.614	0.611	0.612	0.612	0.0016
20	0	0.596	0.594	0.595	0.596	0.594	0.595	0.0010
	0.1	0.598	0.599	0.598	0.6	0.601	0.599	0.0013
	0.2	0.602	0.603	0.604	0.603	0.605	0.603	0.0011
	0.3	0.607	0.608	0.605	0.606	0.606	0.606	0.0011
	0.4	0.61	0.613	0.613	0.611	0.61	0.611	0.0015
	0.5	0.617	0.614	0.616	0.615	0.617	0.616	0.0013
	0.6	0.622	0.62	0.619	0.623	0.619	0.621	0.0018
25	0	0.601	0.601	0.603	0.604	0.602	0.602	0.0013
	0.1	0.608	0.609	0.605	0.606	0.607	0.607	0.0016
	0.2	0.618	0.618	0.616	0.616	0.617	0.617	0.0010
	0.3	0.623	0.622	0.625	0.62	0.621	0.622	0.0019
	0.4	0.627	0.629	0.625	0.628	0.627	0.627	0.0015
	0.5	0.631	0.634	0.629	0.631	0.632	0.631	0.0018
	0.6	0.644	0.641	0.642	0.643	0.642	0.642	0.0011
30	0	0.614	0.615	0.612	0.616	0.613	0.614	0.0016
	0.1	0.621	0.619	0.623	0.619	0.62	0.620	0.0017
	0.2	0.635	0.632	0.635	0.633	0.634	0.634	0.0013
	0.3	0.645	0.645	0.647	0.642	0.644	0.645	0.0018
	0.4	0.658	0.655	0.657	0.658	0.656	0.657	0.0013
	0.5	0.667	0.669	0.67	0.665	0.667	0.668	0.0019
	0.6	0.69	0.691	0.687	0.689	0.688	0.689	0.0016
35	0	0.621	0.622	0.62	0.622	0.621	0.621	0.0008
	0.1	0.635	0.632	0.635	0.631	0.636	0.634	0.0022
	0.2	0.65	0.651	0.65	0.654	0.65	0.651	0.0017
	0.3	0.671	0.673	0.672	0.674	0.67	0.672	0.0016
	0.4	0.684	0.687	0.685	0.686	0.682	0.685	0.0019
	0.5	0.705	0.702	0.703	0.706	0.702	0.704	0.0018
	0.6	0.739	0.738	0.736	0.739	0.736	0.738	0.0015

Appendix G: Thermal conductivity measurements at various temperature

ϕ (%)	T (°C)	Thermal conductivity (W/mK)						stdv
		k1	k2	k3	k4	k5	avg	
0	10	0.578	0.579	0.578	0.577	0.578	0.578	0.0007
	15	0.586	0.587	0.587	0.586	0.585	0.586	0.0008
	20	0.596	0.594	0.595	0.596	0.594	0.595	0.0010
	25	0.601	0.601	0.603	0.604	0.602	0.602	0.0013
	30	0.614	0.615	0.612	0.616	0.613	0.614	0.0016
	35	0.621	0.622	0.62	0.622	0.621	0.621	0.0008
0.1	10	0.580	0.581	0.582	0.578	0.580	0.580	0.0015
	15	0.588	0.588	0.589	0.591	0.591	0.589	0.0015
	20	0.598	0.599	0.598	0.6	0.601	0.599	0.0013
	25	0.608	0.609	0.605	0.606	0.607	0.607	0.0016
	30	0.621	0.619	0.623	0.619	0.62	0.620	0.0017
	35	0.635	0.632	0.635	0.631	0.636	0.634	0.0022
0.2	10	0.583	0.585	0.584	0.583	0.582	0.583	0.0011
	15	0.591	0.593	0.594	0.592	0.591	0.592	0.0013
	20	0.607	0.608	0.605	0.606	0.606	0.6064	0.0011
	25	0.618	0.618	0.616	0.616	0.617	0.617	0.0010
	30	0.635	0.632	0.635	0.633	0.634	0.634	0.0013
	35	0.65	0.651	0.65	0.654	0.65	0.651	0.0017
0.3	10	0.588	0.588	0.590	0.586	0.590	0.588	0.0017
	15	0.597	0.598	0.599	0.595	0.596	0.597	0.0016
	20	0.622	0.62	0.619	0.623	0.619	0.621	0.0018
	25	0.623	0.622	0.625	0.62	0.621	0.622	0.0019
	30	0.645	0.645	0.647	0.642	0.644	0.645	0.0018
	35	0.671	0.673	0.672	0.674	0.67	0.672	0.0016
0.4	10	0.593	0.595	0.591	0.593	0.594	0.593	0.0015
	15	0.603	0.601	0.604	0.599	0.601	0.602	0.0019
	20	0.61	0.613	0.613	0.611	0.61	0.611	0.0015
	25	0.627	0.629	0.625	0.628	0.627	0.627	0.0015
	30	0.658	0.655	0.657	0.658	0.656	0.657	0.0013
	35	0.684	0.687	0.685	0.686	0.682	0.685	0.0019
0.5	10	0.596	0.598	0.597	0.593	0.595	0.596	0.0019
	15	0.605	0.606	0.607	0.604	0.605	0.605	0.0011
	20	0.617	0.614	0.616	0.615	0.617	0.616	0.0013
	25	0.631	0.634	0.629	0.631	0.632	0.631	0.0018
	30	0.667	0.669	0.67	0.665	0.667	0.668	0.0019
	35	0.705	0.702	0.703	0.706	0.702	0.704	0.0018
0.6	10	0.599	0.599	0.601	0.598	0.597	0.599	0.0015
	15	0.610	0.613	0.614	0.611	0.612	0.612	0.0016
	20	0.622	0.62	0.619	0.623	0.619	0.621	0.0018
	25	0.644	0.641	0.642	0.643	0.642	0.642	0.0011
	30	0.69	0.691	0.687	0.689	0.688	0.689	0.0016
	35	0.739	0.738	0.736	0.739	0.736	0.738	0.0015

Appendix H: Thermal conductivity measurements at various parallel magnetic fields

ϕ (%)	B (Gauss)	Thermal conductivity (W/mK)						stdv
		k1	k2	k3	k4	k5	avg	
0.1	0	0.607	0.608	0.609	0.605	0.606	0.607	0.0016
	50	0.613	0.614	0.610	0.612	0.613	0.612	0.0015
	100	0.614	0.617	0.616	0.614	0.616	0.615	0.0013
	150	0.630	0.626	0.627	0.629	0.628	0.628	0.0016
	200	0.643	0.639	0.640	0.641	0.639	0.640	0.0017
	250	0.652	0.649	0.651	0.648	0.650	0.650	0.0016
	300	0.663	0.661	0.663	0.660	0.662	0.662	0.0013
0.2	0	0.618	0.617	0.615	0.618	0.616	0.617	0.0013
	50	0.621	0.618	0.622	0.621	0.620	0.620	0.0015
	100	0.622	0.624	0.625	0.621	0.623	0.623	0.0016
	150	0.635	0.638	0.635	0.633	0.636	0.635	0.0018
	200	0.653	0.654	0.652	0.656	0.655	0.654	0.0016
	250	0.665	0.667	0.668	0.669	0.665	0.667	0.0018
	300	0.684	0.680	0.680	0.682	0.681	0.681	0.0017
0.3	0	0.623	0.624	0.621	0.621	0.62	0.622	0.0016
	50	0.625	0.624	0.624	0.623	0.626	0.624	0.0011
	100	0.634	0.631	0.632	0.633	0.631	0.632	0.0013
	150	0.642	0.641	0.644	0.64	0.642	0.642	0.0015
	200	0.664	0.665	0.662	0.662	0.664	0.663	0.0013
	250	0.682	0.682	0.68	0.683	0.681	0.682	0.0011
	300	0.711	0.714	0.71	0.711	0.711	0.711	0.0015
0.4	0	0.626	0.629	0.627	0.626	0.627	0.627	0.0012
	50	0.632	0.63	0.63	0.633	0.632	0.631	0.0013
	100	0.635	0.637	0.634	0.636	0.636	0.636	0.0011
	150	0.646	0.645	0.648	0.647	0.648	0.647	0.0013
	200	0.671	0.671	0.674	0.672	0.674	0.672	0.0015
	250	0.697	0.699	0.701	0.698	0.697	0.698	0.0017
	300	0.738	0.737	0.74	0.739	0.736	0.738	0.0016
0.5	0	0.632	0.634	0.63	0.633	0.631	0.632	0.0016
	50	0.635	0.637	0.634	0.634	0.636	0.635	0.0013
	100	0.639	0.641	0.637	0.639	0.641	0.639	0.0017
	150	0.652	0.651	0.649	0.653	0.651	0.651	0.0015
	200	0.682	0.68	0.68	0.679	0.681	0.680	0.0011
	250	0.724	0.726	0.724	0.722	0.724	0.724	0.0014
	300	0.766	0.765	0.768	0.766	0.765	0.766	0.0012
0.6	0	0.645	0.642	0.643	0.644	0.643	0.643	0.0011
	50	0.647	0.649	0.646	0.647	0.646	0.647	0.0012
	100	0.654	0.652	0.652	0.653	0.651	0.652	0.0011
	150	0.66	0.661	0.664	0.66	0.662	0.661	0.0017
	200	0.698	0.696	0.696	0.695	0.696	0.696	0.0011
	250	0.745	0.741	0.743	0.742	0.743	0.743	0.0015
	300	0.794	0.791	0.792	0.793	0.793	0.793	0.0011

Appendix I: Thermal conductivity measurements at various perpendicular magnetic fields

ϕ (%)	B (Gauss)	Thermal conductivity (W/mK)						stdv
		k1	k2	k3	k4	k5	avg	
0.1	0	0.608	0.604	0.608	0.607	0.607	0.607	0.0016
	50	0.609	0.606	0.609	0.608	0.609	0.608	0.0013
	100	0.609	0.607	0.609	0.610	0.608	0.609	0.0011
	150	0.609	0.611	0.610	0.612	0.612	0.611	0.0013
	200	0.612	0.613	0.611	0.611	0.613	0.612	0.0010
	250	0.614	0.615	0.613	0.614	0.612	0.614	0.0011
	300	0.614	0.614	0.616	0.612	0.614	0.614	0.0014
0.2	0	0.616	0.618	0.616	0.619	0.617	0.617	0.0013
	50	0.617	0.615	0.618	0.619	0.618	0.617	0.0015
	100	0.618	0.617	0.618	0.619	0.620	0.618	0.0011
	150	0.621	0.623	0.624	0.621	0.621	0.622	0.0014
	200	0.625	0.623	0.624	0.625	0.622	0.624	0.0013
	250	0.625	0.626	0.625	0.624	0.627	0.625	0.0011
	300	0.627	0.628	0.629	0.627	0.626	0.627	0.0011
0.3	0	0.621	0.623	0.624	0.621	0.622	0.622	0.0013
	50	0.622	0.62	0.624	0.624	0.622	0.622	0.0017
	100	0.625	0.625	0.626	0.623	0.627	0.625	0.0015
	150	0.626	0.628	0.629	0.626	0.628	0.627	0.0013
	200	0.629	0.631	0.632	0.629	0.63	0.630	0.0013
	250	0.632	0.634	0.631	0.633	0.632	0.632	0.0011
	300	0.632	0.633	0.634	0.632	0.635	0.633	0.0013
0.4	0	0.627	0.628	0.626	0.629	0.625	0.627	0.0016
	50	0.629	0.627	0.631	0.63	0.629	0.629	0.0015
	100	0.631	0.63	0.634	0.633	0.633	0.632	0.0016
	150	0.636	0.636	0.634	0.633	0.635	0.635	0.0013
	200	0.636	0.637	0.639	0.636	0.639	0.637	0.0015
	250	0.64	0.643	0.639	0.643	0.641	0.641	0.0018
	300	0.643	0.643	0.645	0.641	0.643	0.643	0.0014
0.5	0	0.63	0.632	0.633	0.629	0.63	0.631	0.0016
	50	0.633	0.634	0.633	0.631	0.635	0.633	0.0015
	100	0.637	0.635	0.637	0.634	0.636	0.636	0.0013
	150	0.64	0.639	0.641	0.638	0.639	0.639	0.0011
	200	0.64	0.641	0.643	0.64	0.643	0.641	0.0015
	250	0.646	0.645	0.644	0.643	0.647	0.645	0.0016
	300	0.649	0.652	0.65	0.651	0.65	0.650	0.0011
0.6	0	0.643	0.644	0.642	0.645	0.641	0.643	0.0016
	50	0.643	0.645	0.643	0.646	0.645	0.644	0.0013
	100	0.645	0.646	0.644	0.647	0.645	0.645	0.0011
	150	0.649	0.648	0.646	0.649	0.647	0.648	0.0013
	200	0.65	0.652	0.65	0.653	0.65	0.651	0.0014
	250	0.655	0.653	0.655	0.652	0.656	0.654	0.0016
	300	0.657	0.655	0.656	0.655	0.658	0.656	0.0013

Appendix J: Kinematic viscosity measurements at various particle volume fraction

ϕ	t (sec)	μ (cst)	μ_{avrg} (cst)	stdv
0	335.32	1.306	1.307	0.0019
	335.65	1.307		
	335.69	1.308		
	336.46	1.311		
	335.17	1.305		
0.1	337.65	1.315	1.316	0.0016
	338.65	1.319		
	337.86	1.316		
	337.67	1.315		
	337.98	1.316		
0.2	338.54	1.319	1.319	0.0018
	338.64	1.319		
	338.67	1.319		
	338.3	1.318		
	339.52	1.322		
0.3	339.28	1.321	1.323	0.0017
	339.43	1.322		
	340.32	1.326		
	339.67	1.323		
	340.12	1.325		
0.4	340.89	1.328	1.328	0.0019
	340.41	1.326		
	340.62	1.327		
	341.65	1.331		
	340.57	1.327		
0.5	341.67	1.331	1.332	0.0019
	342.61	1.334		
	341.76	1.331		
	341.85	1.332		
	342.63	1.335		
0.6	343.54	1.338	1.337	0.0012
	342.98	1.336		
	342.78	1.335		
	343.46	1.338		
	343.23	1.337		

Appendix K: Kinematic viscosity measurements at various temperature

T (°C)	t (sec)	μ (cst)	μ_{avrg} (cst)	stdv
10	335.32	1.306	1.307	0.0019
	335.65	1.307		
	335.69	1.308		
	336.46	1.311		
	335.17	1.305		
15	293.86	1.144	1.144	0.0015
	293.76	1.144		
	293.15	1.142		
	294.22	1.146		
	293.55	1.143		
20	256.78	0.999	0.997	0.0023
	255.46	0.994		
	256.43	0.998		
	255.72	0.995		
	256.64	0.999		
25	229.1	0.891	0.889	0.0019
	228.54	0.889		
	227.89	0.887		
	227.98	0.887		
	228.64	0.890		
30	205.23	0.798	0.799	0.0011
	205.54	0.799		
	205.17	0.798		
	205.86	0.801		
	205.43	0.799		
35	187.78	0.730	0.732	0.0012
	188.42	0.733		
	188.19	0.732		
	188.62	0.733		
	188.36	0.732		

Appendix L: Kinematic viscosity measurements at various parallel magnetic fields

Magnetic fields (Gauss)	t (sec)	μ (cst)	μ_{avrg} (cst)	stdv
0	231.67	0.901	0.901	0.0014
	231.54	0.901		
	231.12	0.899		
	231.76	0.902		
	232.14	0.903		
50	232.86	0.906	0.905	0.0017
	232.63	0.905		
	231.72	0.902		
	232.57	0.905		
	232.71	0.905		
100	235.54	0.916	0.914	0.0020
	235.13	0.915		
	234.72	0.913		
	234.81	0.914		
	234.17	0.911		
150	238.56	0.928	0.927	0.0016
	238.91	0.930		
	238.15	0.927		
	237.84	0.925		
	238.28	0.927		
200	241.15	0.938	0.941	0.0015
	242.18	0.942		
	241.65	0.940		
	241.86	0.941		
	241.89	0.941		
250	244.76	0.952	0.952	0.0016
	244.13	0.950		
	245.25	0.954		
	244.61	0.952		
	244.82	0.953		
300	248.73	0.968	0.969	0.0012
	249.16	0.969		
	249.26	0.970		
	248.67	0.968		
	249.32	0.970		

Appendix M: Kinematic viscosity measurements at various perpendicular magnetic fields

Magnetic fields (Gauss)	t (sec)	μ (cst)	μ_{avrg} (cst)	stdv
0	231.67	0.901	0.901	0.0014
	231.54	0.901		
	231.12	0.899		
	231.76	0.902		
	232.14	0.903		
50	232.76	0.906	0.906	0.0015
	232.17	0.903		
	233.27	0.908		
	232.58	0.905		
	232.81	0.906		
100	234.54	0.913	0.912	0.0013
	233.97	0.910		
	234.19	0.911		
	234.84	0.914		
	234.45	0.912		
150	236.14	0.919	0.920	0.0012
	236.72	0.921		
	236.53	0.920		
	236.16	0.919		
	236.76	0.921		
200	238.43	0.928	0.928	0.0022
	237.78	0.925		
	239.36	0.931		
	238.57	0.928		
	238.42	0.928		
250	241.23	0.939	0.938	0.0021
	241.1	0.938		
	240.75	0.937		
	241.72	0.941		
	240.28	0.935		
300	245.52	0.955	0.955	0.0021
	245.98	0.957		
	244.76	0.952		
	244.84	0.953		
	245.72	0.956		

Appendix N: Electrical conductivity measurements at various particle volume fraction

Temp (°C)	ϕ (%)	Electrical conductivity (mS/cm)						stdv
		σ_1	σ_2	σ_3	σ_4	σ_5	σavg	
10	0.1	0.868	0.867	0.866	0.868	0.869	0.868	0.0011
	0.2	1.460	1.462	1.462	1.460	1.463	1.461	0.0013
	0.3	2.164	2.164	2.166	2.163	2.167	2.165	0.0016
	0.4	2.753	2.754	2.753	2.752	2.756	2.754	0.0015
	0.5	3.376	3.378	3.379	3.379	3.377	3.378	0.0013
	0.6	4.046	4.044	4.047	4.045	4.046	4.046	0.0011
15	0.1	0.946	0.946	0.948	0.947	0.948	0.947	0.0010
	0.2	1.644	1.645	1.647	1.643	1.647	1.645	0.0018
	0.3	2.560	2.562	2.563	2.561	2.560	2.561	0.0013
	0.4	3.318	3.316	3.318	3.319	3.317	3.318	0.0011
	0.5	4.203	4.204	4.202	4.205	4.207	4.204	0.0019
	0.6	5.192	5.196	5.193	5.194	5.195	5.194	0.0016
20	0.1	0.991	0.992	0.989	0.988	0.99	0.990	0.0016
	0.2	1.813	1.815	1.813	1.812	1.816	1.814	0.0016
	0.3	2.82	2.818	2.817	2.819	2.82	2.819	0.0013
	0.4	3.689	3.689	3.687	3.689	3.686	3.688	0.0014
	0.5	4.642	4.643	4.642	4.644	4.644	4.643	0.0010
	0.6	5.672	5.674	5.672	5.675	5.673	5.673	0.0013
25	0.1	1.011	1.008	1.01	1.011	1.011	1.010	0.0013
	0.2	1.986	1.987	1.986	1.984	1.987	1.986	0.0012
	0.3	3.111	3.109	3.107	3.11	3.108	3.109	0.0016
	0.4	4.107	4.106	4.104	4.108	4.109	4.107	0.0019
	0.5	4.99	4.991	4.989	4.992	4.993	4.991	0.0016
	0.6	6.618	6.616	6.618	6.619	6.614	6.617	0.0020
30	0.1	1.05	1.049	1.053	1.052	1.051	1.051	0.0016
	0.2	2.168	2.169	2.168	2.167	2.166	2.168	0.0011
	0.3	3.375	3.376	3.374	3.377	3.373	3.375	0.0016
	0.4	4.367	4.368	4.368	4.367	4.366	4.367	0.0008
	0.5	5.455	5.456	5.457	5.458	5.455	5.456	0.0013
	0.6	6.68	6.682	6.682	6.681	6.68	6.681	0.0010
35	0.1	1.101	1.101	1.101	1.103	1.103	1.102	0.0011
	0.2	2.376	2.376	2.377	2.375	2.376	2.376	0.0007
	0.3	3.643	3.644	3.642	3.645	3.644	3.644	0.0011
	0.4	4.744	4.745	4.745	4.746	4.745	4.745	0.0007
	0.5	5.998	5.998	5.998	5.998	5.996	5.998	0.0009
	0.6	7.347	7.348	7.345	7.348	7.35	7.348	0.0018

Appendix O: Electrical conductivity measurements at various temperature

ϕ (%)	T (°C)	Electrical conductivity (mS/cm)						stdv
		σ_1	σ_2	σ_3	σ_4	σ_5	σavg	
0.1	10	0.868	0.867	0.866	0.868	0.869	0.868	0.0011
	15	0.946	0.946	0.948	0.947	0.948	0.947	0.0010
	20	0.991	0.992	0.989	0.988	0.99	0.990	0.0016
	25	1.011	1.008	1.01	1.011	1.011	1.010	0.0013
	30	1.05	1.049	1.053	1.052	1.051	1.051	0.0016
	35	1.101	1.101	1.101	1.103	1.103	1.102	0.0011
0.2	10	1.460	1.462	1.462	1.460	1.463	1.461	0.0013
	15	1.644	1.645	1.647	1.643	1.647	1.645	0.0018
	20	1.813	1.815	1.813	1.812	1.816	1.8138	0.0016
	25	1.986	1.987	1.986	1.984	1.987	1.986	0.0012
	30	2.168	2.169	2.168	2.167	2.166	2.168	0.0011
	35	2.376	2.376	2.377	2.375	2.376	2.376	0.0007
0.3	10	2.164	2.164	2.166	2.163	2.167	2.165	0.0016
	15	2.560	2.562	2.563	2.561	2.560	2.561	0.0013
	20	2.82	2.818	2.817	2.819	2.82	2.819	0.0013
	25	3.111	3.109	3.107	3.11	3.108	3.109	0.0016
	30	3.375	3.376	3.374	3.377	3.373	3.375	0.0016
	35	3.643	3.644	3.642	3.645	3.644	3.644	0.0011
0.4	10	2.753	2.754	2.753	2.752	2.756	2.754	0.0015
	15	3.318	3.316	3.318	3.319	3.317	3.318	0.0011
	20	3.689	3.689	3.687	3.689	3.686	3.688	0.0014
	25	4.107	4.106	4.104	4.108	4.109	4.107	0.0019
	30	4.367	4.368	4.368	4.367	4.366	4.367	0.0008
	35	4.744	4.745	4.745	4.746	4.745	4.745	0.0007
0.5	10	3.376	3.378	3.379	3.379	3.377	3.378	0.0013
	15	4.203	4.204	4.202	4.205	4.207	4.204	0.0019
	20	4.642	4.643	4.642	4.644	4.644	4.643	0.0010
	25	4.99	4.991	4.989	4.992	4.993	4.991	0.0016
	30	5.455	5.456	5.457	5.458	5.455	5.456	0.0013
	35	5.998	5.998	5.998	5.998	5.996	5.998	0.0009
0.6	10	4.046	4.044	4.047	4.045	4.046	4.046	0.0011
	15	5.192	5.196	5.193	5.194	5.195	5.194	0.0016
	20	5.672	5.674	5.672	5.675	5.673	5.673	0.0013
	25	6.618	6.616	6.618	6.619	6.614	6.617	0.0020
	30	6.68	6.682	6.682	6.681	6.68	6.681	0.0010
	35	7.347	7.348	7.345	7.348	7.35	7.348	0.0018

Appendix P: Electrical conductivity measurements at various parallel magnetic fields

ϕ (%)	B (Gauss)	Electrical conductivity (mS/cm)						stdv
		σ_1	σ_2	σ_3	σ_4	σ_5	σavg	
0.1	0	1.011	1.009	1.012	1.010	1.012	1.011	0.0013
	50	1.011	1.012	1.012	1.010	1.012	1.011	0.0009
	100	1.011	1.013	1.010	1.013	1.013	1.012	0.0014
	150	1.012	1.014	1.011	1.013	1.013	1.013	0.0011
	200	1.013	1.011	1.013	1.014	1.012	1.013	0.0011
	250	1.015	1.011	1.014	1.015	1.014	1.014	0.0016
	300	1.014	1.014	1.015	1.015	1.016	1.015	0.0008
0.2	0	2.018	2.018	2.020	2.017	2.020	2.019	0.0013
	50	2.021	2.019	2.018	2.020	2.021	2.020	0.0013
	100	2.018	2.021	2.021	2.018	2.020	2.020	0.0015
	150	2.022	2.021	2.020	2.022	2.022	2.021	0.0009
	200	2.021	2.019	2.022	2.022	2.020	2.021	0.0013
	250	2.023	2.021	2.020	2.022	2.023	2.022	0.0013
	300	2.022	2.022	2.023	2.024	2.022	2.023	0.0009
0.3	0	3.159	3.162	3.161	3.159	3.159	3.160	0.0014
	50	3.16	3.161	3.16	3.162	3.16	3.161	0.0009
	100	3.16	3.162	3.161	3.16	3.162	3.161	0.0010
	150	3.161	3.163	3.161	3.164	3.163	3.162	0.0013
	200	3.162	3.164	3.163	3.162	3.161	3.162	0.0011
	250	3.162	3.162	3.164	3.165	3.162	3.163	0.0014
	300	3.164	3.165	3.162	3.164	3.165	3.164	0.0012
0.4	0	4.11	4.108	4.109	4.11	4.108	4.109	0.0010
	50	4.114	4.114	4.111	4.112	4.113	4.113	0.0013
	100	4.113	4.112	4.114	4.112	4.113	4.113	0.0008
	150	4.114	4.113	4.115	4.116	4.115	4.115	0.0011
	200	4.117	4.115	4.117	4.114	4.115	4.116	0.0013
	250	4.116	4.116	4.116	4.117	4.118	4.117	0.0009
	300	4.12	4.118	4.118	4.119	4.119	4.119	0.0008
0.5	0	4.993	4.992	4.993	4.995	4.995	4.994	0.0013
	50	4.995	4.997	4.996	4.998	4.995	4.996	0.0013
	100	4.997	4.999	4.998	4.997	4.999	4.998	0.0010
	150	5.003	5.002	5.003	5.001	5.003	5.002	0.0009
	200	5.003	5.003	5.001	5.004	5.005	5.003	0.0015
	250	5.003	5.003	5.006	5.005	5.003	5.004	0.0014
	300	5.006	5.005	5.006	5.004	5.006	5.005	0.0009
0.6	0	6.623	6.625	6.624	6.626	6.623	6.624	0.0013
	50	6.626	6.627	6.626	6.628	6.628	6.627	0.0010
	100	6.631	6.631	6.631	6.629	6.63	6.630	0.0009
	150	6.63	6.632	6.63	6.631	6.633	6.631	0.0013
	200	6.631	6.633	6.631	6.63	6.633	6.632	0.0013
	250	6.635	6.635	6.633	6.632	6.633	6.634	0.0013
	300	6.636	6.636	6.634	6.635	6.634	6.635	0.0010

Appendix Q: Electrical conductivity measurements at various perpendicular magnetic fields

ϕ (%)	B (Gauss)	Electrical conductivity (mS/cm)						stdv
		σ_1	σ_2	σ_3	σ_4	σ_5	σavg	
0.1	0	1.011	1.013	1.014	1.012	1.013	1.013	0.0011
	50	1.015	1.017	1.015	1.016	1.017	1.016	0.0010
	100	1.019	1.016	1.019	1.017	1.018	1.018	0.0013
	150	1.019	1.020	1.019	1.021	1.021	1.020	0.0010
	200	1.020	1.022	1.023	1.021	1.021	1.021	0.0011
	250	1.021	1.022	1.023	1.024	1.021	1.022	0.0013
	300	1.022	1.023	1.024	1.023	1.021	1.023	0.0011
0.2	0	2.020	2.019	2.019	2.018	2.018	2.019	0.0008
	50	2.023	2.022	2.023	2.021	2.023	2.022	0.0009
	100	2.022	2.023	2.024	2.024	2.022	2.023	0.0010
	150	2.024	2.025	2.024	2.025	2.023	2.024	0.0008
	200	2.024	2.024	2.025	2.026	2.026	2.025	0.0010
	250	2.028	2.026	2.027	2.028	2.028	2.027	0.0009
	300	2.027	2.027	2.028	2.029	2.027	2.028	0.0009
0.3	0	3.131	3.13	3.132	3.13	3.129	3.130	0.0011
	50	3.134	3.133	3.132	3.134	3.132	3.133	0.0010
	100	3.136	3.133	3.136	3.135	3.136	3.135	0.0013
	150	3.136	3.137	3.135	3.137	3.139	3.137	0.0015
	200	3.14	3.139	3.138	3.14	3.137	3.139	0.0013
	250	3.138	3.139	3.14	3.138	3.14	3.139	0.0010
	300	3.14	3.141	3.14	3.142	3.139	3.140	0.0011
0.4	0	4.117	4.118	4.119	4.118	4.12	4.118	0.0011
	50	4.119	4.121	4.121	4.119	4.12	4.120	0.0010
	100	4.121	4.121	4.122	4.12	4.122	4.121	0.0008
	150	4.122	4.123	4.122	4.124	4.124	4.123	0.0010
	200	4.123	4.123	4.124	4.121	4.125	4.123	0.0015
	250	4.125	4.123	4.125	4.125	4.124	4.124	0.0009
	300	4.124	4.125	4.126	4.126	4.124	4.125	0.0010
0.5	0	5.008	5.006	5.007	5.009	5.008	5.008	0.0011
	50	5.01	5.011	5.012	5.012	5.01	5.011	0.0010
	100	5.011	5.012	5.013	5.014	5.011	5.012	0.0013
	150	5.013	5.014	5.013	5.015	5.015	5.014	0.0010
	200	5.015	5.014	5.016	5.016	5.015	5.015	0.0008
	250	5.014	5.016	5.015	5.017	5.016	5.016	0.0011
	300	5.018	5.018	5.017	5.016	5.017	5.017	0.0008
0.6	0	6.627	6.627	6.629	6.627	6.628	6.628	0.0009
	50	6.630	6.631	6.630	6.632	6.629	6.630	0.0011
	100	6.63	6.629	6.632	6.632	6.63	6.631	0.0013
	150	6.633	6.633	6.634	6.632	6.635	6.633	0.0011
	200	6.632	6.634	6.632	6.635	6.634	6.633	0.0013
	250	6.633	6.635	6.634	6.633	6.634	6.634	0.0008
	300	6.634	6.635	6.636	6.634	6.634	6.635	0.0009